On-surface coupling reactions on calcium carbonate

Chiara Venturini

THÈSE

En vue de l'obtention du

DOCTORAT DE L'UNIVERSITÉ DE TOULOUSE

Délivré par *l'Université Toulouse III – Paul Sabatier (UT3 Paul Sabatier)*
Discipline ou spécialité : *Chimie moléculaire – CO 046*

Présentée et soutenue par

Chiara VENTURINI

Le 25 Novembre 2015

On-surface coupling reactions on calcium carbonate

JURY

Dr. Evelina COLACINO	Maître de conférences, Université de Montpellier	**Rapporteur**
Dr. Cédric BOISSIERE	Chargé de Recherche, UPMC Collège de France	**Rapporteur**
Prof. Brigitte CAUSSAT	Professeur, ENSIACET Toulouse	**Examinateur**
Dr. Hubert MUTIN	Directeur de Recherche, ICG Montpellier	**Examinateur**
Prof. Marc VERELST	Professeur, Université Paul Sabatier (Toulouse)	**Examinateur**
Dr. André GOURDON	Directeur de Recherche, CEMES-CNRS, Toulouse	**Directeur de thèse**

Ecole doctorale : Sciences de la Matière SDM
Unité de recherche : CEMES-CNRS (UPR 8011)
Directeur de Thèse : Dr. André GOURDON

THÈSE

En vue de l'obtention du

DOCTORAT DE L'UNIVERSITÉ DE TOULOUSE

Délivré par *l'Université Toulouse III – Paul Sabatier (UT3 Paul Sabatier)*
Discipline ou spécialité : *Chimie moléculaire – CO 046*

Présentée et soutenue par

Chiara VENTURINI

Le 25 Novembre 2015

On-surface coupling reactions on calcium carbonate

JURY

Dr. Evelina COLACINO	Maître de Conférences, Université de Montpellier	**Rapporteur**
Dr. Cédric BOISSIERE	Chargé de Recherche, UPMC Collège de France	**Rapporteur**
Prof. Brigitte CAUSSAT	Professeur, ENSIACET, Toulouse	**Examinateur**
Dr. Hubert MUTIN	Directeur de Recherche, ICG, Montpellier	**Examinateur**
Prof. Marc VERELST	Professeur, Université Paul Sabatier, Toulouse	**Examinateur**
Dr. André GOURDON	Directeur de Recherche, CEMES-CNRS, Toulouse	**Directeur de thèse**

Ecole doctorale : Sciences de la Matière SDM
Unité de recherche : CEMES-CNRS (UPR 8011)
Directeur de Thèse : Dr. André GOURDON

Acknowledgements

First and foremost I wish to express my sincere appreciation and gratitude to my supervisor, Dr. André Gourdon, for supporting my study and research during these three years, for his patience, motivation and knowledge. His guidance helped me in all the time of research and writing of this thesis. I appreciate his contributions in terms of time, ideas, and funding to make my Ph.D. experience productive and stimulating. I would also like to thank the director of the laboratory, Dr. Alain Claverie, for providing me an excellent atmosphere for doing research.

Besides my supervisor, I am also grateful to my thesis commission: Dr. Evelina Colacino and Dr. Cédric Boissière for taking the time to deeply evaluate my work and Prof. Brigitte Caussat, Dr. Hubert Mutin, Prof. Marc Verelst for their encouragement, insightful comments and scientific discussion.

My sincere thank also goes to Prof. Angelika Kühnle and the entire research group at the University of Mainz for kindly hosting me during my Ph.D. and especially to Robert Lindner to reveal me all the secrets of the nc-AFM: *vielen Dank!*

I would also like to thank the entire group GNS, in particularly the chemists who have contributed immensely to my personal and professional formation. A particular thank goes to the other members of the laboratory that helped me during this thesis (especially David Neumeyer and Dr. Nicolas Ratel-Ramond).

I wish to express my appreciation to all the common services of the University of Toulouse Paul Sabatier and to the staff of different groups (Dr. Brigitte Guidetti, SPCMIB and Prof. Catherine Amiens, LCC).

My sincere gratitude goes to my beloved family who always supported my work and Vincent for his encouragement and help throughout the course of this thesis.

The financial support of ANR ICMADS is gratefully acknowledged.

Table of contents

General introduction 1
References 2

1. Coupling reaction on surface in UHV conditions 5
1.1 State of art 5
1.2 Coupling reactions on metal surface 7
1.2.1 Ullmann reaction 7
1.2.2 Glaser-Hay reaction 11
1.2.3 Polycondensation reaction 15
1.2.4 Summary of reactions on metal surfaces 17
1.2.5 Example of molecular devices obtained by couplingon metal surface 18
1.3 Coupling reactions on insulating surfaces 19
1.3.1 Coupling reaction on NaCl thin film 20
1.3.2 Coupling reaction on TiO_2 20
1.3.3 Coupling reactions on calcite 21
1.3.3.1 Photochemical activation on calcite 28
1.4 Limits 30
1.5 References 31

2. Molecules designed for covalent coupling on calcite in UHV conditions 35
2.1 Conception of molecules 36
2.2 Molecules for homocoupling of ethynes 37
2.2.1 Introduction and objective 37
2.2.2 Results and discussion 38
2.2.2.1 Retrosynthetic analysis 38
2.2.2.2 Synthesis 38
2.2.2.3 Deposition on $CaCO_3$ surface 40
2.2.3 Conclusion 43
2.3 Molecules for photopolymerization 43
2.3.1 Introduction and objective 43
2.3.2 Results and discussion 45
2.3.2.1 Retrosynthetic analysis 45

2.3.2.2 Synthesis 45
2.3.2.3 Characterization 48
2.3.2.4 Deposition on $CaCO_3$ surface 49
2.3.3 Conclusion 50
2.4 Molecules for polycondensation 50
2.4.1 Introduction and objective 50
2.4.2 Results and discussion 55
2.4.2.1 Synthesis 55
2.4.2.2 Characterization 58
2.4.3 Conclusion 59
2.5 Molecules for Ullmann Coupling 60
2.5.1 Introduction and objective 60
2.5.2 Results and discussion 60
2.5.2.1 Retrosynthetic analysis 60
2.5.2.2 Synthesis 61
2.5.2.3 Characterization 69
2.5.3 Conclusion 73
2.6 General conclusion 73
2.7 References 74

3. Preparation of $CaCO_3$ particles for solid state reaction 77
3.1 Calcium carbonate 78
3.1.1 Calcium carbonate characteristics and properties 78
3.1.2 Calcium carbonate formation 80
3.1.3 Historical background 80
3.1.3.1 Calcium carbonate as construction material 81
3.1.4 Modern uses and production 82
3.2 Preparation methods of $CaCO_3$ particles 83
3.3 Preparation of calcium carbonate microparticles 85
3.3.1 Specific surface for coupling reaction on $CaCO_3$ particles 86
3.3.1.1 Results and discussion 86
3.3.2 $CaCO_3$ particles by grinding 87
3.3.2.1 Results and discussion 87
3.3.2.2 Conclusion on $CaCO_3$ by grinding 89
3.3.3 $CaCO_3$ particles *via* spray pyrolysis technique 89
3.3.3.1 Results and discussion 90
3.3.3.2 Conclusion on $CaCO_3$ particles *via* spray pyrolysis technique 110

3.3.4 General conclusion on preparation of $CaCO_3$ particles for solid state reaction 110
3.4 References 110

4. Coupling reaction on $CaCO_3$ particles 113
4.1 Reaction on solid surface by mechanochemistry 114
4.1.1 Introduction and objective 114
4.1.2 Experimental 116
4.1.3 Results and discussion 119
4.1.4 Conclusions on reaction by mechanochemistry activation 120
4.2 Coupling reaction on solid surface by thermal activation 121
4.2.1 Introduction and objective 121
4.2.2 Experimental 121
4.2.3 Results and discussion 121
4.2.4 Other reactions studied in this work 125
4.2.5 Conclusions on coupling reaction by thermal activation on $CaCO_3$ microparticles 129
4.3 General conclusion on coupling reactions on solid surface 129
4.4 References 131

General conclusion 133
References 135

Experimental part 137
Experimental part Chapter 2 139
Generalities 139
Solvents and Reagents 139
Chromatographic supports 139
Analytical tools and devices 139
Synthesis 140
Experimental techniques 150
Experimental part Chapter 3 151
Grinding of commercial calcium carbonate 151
Synthesis of particles *via* spray pyrolysis 151
Characterization of calcium carbonate particles 151
Fourier-transform infrared spectroscopy (FTIR) 152
Thermogravimetry and differential thermal analysis (TG/DTA) 152

X-ray powder diffraction (XRD) 152
Scanning electron microscopy (SEM) 152
Adsorption and BET 153
Laser granulometry (LG) 154
Transmission Electron Microscopy (TEM) 154
Experimental part Chapter 4 155
Mechanochemistry experiments 155
Thermal experiments 155
References 155

Annex 157
X-Ray structure of 3-ethynylbenzoic acid (11) 159
Résumé en français 161

List of abbreviations

ACC	Amorphous Calcium Carbonate
(nc)-AFM	(non contact)-Atomic Force Microscopy
amb.	ambient
anh.	anhydrous
approx.	approximately
aq.	aqueous
atm.	atmosphere
ARPES	Angle-Resolved Photoemission Spectroscopy
BET	Brunauer–Emmett–Teller (theory)
cal.	calculated
cat.	catalyst
conc.	concentrated
cyclohex.	cyclohexane
DOX	doxorubicin
eq.	equivalent
FFT	Fast Fourier Transform
FTIR	Fourier Transform Infrared Spectroscopy
GCC	Ground Calcium Carbonate
hex.	hexane
HRMS	High Resolution Mass Spectroscopy
LG	Laser Granulometry
MOFs	Metal Organic Frameworks
MOSFETs	Metal-Oxide-Semiconductor Field-Effect Transistors
MR	Molecular Ratio
NMR	Nuclear Magnetic Resonance spectroscopy
Pc	Phthalocyanine
PCC	Precipitated Calcium Carbonate
PDAs	Polydiacetylenes
PPC	Poly Phthalocyanine
Recryst.	Recrystallization
ref.	Reference
RT	Room Temperature (25 °C)
SEM	Scanning Electron Microscopy
SCOFs	Surface Covalent Organic Frameworks
SP	Spray Pyrolysis
SSA	Specific Surface Area
STM	Scanning Tunneling Microscopy
TBAF	Tetra-*n*-butylammonium fluoride
TEM	Transmission Electron Microscopy
TES	Triethylsilane
TG/DTA	Thermogravimetry/Differential Thermal Analysis
TLC	Thin Layer Chromatography
TMEDA	*N,N,N',N'*-tetramethylethylenediamine
TMSA	Trimethylsilylacetylene

TS	Transition State
UHV	Ultra High Vacuum
UV-Vis	Ultraviolet-Visible Spectroscopy
XPS	X-ray Photoelectron Spectroscopy
XRD	X-Ray Diffraction

General introduction

From many decades, miniaturization has allowed the fabrication of electronic devices down to the nanoscale dimension. In forty years (1970-2011) transistors size has been reduced dramatically and its density on electronic chips increased exponentially. For instance, the MOSFETs gate length decreased from 10 μm to 28 nm (yellow circles, *y* axis right; in the picture below). The number of transistors, on the other hand, augmented from 200 to over 1 million (all the other symbols, *y* axis left; in the picture below)[1] and today more than 9 millions.

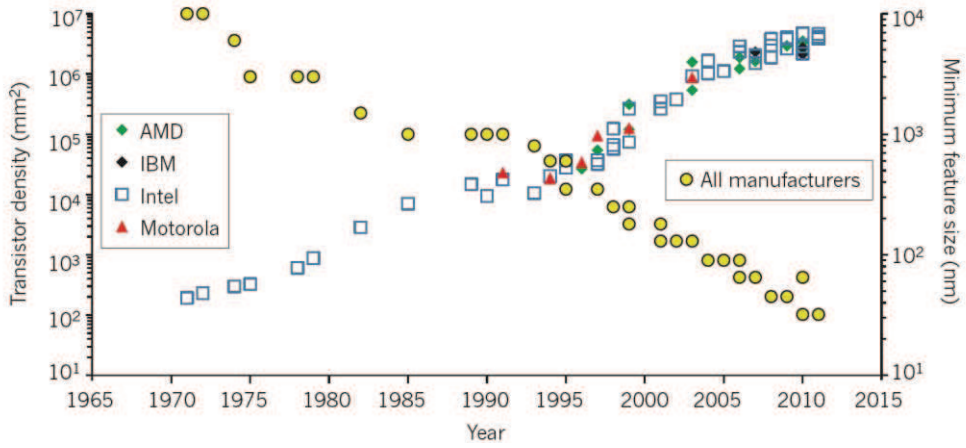

Figure 1 Density and size evolution of transistors from 1970 to 2011. The yellow circles show the size reduction of gate length in MOSFETs (*y* axis right); the other symbols represent the increasing number of transistors per square millimeters (*y* axis left). From ref.[1].

This was achieved by top-down approach, by creating the desired pattern on the surface (lithography). However, this method is reaching the limit for physical and technical reasons such as the difficulty of fabricate smaller silicon transistor and their interconnections down to the nanoscale.

These limitations led to the development of "molecular electronics" concept. A. Aviram and M. A. Ratner, pioneers on this subject, proposed for the first time (in 1970s)[2] the use of a single molecule as an electronic device ("molecular rectifier") and an electronic circuit constituted by molecules and electrodes[3]. The introduction of molecules as parts of electronic circuits, remained at the beginning almost a theoretical concept due to the gap with the technology at that period. However, recent technological and theoretical development now allows the possibility of a bottom-up approach towards molecular electronics circuits.

In order to obtain complex devices, one recent possibility is to use on-surface synthesis by bottom-up approach: small precursor molecules are assembled on a very clean (ideally insulating for electronic devices applications) surface by covalent coupling in order to obtain complex structure.

Until now, the covalent coupling has been studied mainly on metallic surface, due to several reasons, such as the technological instrument availability (scanning tunneling microscope -STM- for instance), the strong van der Waals interaction between the precursor molecules and metallic surface, and the catalyst role of the metal itself.

The objective of this thesis is inserted in this context: the exploration of the coupling reactions on insulating surface of calcium carbonate. The first results of coupling (Ullmann reaction) obtained on $CaCO_3$[4–6] encouraged the choice of this material.

This work is presented in two parts: the first part is dedicated to the synthesis of molecules for coupling reaction on insulating surface of $CaCO_3$ in ultra high vacuum (UHV) conditions. Then, in the second part of this work we extend this investigation to the macroscale conditions (semi-preparative) by preparing $CaCO_3$ microparticles and investigating the coupling reaction of smaller molecules anchored on this substrate.

Chapter 1 is devoted to the state-of-art of the coupling reaction on surface in UHV conditions, from the first results on metallic surface to insulating surfaces.

In **chapter 2** we detail the synthesis of molecules for different type of reactions on insulating surface of $CaCO_3$ in UHV: homocoupling of ethynes, photopolymerization, polycondensation and Ullmann coupling.

In **chapter 3** we describe the preparation and characterization of $CaCO_3$ microparticles *via* two different approaches: by grinding the commercial product and by spray pyrolysis.

Finally **chapter 4** is dedicated to the synthesis of molecules on $CaCO_3$ microscale particles.

General conclusions close the manuscript.

References

1. Ferain, I., Colinge, C. A. & Colinge, J.-P. Multigate transistors as the future of classical metal–oxide–semiconductor field-effect transistors. *Nature* **479,** 310–316 (2011).
2. Does molecular electronics compute? *Nat. Nanotechnol.* **8,** 377–377 (2013).
3. Aviram, A. & Ratner, M. A. Molecular rectifiers. *Chem. Phys. Lett.* **29,** 277–283 (1974).
4. Kittelmann, M. *et al.* On-Surface Covalent Linking of Organic Building Blocks on a Bulk Insulator. *ACS Nano* **5,** 8420–8425 (2011).

5. Kittelmann, M., Rahe, P., Gourdon, A. & Kühnle, A. Direct Visualization of Molecule Deprotonation on an Insulating Surface. *ACS Nano* **6,** 7406–7411 (2012).
6. Kittelmann, M., Nimmrich, M., Lindner, R., Gourdon, A. & Kühnle, A. Sequential and Site-Specific On-Surface Synthesis on a Bulk Insulator. *ACS Nano* **7,** 5614–5620 (2013).

1 Coupling reactions on surface in UHV conditions

1.1 State of art 5
1.2 Coupling reactions on metal surface 7
1.2.1 Ullmann reaction 7
1.2.2 Glaser-Hay reaction 11
1.2.3 Polycondensation reaction 15
1.2.4 Summary of reactions on metal surfaces 17
1.2.5 Example of molecular devices obtained by coupling on metal surface 18
1.3 Coupling reactions on insulating surfaces 19
1.3.1 Coupling reaction on NaCl thin film 20
1.3.2 Coupling reaction on TiO_2 20
1.3.3 Coupling reactions on calcite 21
1.3.3.1 Photochemical activation on calcite 28
1.4 Limits 30
1.5 References 31

1.1 State of art

Self-assembly of molecules on surfaces in ultra high vacuum (UHV) conditions has been widely investigated in the recent years. The structures are formed by reversible and weak interactions (van der Waals, hydrogen bonds for instance). However those structures are fragile, not stable outside UHV environment and the intermolecular charge transport is precluded[1–3]. For this reason, one of the most recent challenges is the construction of devices by bottom-up approach *via* covalent linking in UHV conditions.

Precursor molecules are sublimated on a very clean surface under high vacuum (10^{-9} mbar); then they are activated (by annealing) to react and form a more complex molecule with a specific function (electrical, mechanical and so on).

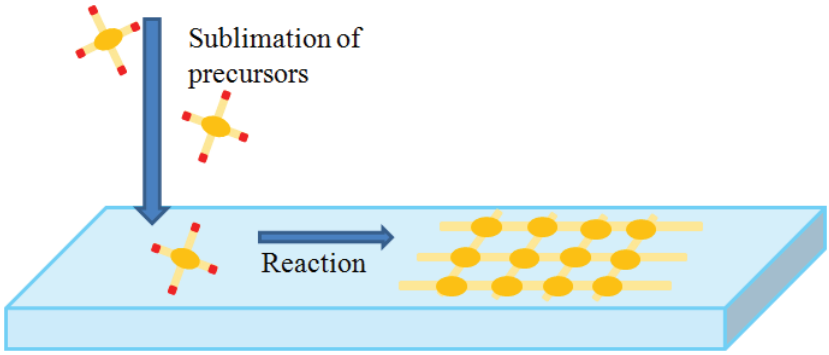

Figure 1.1 Bottom-up approach in ultra high vacuum conditions.

Indeed deposing precursor molecules directly on surface in UHV in order to obtain covalent coupling has many advantages[1,4]:

- The so-obtained structures have high thermal stability due to the formation of covalent bonds instead of weak interactions.
- The preparation of 0D, 1D or 2D structures (not reachable in standard solution chemistry due to solubility problems) directly on the surface is possible.
- Reaction temperatures might be higher due to the absence of solvents.
- The system structure might be "controlled" by using determined pre-template precursor molecules.
- Scanning probe microscopy (STM) and on-surface spectroscopy techniques can be used for deeper investigation directly on surface.

The surface plays a crucial role: the precursor molecules "anchor" the metal substrate with strong interaction (therefore the desorption is limited even at "high" temperature) and the metal surface acts as catalyst (reducing the activation temperature)[5].

For this reason, up to now, this approach has been developed mainly on metallic surface (paragraph 1.2). However, its extension to insulating surfaces is a primary objective for future applications (such as molecular electronics, catalysis and so on), as will be discussed in paragraph 1.3.

1.2 Coupling reactions on metal surface

On-surface synthesis represents a very recent and active field of research. Since the first studies in 2007 on metal surface, important progress have been done during the last decades[1,4,6]. In this paragraph we will briefly recall the milestone papers of on-surface coupling reaction in UHV on metal surfaces.

1.2.1 Ullmann reaction

One of the first and most studied reactions on metal surface in UHV is the Ullmann coupling. The reaction is well known since early 20th century and involves the use of Cu catalyst for the coupling of two aryl halides[7].

$$\text{Ar-X} + \text{X-Ar} \xrightarrow{\text{Cu cat.}} \text{Ar-Ar}$$

Figure 1.2 Ullmann reaction.

L. Grill and others, presented for the first time in 2007 the coupling reaction on a metal surface[8]. They started with small precursors, as tetra(4-bromophenyl)porphyrin (Br_4TPP) in Figure 1.3b, in which the bromine reactive groups are connected *via para*-phenylene to a central porphyrin core. The precursor molecules were activated by annealing and consequently the C-Br bonds were broken giving a reactive intermediate. The latter diffused on the surface and by bonding with similar molecules afforded the final more complex product (Figure 1.3a).

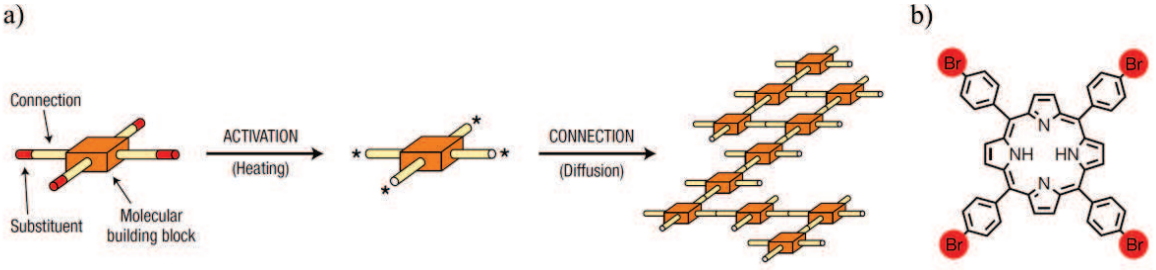

Figure 1.3 a) Scheme of the reaction; b) precursor molecule tetra(4-bromophenyl)porphyrin (Br_4TPP) from ref.[8].

The authors presented two different approaches in order to activate the starting molecule. In the first method, once the starting molecule is deposited on the surface, the C-Br bonds were broken by heating. In the second method, the activation occurred during the evaporation phase and the molecules (already activated) were deposed on the cold surface. Both the methods afforded the same covalently linked molecules.

With this approach the authors successfully reported the coupling of tetraphenylporphyrins (TTPs) with different number of Br substituents (one, two or four respectively, as showed in Figure 1.4), affording 1D or 2D arrays. They activated the precursors with the two different approaches previously explained (from left to right in Figure 1.4: method II, method I, method I). In both cases, the obtained "radical" molecules diffuse on the surface and react in order to form the final product.

STM provides the proof of the new C-C bonds (broad peak at 3eV over the intramolecular connections)[1,8].

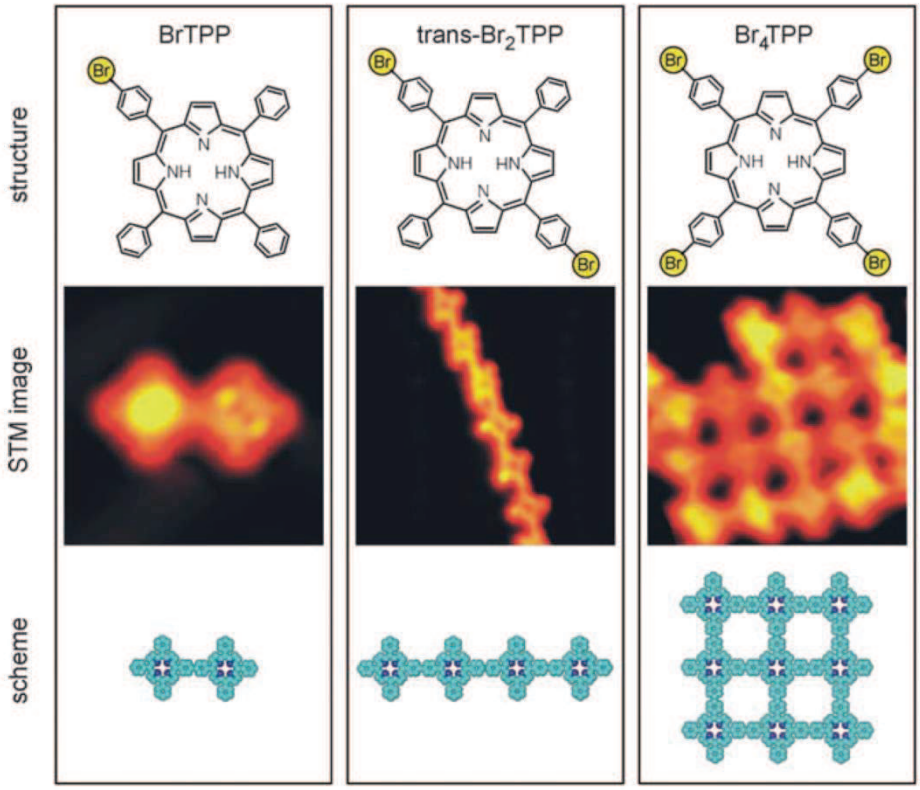

Figure 1.4 Results of tetraphenylporphyrins covalent coupling on metal surface, from ref.[1].

To date, the mechanism commonly accepted for this reaction consists in a first step of physisorption in which the molecules are, generally, lying flat on the surface. Then, by heating, the carbon-halogen bond is broken and the molecules bind the surface *via* an organometallic bond. Then, by diffusion the molecules approach and a metallic atom pops-out (some researchers affirm that this intermediate state is more favored than the previous – Bjork, Springer book, in the press) promoting the coupling reaction. If the molecules are too sterically crowded, they do not coalesce. The process is shown in Figure 1.5.

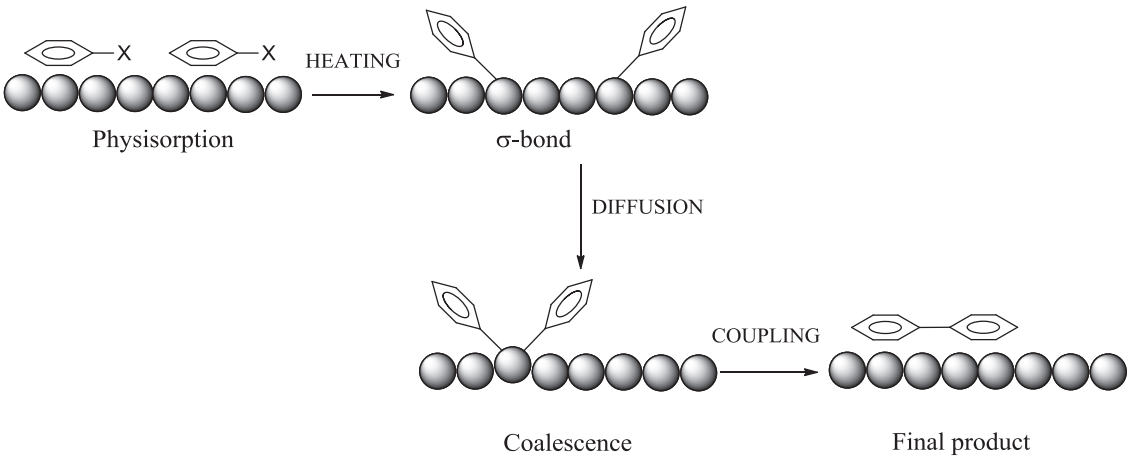

Figure 1.5 On-surface Ullmann coupling proposed mechanism.

In a remarkable paper, M. Bieri and others achieved with this approach bidimentional polyphenylene on metal surface[9]. The polymeric structure was obtained by aryl-aryl coupling reaction from precursor molecule hexaiodo cyclo-*m*-phenylene (CHP), Figure 1.6.

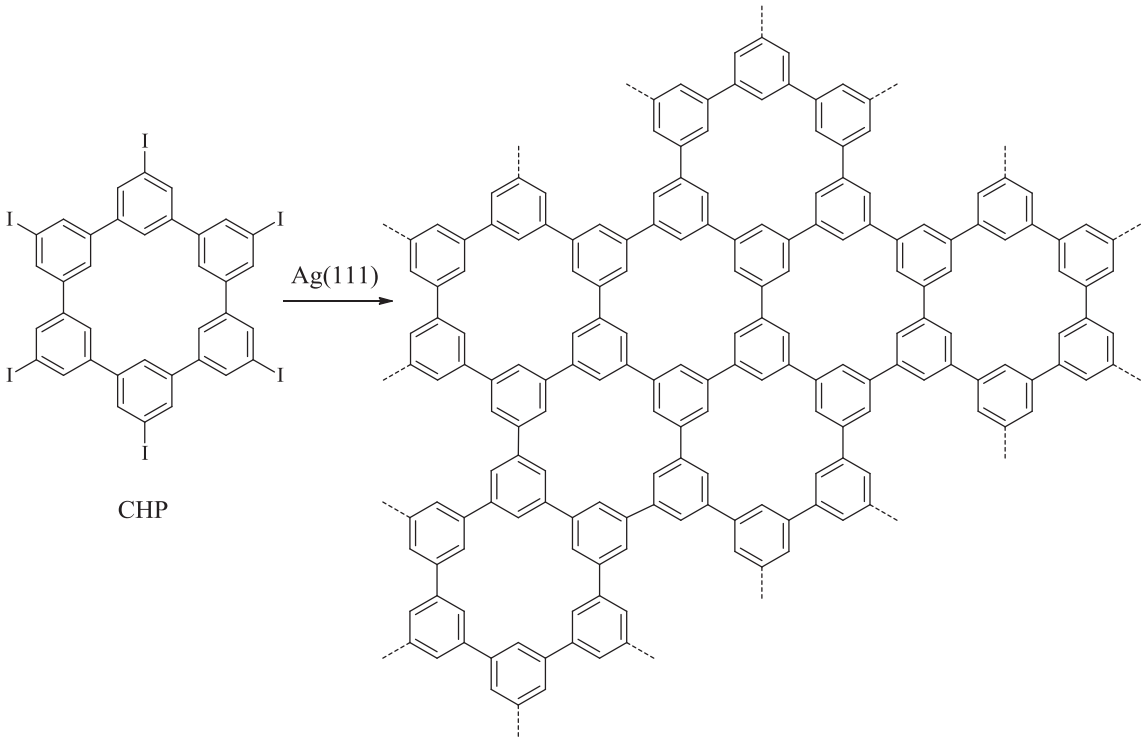

Figure 1.6 Scheme of the reaction from the starting molecule (CHP) to the polyphenylene superhoneycomb structure (fraction in the picture), readapted from ref.[9].

The same authors proposed in another paper, the bottom-up fabrication of graphene nanoribbon[10]. In their work, 10,10'-dibromo-9,9'-bianthryl (precursor molecule in Figure 1.7) was sublimated on metal surface. The molecules lost bromine giving intermediate molecules probably linked to the metal surface with the mechanism proposed above. After a first thermal

treatment, the intermediates approached and coupled to give linear polyanthryl polymer. Finally after a second thermal treatment, cyclodehydrogenation of the linear polymer afforded the graphene nanoribbon.

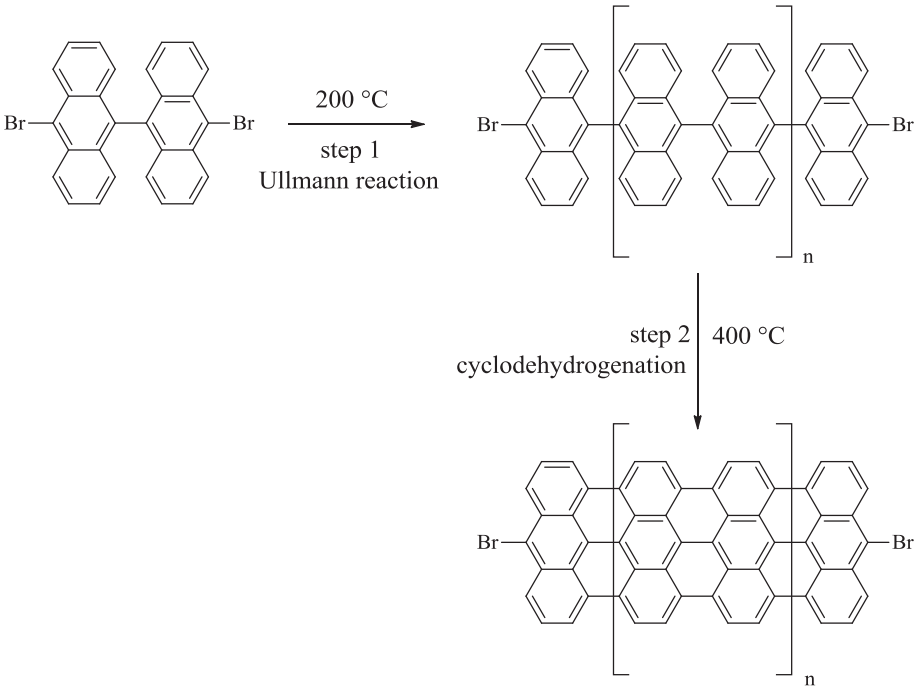

Figure 1.7 Bottom-up fabrication of graphene nanoribbon, readapted from ref.[10].

The choice of this precursor molecule is justified by the interactions with the metallic surface. In fact, if a simple anthracene core molecule is chosen, the interactions with the metallic surface forced the molecule to a flat lying conformation. In this case, the intermolecular steric repulsion of hydrogen atoms belonging to different anthracene molecules, prevents the Ullmann reaction.

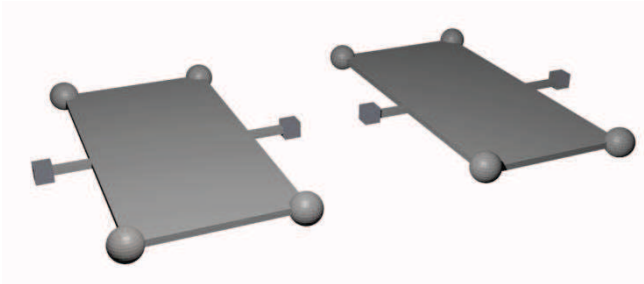

Figure 1.8 Model of two anthracene precursor molecules. The squares represent the brome atoms and the spheres the hydrogen atoms. If the molecules are flat lying on the surface, the intermolecular steric repulsion of hydrogen atoms belonging to different anthracene molecules prevents the covalent coupling *via* C-Br bond breaking.

The 10,10'-dibromo-9,9'-bianthryl molecule, however, assumed a twisted arrangement on the surface, allowing the C-C coupling reaction to give the linear polymer.

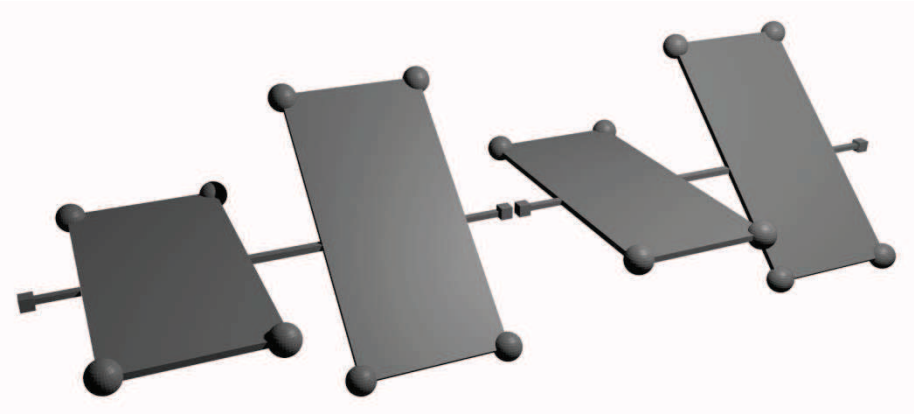

Figure 1.9 Model of 10,10'-dibromo-9,9'-bianthryl precursor molecules. The molecules are slightly twisted, therefore the intermolecular steric repulsion of hydrogen atoms belonging to different anthracene molecules does not prevent the covalent coupling *via* C-Br bond breaking.

Recently two different groups obtained with the same technique a boron-doped graphene nanoribbon[11,12], showing the versatility of this approach and paving the way for new reactions yielding chemical products otherwise impossible to obtain in solutions.

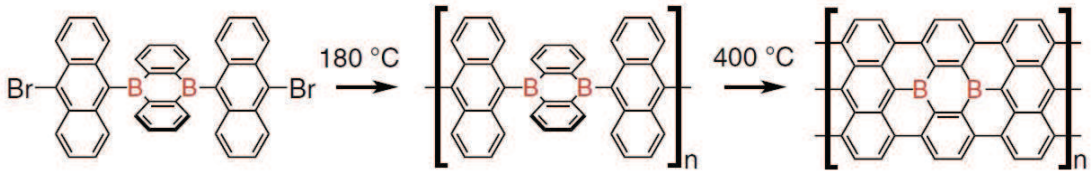

Figure 1.10 Bottom-up synthesis of boron doped graphene nanoribbon (B-GNRs), from ref.[11].

Finally, researchers studied also the photochemical activation of Ullmann coupling induced by irradiation on silver surface[13]. 4-bromo-4'-hydroxybiphenyl molecules were deposited on surface in UHV condition and irradiated by 266 nm UV lamp at 80 K for 10 min. The cleavage of C-Br or C-OH bond led to an intermediate hexagonal nanopore structure. Finally, after one hour at room temperature polymer chains were obtained. This example offers new possibility for C-halogen and C-O cleavage on surface in UHV conditions at "moderate temperature".

1.2.2 Glaser-Hay reaction

Another key reaction widely studied on metal surface is the Glaser-Hay (Figure 1.11). In solution, the reaction was proposed for the first time by C. Glaser in 1869 and successively modified several times. Notably, A. S. Hay carried out in 1962 this reaction in presence of

catalytic amount of bidentate ligand *N,N,N',N'*-tetramethylethylenediamine (TMEDA) (that increases the solubility of the reactive species), copper (I) chloride in presence of oxygen[14–16].

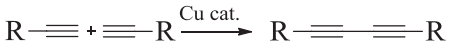

Figure 1.11 Glaser-Hay reaction.

Recently the reaction has been studied on surface as well[16].

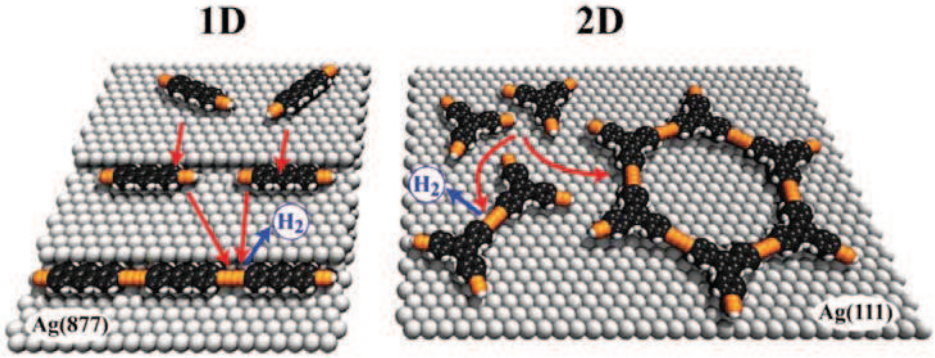

Figure 1.12 1D and 2D structures obtained by Glaser-Hay reaction on surface, from ref.[16].

To date, the reaction pathway is still debated in the scientific community. Two mechanisms are proposed, as shown in figure below.

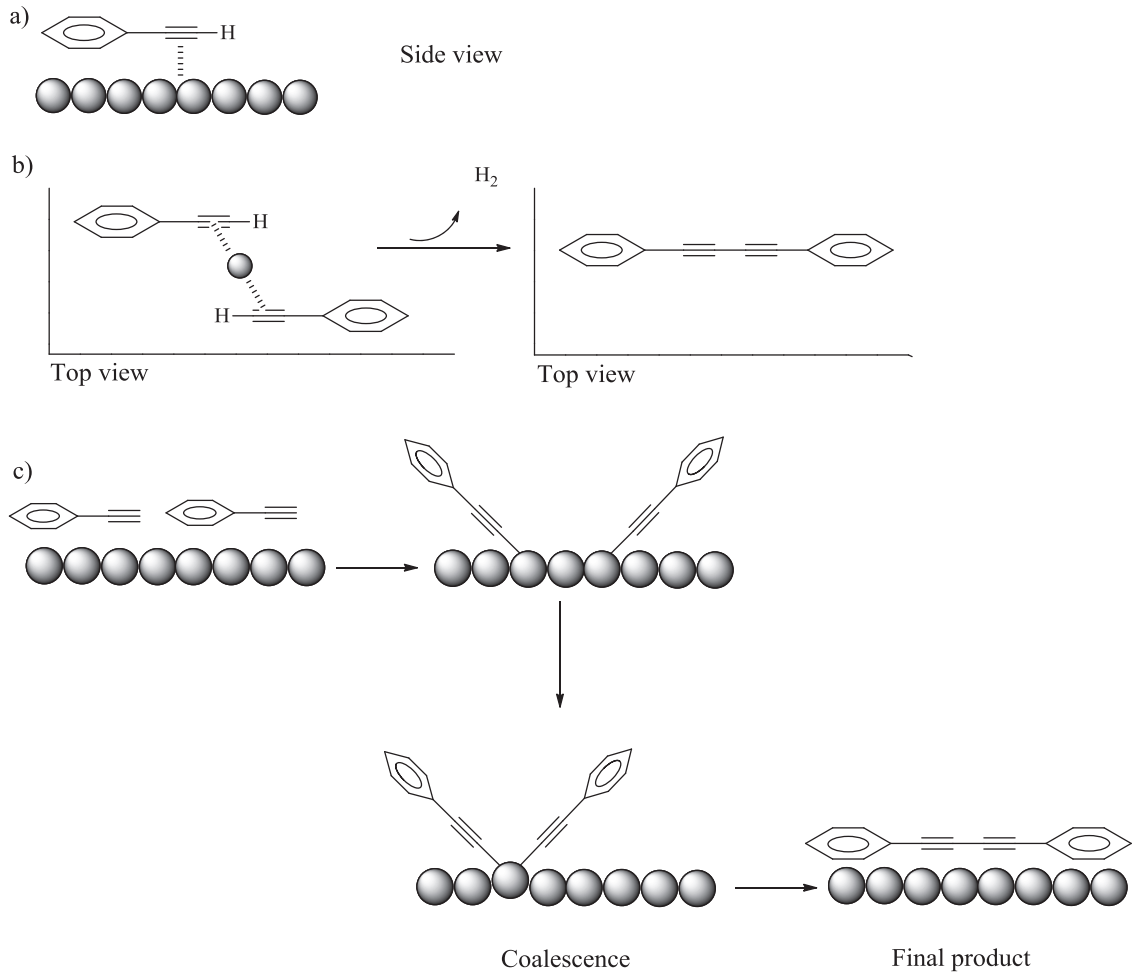

Figure 1.13 a-b) Side view and top view for Barth's proposed mechanism for Glaser-Hay reaction; c) Fuch's proposed mechanism for Glaser-Hay reaction.

The first mechanism was proposed by J. V. Barth and others. In their publication the authors presented the homocoupling reaction of alkynes in UHV conditions on silver surface without using an external catalyst, with hydrogen as the only side product. They obtained several final chemical structures, depending on the starting monomers (Figure 1.14 and Figure 1.15)[17].

The authors calculated by DFT the energy barriers corresponding to initial, transition, intermediate and final state, and they suggested a mechanism by π-complexation of the alkyne with the metal surface (Figure 1.13 a and b). The two molecules approached and reacted in order to form a intermediate dimer stabilized *via* π-complexation. Then, dehydrogenation afforded the final molecule.

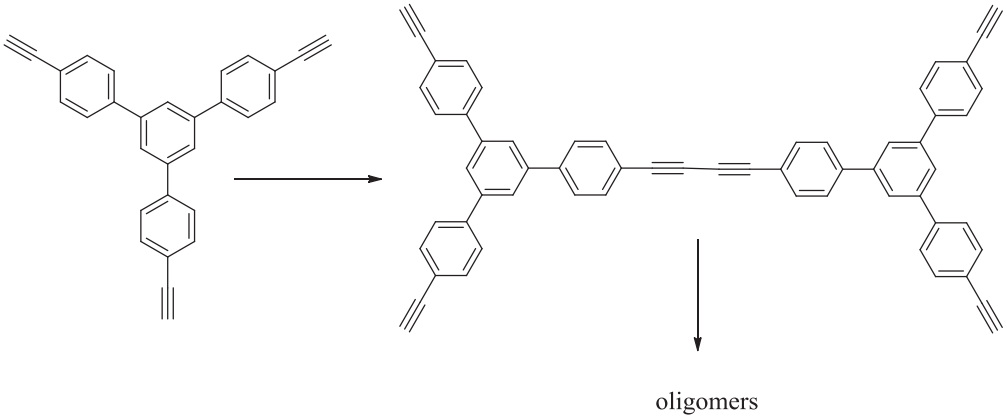

Figure 1.14 Glaser-Hay reaction on metal surface, readapted from ref.[17].

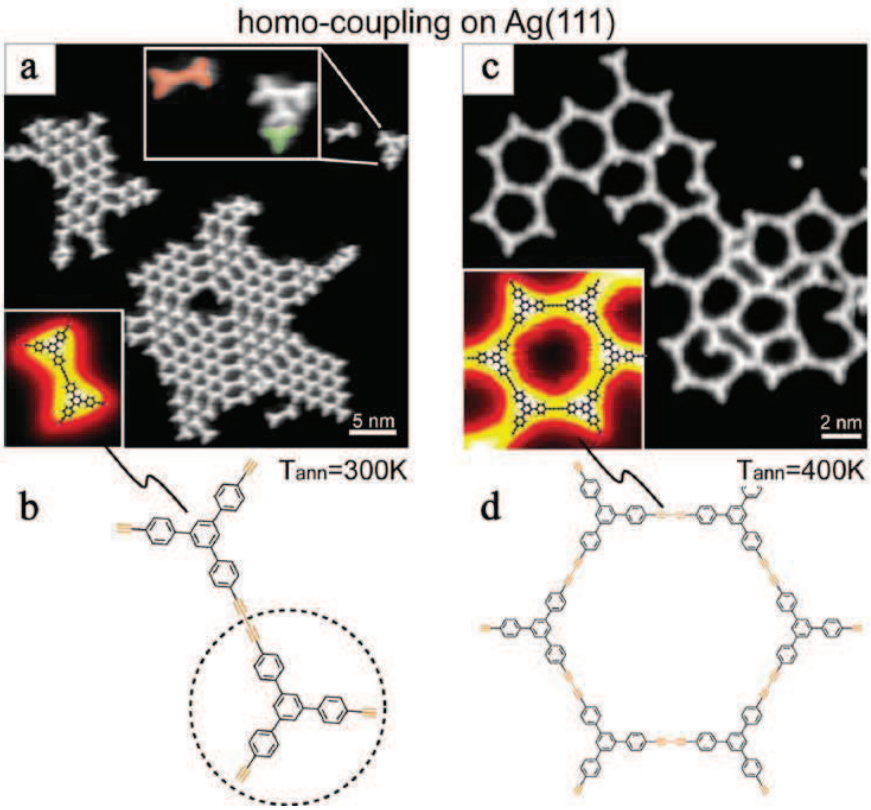

Figure 1.15 a-d) Homo-coupling on Ag (111) surface. Annealing at 300 K (a-b) led to dimer, while annealing at 400 k (c-d) to oligomers. From ref.[16].

However, this mechanism has been criticized mainly on its lack of clarity on its intermediate dimer. Additionally, the DFT is a method with several adjustable parameters so that the calculated energy barriers are questionable.

On the other hand, H. Fuchs and coworkers proposed a different mechanism similar to Ullmann coupling by oxidative addition, coalescence and reductive elimination (Figure 1.13 c). They reported the Glaser coupling of arylalkyne and bisethynylarenes on different metal

surfaces in UHV conditions (Figure 1.16 a and b)[18]. The molecules deposited were studied by STM and the reactions were found more efficient on Ag(111) surface than Au(111) or Cu(111)[18].

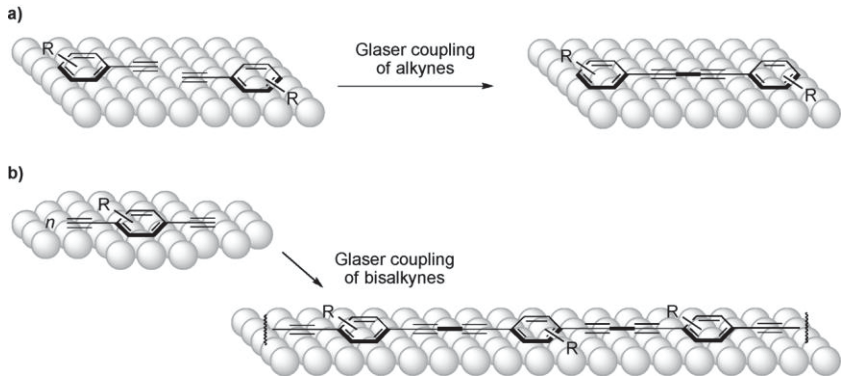

Figure 1.16 a) Glaser coupling of alkynes. b) Glaser coupling of bisalkynes[18]. The mechanism is similar to Ullmann coupling by oxidative addition, coalescence and reductive elimination.

In this paper the authors stated that annealing monomers on surface leads to a molecule-metal intermediate, which gives the Glaser product by reductive coupling. The surface, they stated, gives the support to the molecules for adsorption and orientation. The authors, differently from Barth's mechanism, speculate that the metal takes part in the reaction by cleavage of C-H bond.

Even this second approach has been criticized: the authors obtained alkyne chains but also trimers (those products cannot be explained with this approach, but with Barth's mechanistic model).

We can conclude that to date, the reaction pathway cannot be explained with only one of the two suggested mechanism. Further studies are necessary to deeper investigate the problem.

If we agree with Barth's mechanism for surface role (π-interaction and not oxidative interaction and reductive elimination), the results obtained in their paper might pave the way for the application of acetylenic coupling on non-catalystic surfaces in UHV conditions.

1.2.3 Polycondensation reaction

Another interesting reaction is the polycondensation of phthalocyanine in presence of metal such as Fe (Figure 1.17).

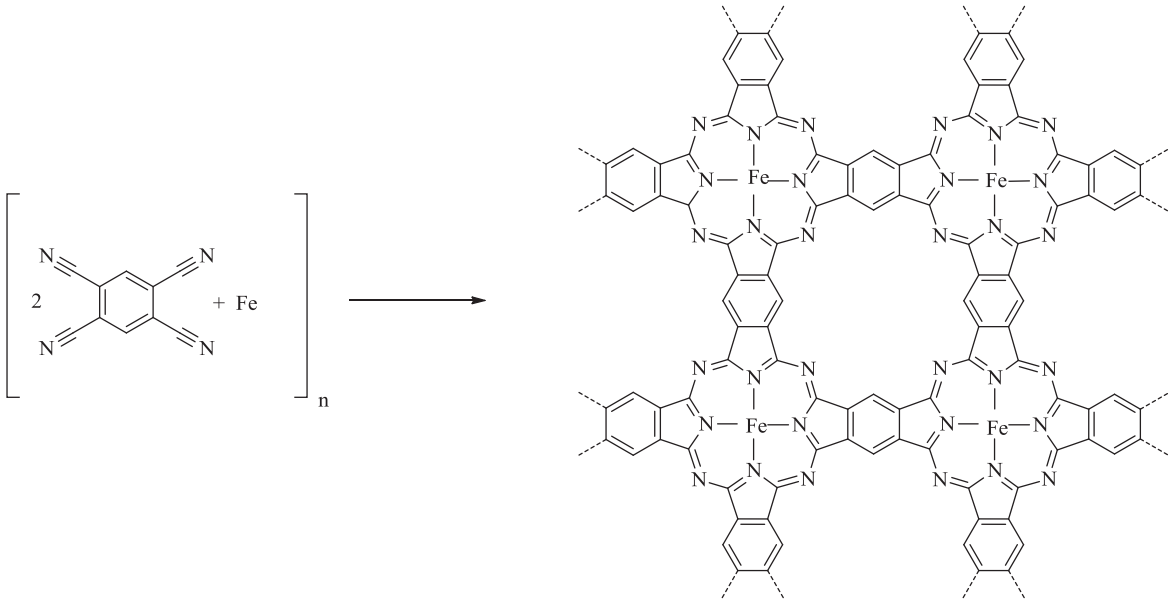

Figure 1.17 Polycondensation reaction of TCNB. Readapted from the ref.[19].

The reaction has been studied on metal surface in UHV conditions[19] (M. Abel and coworkers). In this experiment by co-evaporation of Fe and 1,2,3,4-tetracyanobenzene (TCNB), the authors obtained an organometallic polymer of phthalocyanine on Au (111) and Ag (111)[19] (Figure 1.18).

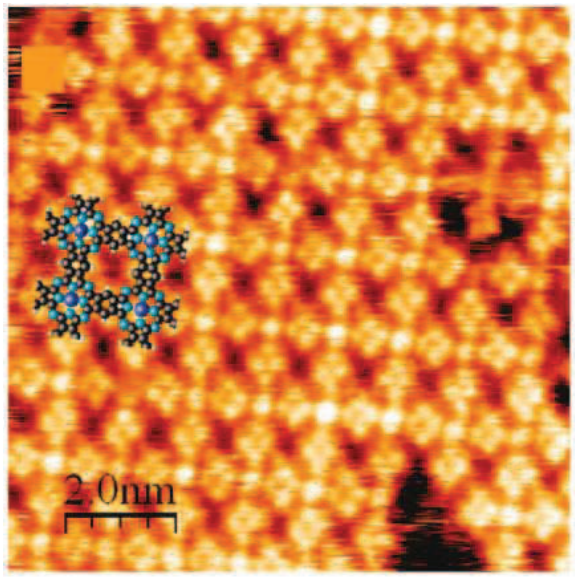

Figure 1.18 STM image of phthalocyanine network on Ag (111), from ref.[19].

In another paper, the same authors studied the on-surface synthesis in UHV conditions of (TCNB) and Mn atoms on metal Ag (111) surface.

At room temperature the deposition of the starting molecule (TCNB) and Mn atoms on surface led to the formation of Mn atoms and TCNB metallic-organic network (as shown in Figure 1.19 a).

By heating at 415 K the authors observed the formation of $MnPc(CN)_8$ in two domains: either self-assembled by hydrogen bonded (Figure 1.19 b) or metal-ligand coordinated (Figure 1.19 c).

Additional heating at 615 K, led to a polymeric network[20] (Figure 1.19 d).

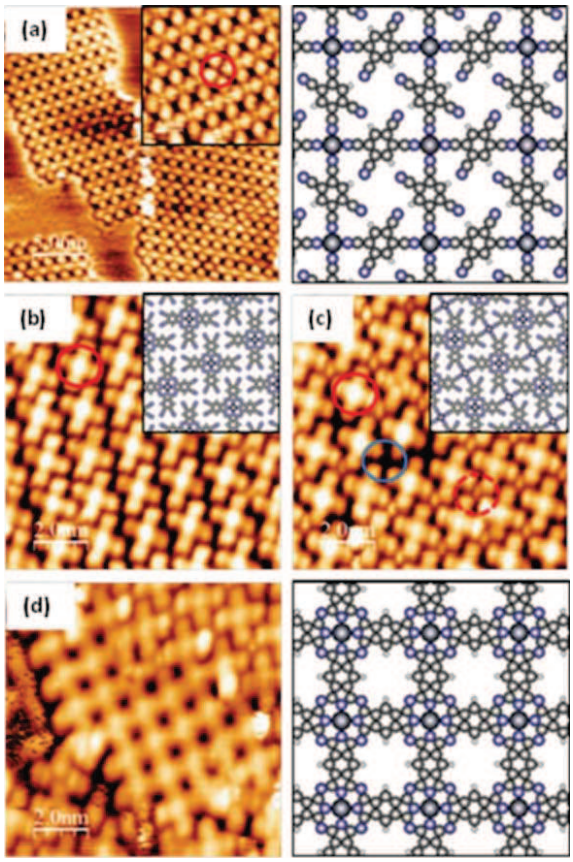

Figure 1.19 a) STM images of metal-organic framework at room temperature and its DFT model; b) STM images of $MnPC(CN)_8$ molecules and its DFT models (the circle indicates a Mn atom covalently bonded); c) STM images of metal-organized $MnPC(CN)_8$ molecules and Mn atoms (the circle in red solid line indicates a Mn atom covalently bonded; in blue solid line indicates a missing Mn atom and in red dashed lines a Mn-coordinated atom); d) STM image of bidimentional Mn phthalocyanine organometallic polymer and its DFT model. Adapted from ref.[20].

1.2.4 Summary of reactions on metal surfaces

Without getting into details for all the reactions, we briefly summarize in the following table the most important examples in literature.

Reaction name	Substrate
Ullmann coupling	Cu[21], Ag[22], Au[8] and others
Glaser coupling	Cu[23], Ag[17], Au[18]
Bergman cyclization	Cu[24], Ag[25]
Huisgen cycloaddition	Cu[26], Au[27]
Scholl reaction	Cu[28], Au[10], Pt[29], Ru[30] and others
Ring-opening polymerization	Cu[31]
Condensation reaction	Cu[32], Ag[33], Au[34]
[2+2+2] cycloaddition	Au[35]
[2+2] cycloaddition	Au[36]

Table 1.1 Selection of on-surface reactions in UHV conditions, readapted from ref.[6].

1.2.5 Example of molecular devices obtained by coupling on metal surface

The synthesis on metal surface in UHV allows carrying out experiments in ultra-clean conditions on single molecule impossible to synthesize in solution. For instance L. Grill, C. Joachim and others measured for the first time the conductance of a single molecule in function of its length (2009)[37].

First, the authors sublimated on Au (111) surface dibromoterfluorene (DBTF) molecules. Then, annealing at 520 K led to C-Br bond breaking and consequently to the formation of a covalent bond to form polyfluorenes molecules (left in Figure 1.20) of above 100 nm length. Those molecules are impossible to obtain in solution due to their low solubility.

The authors demonstrated the covalent linking of the monomers by lifting up the chain with the STM tip and they measured its electrical properties (conductance). In this experiment part of the molecule is between two electrodes (tip and metal surface), so that at every tip position, the measurement of the current gives the conductance. By varying the tip height (Figure 1.20 a-c) the length of the molecule between the two electrodes changes, therefore is it possible to measure the variation of conductance in function of the length of a single molecule.

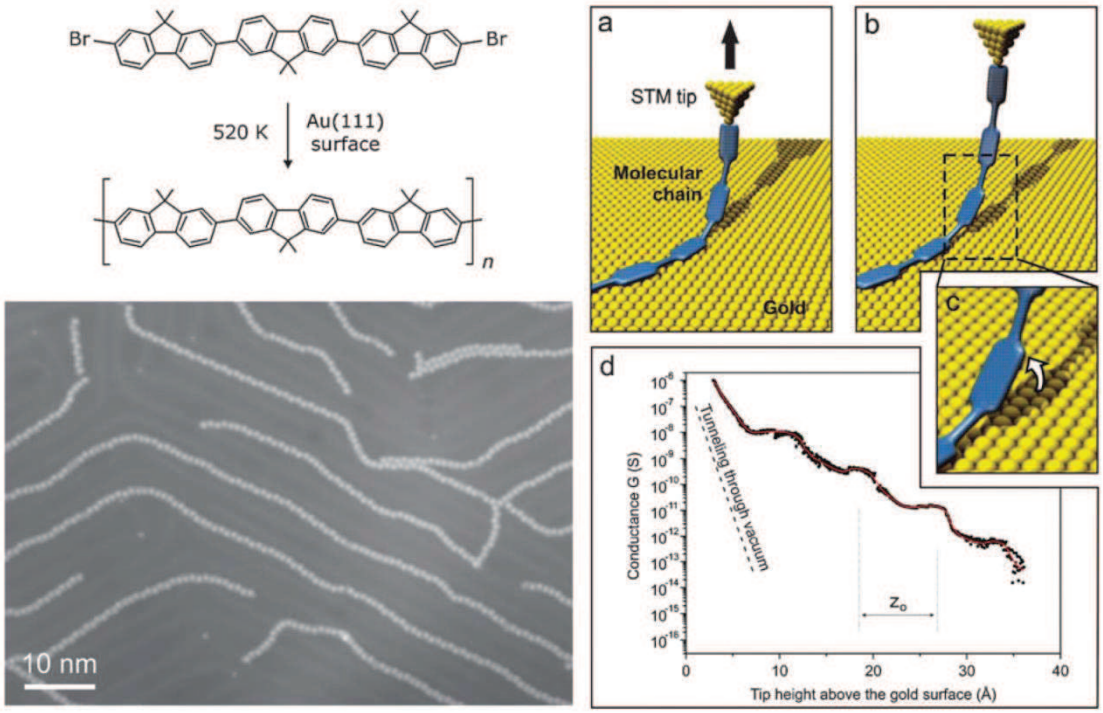

Figure 1.20 Left: synthesis of polyconjugated molecule on Au(111) surface; a-c) scheme of the lifting by STM tip and conductance measured (d). From ref.[4].

1.3 Coupling reactions on insulating surfaces

In this paragraph we present the recent state-of-art of coupling reactions focused on insulating substrates. Up to now, coupling reactions on insulating surfaces remains less investigated field. The main problem, in this case, is the weak molecule/surface interaction: the molecules tent to desorb easily or to form 3D clusters. Additionally the surfaces do not take part to the reaction (as catalyst) as the metal surfaces.

Type of interaction	Typical energy kJ/mol*	Interacting species
ion-ion	250	ions only
ion-dipole	15	ions and polar molecules
dipole-dipole	2	stationary polar molecules
	0.3	rotating polar molecules
London (dispersion)	2	all the types of molecules
hydrogen bonding	20	N,O,F; the link is a shared H atoms

Table 1.2 Type of interactions, from ref.[38]. (*Typical strength are for distance of 500 pm).

1.3.1 Coupling reaction on NaCl thin film

M. Abel and coworkers synthesized for the first time a bidimentional network of phthalocyanine on NaCl film supported by metal surface (Ag 100)[19] (reaction showed in Figure 1.17). In this work, they prepared a surface of monoatomic NaCl on Ag at room temperature in UHV conditions. First, they evaporated the precursor molecule TCNB from a crucible and successively Fe using an electron-beam heating evaporator. Then, phthalocyanines formed polymeric phase over the insulating layer. Attempts to repeat this experiment on bulk NaCl surface led to the formation of clusters of TCNB molecules (private communication of the authors).

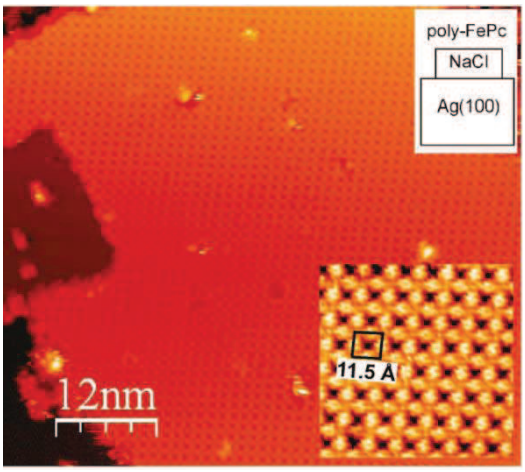

Figure 1.21 Phthalocyanine polymeric phase over NaCl on Ag (100), from ref.[19].

1.3.2 Coupling reaction on TiO_2

In a recent paper, M. Szymonski and others achieved the polymerization of polyanthrylene on TiO_2 surface[39].

The authors deposited the precursor molecule 10,10'-dibromo-9,9'-bianthryl (DBBA, Figure 1.22 a) by sublimation at 135 °C on TiO_2 surface in UHV heated at ~270-300 °C. They obtained randomly distributed oligomers (Figure 1.22 b) by coupling of bianthryl precursor molecules as already demonstrated on metal surface (first step of the reaction represented in Figure 1.7).

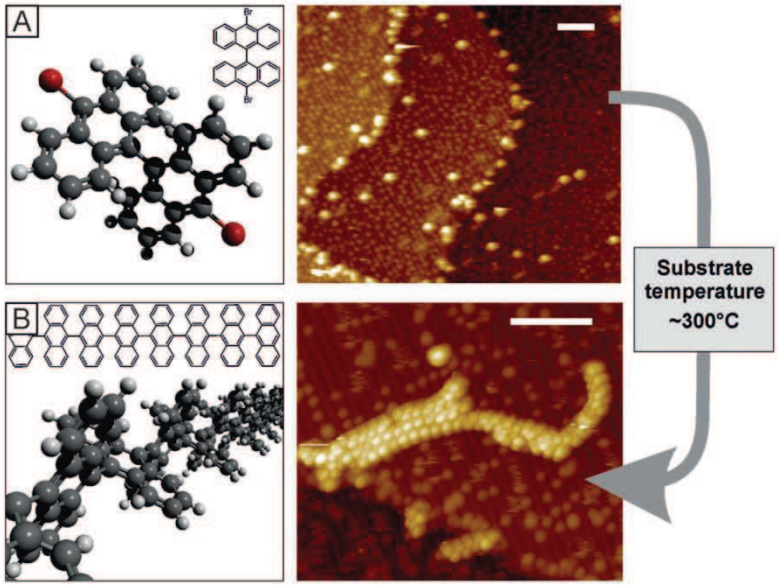

Figure 1.22 Polymerization of DBBA precursor molecule on TiO_2 surface in UHV (scale bars 5 nm). From ref.[39].

As reported previously, on metallic surface heating the polyanthryl at 400 °C led to cyclodehydrogenation and consequently to a graphene nanoribbon (step 2 in the reaction in Figure 1.7). For this reason, the authors tried the same reaction on TiO_2. However in this case, heating up to 450 °C did not afford the graphene nanoribbon and only polyanthrylenes were recovered on the surface.

They concluded that although covalent coupling of starting monomer easily afforded oligomers, cyclodehydrogenation was not observed on TiO_2 in these conditions.

1.3.3 Coupling reactions on calcite

Investigations on insulating surface have been carried out on calcite by A. Kühnle's group (University of Mainz, Germany) and Nanoscience group (CNRS Toulouse, France).

Calcite, the most stable polymorph of calcium carbonate, is an insulator with 6.0 eV band gap and can be easily cleaved (natural cleavage plane 104) in UHV conditions.

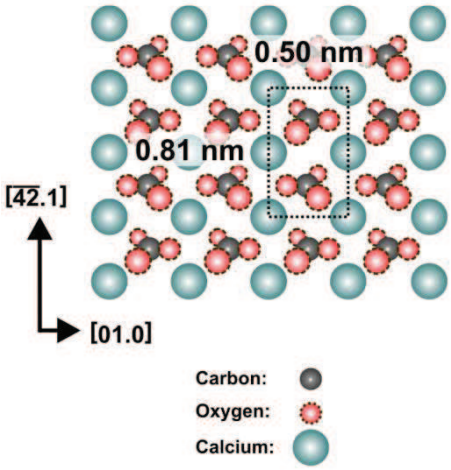

Figure 1.23 Calcite crystal structure, readapted from the reference: Springer book, in the press.

Working with this substrate, A. Kühnle's and A. Gourdon's groups proposed the use of electrostatic interaction to fix the molecules on the surface. They suggested the use of carboxylic groups as anchoring groups[40].

In a first approach the authors induced the reaction *via* thermal activation and they studied for the first time the "Ullmann" coupling on calcite in UHV conditions. The two groups investigated several benzoic acid derivatives in which the carboxylic acid is the anchoring group and the halogen group the leaving group.

In all those cases, a first step of deprotonation is necessary in order to anchor the molecule on the surface (through the interaction between the carboxylate and Ca^{2+}). Therefore, depending from the pK_a of the carboxylic acid derivative, this deprotonation step might be spontaneous or needs an annealing step[40–42]. In particularly the molecules with pK_a (calculated) equal or smaller than 3, are deprotonated on the surface (the process can be followed *via* nc-AFM) at RT or below. Molecules with pK_a higher than 3 require a further annealing step (Springer book, in the press).

The proposed mechanism for the coupling reaction is depicted in Figure 1.24. Once the precursor molecule is sublimated and deprotonated on the surface, the presence of carboxylate group is expected to weaken the phenyl-halide bond, therefore favors homolytic cleavage. The reactive phenyl species react at specific temperatures (at ~520 K, depending from the sample) without the need of catalysts in order to form the coupling product. The mechanism suggested proceeds *via* "radical" reaction (Figure 1.24).

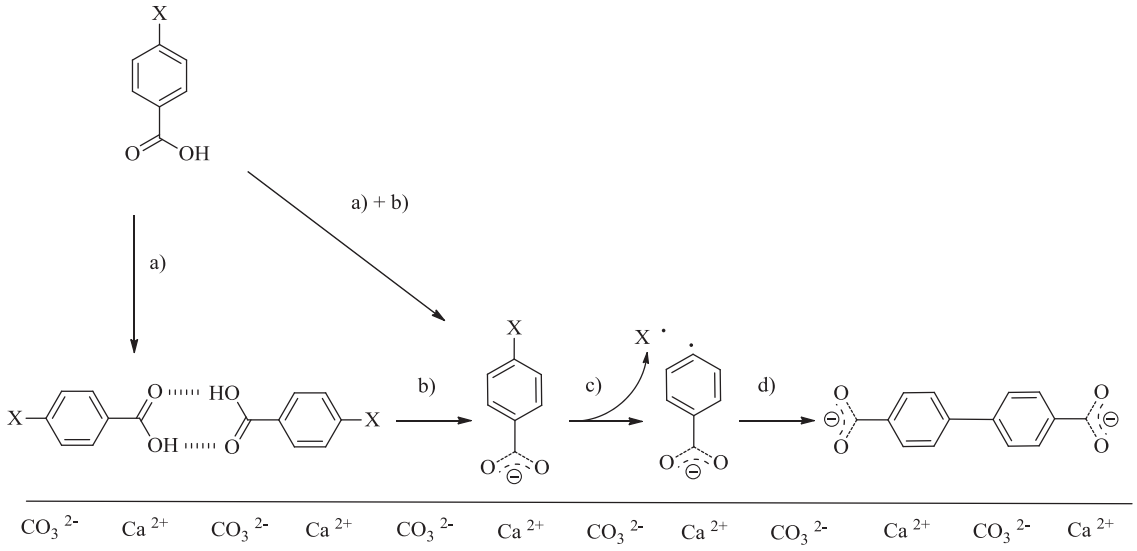

Figure 1.24 Mechanism proposed for 4-halobenzoic acid reaction on calcite in UHV. Steps: a) sublimation; b) deprotonation; c) homolytic cleavage and d) coupling.

In a first paper the authors described the deposition of 4-iodobenzoic acid on calcite[40]. The precursor molecule was sublimated on cleaved calcite in UHV conditions, and at room temperature, formed islands with apparent height of 0.5 nm. Due to their highly mobility, the molecules were observed at RT only if confined for instance in surface troughs (Figure 1.25 a).

However, after a first annealing step at 520 K the structure changed and the domains had an apparent height of 0.8 nm (Figure 1.25 b). The authors suggested that the precursor molecules passed from a lying to an upright-standing conformation due to the deprotonation step (*p*Ka of 4-iodobenzoic acid = 4.02).

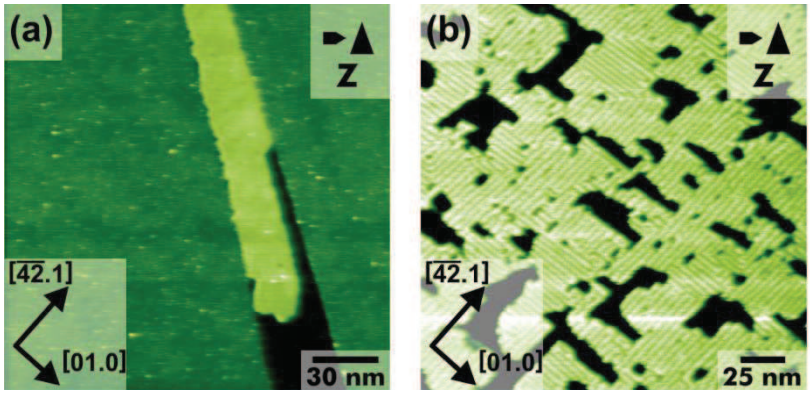

Figure 1.25 a) Deposition of 4-iodobenzoic acid on calcite at room temperature. Due to their mobility, the molecules are observable only when lying in surface troughs; b) after a first annealing step at 520 K the deprotonation step changed the self-assembly. Figure readapted from Springer book (in the press).

A second annealing step at 580 K revealed a different structure (rows) with apparent high of 0.4 nm (Figure 1.26). The authors suggested that the second annealing afforded 4,4'-biphenyldicarboxylic acid molecules on calcite.

This assignment was confirmed by the deposition of the dimer (biphenyl-4,4'-dicarboxylic acid) directly on the surface[40]. The latter, once deposited, resulted in two structures: side-by-side (same result obtained by the reaction of 4-iodobenzoic acid) and head-to-tail type. In fact when biphenyl-4,4'-dicarboxylic acid is sublimated on the surface is not deprotonated as 4-iodobenzoic, therefore it could form either hydrogen-bonded (head-to-tail) or side-by-side structures Springer book (in the press).

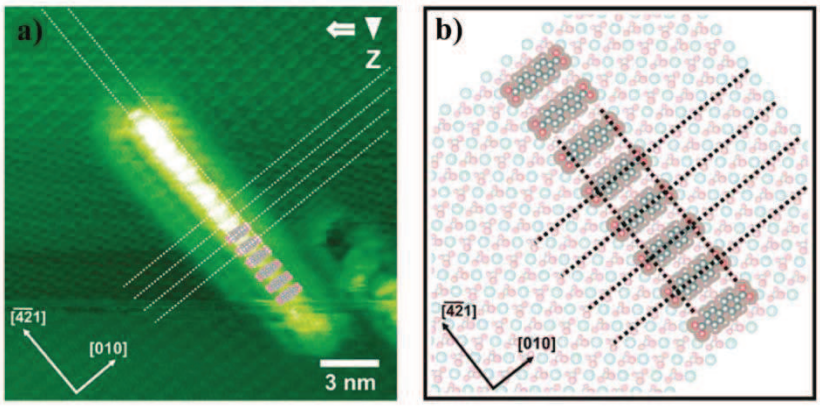

Figure 1.26 a-b) 4,4'-biphenyldicarboxylic acid after annealing at 580 K (nc-AFM image and model). Readapted from ref.[40].

Another remarkable example proposed by the same groups concerns the 3,5-diiodosalicylic acid. In this case the molecule has a *p*Ka of 2.07, so once deposited on the surface, is already deprotonated at room temperature (apparent height of 0.6 nm). Annealing at 580 K led to a flat-lying (apparent high 0.35 nm) zigzag structure, as shown in figures below[40] (Figure 1.27 and Figure 1.28).

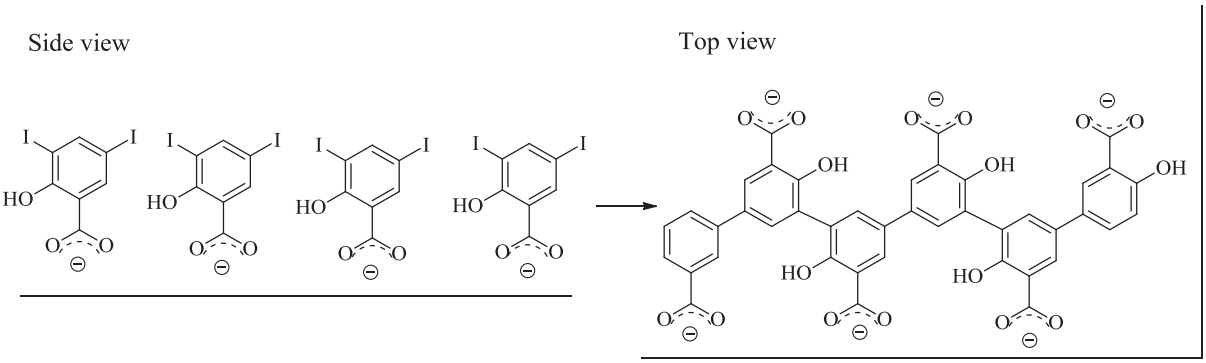

Figure 1.27 Mechanism proposed for the coupling reaction of 3,5-diiodosalicylic acid.

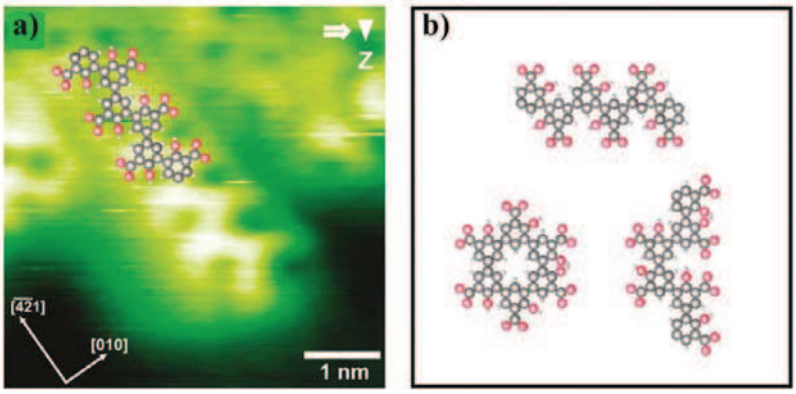

Figure 1.28 a) Zigzag structure due to the covalent coupling of 3,5-diiodosalicylic acid after annealing at 580 K; b) model of different observed structures obtained from this molecule, readapted from ref.[40].

From those examples we deduce that the shape of the final coupling product could be controlled by varying the position of the reactive halide groups[6].

Depending of the phenyl-halide bond strength, the cleavage temperature expected to increase in the order iodine, bromine, chlorine (bond energies: 268, 336 and 399 kJ/mol respectively).

Having this data in mind the same groups carried out a two-step sequential activation by using as starting monomer a molecule including two different halogen atoms (bromine and chlorine)[42]. The precursor 2-(4-bromophenyl)-6-(4-chlorophenyl)pyridine-4-carboxylic acid (named as BPCPPCA), in depicted in the figure below.

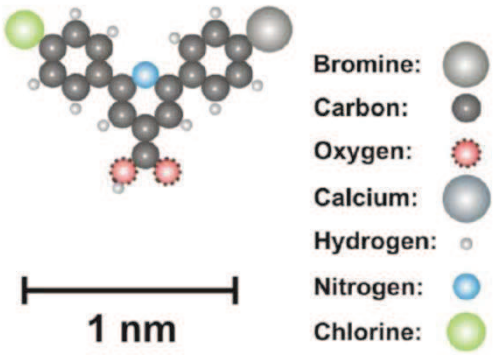

Figure 1.29 Precursor molecule 2-(4-bromophenyl)-6-(4-chlorophenyl)pyridine-4-carboxylic acid (BPCPPCA), from ref.[42].

Once the molecules were deposited on the surface at room temperature, the authors observed two different types of islands with a mirror symmetry axis. In fact the molecules could form a (2x4) superstructure on the calcite surface in two mirror-symmetric ways (Figure 1.30 a).

Figure 1.31 a-b shows in detail the two islands A and B. The authors suggested a tilted conformation of the deprotonated molecules on calcite (*p*Ka of BPCPPCA =3.5).

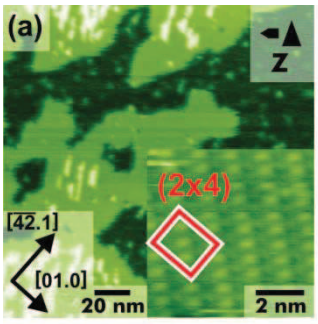

Figure 1.30 a) Deposition of BPCPPCA precursor molecules on calcite at room temperature and detail of (2x4) superstructure. Readapted from[6,42] and Springer book, in the press.

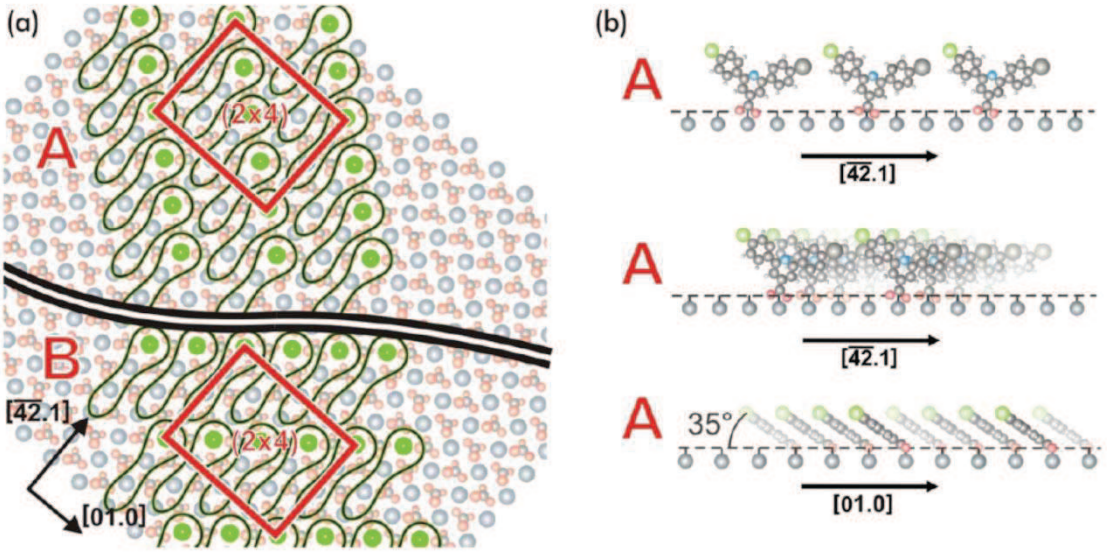

Figure 1.31 a) Suggested model for molecules arrangements (islands A and B) after deposition on calcite. The ellipses correspond to the molecules size. b) Side view of the proposed model: the molecules are anchored on the surface (*via* electrostatic interactions of the carboxylate moiety) and tilted. The island A and B are mirror images. From ref.[42].

Annealing at 570 K changed the self-assembly from islands to row-like type (Figure 1.32 b). The authors suggested a homolytic cleavage reaction of phenyl-bromine bond and consequent coupling of the intermediate molecules. The dimers obtained have two possible arrangements: “S” type or “U” type (Figure 1.33).

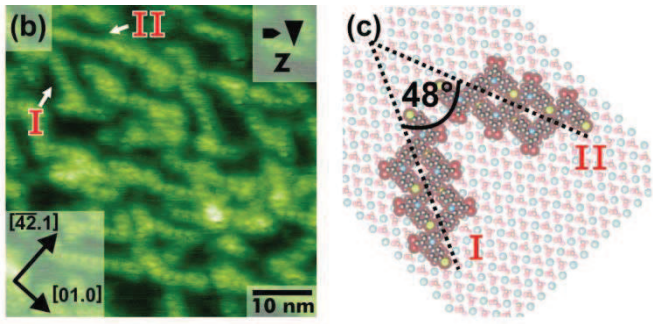

Figure 1.32 b) after annealing at 570 K row-like features are observed on the surface with an opening angle of 48°; c) model of the possible arrangement of the dimers. Readapted from[6,42] and Springer book, in the press.

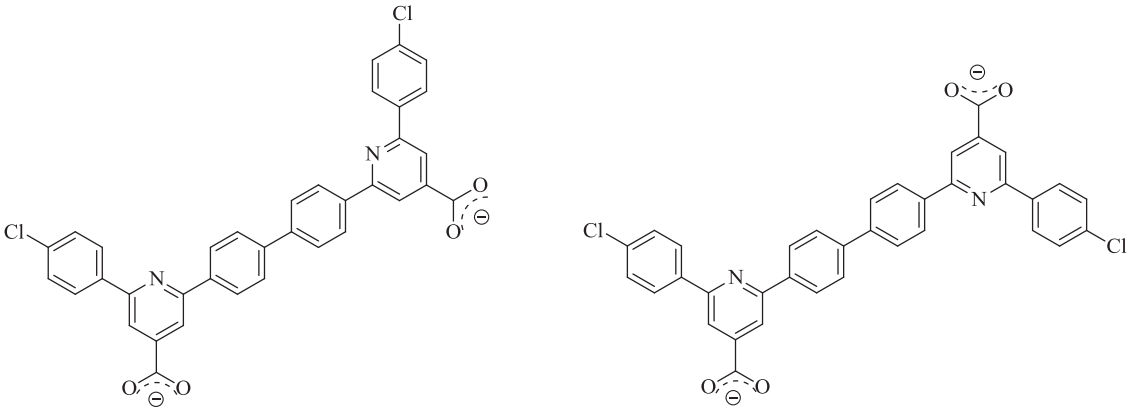

Figure 1.33 Two possible type of dimer.

When the "S" dimers are arranged side-by-side, the intermolecular interaction is higher. Having this in mind, only two directions are possible with an opening angle of about 48° (the model is showed in Figure 1.32 c).

Finally annealing at 610 K induced the coupling of the carbon atoms having the chlorine atoms, affording zigzag chain (Figure 1.34 d-e)[42] and small ring-like features (Figure 1.34 f).

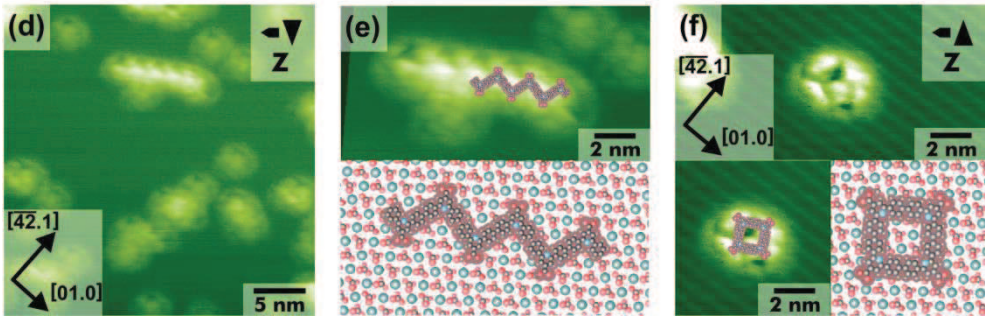

Figure 1.34 d) second annealing at 610 K changed the structures on the surface; e-f) detail and model of zigzag chain and ring features respectively. Readapted from[6,42] and Springer book, in the press.

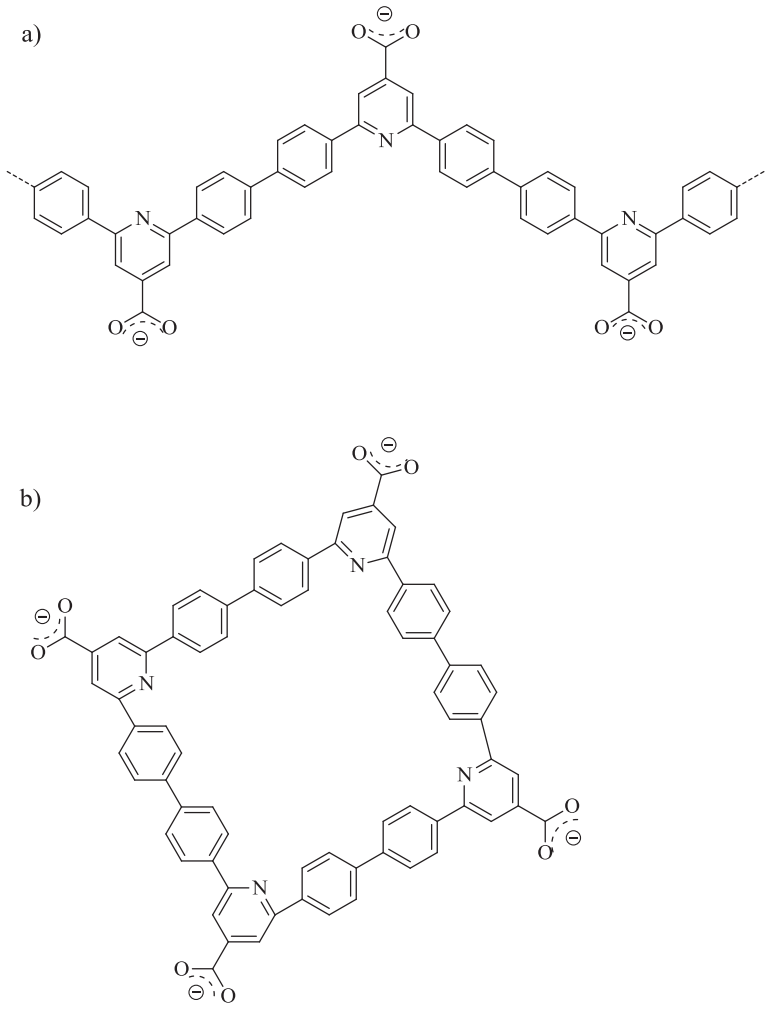

Figure 1.35 a) Zigzag and b) ring feature.

1.3.3.1 Photochemical activation on calcite

In all the previous examples, the reactions were induced by thermal activation: annealing the substrate led to the homolytic cleavage of phenyl-halide bond. However, recently the same groups moved from the thermal activation to the photochemical activation.

The advantage in this case is that it does not require high temperature, therefore the desorption of precursor molecules is limited.

As a first example, the authors selected C_{60} molecules, known to undergo to [2+2] cycloaddition under irradiation.

Once C_{60} molecules were deposited on calcite at room temperature, the authors observed the formation of large islands (Figure 1.36 a). C_{60} molecules arranged *via* van der Waals interactions. C_{60} diameters did not match with the substrate which led to the formation of a moiré pattern. Only the molecules (in red) marked with the black arrows in Figure 1.36 d matched perfectly with the correct site of adsorption on calcite substrate.

After irradiation (with a laser 405 nm), the assemblies started to degrade (Figure 1.36 b); successive irradiations drastically changed the features, and gaps (marked with arrows in Figure 1.36 c) became then visible. The authors suggested that after successive irradiations, the molecules were linked *via* covalent bond (shorter than van der Waals interaction), leading to the formation of islands and irregularities as depicted in the model (Figure 1.36 e)[43].

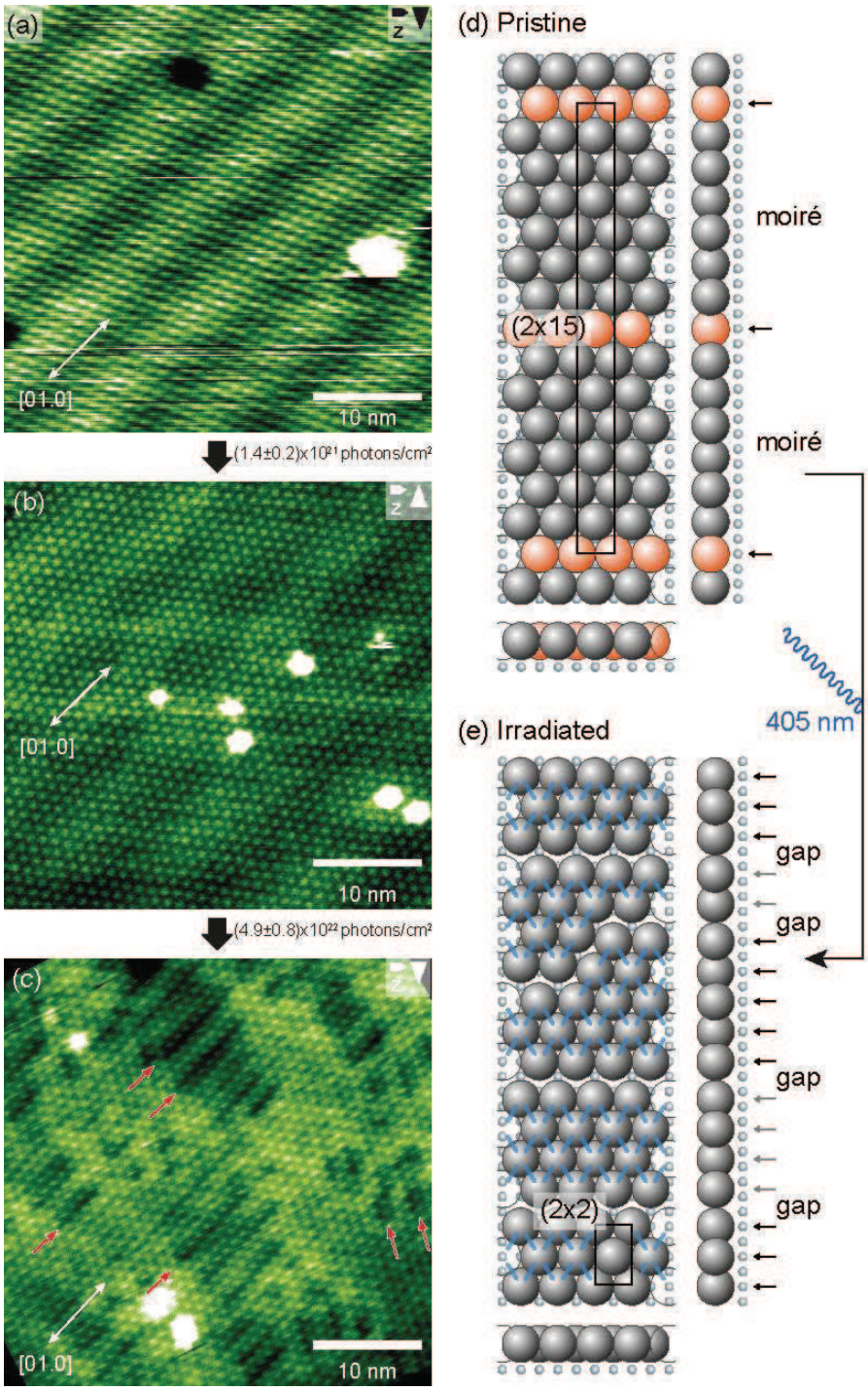

Figure 1.36 a) Model of pristine C_{60} adsorption; b) model of formation of covalent bond (marked in blue) after irradiation. The molecules with the same adsorption position are marked with either black or grey arrow. Readapted from the reference Springer book, in the press.

1.4 Limits

On-surface synthesis is a useful tool to obtain complex structures that, however, cannot be exported outside of the UHV environment for further analysis. Furthermore, the

spectroscopic techniques accessible on metal surface (XPS, ARPES) are not compatible with the insulating surfaces.

For these reasons we extended the investigation at macroscale level on particles in order to easily recover the final product and characterize with routine analysis.

1.5 References

1. Gourdon, A. On-Surface Covalent Coupling in Ultrahigh Vacuum. *Angew. Chem. Int. Ed.* **47,** 6950–6953 (2008).
2. Tait, S. L. Function Follows Form: Exploring Two-Dimensional Supramolecular Assembly at Surfaces. *ACS Nano* **2,** 617–621 (2008).
3. Lafferentz, L. *et al.* Controlling on-surface polymerization by hierarchical and substrate-directed growth. *Nat. Chem.* **4,** 215–220 (2012).
4. Franc, G. & Gourdon, A. Covalent networks through on-surface chemistry in ultra-high vacuum: state-of-the-art and recent developments. *Phys. Chem. Chem. Phys.* **13,** 14283 (2011).
5. Björk, J. & Hanke, F. Towards Design Rules for Covalent Nanostructures on Metal Surfaces. *Chem. – Eur. J.* **20,** 928–934 (2014).
6. Lindner, R. & Kühnle, A. On-Surface Reactions. *ChemPhysChem* **16,** 1582–1592 (2015).
7. Sambiagio, C., Marsden, S. P., Blacker, A. J. & McGowan, P. C. Copper catalysed Ullmann type chemistry: from mechanistic aspects to modern development. *Chem. Soc. Rev.* **43,** 3525 (2014).
8. Grill, L. *et al.* Nano-architectures by covalent assembly of molecular building blocks. *Nat. Nanotechnol.* **2,** 687–691 (2007).
9. Bieri, M. *et al.* Porous graphenes: two-dimensional polymer synthesis with atomic precision. *Chem. Commun.* 6919 (2009). doi:10.1039/b915190g
10. Cai, J. *et al.* Atomically precise bottom-up fabrication of graphene nanoribbons. *Nature* **466,** 470–473 (2010).
11. Kawai, S. *et al.* Atomically controlled substitutional boron-doping of graphene nanoribbons. *Nat. Commun.* **6,** 8098 (2015).
12. Cloke, R. R. *et al.* Site-Specific Substitutional Boron Doping of Semiconducting Armchair Graphene Nanoribbons. *J. Am. Chem. Soc.* **137,** 8872–8875 (2015).
13. Shen, Q. *et al.* Self-assembled two-dimensional nanoporous molecular arrays and photoinduced polymerization of 4-bromo-4′-hydroxybiphenyl on Ag(111). *J. Chem. Phys.* **142,** 101902 (2015).
14. Siemsen, P., Livingston, R. C. & Diederich, F. Acetylenic Coupling: A Powerful Tool in Molecular Construction. *Angew. Chem. Int. Ed.* **39,** 2632–2657 (2000).
15. Hay, A. S. Oxidative Coupling of Acetylenes. *J. Org. Chem.* **27,** 3320–3321 (1962).
16. Klappenberger, F. *et al.* On-Surface Synthesis of Carbon-Based Scaffolds and Nanomaterials Using Terminal Alkynes. *Acc. Chem. Res.* **48,** 2140–2150 (2015).
17. Zhang, Y.-Q. *et al.* Homo-coupling of terminal alkynes on a noble metal surface. *Nat. Commun.* **3,** 1286 (2012).
18. Gao, H.-Y. *et al.* Glaser Coupling at Metal Surfaces. *Angew. Chem. Int. Ed.* **52,** 4024–4028 (2013).
19. Abel, M., Clair, S., Ourdjini, O., Mossoyan, M. & Porte, L. Single Layer of Polymeric Fe-Phthalocyanine: An Organometallic Sheet on Metal and Thin Insulating Film. *J. Am. Chem. Soc.* **133,** 1203–1205 (2011).

20. Koudia, M. & Abel, M. Step-by-step on-surface synthesis: from manganese phthalocyanines to their polymeric form. *Chem. Commun.* **50,** 8565 (2014).
21. Hla, S.-W., Bartels, L., Meyer, G. & Rieder, K.-H. Inducing All Steps of a Chemical Reaction with the Scanning Tunneling Microscope Tip: Towards Single Molecule Engineering. *Phys. Rev. Lett.* **85,** 2777–2780 (2000).
22. Gutzler, R. *et al.* Ullmann-type coupling of brominated tetrathienoanthracene on copper and silver. *Nanoscale* **6,** 2660 (2014).
23. Eichhorn, J., Heckl, W. M. & Lackinger, M. On-surface polymerization of 1,4-diethynylbenzene on Cu(111). *Chem. Commun.* **49,** 2900 (2013).
24. Sun, Q. *et al.* On-Surface Formation of One-Dimensional Polyphenylene through Bergman Cyclization. *J. Am. Chem. Soc.* **135,** 8448–8451 (2013).
25. de Oteyza, D. G. *et al.* Direct Imaging of Covalent Bond Structure in Single-Molecule Chemical Reactions. *Science* **340,** 1434–1437 (2013).
26. Bebensee, F. *et al.* On-Surface Azide–Alkyne Cycloaddition on Cu(111): Does It 'Click' in Ultrahigh Vacuum? *J. Am. Chem. Soc.* **135,** 2136–2139 (2013).
27. Díaz Arado, O. *et al.* On-Surface Azide–Alkyne Cycloaddition on Au(111). *ACS Nano* **7,** 8509–8515 (2013).
28. In't Veld, M., Iavicoli, P., Haq, S., Amabilino, D. B. & Raval, R. Unique intermolecular reaction of simple porphyrins at a metal surface gives covalent nanostructures. *Chem. Commun.* 1536 (2008). doi:10.1039/b718865j
29. Otero, G. *et al.* Fullerenes from aromatic precursors by surface-catalysed cyclodehydrogenation. *Nature* **454,** 865–868 (2008).
30. Rim, K. T. *et al.* Forming Aromatic Hemispheres on Transition-Metal Surfaces. *Angew. Chem. Int. Ed.* **46,** 7891–7895 (2007).
31. Lin, Y.-P. *et al.* Self-Assembled Melamine Monolayer on Cu(111). *J. Phys. Chem. C* **117,** 9895–9902 (2013).
32. Clair, S., Abel, M. & Porte, L. Growth of boronic acid based two-dimensional covalent networks on a metal surface under ultrahigh vacuum. *Chem. Commun.* **50,** 9627 (2014).
33. Zwaneveld, N. A. A. *et al.* Organized Formation of 2D Extended Covalent Organic Frameworks at Surfaces. *J. Am. Chem. Soc.* **130,** 6678–6679 (2008).
34. Weigelt, S. *et al.* Covalent Interlinking of an Aldehyde and an Amine on a Au(111) Surface in Ultrahigh Vacuum. *Angew. Chem. Int. Ed.* **46,** 9227–9230 (2007).
35. Liu, J., Ruffieux, P., Feng, X., Müllen, K. & Fasel, R. Cyclotrimerization of arylalkynes on Au(111). *Chem. Commun.* **50,** 11200 (2014).
36. Fesser, P. *et al.* Visualizing the Product of a Formal Cycloaddition of 7,7,8,8-Tetracyano-p-quinodimethane (TCNQ) to an Acetylene-Appended Porphyrin by Scanning Tunneling Microscopy on Au(111). *Chem. - Eur. J.* **17,** 5246–5250 (2011).
37. Lafferentz, L. *et al.* Conductance of a Single Conjugated Polymer as a Continuous Function of Its Length. *Science* **323,** 1193–1197 (2009).
38. Atkins, P. W. & Beran, J. A. *General Chemistry*. (Scientific Americans Books).
39. Kolmer, M. *et al.* Polymerization of Polyanthrylene on a Titanium Dioxide (011)-(2×1) Surface. *Angew. Chem. Int. Ed.* **52,** 10300–10303 (2013).
40. Kittelmann, M. *et al.* On-Surface Covalent Linking of Organic Building Blocks on a Bulk Insulator. *ACS Nano* **5,** 8420–8425 (2011).
41. Kittelmann, M., Rahe, P., Gourdon, A. & Kühnle, A. Direct Visualization of Molecule Deprotonation on an Insulating Surface. *ACS Nano* **6,** 7406–7411 (2012).
42. Kittelmann, M., Nimmrich, M., Lindner, R., Gourdon, A. & Kühnle, A. Sequential and Site-Specific On-Surface Synthesis on a Bulk Insulator. *ACS Nano* **7,** 5614–5620 (2013).

43. Lindner, R. *et al.* Substrate Templating Guides the Photoinduced Reaction of C 60 on Calcite. *Angew. Chem. Int. Ed.* **53,** 7952–7955 (2014).

2. Molecules designed for covalent coupling on calcite in UHV conditions

2.1 Conception of molecules 36
2.2 Molecules for homocoupling of ethynes 37
2.2.1 Introduction and objective 37
2.2.2 Results and discussion 38
2.2.2.1 Retrosynthetic analysis 38
2.2.2.2 Synthesis 38
2.2.2.3 Deposition on $CaCO_3$ surface 40
2.2.3 Conclusion 43
2.3 Molecules for photopolymerization 43
2.3.1 Introduction and objective 43
2.3.2 Results and discussion 45
2.3.2.1 Retrosynthetic analysis 45
2.3.2.2 Synthesis 45
2.3.2.3 Characterization 48
2.3.2.4 Deposition on $CaCO_3$ surface 49
2.3.3 Conclusion 50
2.4 Molecules for polycondensation 50
2.4.1 Introduction and objective 50
2.4.2 Results and discussion 55
2.4.2.1 Synthesis 55
2.4.2.2 Characterization 58
2.4.3 Conclusion 59

2.5 Molecules for Ullmann Coupling 60
2.5.1 Introduction and objective 60
2.5.2 Results and discussion 60
2.5.2.1 Retrosynthetic analysis 60
2.5.2.2 Synthesis 61
2.5.2.3 Characterization 69
2.5.3 Conclusion 73
2.6 General conclusion 73
2.7 References 74

In this chapter we present the synthesis of four families of molecules designed for different reactions on $CaCO_3$ surface: homocoupling of ethynes, photopolymerization, polycondensation (phthalocyanine networks) and Ullmann reaction. The molecules were synthesized by standard organic routes.

Then, the molecules will be deposited on calcite in UHV conditions. During the redaction of this manuscript only the first two families were deposited. The others two families will be studied soon. The work was done by Prof. A. Kühnle's group (R. Lindner, A. Richter and others), University of Mainz, Germany.

2.1 Conception of molecules

As our molecules will be deposited on calcite in UHV conditions, we decided to adopt the same strategy of carboxylic acid anchoring groups. The design of the target molecule should take into account all the constraints due to the insulating material: the exigency of anchoring groups (due to the low interaction molecule-substrate) and the technique used in order to investigate the surface (nc-AFM). Therefore, the ideal molecule should have a central core (ideally visible or recognizable with the nc-AFM), arms with the anchoring groups (carboxylic acid) and some reactive groups.

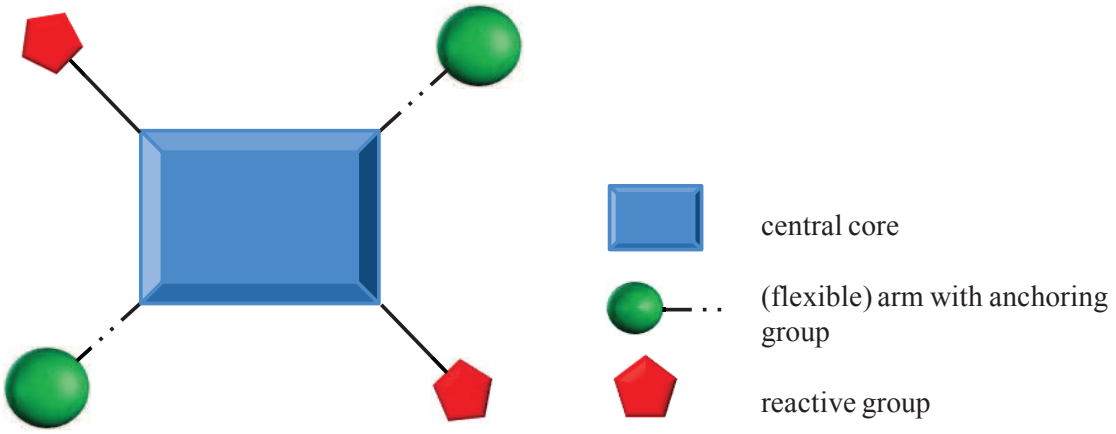

Figure 2.1 Scheme of the target molecule.

2.2 Molecules for homocoupling of ethynes

2.2.1 Introduction and objective

The objective of this section was the synthesis of molecules for homocoupling of ethynes. Many papers have been published on this family of molecules due to their high versatility. Acetylenic coupling, represents a powerful tool in order to obtain different scaffold materials using ethynes as building blocks. By molecular assembly, these compounds can form new molecular materials for different applications such as catalysis, molecular recognition and so on.

In this work we decided to investigate, for the first time, the Glaser-Hay reaction on insulating surface of $CaCO_3$. As already introduced previously, the mechanism of Glaser-Hay reaction on metallic surface is still well debated in the scientific community.

In this work the target molecule designed for homocoupling reaction is the 4-ethynyl benzoic acid **6** (Figure 2.2 b). In addition, the dimer **5** (Figure 2.2 a) was also synthesized in order to have a reference for nc-AFM.

a)

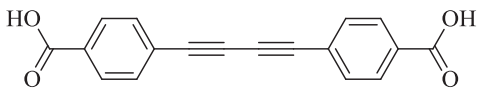

5

b)

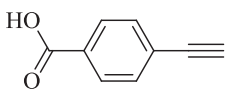

6

Figure 2.2 a) 4,4'-(buta-1,3-diyne-1,4-diyl)dibenzoic acid, product **5**. b) 4-ethynylbenzoic acid, product **6.**

The monomer 4-ethynylbenzoic acid (**6**) was chosen because it contains all the characteristics needed for the homocoupling of ethynes. In fact, while the triple bond moiety is involved in the coupling reaction, the carboxylic group, once deprotonated, is expected to

bind strongly calcite. As already introduced previously the anchoring groups assure the stability of the molecule on the surface. Once deposited, the monomer is expected to be upright standing on calcite.

The dimer 4,4'-(buta-1,3-diyne-1,4-diyl)dibenzoic acid (**5**) was synthesized in order to have a reference for the nc-AFM measurements. The homocoupling reaction product, the dimer, is expected to be flat lying on the surface, due to the carboxylate groups pointing in opposite directions.

This section describes the synthesis and the deposition of the molecules on $CaCO_3$ surface and it will conclude with future perspectives.

2.2.2 Results and discussion

2.2.2.1 Retrosynthetic analysis

From the retrosynthetic approach all the compounds were prepared from methyl esters in order to protect the acid moieties in the reaction conditions.

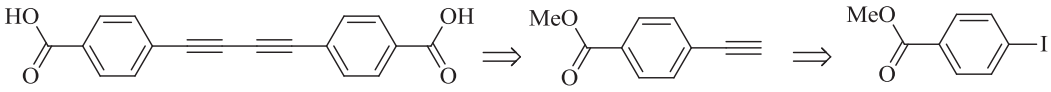

Figure 2.3 Retrosynthetic analysis.

2.2.2.2 Synthesis

The synthesis of the target molecules was carried out following procedures already reported in literature, as shown in the scheme:

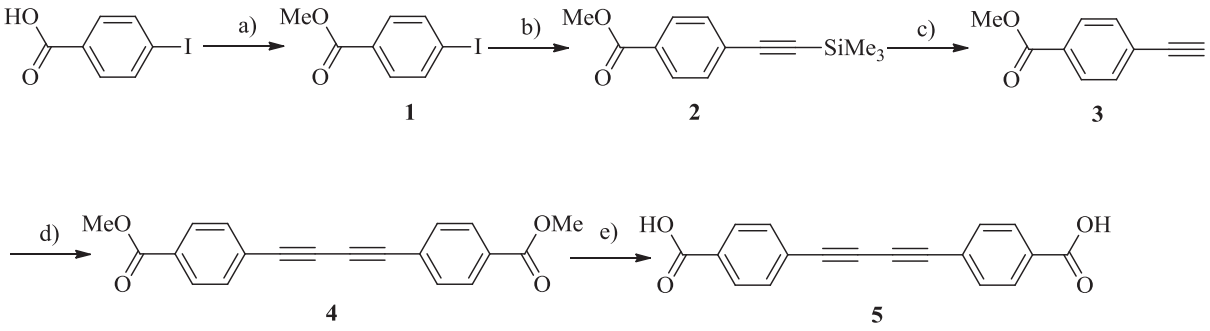

Figure 2.4 Synthesis of target molecule **5**. Conditions: a) MeOH, reflux, overnight, 81%; b) TMSA, $Pd(PPh_3)_3Cl_2$ (3%), CuI (5%), Et_3N, 25 °C, 2h, 94%; c) K_2CO_3, $MeOH/CH_2Cl_2$, 25 °C, 3h, 87% ; d) I_2, $Pd(PPh_3)_3Cl_2$ (2.5%), CuI (6.3%), $^iPr_2NH$, 25 °C, 6h, 81%; e) LiOH, THF, 25 °C, 5 days, 61%.

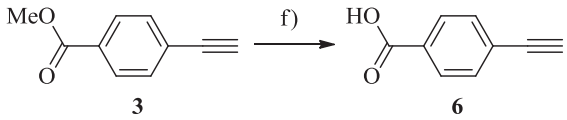

Figure 2.5 Synthesis of target molecule **6**. Conditions: f) LiOH, MeOH/H_2O, 25 °C, 5h, 42%.

Step a) to f)

Step a) The first step was a standard esterification[1] in order to protect the carboxylic group. 4-iodobenzoic acid was treated with methanol and sulfuric acid as catalyst at reflux for all the night. Standard work-up followed the reaction, with triethylamine (NEt_3) neutralization and extraction in order to obtain product **1** (81%).

Step b) In the following step the alkyne moiety (protected with trimethylsilyl) was introduced by Sonogashira cross coupling[2,3] on methyl *p*-iodo benzoate. The conditions employed were 3% $Pd(PPh_3)_2Cl_2$ and 5% CuI in triethylamine. The high reaction rate at room temperature (2h) and high yield (94%) can be justified by considering the activation by the benzoate function in *para* position.

Step c) The deprotection of trimethylsilyl group was obtained as reported in literature[2,4] by dissolving in a mixture of methanol:dichloromethane with potassium carbonate. Standard work-up affords the product **3** with 87% yield.

Step d) Product **4** was obtained in good yield (81%) by oxidative homo-coupling of product **3** using iodine, 2.5% of $Pd(PPh_3)_3Cl_2$ and 6.3% of CuI as catalyst in diisopropylamine ($^iPr_2NH$) at room temperature[5].

The acetylenic coupling has been deeply investigated during the last decades due to its high versatility (for instance cross coupling reactions such as Sonogashira). In this step palladium and copper were used as catalysts and iodine as oxidant following the wide literature on acetylenic coupling reactions[5–8] under these conditions. For these reactions, the absence of iodine lowers the yield at 20-30%, while the absence of one of the metal catalysts leads to mixtures of different side products[7].

Step e) Final deprotection of compound **4** was obtained in tetrahydrofuran (THF) at room temperature with lithium hydroxide in water followed by acidification with 3M HCl. The reaction was performed several times, changing different conditions, but it was not possible to obtain yields similar to the published ones[9]. The high polarity of the product let it difficult to follow the reaction *via* TLC.

Entry	Days	Temperature	Yield
Ref. lit. [9]	3	RT	89%
1	2	RT	21%
2	3	RT	47%
3	5	RT	61%
4	3	35 °C	30 %

Table 2.1 Experimental details for deprotection reaction. Each experiment was performed on average two times.

The reaction was performed, in a first experiment, in conditions similar to literature but the yield was drastically lower (entry 1 and 2 in Table 2.1). Then, the reaction time was increased and the work-up changed. In this way the yield was improved (entry 3). In this work-up the precipitation was performed in ice bath in order to optimize the precipitation process. Finally, the reaction was also performed by gently heating at 35 °C (entry 4) in order to increase the reaction rate. We did not get further for the optimization of this reaction because it was not the purpose of this work.

Once the dimer (molecule **5**) was synthetized, we focused on the single monomer (molecule **6**).

Step f) 4-ethynylbenzoic acid is commercially available. In this work it was synthesized as reported in literature[10]. 4-ethynylbenzoic in methanol:water solution was deprotected with lithium hydroxide followed by an acidification step (3M HCl). The final product was obtained with 42% yield. The spectra of product **6** are in agreement with the reference in the literature[10,11].

2.2.2.3 Deposition on $CaCO_3$ surface

The monomer **6** and the dimer **5** were deposited on calcite surface in UHV conditions by sublimation. The images were recorded at 10^{-9} mbar on a calcite crystal, previously cleaved.

Molecule **6** was sublimated for 2.5 minutes at 189 °C. From the recorded images (Figure 2.6) it can be assumed that the molecules form mainly double lines of five or six rows. The apparent height measured is 0.8 nm and periodicity of 0.5 nm. So it can be assumed that the molecules are probably upright standing.

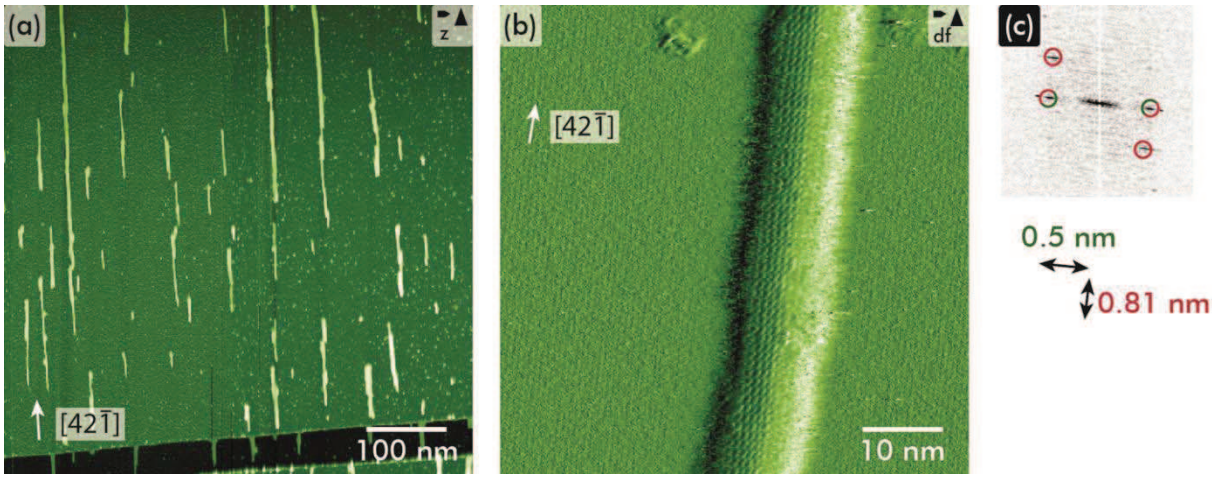

Figure 2.6 a) Deposition of monolayers of 4-ethynylbenzoic acid (**6**) on $CaCO_3$ (10.4) stripes along the [42$\bar{1}$] direction are observed. b) Molecular resolution reveals single molecules with an imaging height of 0.8 nm and periodicities of 0.5 nm and 0.81 nm, resulting in a (1x1) superstructure. This is also evident from the respective FFT (Fast Fourier Transform) (c).

The model below shows the orientation of the molecules on the surface.

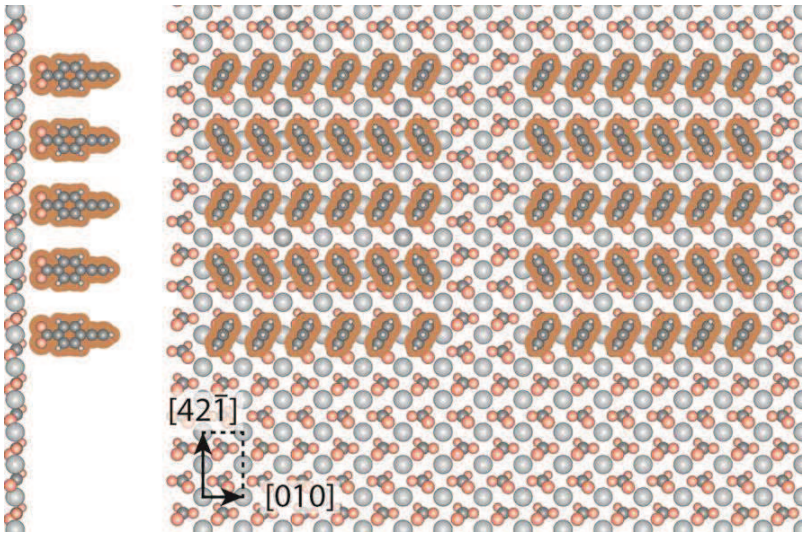

Figure 2.7 Adsorption model of 4-ethynylbenzoic acid (**6**), molecule on $CaCO_3$ (10.4).

The molecules occupy one calcite unit cell (dashed rectangle) each. Within one row, the molecules are tilted ±31° with respect to the [42$\bar{1}$] substrate direction. From the geometry we supposed the presence of at most five or six molecules. In fact the distance between the molecules does not correspond exactly to the lattice parameters, and the molecules are tilted due to the combination of different factors (van der Waals interactions between aromatic cores, steric repulsions).

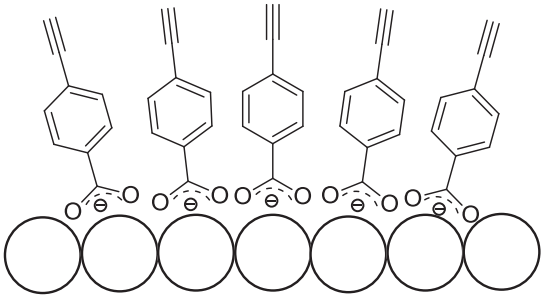

Figure 2.8 Illustration of tilted molecules on surface.

After sublimation onto the surface, the molecules were heated in order to induce the thermal coupling. Unfortunately no changes of the structures were observed. Therefore the sample was irradiated at 254 nm for 1h in order to photopolymerize the molecules. But also in this case, no structural changes were observed (Figure 2.9).

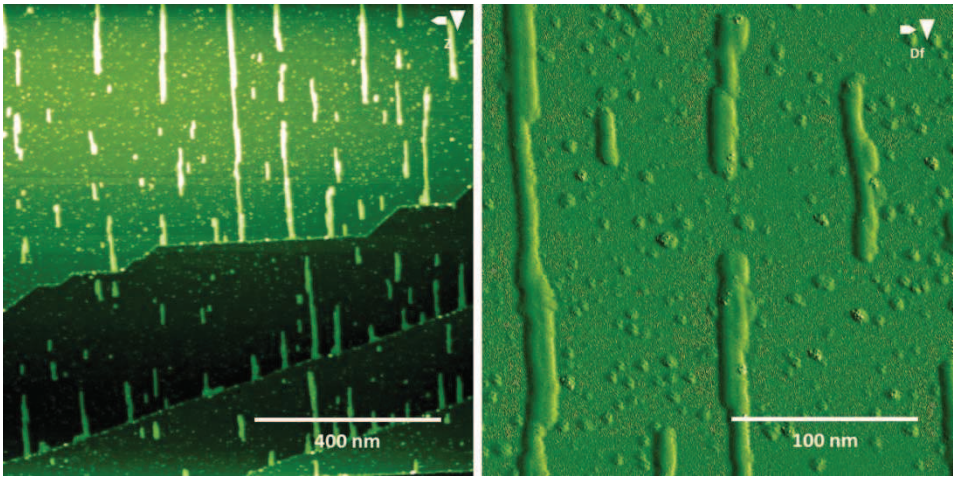

Figure 2.9 Picture of 4-ethynylbenzoic acid (**6**) on $CaCO_3$ after irradiation.

Molecule **5** was sublimated on the surface in order to have a reference for the coupling reaction. The product was sublimated for 5 minutes at 103 °C. It seemed to be flat lying on the surface and to form preferentially double rows as the monomer. The apparent height is 0.4 nm.

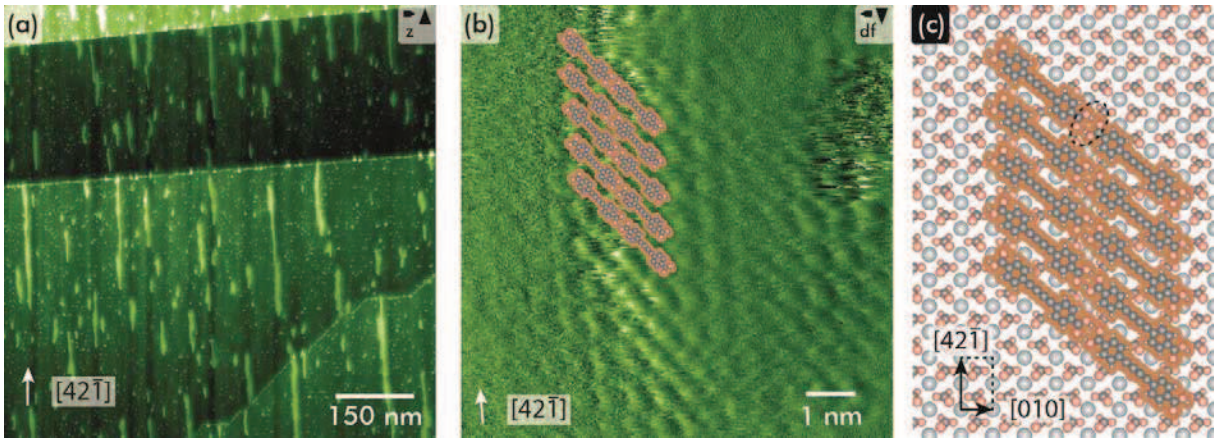

Figure 2.10 (a) Similar to 4-ethynylbenzoic acid (**6**), the 4-ethynylbenzoic acid dimer (**5**) forms stripes along[42$\bar{1}$]. (b) Molecular resolution reveals rows of molecules tilted by 50° with respect to [42$\bar{1}$] direction. (c) Adsorption model of 4-ethynylbenzoic acid dimer (**5**) on $CaCO_3$.

2.2.3 Conclusion

In this section we presented the synthesis of ethynes for homocoupling reaction on calcite. The molecules synthesized have been successfully deposited on insulating surface. The first preliminary tests of homocoupling did not afford the expected product on the surface. Further studies will be carried out in order to better investigate the reaction on $CaCO_3$ surface.

Polycarboxylic acids could be used as scaffold material for different structures, such as Metal Organic Frameworks (MOFs). Those, in particularly, has been widely studied during the last years for many applications (catalysis, gas storage or adsorption and so on)[12]. Molecule **5** has already been used as ligand for MOFs, as reported in some examples in literature[9,12–15]. With this objective the molecule was sent in Greece, to Dr. E. Manos' group in order to test it for new MOFs.

2.3 Molecules for photopolymerization

2.3.1 Introduction and objective

Photochemical reactions are the second field of reaction investigated in this work. As has been already discussed previously, one of the major advantage of these reactions is that they do not need high temperature to be activated, so the desorption and decomposition of starting monomer on the surface are less probable.

Having these results in mind, we decided to investigate the photopolymerization reaction on calcite. The precursor molecules chosen for this reaction are diacetylenes. Those

compounds are characterized by two bonds in conjugations. For many years they were the objective of intense study due their particular property of polymerization if excited by UV light, heating or exposure to some gases[16,17]. Once polymerized, diacetylenes form various organized structures such as single crystals, Langmuir-Blodgett films, self-assembled monolayers and so on[17]. Polydiacetylenes (PDAs) have interesting optical and electronic properties that make them an attractive field for many researches. Figure 2.11 represents one of the possible arrangements suggested for diacetylene polymerization.

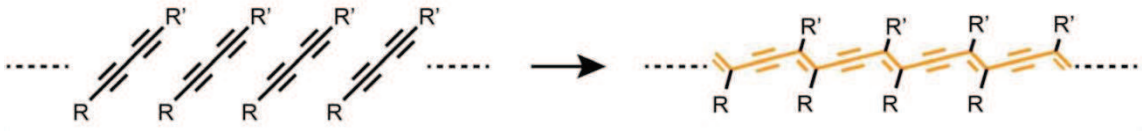

Figure 2.11 Polymerization reaction of diacetylene compounds from ref.[18].

Many papers have been written on the kinetics mechanism of the solid-state (crystalline) polymerization process[16]. In the case of thermal or photopolymerization, one of the possible the mechanism is showed in Figure 2.12. When energy of 1eV is supplied in the form of heating or UV irradiation, a TS dimer is formed. The latter can revert to the monomer or start the chain propagation.

Little is known about the chain termination event. It has been suggested a biradical structure for the dimer instead of dicarbene type[19]. The first, in fact, should have a lower energy because its formation requires disruption of only one carbon-carbon π-bond instead of two in the case of carbine formation[19].

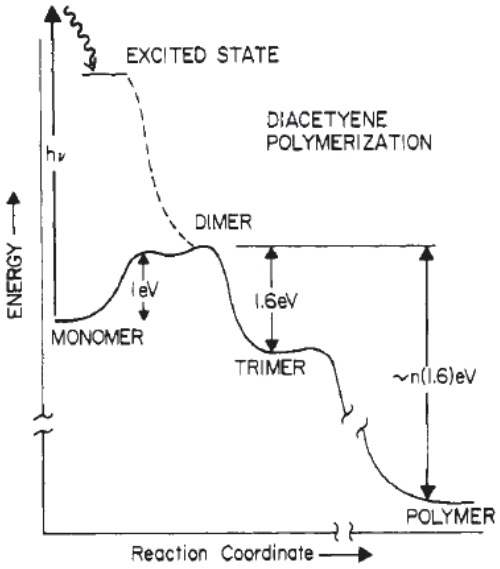

Figure 2.12 Energy reaction diagram of solid-state diacetylene polymerization from ref.[16].

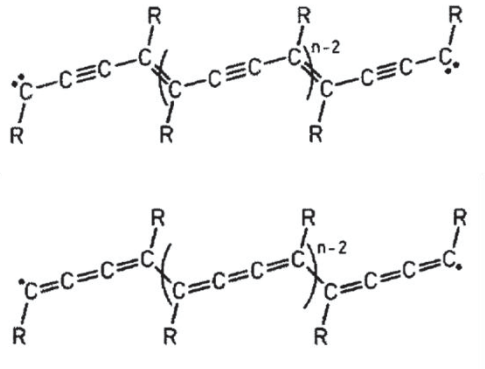

Figure 2.13 Dicarbene and diradical intermediate from ref. [19].

In this work the starting molecule envisaged for the photopolymerization is the 3,3'-(buta-1,3-diyne-1,4-diyl)dibenzoic acid (molecule **10)**. In fact, due to its conformation, the molecule should not lie flat on the surface and consequently more prone to polymerization. The monomer in *meta*-position (molecule **11**) was also synthesized in order to test it for homocoupling of ethynes.

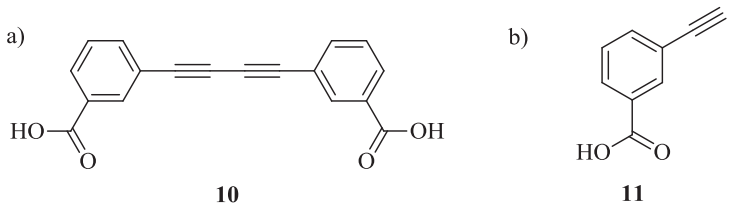

Figure 2.14 a) 3,3'-(buta-1,3-diyne-1,4-diyl)dibenzoic acid, product **10**. b) 3-ethynylbenzoic acid, product **11**.

2.3.2 Results and discussion

2.3.2.1 Retrosynthetic analysis

The molecules were synthesized from the corresponding esters.

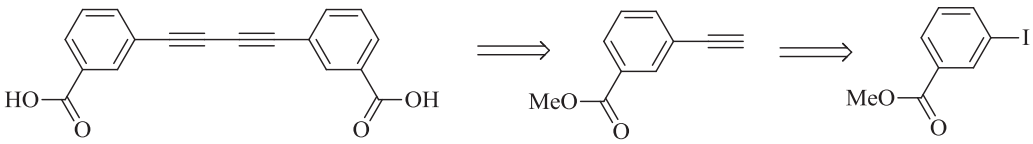

Figure 2.15 Retrosynthetic analysis.

2.3.2.2 Synthesis

The synthesis of the target molecules was carried out following procedures already reported in literature, as shown in Figure 2.16.

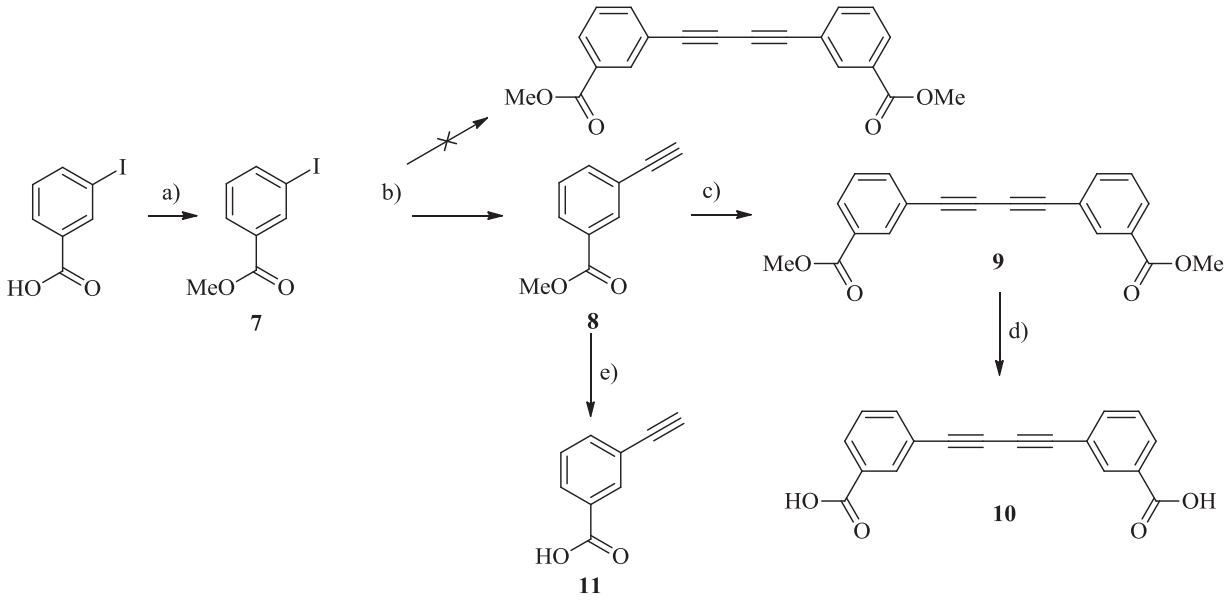

Figure 2.16 Synthesis of target molecules **10** and **11**. Conditions: a) MeOH, reflux, overnight, 89%; b) 1.TMSA, $Pd(PPh_3)_3Cl_2$ (2%), CuI (4%), THF, Et_3N, 25 °C, 3h; 2. TBAF, THF, molecular sieves 3 Å, air, 25 °C, overnight 64%; c) TMEDA (30%), CuCl (10 %), CH_2Cl_2, molecular sieves 3 Å, 2h, 91% ; d) LiOH, THF, 25 °C, overnight, 37%; e) LiOH, MeOH/H_2O, 25 °C, overnight, 54%.

Step a) to e)

Step a) The first step was a standard esterification[20] in order to protect the carboxylic group. 3-iodobenzoic acid was treated with methanol and sulfuric acid as catalyst at reflux for all the night. Standard work-up afforded product **7** with 89% yield.

Step b) The following step was a concatenating Sonogashira and Glaser coupling reaction in a one-pot sequence[21,22]. The methyl 3-iodobenzoate was treated with trimethylsilylacetylene (TMSA) under Sonogashira standard conditions (2% $Pd(PPh_3)_2Cl_2$, 4% CuI and triethylamine). The compound was let to react by monitoring *via* TLC for three hours at room temperature. Then tetra-*n*-butylammonium fluoride (TBAF) in tetrahydrofuran and molecular sieves (3Å) were added in order to remove the protecting group and the reaction mixture was stirred under air atmosphere (Glaser coupling reaction). The ideal salt for the deprotection was actually potassium fluoride (as reported in the procedure[22]), but in our case TBAF was used. The mechanistic sketch is reported in Figure 2.17.

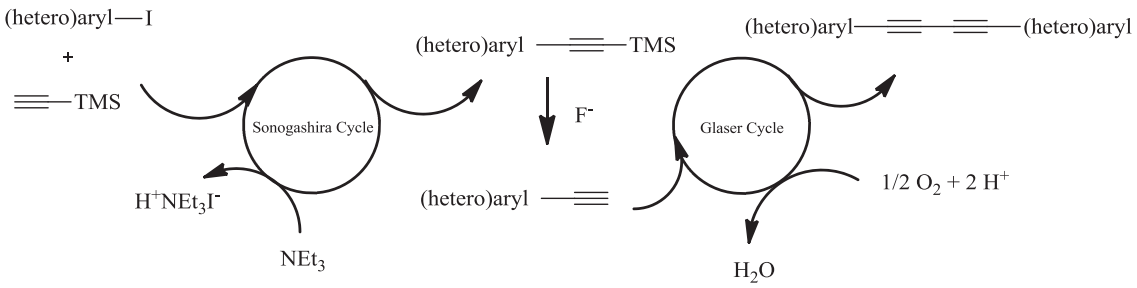

Figure 2.17 Mechanistic sketch of concatenate Sonogashira-Glaser coupling reaction from ref.[22].

In the same paper the authors show the influence of precatalysts in the Glaser-Hay coupling step. When the reactions are carried out without additives, palladium or copper catalysts, the yield of the Glaser cycle is drastically lower than the reaction obtained by the complete sequence. It has been thought that the ammonium iodide generated by the Sonogashira cycle could influence the Glaser cycle. Additionally molecular sieves were added in the reaction. The role of the molecular sieves is explained in another paper[23] in which the authors present the optimization of the Glaser-Hay reaction based on a NMR kinetic experiment. The paper shows that in a standard Hay reaction (conditions 5% CuCl, 10% TMEDA) the kinetics are zero-order and after a while they decrease is slower kinetics with the same order. The authors suggested that water could have a negative influence. For this reason, they recommend performing the reaction in presence of molecular sieves in order to reduce the problem.

In our case the reaction afforded methyl 3-ethynylbenzoate already deprotected[2], with 64% yield. We hypothesized that the interface of exchange with O_2 (for the Glaser cycle) in the Schlenk flask was not enough large. Therefore the cycle was not completed.

Step c) Product **9** was obtained in good yield (91%) following a procedure already published in literature[22,23]. The conditions adopted were copper(I) chloride (10%), *N*,*N*,*N'*,*N'*-tetramethylethylenediamine (TMEDA) (30%) and molecular sieves (3Å) under air condition.

Step d) Final deprotection of compound **9** was obtained in tetrahydrofuran at room temperature with lithium hydroxide in water. The reaction was performed in similar conditions that product **5** but for shorter time (that might explain the lower yield, 37%)[9]. Product **10** has been already reported in literature without characterization details[24].

Once the dimer (molecule **10**) was synthesized, we focused on the single monomer (molecule **11**).

Step e) 3-ethynylbenzoic acid is commercially available. In this work it was synthetized by analogy to product **6**, by deprotection of the corresponding ester in

methanol:water with lithium hydroxide followed by an acidification step (3M HCl). The product **11** was afforded with 54% yield and its spectrum is in agreement with the reference in the literature[25].

2.3.2.3 Characterization

All the molecules **1-9** are already known in the literature, while molecule **10** and **11** only partially. A complete characterization was done by multinuclear (^{1}H and ^{13}C) mono and bi-dimensional NMR spectroscopy and high-resolution mass spectroscopy for both the molecules. The ^{13}C spectrum of molecule **10** is showed below.

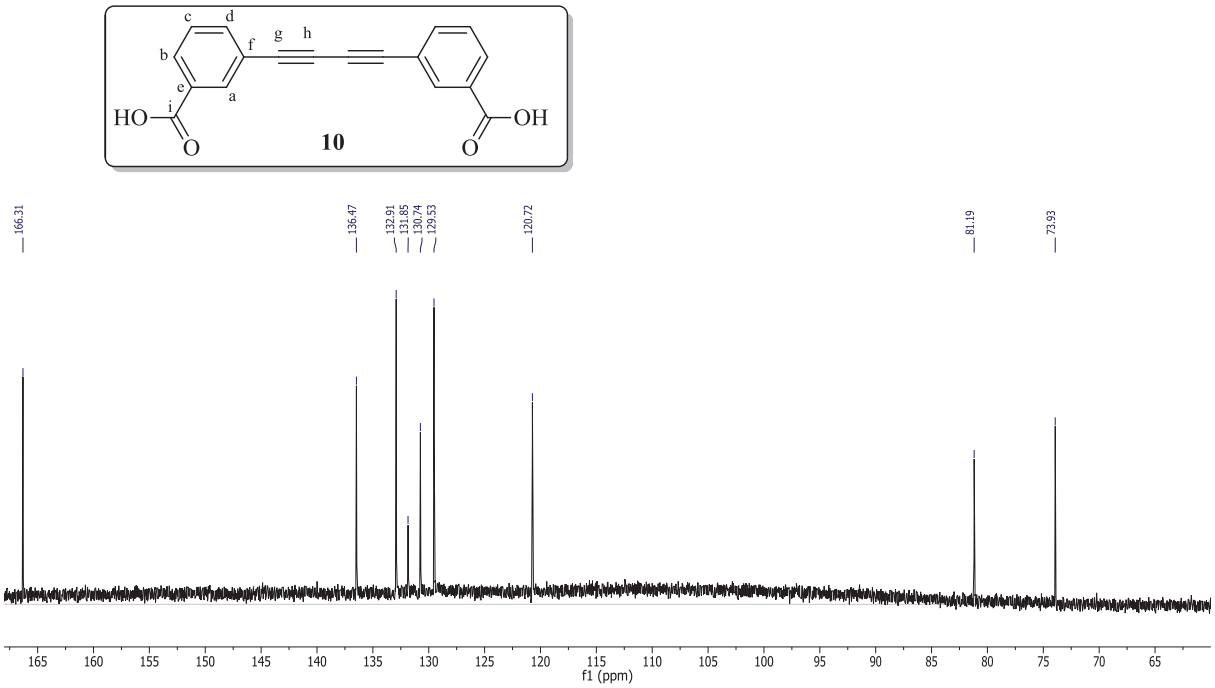

Figure 2.18 ^{13}C NMR of molecule **10**.

	C_a	C_b	C_c	C_d	C_e	C_f	C_g	C_h	C_i
δ_C **(ppm)**	132.9	130.7	129.5	136.5	*131.9*	*120.7*	81.2	73.9	166.3

Table 2.2 ^{13}C NMR chemical shift of molecule **10**. The chemical shifts in italic were attributed by analogy to molecule **11**.

From the multinuclear spectra it was possible to assign the carbon signals. High resolution mass spectra (ES in negative mode) confirms the product, showing a molecular peak at m/z 289.0498 (calculated mass 289.0501).

Molecule **11**, has been characterized only by ^{1}H NMR in the literature[25]. In this work it has been characterized by multinuclear (^{1}H and ^{13}C) mono and bi-dimensional NMR spectroscopy and high-resolution mass spectroscopy. ^{13}C spectrum is showed below.

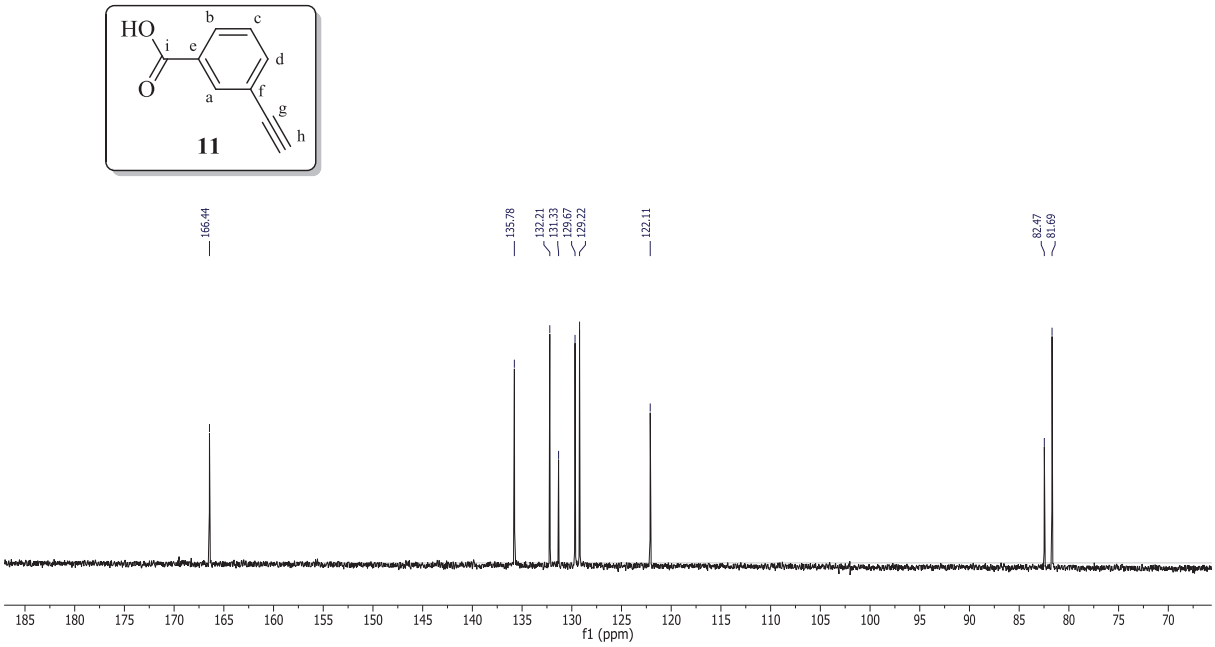

Figure 2.19 ^{13} C NMR of molecule **11**.

	C_a	C_b	C_c	C_d	C_e	C_f	C_g	C_h	C_i
δ_C **(ppm)**	*132.2*	*129.7*	129.2	*135. 8*	131.4	122.1	82.5	81.7	166.4

Table 2.3 ^{13}C NMR chemical shift of molecule **11**. The chemical shifts in italic were attributed by analogy to molecule **10** .

The proton spectrum is in agreement with the reference in the literature. The signals corresponding at C_a, C_b and C_d at 132.2, 129.7 and 135.8 ppm cannot be assigned for certain. In this work these signals (in italic in the table) have been assigned by analogy to the molecule **10**.

High resolution mass spectroscopy (DCl/CH_4) confirms the product 147.0457 in the protonated form (calc. mass 147.0446).

2.3.2.4 Deposition on $CaCO_3$ surface

Molecules **10** and **11** were deposited on calcite surface on UHV conditions by sublimation. The images were recorded in the same conditions, at 10^{-9} mbar on a calcite crystal, previously cleaved.

Molecule **10** was sublimated for five minutes at 80 °C. As shown the picture it forms very few stripes.

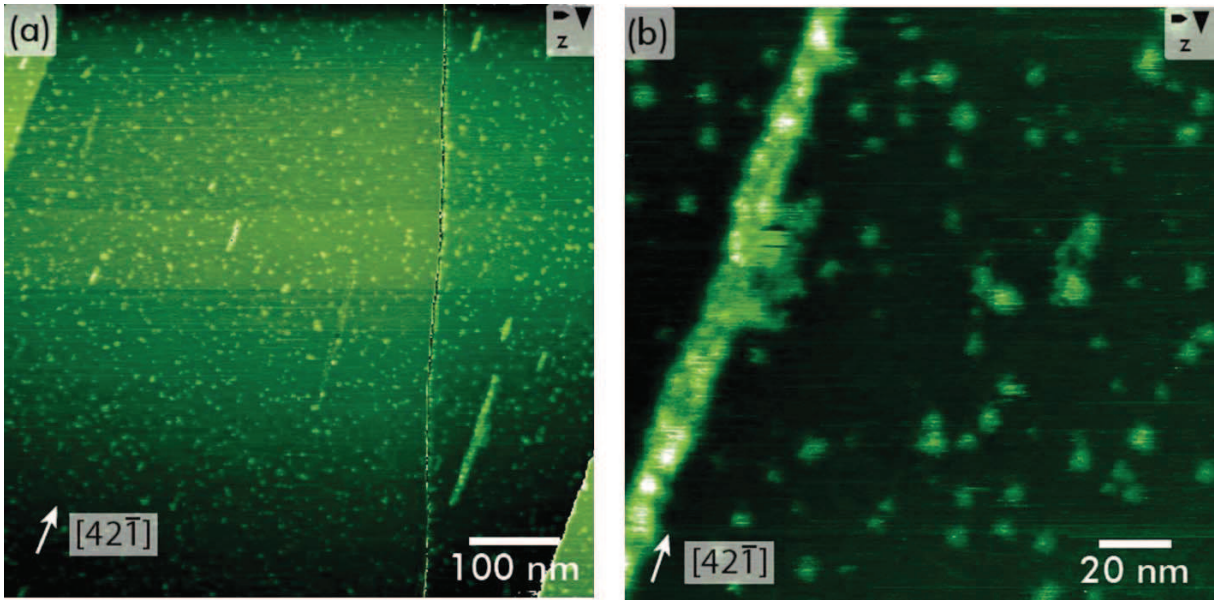

Figure 2.20 a-b) 3-ethynylbenzoic acid (**10**) dimer on $CaCO_3$.

The sample was irradiated for two hours at 254 nm without relevant differences. Several attempts were done in order to sublimate the molecule. Unfortunately it turned that the molecule reacts already in the crucible and it was no possible to depose it on the surface. Further experiment will be needed.

2.3.3 Conclusion

In this paragraph we presented the synthesis of two molecules for different purposes. The first molecule (**10**) was synthetized for photopolymerization reaction on the surface. The latter (**11**) was prepared for homocoupling reaction (the same as *para*-position molecules). In addition, molecule **11** has been characterized by single crystal X-ray diffraction (details in Annex).

2.4 Molecules for polycondensation

2.4.1 Introduction and objective

Since their discovery at the beginning of 20th century, phthalocyanines have been immediately the object of intense research for their industrial and academic importance (paints, fabrics, organic semiconductors in photovoltaic, organic catalysis, photocatalysis and so on)[26–28]. Phthalocyanines can be used as building blocks for many applications (organic

light emitting diodes, data storage devices, field effect transistors) and they show interesting chemical and optoelectronical properties[27,29].

Polymeric phthalocyanines are insoluble in standard organic solvents (except concentrated sulfuric acid in some cases) and not sublimable. For this reason special techniques are employed for treating these compounds[28]. Today, two principal methods are known in order to obtain phthalocyanine networks[27,28].

The first is the synthesis by cyclotetramerization of bifunctional monomers (such as 1,2,4,5-tetracyanobenzene or pyromellitic dianhydride) in order to obtain an extended bidimentional polymer, often called polyphthalocyanine (PPc), as shown in the picture above. This method has been deeply studied by Wörle and coworkers: the starting monomers polymerize in presence of metal salts or metal bulk at high temperature (350-400 °C)[27,28]. Additionally, the starting monomers can be deposited on metallic surface by chemical vapor deposition (CVD) and then they polymerize giving a thin film of PPc[27].

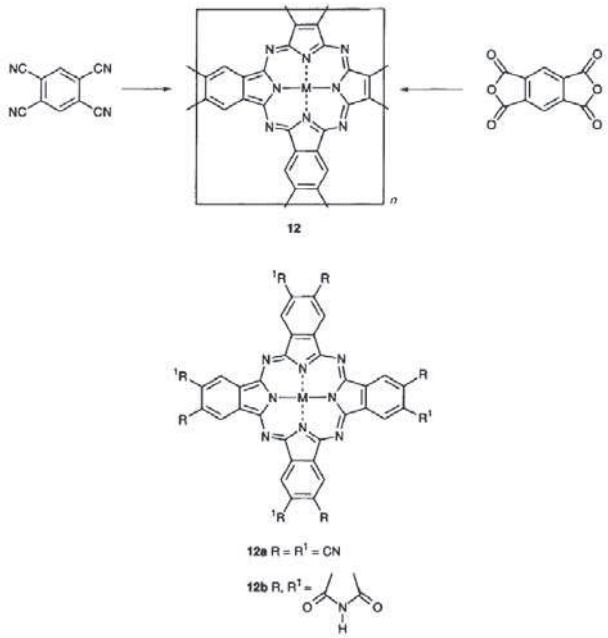

Figure 2.21 Polymeric phthalocyanine obtained by cyclotetramerization, from ref.[27].

The second important method involves the condensation of tetra or disubstituted Pc derivatives at low-molecular weight with other bifunctional compounds (or by self-condensation). In this method the number of Pcs in the final network is easier to control (comparing to the previous method). In the figure above is shown the polyimide (**13** in the figure) obtained with this method from a modified Pc (**12**) and other compounds, by an intermediate film of polyamide-acid.

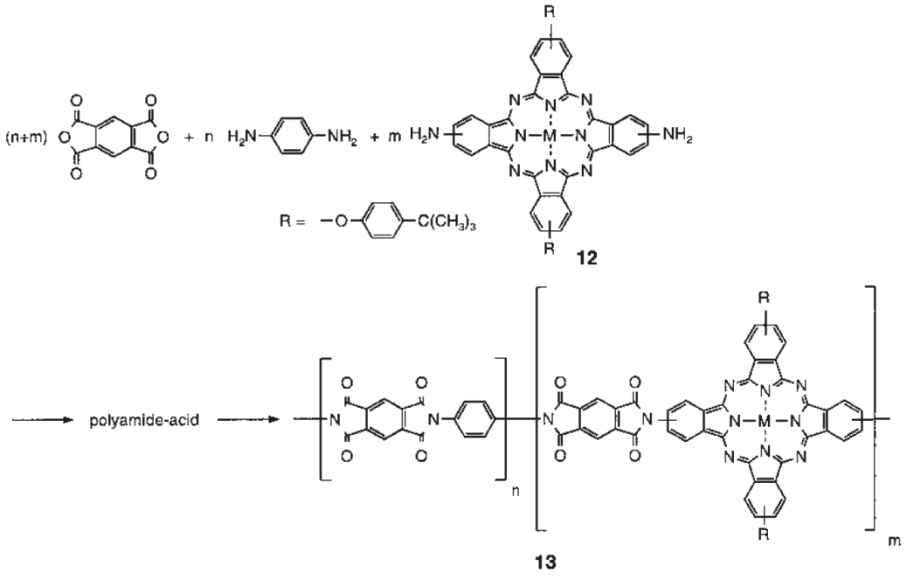

Figure 2.22 Polymeric phthalocyanine obtained by polycondensation from ref.[28].

Finally, others methods (less important) exist to obtain phthalocyanine networks but we will not get into details for them (such as plasma polymerization or polymerization on the surface of electrodes)[27].

Polycondensation of phthalocyanine has been already carried out on metal surface and on NaCl monolayer in UHV conditions at room temperature[29] by M. Abel and coworkers as already discussed previously (chapter 1).

In the present work we envisaged to synthesize molecules in order to obtain a single phthalocyanine molecule and phthalocyanines network on $CaCO_3$ surface (Figure 2.26 a and b). Calcite, comparing to NaCl, has a higher surface energy, so molecules are expected to bind strongly the surface. We can imagine three different approaches:

- First the metal deposition and then molecule sublimation.
- Both molecule and metal together (co-evaporation).
- First the molecule deposition and then the metal.

The first method can be excluded because we presume that metal atoms, if sublimated on an insulating surface, might form clusters due to the low interaction with the surface.

Both the second and the third method could be possible. Among these maybe the latter could be the best option because it should prevent diffusion or undesirable side-products that might be formed by co-evaporation. Additionally, the molecule/metal ratio plays a crucial

role: in this work we envisaged to test at the beginning 4:1 (phthalocyanine synthesis, Figure 2.26 a) or 2:1 (polyphthalocyanine synthesis, Figure 2.26 b).

Assuming that the reaction occurs at room temperature in UHV conditions, the grafting carboxylic groups are no more necessary because the cyano groups interact with the surface. The metal acts as a template for the formation of phthalocyanine. Finally, the target monomer was envisaged with a central naphthalene core (instead of benzene as in the reference paper) in order to easily recognize the network on nc-AFM images.

Researchers in A. Foster's group (Aalto University, Finland) carried out calculation on the naphthalene-2,3,6,7-tetracarbonitrile (Figure 2.23). The nitrogen atoms of the molecule (blue in the picture) interact with the calcium atoms (green in the image) of the substrate (Figure 2.24). The adsorption energy ($E_{ads} = E_{surf+mol} - E_{empty\ surface} - E_{mol\ in\ vacuum}$) is - 41.9 kcal/mol, so the molecule is likely to adsorb strongly on calcite at room temperature.

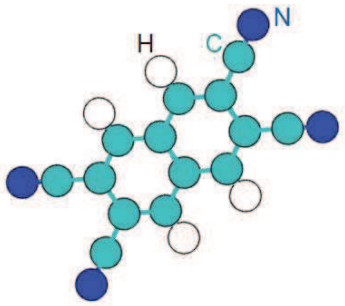

Figure 2.23 Picture of naphthalene-2,3,6,7-tetracarbonitrile molecule (private communication).

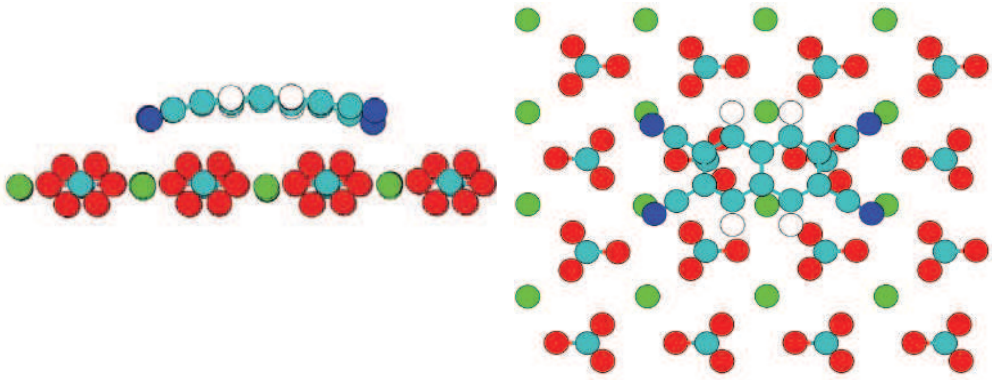

Figure 2.24 Simulation of naphthalene-2,3,6,7-tetracarbonitrile molecule on calcite (private communication).

Au atoms were added in the calculation in order to estimate if the metal forms clusters or not in the surface. Au atoms (yellow in figure Figure 2.25) are localized in specific sites

between carbonate ions. In presence of Au atoms, the adsorption energy of molecules decreases at - 85.3 kcal/mol.

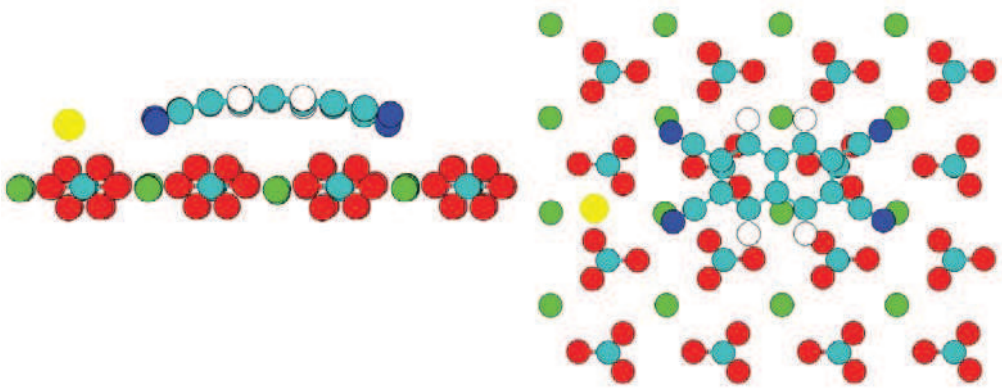

Figure 2.25 Simulation of naphthalene-2,3,6,7-tetracarbonitrile molecule and Au atom on calcite (private communication).

Having these considerations in mind we decided to work with two different approaches: starting with 2,3-dicyanonaphthalene in order to obtain the single phthalocyanine molecule on surface and naphthalene-2,3,6,7-tetracarbonitrile in order to obtain the polymeric network, as pictured in Figure 2.26 (a and b respectively) .

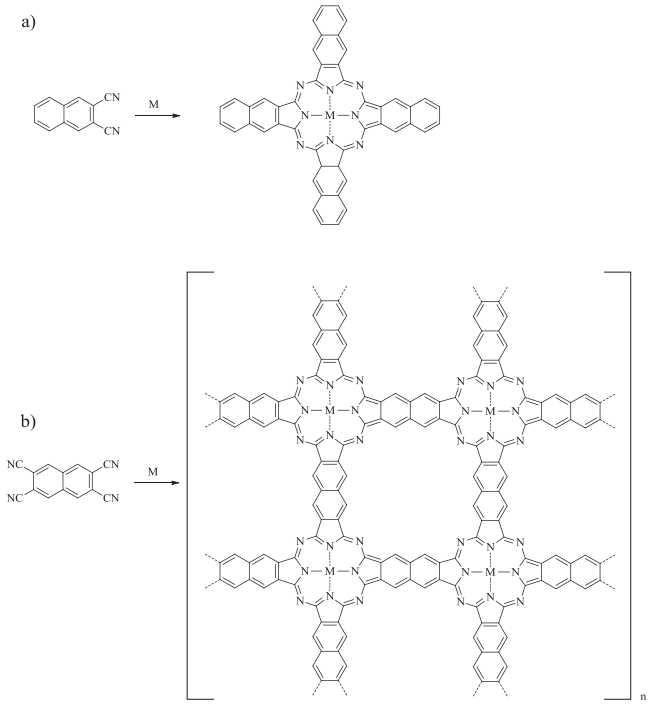

Figure 2.26 Two different approaches envisaged for phthalocyanine synthesis on surface (a) or phthalocyanine network (b).

The first molecule is commercially available, while the second was synthesized in this work (molecule **13**).

2.4.2 Results and discussion

2.4.2.1 Synthesis

The synthesis of the target molecule naphthalene-2,3,6,7-tetracarbonitrile (**13**) can be achieved by modification of two procedures already reported in literature[30,31].

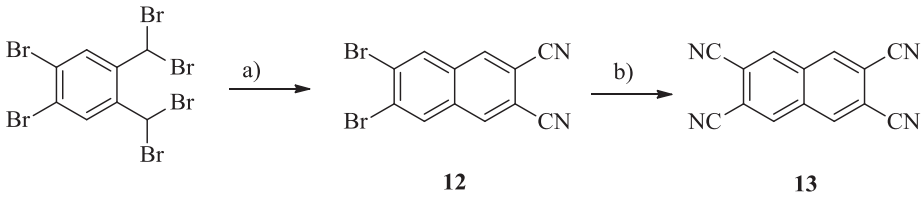

Figure 2.27 Synthesis of target molecule naphthalene-2,3,6,7-tetracarbonitrile (**13**). Conditions: a) Fumaronitrile, NaI, DMF, 80 °C, 5h, 72%; b) CuCN, DMF reflux, 5h, 80%.

The first step (a) afforded an intermediate molecule 6,7-dibromodicarbonnaphthalene-2,3-dicarbonitrile (**12**) *via* the reaction mechanism is reported below:

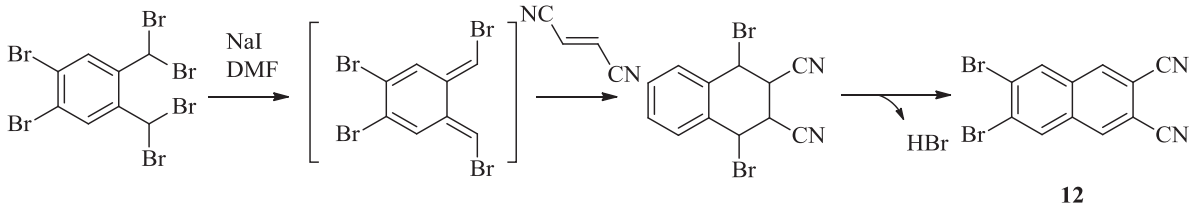

Figure 2.28 Reaction mechanism for molecule **12**.

The elimination of one bromine atom of each dibromomethyl substituent gives an intermediate derivative (5*E*,6*E*)-2,3-dibromo-5,6-bis(bromomethylene)cyclohexa-1,3-diene, which interacts with fumaronitrile by a Diels-Alder reaction. Then, elimination of HBr, moved by the driving force of aromaticity, affords the final compound 6,7-dibromodicarbonnaphthalene-2,3-dicarbonitrile (**12**)[30,31].

The second step (b) affords the final molecule naphthalene-2,3,6,7-tetracarbonitrile (**13**). It can be achieved through a standard method for preparation of aromatic nitriles from aryl halides (Rosenmund-von Braun)[31–34].

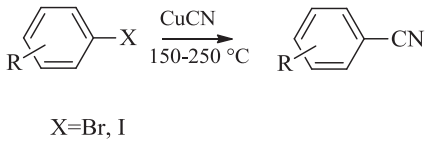

Figure 2.29 Rosenmund-von Braun reaction.

The proposed mechanism involves two steps: first the oxidative addition of the aryl halide that leads to the formation of a Cu(III) species; then the reductive elimination affords the aromatic nitrile.

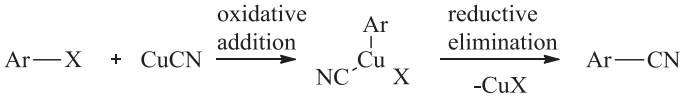

Figure 2.30 Mechanism of Rosenmund-von Braun reaction.

However this reaction has many inconveniences such as the use large quantities of toxic copper (I) cyanide (that make also difficult the separation) or the high temperature required that may not be compatible with all the substrates. Today many efforts have been done in order to use more convenient and less hazardous methods[34–36]. Palladium or nickel catalysts aryl cyanation, in fact, has replaced the previous method. As reported in the literature, addition of CuI 10% increases the efficiency of the reaction. Aryl nitriles are obtained from aryl bromides through the corresponding *in situ* formation of aryl iodide (by using catalytic amount of CuI and KI). In a recent protocol acetone cyanidrine is used as alternative cyanating agent (instead of sodium cyanide).

Step a) and b)

Step a) The reaction has been already described in literature[30,31] with two similar procedures but slightly different work-up and yield (65% and 89% respectively). Even if the second paper presents a higher yield, the procedure involves the use of carbon tetrachloride (CCl_4) and TLC monitoring with benzene. For this reason, in the present work, both the procedures were combined and the work-up was adapted.

1,2-dibromo-4,5-bis(dibromomethyl)benzene was stirred in *N*,*N*-dimethylformamide (DMF) with fumaronitrile and sodium iodide at 80 °C for 5 hours. Once the reaction was finished (monitoring *via* TLC), the mixture was cooled at room temperature. The mixture was diluted with water (in order to precipitate the solid) and treated with saturated solution of sodium thiosulfate in order to reduce bromine. Filtering and washing with saturated solution

of sodium thiosulfate, water and diethyl ether affords the final product 6,7-dibromodicarbonnaphthalene-2,3-dicarbonitrile (**12**), entry 4 in summary Table 2.4.

The reaction was performed in slightly different conditions, as reported in the Table 2.4. First, after the filtration, the reaction was recrystallized from toluene/hexane mixture (1:1) as reported in literature[30]. It turned that this step was not necessary because the product was already sufficiently clean and the recrystallization decreased the yield drastically (entry 1). The reaction was performed also in a different concentration (entry 2), but in this condition the product did not precipitate. Finally the reaction was performed in a different solvent (entry 3). Acetone was chosen to test this reaction because it dissolves easily sodium iodide (50.44 g NaI/100 g acetone; while 3.7-3.6 g NaI/100 g DMF), while some impurities (for example sodium bromide) are not soluble in this solvent, allowing an easier filtration. Standard work-up affords the product **12** in very low yield (<1%). In conclusion, for this reaction the best conditions found are summarized in the table (entry 4).

Entry	Solvent	Concentration	Work up	Yield
Ref. lit.[30]	DMF	0.145 g/mL	Recryst. tol./hex.	65%
Ref. lit.[31]	DMF	0.109 g/mL	Recryst. CCl_4 and sublimation	89%
1	DMF	0.109 g/mL	Recryst. tol./hex.	37%
2	DMF	0.006 g/mL	/	/
3	Acetone	0.006 g/mL	Filtration	<1%
4	DMF	0.100 g/mL	Filtration	72%

Table 2.4 Reaction details. Each experiment was performed at least two times (except entry 2 and 3 just once).

Step b) The reaction has been already described in literature[31], but the work-up was changed due to the presence of benzene in the experimental protocol. Compound **12** was stirred with copper (I) cyanide under reflux of dimethylformamide and then treated with saturated solution of iron (III) chloride hexahydrate in order to neutralize the excess of cyanide as iron complexes. The dark precipitate was washed with ammonium hydroxide solution, redissolved and heated to reflux in acetonitrile in order to remove the insoluble admixtures. The filtrate was evaporated resulting in the final product **13** (80%).

The reaction was performed with different concentration as reported in Table 2.5. If the reaction is carried out in the same conditions as the reference (0.050 g/mL), entry 1, the spectrum of the crude product presents two broad signals around 5.5-6.3 ppm of an impurity and the 7-bromonaphthalene-2,3,6-tricarbonitrile. Additional recrystallization, followed by a

passage through a short column of silica gel (toluene/acetone 30:1 → 30: 1.5) afforded the target molecule **13**. The same result was obtained when the concentration is 0.042 g/mL (entry 2) with again very low yield. Finally, when the concentration is 0.047 g/mL, the NMR spectrum does not show the broad signals around 5.5-6.3 ppm neither of the 7-bromonaphthalene-2,3,6-tricarbonitrile. In this case the target molecule was obtained with 80% yield.

Entry	Concentration	Work up	Yield	Comments
Ref. lit.[31]	0.050 g/mL	Filtration and column chromatography	68%	
1	0.050 g/mL	Filtration, recryst. and column chromatography	10%	Impurity and 7-bromonaphthalene-2,3,6-tricarbonitrile
2	0.042 g/mL	Filtration, recryst. and column chromatography	16%	Impurity and 7-bromonaphthalene-2,3,6-tricarbonitrile
3	0.047 g/mL	Filtration	80%	

Table 2.5 Reaction details. Each reaction was performed in average two times.

2.4.2.2 Characterization

The molecule naphthalene-2,3,6,7-tertracarbonitrile (**13**) has not been described completely in the literature[31]. In the present work it has been characterized by multinuclear (^{1}H and ^{13}C) mono and bi-dimensional NMR spectroscopy and high-resolution mass spectroscopy. The proton spectrum matches with the reference. The ^{13}C spectrum is reported here below.

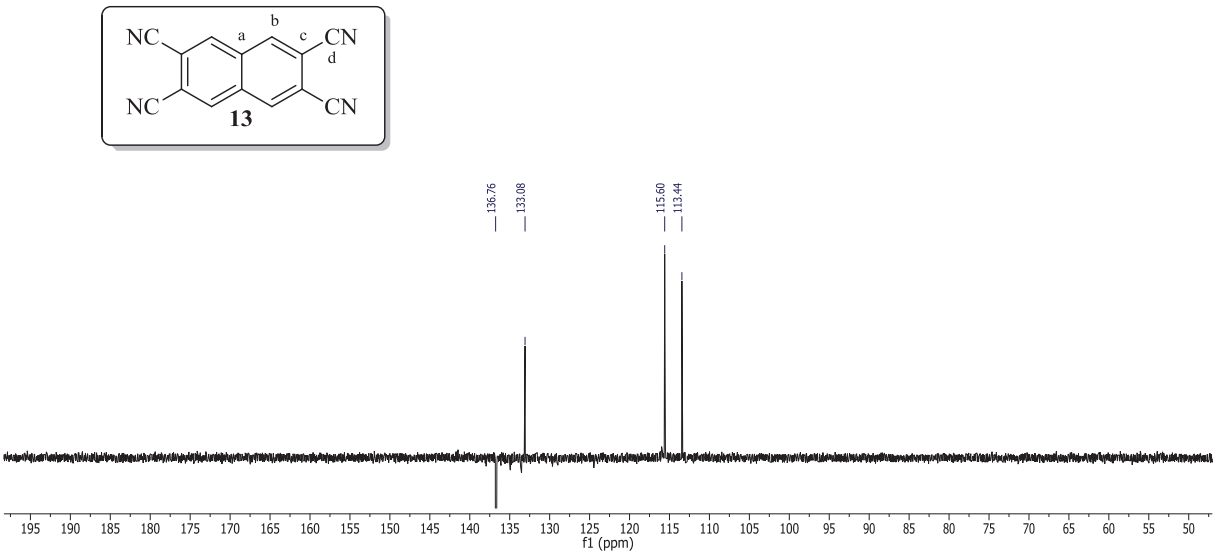

Figure 2.31 ^{13}C spectra of naphthalene-2,3,6,7-tertracarbonitrile molecule (**13**).

	C_b	C_a	C_c	C_d
δ_C **(ppm)**	136.8	*133.1*	*113.4*	*115.6*

Table 2.6 ^{13}C NMR chemical shift of naphthalene-2,3,6,7-tertracarbonitrile molecule (**13**). The signals in italic are assigned by analogy to 6,7-dibromodicarbonnaphthalene-2,3-dicarbonitrile molecule (**12**) (not reported in this manuscript).

Due to the high symmetry of the molecule, it turns difficult to assign all the carbons signals with certitude. It is possible to attribute the C_b signal (136.8 ppm), which it can be identified by multinuclear (^1H and ^{13}C) mono and bi-dimensional NMR spectroscopy. By analogy of the previous molecule (**12**), characterized by multinuclear (^1H and ^{13}C) mono and bi-dimensional NMR spectroscopy and fully described in the literature[30,31], the signal at 133.1 ppm could be attributed to C_a, at 113.4 ppm to C_c and 115.6 ppm to C_d.

The high resolution mass spectra (DCl-CH_4) confirms the product, showing a molecular peak at m/z 229.0504 that corresponds to the protonated form $[M+H]^+$(cal. mass 229.0514).

2.4.3 Conclusion

In this section we described the synthesis of naphthalene based molecule for polycondensation reaction on $CaCO_3$ surface. At the moment of the redaction of this manuscript the molecule has been sent in Germany for the deposition on calcite.

From the synthetic point of view, the work could continue with alternative methods for the synthesis of naphthalene-2,3,6,7-tetracarbonitrile. In fact, as already stated, the

Rosenmund-von Braun reaction has many inconvenient and today is not very frequently adopted. Investigations on new reactions methods could be carried out in order to optimize the reaction.

2.5 Molecules for Ullmann Coupling

2.5.1 Introduction and objective

The last reaction studied in this work is the Ullmann reaction. As already discussed in the first chapter, Ullmann reaction has been deeply investigated on metal surface in UHV conditions. Having in mind the results published by Cai and coworkers[37] on metal surface (presented in the previous chapter), we envisaged to design a similar target molecule (**18**) for coupling on calcite, showed in Figure 2.32.

In our case the target molecule is characterized by an anthracene central core, two flexible arms with carboxylic groups at the moieties and bromine in position 9 and 10 of anthracene.

As we work on calcite, the molecule-surface interactions are weaker than the corresponding ones on metal surface; therefore molecule **18** is expected to be slightly mobile and not completely flat on the surface. In this position the intermolecular steric repulsion of hydrogen atoms belonging to different molecules, do not prevent the coupling reaction, as observed on metallic surface (see chapter 1). Once the intermediate polymer is formed, the second step involves (for the first time on insulating surface) cyclodehydrogenation in order to obtain graphene nanoribbon.

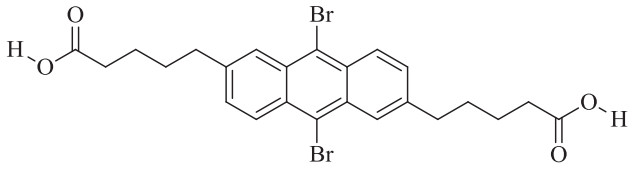

Figure 2.32 Target molecule **18**.

2.5.2 Results and discussion

2.5.2.1 Retrosynthetic analysis

The retrosynthetic analysis for molecule **18** is reported here below:

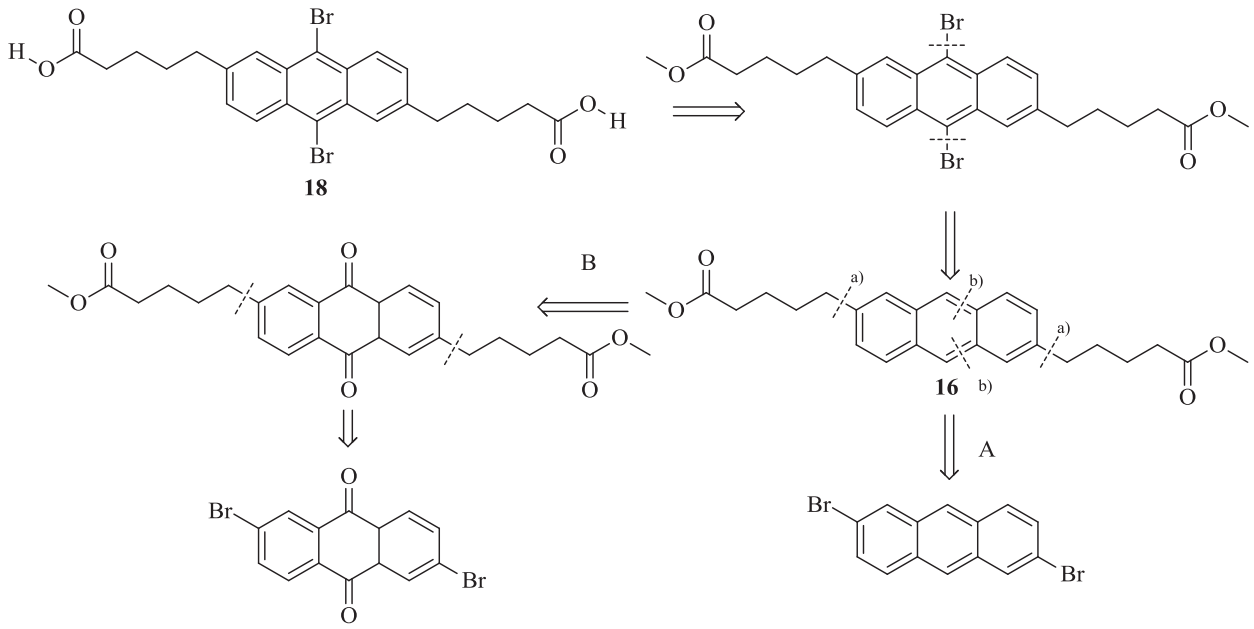

Figure 2.33 Simplified retrosynthetic analysis for molecule **18**.

The target molecule (**18**) can be achieved from a key precursor (molecule **16**). The latter can be obtained by a double Sonoghasira coupling reaction on 2,6-dibromoanthracene (commercially available) (Method A), followed by reduction of triple bonds. Then, bromination of position 9 and 10 of anthracene followed by deprotection of carboxylic group affords the target molecule **18**. The intermediate molecule **16** can be also obtained by a second route (Method B), involving a double Sonogashira coupling reaction on 2,6-dibromoanthraquinone (commercially available), followed by re-aromaticity step. Then the pathway is the same as for the previous method.

2.5.2.2 Synthesis

4-pentynoic methyl ester, molecule **14**, is used as alkyne for Sonogashira coupling. The molecule was synthesized as already reported in the literature[38].

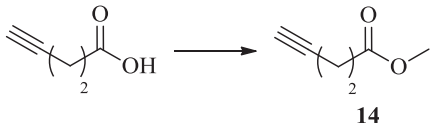

Figure 2.34 Synthesis of 4-pentynoic methyl ester (**14**). Conditions: MeOH reflux, overnight, 68%.

4-penynoic acid was esterificated in methanol at reflux with concentrated sulfuric acid as catalyst, as reported in literature[38]. Standard work-up afforded molecule **14** with 68% yield.

Method A

The synthesis of target molecule **18** *via* method A is reported below.

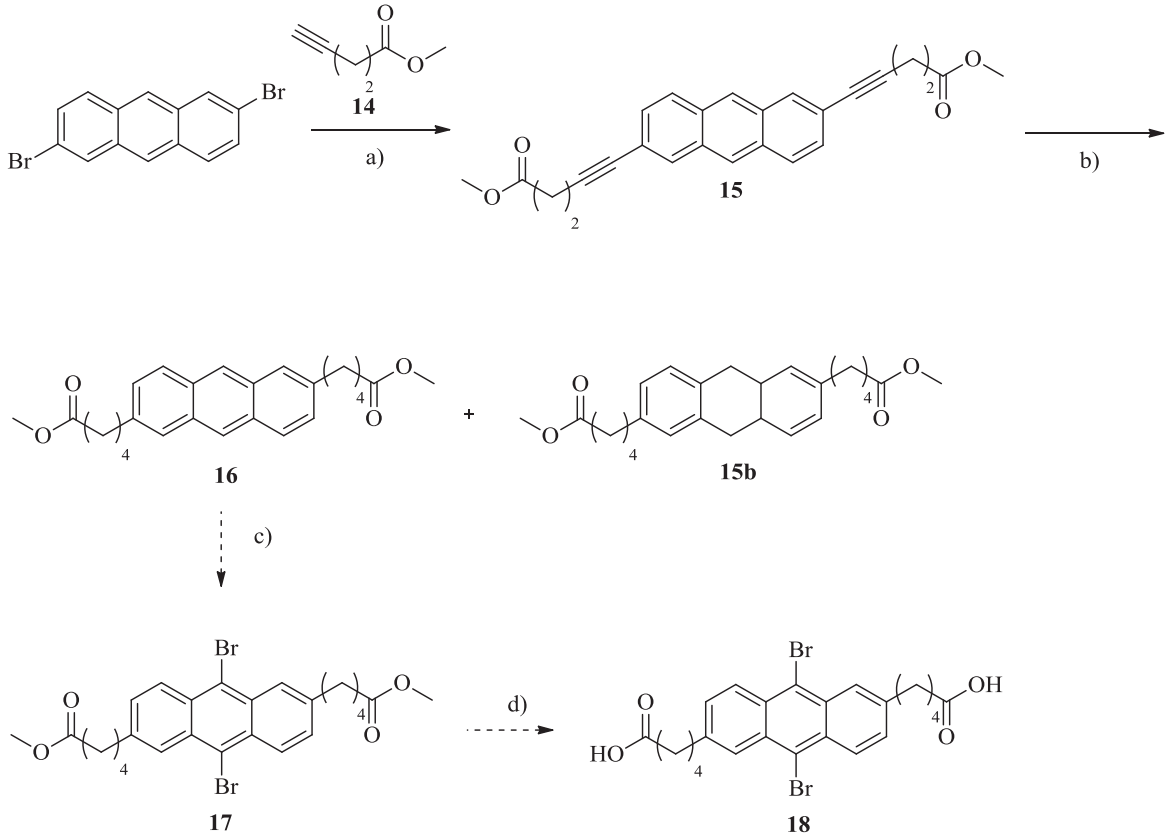

Figure 2.35 Reaction path A for the target molecule **18**. Conditions: a) **14**, $Pd(PPh_3)_3Cl_2$ (2%), CuI (6%), Et_3N, reflux, 5 days, 66%; b) **15**, TES, 10% Pd/C, MeOH, 4h, 27%.

Step a) to d)

Step a) The first step is a double Sonogashira reaction on the substrate of 2,6-dibromoanthracene in order to obtain molecule **15**. The reaction is more efficient with electron poor systems (such as anthraquinone for instance, instead of anthracene) and iodine as halogen (instead of bromine).

Here we report some examples in literature of this reaction on similar substrate[39–41].

In the first paper[39] E. Quesada and coworkers synthesized fluorescent diester molecules with an anthracene core. They proposed two different approaches: in a first experiment they inserted the acyl chains by Sonogashira coupling ($[Pd(PPh_3)_2Cl_2]$/CuI catalysts, diethylamine as solvent) on 2,6-dibromoanthracene (70% yield), followed by Raney-Nickel® reduction of triple bond (55% yield). In the second approach they used 2,6-dibromoanthraquinone as substrate for the coupling reaction (73% yield) and then the reduction of triple bonds was carried out with H_2, PtO_2, followed by oxidation with 2,3-

dichloro-5,6-dicyano-1,4-benzoquinone (DDQ) in order to restore the aromaticity on anthracene core (31% and 50% yield, respectively).

M. Saito and coworkers[40], on the other hand, carried out a double Sonogashira coupling reaction on 2,6-dibromoanthracene using different conditions and catalysts: $Pd(PPh_3)_4$/CuI (0.046:0.098) in triethylamine with a 64% yield.

Finally in a third paper[41], B. Khanna and coworkers carried out the same reaction in different conditions: $[Pd(PPh_3)_2Cl_2]$/CuI catalysts (0.02:0.06) in triethylamine. They obtained their target molecules with 54% and 73% yields.

In this work we tried various conditions from the literature, as summarized in Table 2.7.

In a first experiment we used $[Pd(PPh_3)_2Cl_2]$/CuI (0.10:0.20) as catalyst in diethylamine, as suggested in the first paper[39]. In this case the reaction afforded several side products and, even after the purification by column chromatography (ethyl acetate/hexane 1:9), it was no possible to isolate the target molecule. By changing the ratio of catalysts $[Pd(PPh_3)_2Cl_2]$/CuI (0.20:0.10), the reaction did not afford the target molecule but mainly the monobromine substituted derivative. In both the case, the presence of high amount of starting material suggested that the reaction did not completely work.

Then the catalysts quantities $[Pd(PPh_3)_2Cl_2]$/CuI (0.20:0.20), alkyne (1:7 instead of 1:3 for the previous reactions) and solvent (triethylamine/toluene 1:1) were slightly changed, as reported in another paper[42]. Recrystallization from dichlomethane/pentane afforded molecule **15** with 5% yield.

Having in mind the results published by M. Saito[40], we changed the catalysts, the quantity of alkyne and the solvent: $Pd(PPh_3)_4$/CuI (0.010:0.030) in triethylamine. The reaction mixture was purified by column chromatography (ethyl acetate/dichloromethane/cyclohexane 1:3:6) affording molecule **15** (not completely pure even after two columns chromatography) with an approximated 64% yield.

Finally the best results were obtained with $[Pd(PPh_3)_2Cl_2]$/CuI (0.020:0.060) in triethylamine, as suggested in another paper (B. Khanna)[41]. The reaction was stirred for three days (monitoring *via* TLC) at reflux (alkyne and catalysts were added again in the same quantities after one day). Standard work-up followed by flash chromatography purification (SiO_2, cyclohexane/dichloromethane 70:30→ dichloromethane pure, with a gradual increment of polarity 20% every time) afforded molecule **15** with 66% yield.

Entry	Catalysts	MR catalysts	MR st.mat./alkyne	Solvent	Yield	Reference
1	a	0.20:0.10	1:3	$NHEt_2$	/	Ref.[39]
2	a	0.10:0.20	1:3	$NHEt_2$	/	Ref.[39]
3	a	0.20:0.20	1:7	NEt_3 / toluene 1:1	5%	Ref.[42]
4	b	0.01:0.03	1:4	NEt_3	Approx.64%	Ref.[43]
5	a	0.02:0.06	1:2.4	NEt_3	66%	Ref.[41]

Table 2.7 Different reactions tested for molecule **15**. Catalysts a: $[Pd(PPh_3)_2Cl_2]$/CuI; catalysts b: $[Pd(PPh_3)_4]$/CuI. Each reaction was performed at least three times, except reaction 3 and 4.

Step b) The following reaction is the reduction of the triple bond. This reaction is necessary because if we brominate directly molecule **15**, the triple bonds will react immediately and the molecule obtained would probably decompose during the sublimation step in UHV. The ester moieties and the anthracene core make this reduction a synthetic challenge.

From the milder methods (catalytic transfer of hydrogen for example) to the H_2 gas, reduction reactions have been deeply investigated in the past. In this manuscript we present a selection of the most common method. We tested all of them on our substrate, following some literature examples[39,43–45].

The first method investigated in this work in the catalytic transfer of hydrogen. Instead of using hydrogen gas, the reduction is carried out by a hydrogen donor in presence of catalyst. In a remarkable paper P. K. Mandal[44] proposed a mild reduction using excess of triethylsilane (TES) and 10% Pd/C (20% by weight) as catalyst in methanol. The reaction mechanism is showed below:

Figure 2.36 Reduction with triethylsilane, from ref.[44].

The authors stated that this method has a great tolerance for many functional groups. This method is also employed in other examples in literature[46,47] for the synthesis of γ-aryl or β-amino acids or perylene derivatives respectively.

An alternative method was proposed in a recent paper by R. Shen[45] and coworkers. They published the selective hydrogenation with formic acid and palladium catalyst. This

reduction affords three possible products: *cis*-, *trans*-alkenes or alkanes, depending from the reaction conditions.

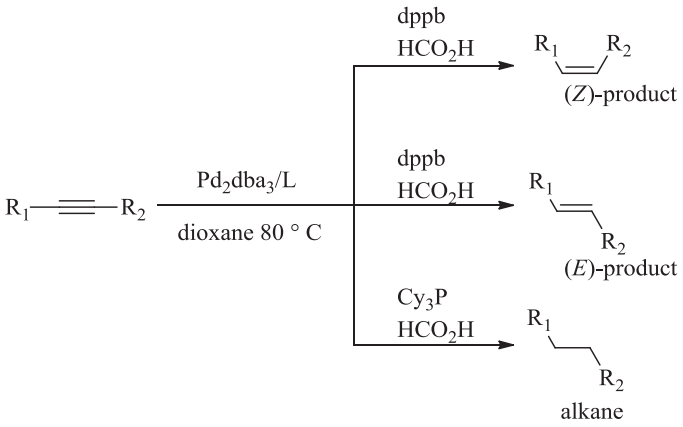

Figure 2.37 Hydrogenation of alkyne to akenes or alkane with palladium catalyst and formic acid, readapted from the literature[45].

To obtain the alkane product, they used as conditions: $Pd_2(dba)_3$, Cy_3P (1% and 4% respectively) and aqueous solution (25%) of formic acid (6.0 eq.) in dioxane. They stated that this reduction is a good alternative even for sensible substrate.

Another possible route for reduction reaction is to use Raney-Nickel®. This reagent represents a useful and common tool for organic chemistry reduction. In the previous paper of E. Quesada[39], for instance, the authors used this reagent for triple bond reduction.

Finally the last method studied in this work is the standard hydrogenation with H_2 gas at atmosphere pressure with Pd/C as catalyst in ethanol[50]. This route requires H_2 gas, that need special equipment and the reduction capacity is harsh so they might decompose the substrate or the ester moieties.

In this work we tested all the listed methods with different results (Table 2.8).

In a first experiment we tested TES (10 eq.) in methanol solution with 10% Pd/C as catalyst (23% by weight), as described in the literature[44]. Standard work-up followed by preparative TLC (ethyl acetate/dichloromethane/cyclohexane 1:3:6) afforded the target molecule with a yield of 27%. The presence of good amount of starting material, suggested that the reaction did not completed. For this reason the reaction was performed again in the same condition but this time TES and catalysts were added three times every hour in order to increase the yield and the reaction was left all the night. Standard work-up followed by preparative TCL (same conditions) afforded the product with an impurity (approximate yield 24%). A second preparative TLC was carried out, but did not completely purify the product. Finally we tested a third different condition. As we speculated that the reaction had a high

kinetic rate, we decided to add TES diluted in methanol drop by drop in a dropping funnel over 10 minutes. The reaction was let to react for 2 days (adding the catalyst and TES every day). Standard work-up followed by preparative TLC (same conditions) afforded the target molecule with a yield of 3%. We tried several times to reproduce the reaction again with the first conditions, but we never achieved the results obtained before. In every case more than 50% of the starting material did not react. We suggested that the catalyst is poisoned preventing the success of the reaction. We also obtained and characterized dihydroanthracene derivative (molecule **15 b**) as side product.

We decided to change the strategy using the conditions proposed in R. Shen's paper[45]. In this case, first we form the complex between the ligand Cy_3P and $Pd_2(dba)_3$ (20% and 5% respectively) in dioxane (the reaction color switches from dark red into dark orange), we added molecule **15** and finally formic acid (aqueous solution at 25%, 6 eq.). The reaction mixture was heated at 80 °C overnight. Standard work-up followed by preparative TLC (ethyl acetate/dichlomethane/cyclohexane 1:4:5) afforded a degraded product that did not correspond to the target molecule.

We also tested the Raney-Nickel® reaction in tetrahydrofurane for three hours following the procedure already reported in the literature[39]. Standard work-up, followed by purification afforded a degraded product that did not correspond to the target molecule.

Probably in both cases the reaction conditions (formic acid or Raney-Nickel®) were too harsh and the anthracene derivative has been over reduced affording complex mixtures. After a first purification the mixtures were not separated and we abandoned this route.

The other approach tested in this work is the in hydrogenation with H_2 gas, as suggested in the literature[43]. The reaction was conducted in ethanol with 10% Pd/C (0.28 eq. of palladium) as catalyst in a presence of H_2 gas at 0.4 bar. After four hours, the starting material was still present so the reaction was left 48 hours under H_2 atmosphere and rapid stirring. Standard work-up followed by preparative TLC (ethyl acetate/cyclohexane 2:8) afforded an unknown product. Characterization by NMR spectroscopy did not help in the identification of the product; high resolution mass spectroscopy is in progress during the redaction of the manuscript. The reaction was also carried out in similar conditions but for a shorter time. The reaction was conducted in ethanol with 10% Pd/C (1.4 eq.) as catalyst in a presence of H_2 gas at ambient pressure. After 6 hours the starting materials was still present but in smaller quantity. Standard work-up, followed by preparative TLC (ethyl acetate/dichloromethane/cyclohexane 1:3:6) afforded the same product as in the previous case (reduction with H_2 gas at 0.4 bar) and starting material. Therefore we can deduce that when

the reduction is carried out with H_2 gas the reaction afford one product which characterization is still in progress.

Finally, in already mentioned paper[39], E. Quesada and coworkers used H_2 under pressure (10 bar) for 16 hours in presence of PtO_2 (yield of 31%). After the results obtained with H_2 gas at ambient pressure, we did not follow this route because we estimated the conditions too harsh for our substrate.

Entry	Method	Yield	Ref.
1a	TES+10% Pd/C (23% by weight) in MeOH	27%	Ref.[44]
1b	TES+10% Pd/C (23% by weight) in MeOH overnight (several adds)	Approx. 24%	Ref.[44]
1c	TES+10% Pd/C (23% by weight) in MeOH for 2 days; TES added by dropping funnel	3%	Ref.[44]
2	$Pd_2(dba)_3$ and Cy_3P (5% and 20% resp.) in dioxane and aq. formic acid (6 eq.)	/	Ref.[45]
3	Nickel-Raney® in THF for 3 hours	/	Ref.[39]
4a	H_2 gas at P 0.4 bar for 48 hours	/	Ref.[43]
4b	H_2 gas at P amb. for 6 hours	/	Ref.[43]

Table 2.8 Summary table of tested reduction reaction on molecule **15** (the yield is referred to the target molecule).

At the moment of the redaction of this manuscript the molecule was not completed and the work will be pursed in order to afford the target molecule **18**.

Step c) Once the molecule is obtained, the following step will be bromination as reported in literature[48–50], using dichloromethane as solvent (less toxic than carbon tetrachloride often used for this reaction).

Step d) Finally deprotection of molecule **17** will be carried out with lithium oxide in water, followed by acidification step, as already carried out for the previous molecules (molecules **5** and **10**).

Method B

As already mentioned, we simultaneously started a second method in order to easily recover target molecule **15**. From the latter, the pathway is the same of route A.

The synthesis *via* method B is reported below in Figure 2.38. However, as we optimized with satisfactory results of the first steps of method A, we did not continue with this route.

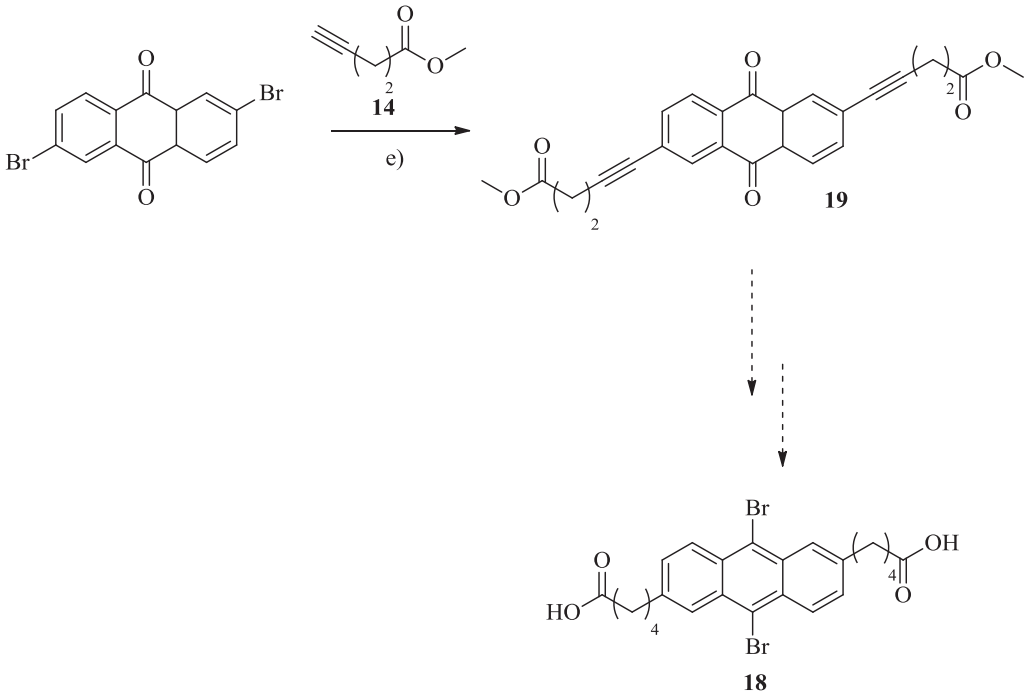

Figure 2.38 Reaction path B for the target molecule **18**. Conditions: e) **14**, $Pd(PPh_3)_3Cl_2$ (10%), CuI (10%), Et_2NH, reflux, 24h, 85%.

Step e) to g)

Step e) Double Sonogashira coupling reaction was carried out on 2,6-dibromoanthraquinone substrate as reported in the literature for a similar substrate[46] to afford molecule **19**. The reaction conditions were: $[Pd(PPh_3)_2Cl_2]$/CuI (0.10:0.10) in diethylamine ($NHEt_2$). Standard work-up followed by column chromatography (ethyl acetate/cyclohexane 3:7) afforded molecule **19** with 85% yield.

Molecule **19** was hydrogenated in order to obtain the dihydroanthracene core derivative, as reported in the literature for similar substrate[51]. Molecule **19** was heated to reflux for 5 days in the dark in presence of aqueous hydroiodic acid (HI) (47% by weight) and glacial acetic acid. Standard work-up and preparative TLC purification (ethyl acetate/cyclohexane 3:7) followed the reaction. However the reaction conditions were too harsh and the anthraquinone derivative has been completely degraded.

As the first route afforded the intermediate molecule (**15**) with satisfactory yield we did not continue this route.

2.5.2.3 Characterization

Molecules **15**, **16** and **19** are not known in the literature and have been characterized by multinuclear (^{1}H and ^{13}C) mono and bidimentional NMR spectroscopy and high-resolution mass spectroscopy.

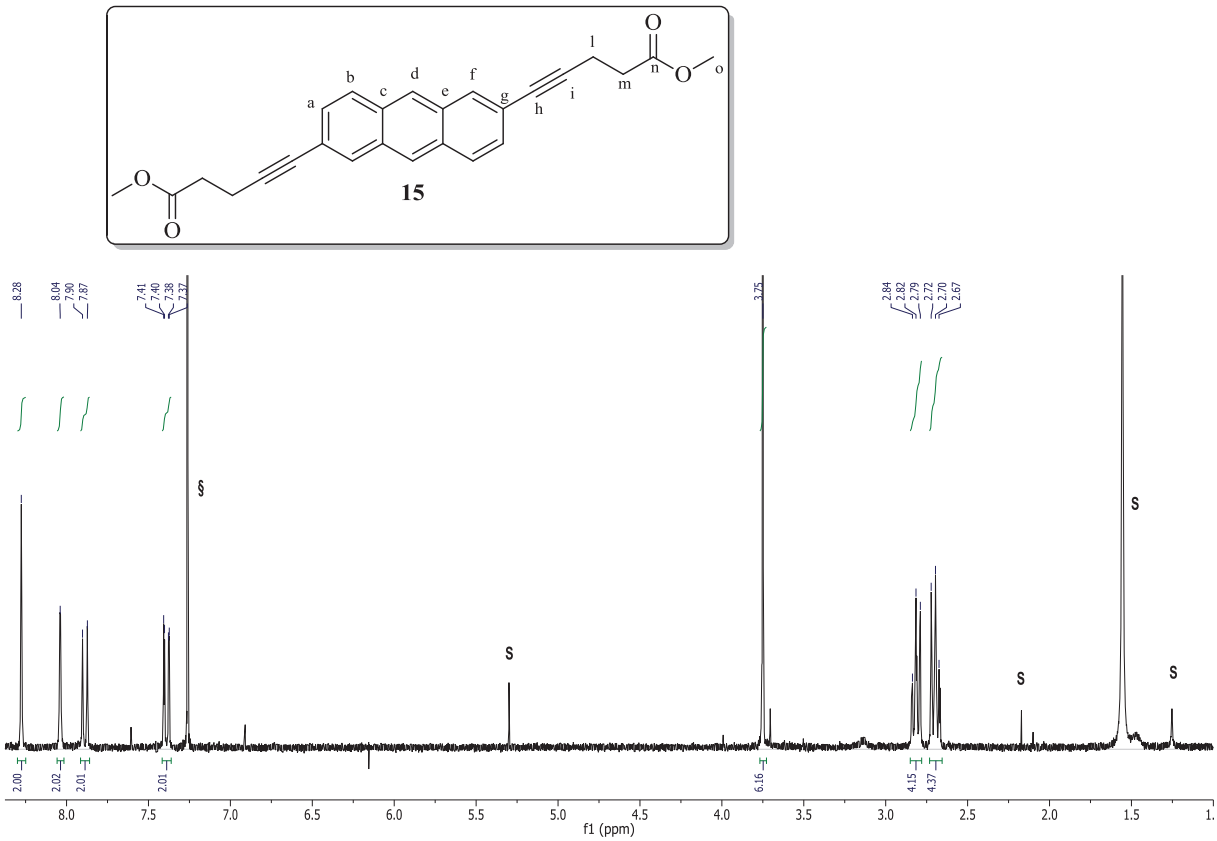

Figure 2.39 ^{1}H Spectra of molecule **15**. Signals marked with "S" at 5.30, 2.17, 1.55 and 1.2 ppm are dichloromethane, acetone, water and grease respectively; signal marked with "§" is $CDCl_3$.

	H_a	H_b	H_d	H_f	H_l	H_m	H_o
δ_H **(ppm)**	*7.40*	*7.90*	8.28	8.04	2.83	2.70	3.75

Table 2.9 ^{1}H NMR chemical shift of molecule **15**. The chemical shift of H_a and H_b cannot be assigned with certitude.

	H_a	H_b
^{3}J **(Hz)**	9	9
^{4}J **(Hz)**	3	-

Table 2.10 *J* values of molecule **15**.

Bidimentional experiments (HSQC and HMBC) allowed the attribution of the carbon spectra (not reported) for almost all the signals. However the proton signals at 7.90 and 7.40

ppm cannot be assigned with certitude. The assignation proposed here is in agreement with similar molecules in literature.

	C_a	C_b	C_c	C_e	C_d	C_f	C_g
δ_C (ppm)	*128.6 or 128.5*	*128.6 or 128.5*	*131.7 or 131.2*	*131.7 or 131.2*	126.3	131.8	120.9

Table 2.11 ^{13}C NMR chemical shift of molecule **15** (from C_a to C_g). The chemical shift of C_a, C_b or C_c and C_e cannot be assigned with certitude.

	C_h	C_i	C_l	C_m	C_n	C_o
δ_C (ppm)	82.1	89.5	15.9	33.8	172.7	52.2

Table 2.12 ^{13}C NMR chemical shift of molecule **15** (from C_h to C_o).

High resolution mass spectroscopy (DCI/CH_4) confirms the product (molecule **15**), showing a molecular peak at m/z 398.1534 (calculated mass: 398.1518).

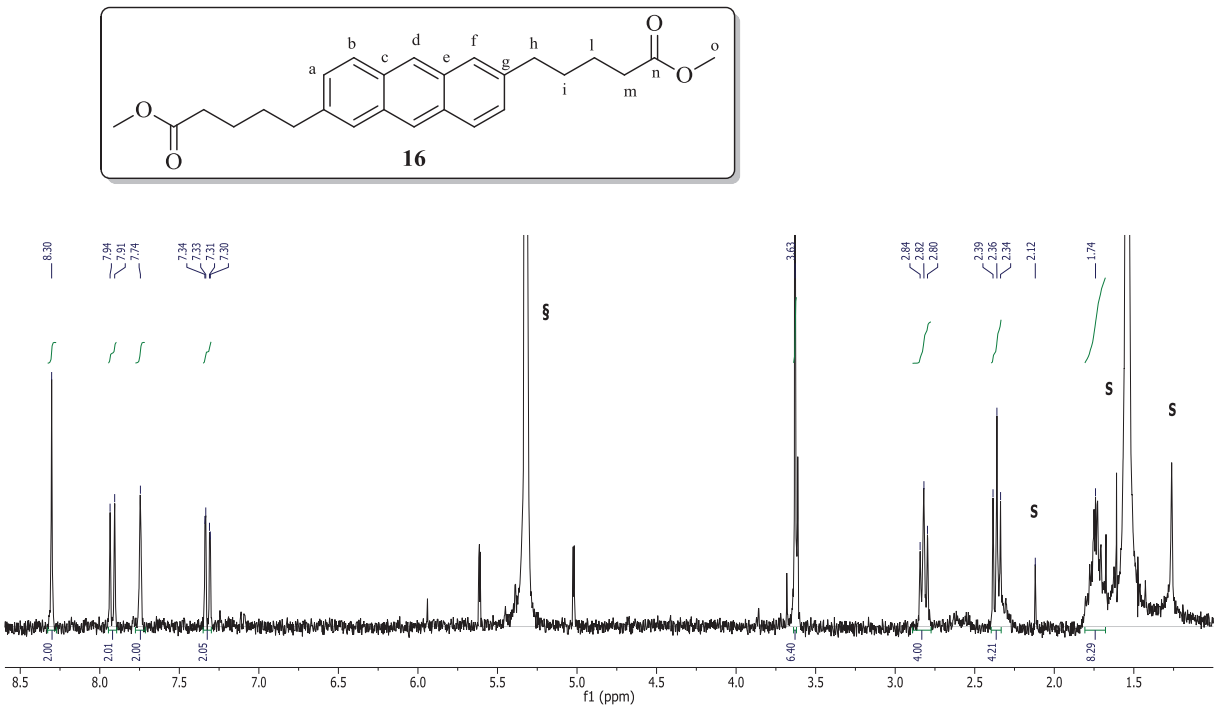

Figure 2.40 1H spectra of molecule **16**. Signals marked with "S" at 2.12, 1.52 and 1.26 ppm are acetone, water and grease respectively; signal marked with "§" is CD_2Cl_2.

	H_a	H_b	H_d	H_f	H_h	H_{i-l}	H_m	H_o
δ_H (ppm)	*7.32*	*7.92*	8.30	7.74	2.82	1.69-1.79	2.36	3.63

Table 2.13 ^{1}H chemical shift of molecule **16**. The chemical shift of H_a and H_b cannot be assigned with certitude.

	H_a	H_b
^3J **(Hz)**	9	9
^4J **(Hz)**	3	-

Table 2.14 *J* values of molecule **16**.

The bidimentional experiments (HSQC and HMBC) allowed the attribution of the carbon spectra for almost all the signals. As in the previous case, the proton signals at 7.92 and 7.32 ppm cannot be assigned with certitude. Here we assigned by analogy to the previous molecule. The assignation is in agreement with similar molecules in literature.

	C_a	C_b	C_c	C_e	C_d	C_f	C_g
δ_C **(ppm)**	*128.3 or 127.7*	*128.3 or 127.7*	*131.9 or 131.2*	*131.9 or 131.2*	126.2	125.4	139.6

Table 2.15 ^{13}C chemical shift of molecule **16** (from C_a to C_g). The chemical shift of C_a, C_b or C_c and C_e cannot be assigned with certitude.

	C_h	C_i	C_l	C_m	C_n	C_o
δ_C **(ppm)**	36.2	30.8	25.0	34.2	174.2	51.7

Table 2.16 ^{13}C chemical shift of molecule **16** (from C_h to C_o).

High resolution mass spectroscopy (DCI/CH_4) confirms the product (molecule **16**), showing a molecular peak at m/z 407.2226 for the protonated form (calculated mass 407.2222).

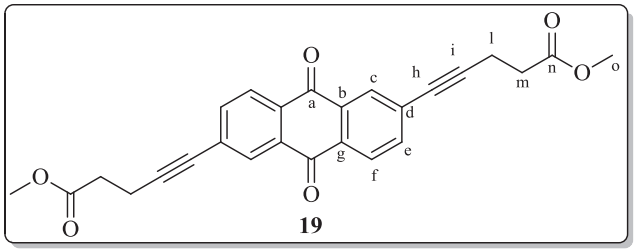

19

	H_c	H_e	H_f	H_l	H_m	H_p
δ_H **(ppm)**	8.21	7.71	8.17	2.78	2.66	3.73

Table 2.17 ^{1}H chemical shift of molecule **19**.

	H_e
^3J (Hz)	10
^4J (Hz)	5

Table 2.18 *J* values of molecule **19**.

	C_a	C_b	C_c	C_d	C_e	C_f	C_g
δ_C (ppm)	182.0	133.4	130.3	132.1	136.8	127.4	130.1

Table 2.19 ^{13}C chemical shift of molecule **19** (from C_a to C_g).

	C_h	C_i	C_l	C_m	C_n	C_o
δ_C (ppm)	80.2	93.8	15.6	33.2	172.2	52.1

Table 2.20 ^{13}C chemical shift of molecule **19** (from C_h to C_o).

As the previous molecules, mono and bidimentional NMR spectra allowed the attribution of the signals. The attribution is in agreement with similar molecules in literature.

High resolution mass spectroscopy (DCI/CH_4) confirms the product (molecule **19**), showing a molecular peak at m/z 429.1349 of the protonated form (calculated mass 429.1338).

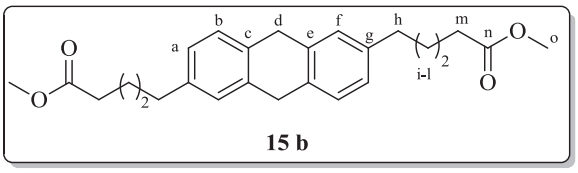

15 b

	H_a	H_b	H_d	H_f	H_h	H_{i-l}	H_m	H_o
δ_H (ppm)	*7.19 or 6.98*	*7.19 or 6.98*	3.87	7.09	2.60	1.66	2.33	3.66

Table 2.21 ^{1}H chemical shift of molecule **15 b**. The chemical shift of H_a and H_b cannot be assigned with certitude.

	C_a	C_b	C_c	C_d	C_e	C_f	C_g
δ_C (ppm)	*127.4 or 126.2*	*127.4 or 126.2*	*136.9 or 134.3*	35.9	*136.9 or 134.3*	127.5	140.0

Table 2.22 ^{13}C chemical shift of molecule **15 b** (from C_a to C_g). The chemical shift of C_a, C_b or C_c and C_e cannot be assigned with certitude.

	C_h	C_{i-l}	C_m	C_n	C_o
δ_C **(ppm)**	35.3	31.2 and 24.7	34.1	174.3	51.6

Table 2.23 ^{13}C chemical shift of molecule **15 b** (from C_h to C_o).

As we already mentioned, we obtained as side product of the reduction reaction of molecule **15** (Figure 2.35, reaction b), the dihydroanthracene derivative (molecule **15 b**). Even if very instable due to its sensibility to air and light, we managed to characterize with mono and bidimentional NMR spectra. As for the previous cases, some signals cannot be assigned with certitude. The assignation is in agreement with similar molecules in the literature.

2.5.3 Conclusion

In this section we presented the synthesis of anthracene molecule in order to obtain the graphene nanoribbon on calcite surface. With this purpose, first we synthesized an intermediate molecule (molecule **15**). This was obtained with satisfactory results by double Sonogashira coupling reaction on anthracene core. We also investigated a second method (method B) to obtain this key intermediate. Then, in order to reduce the triple bond we studied different reduction reactions with several methods (triethylsilane, formic acid, Raney- Nickel® and hydrogenation with H_2 gas). A complete characterization (mono and bidimentional NMR spectra and high resolution mass spectroscopy) was carried out on the molecules not already described in the literature. Further studies will be carried on in order to optimize the reduction and complete the final product (molecule **18**) by bromination and deprotection steps.

2.6 General conclusion

In this chapter we presented the synthesis of four families of molecules for coupling reactions on calcite in UHV conditions. Investigation of this new stimulating field of study might pave the way for future applications in molecular electronics.

This exploratory work leads us to study four different types of reactions with particular properties. First we synthesized molecules for homocoupling reactions on calcite surface. Then, we focused on the synthesis of the analogous dimers for photopolymerization reaction on surface. We continued the study with the synthesis of cyanonaphthalene derivative for polycondensation reaction in order to obtain phthalocyanine network. Finally we concluded the work with the study of anthracene derivative in order to reproduce the Ullmann reaction on calcite. The molecules studied were synthetized with standard organic

routes and are being studied by nc-AFM by A. Kühnle's group in Germany. Characterization by NMR and mass spectroscopy of the molecules completed the work. In addition to this, some molecules were also used for MOFs.

2.7 References

1. Shao, M. & Zhao, Y. TTFAQ-cored D/A ensembles: synthesis, electronic properties, and redox responses to transition metal ions. *Tetrahedron Lett.* **51,** 2892–2895 (2010).
2. Feng, Y.-S., Xie, C.-Q., Qiao, W.-L. & Xu, H.-J. Palladium-Catalyzed Trifluoroethylation of Terminal Alkynes with 1,1,1-Trifluoro-2-iodoethane. *Org. Lett.* **15,** 936–939 (2013).
3. Niamnont, N., Siripornnoppakhun, W., Rashatasakhon, P. & Sukwattanasinitt, M. A Polyanionic Dendritic Fluorophore for Selective Detection of Hg2+ in Triton X-100 Aqueous Media. *Org. Lett.* **11,** 2768–2771 (2009).
4. Zanotti, G. *et al.* Synthesis of a novel unsymmetrical Zn(II) phthalocyanine bearing a phenyl ethynyl moiety as sensitizer for dye-sensitized solar cells. *Dalton Trans.* **40,** 38–40 (2010).
5. Fasina, T. M. *et al.* Synthesis, optical properties, crystal structures and phase behaviour of symmetric, conjugated ethynylarene-based rigid rods with terminal carboxylate groups. *J. Mater. Chem.* **15,** 690–697 (2005).
6. Siemsen, P., Livingston, R. C. & Diederich, F. Acetylenic Coupling: A Powerful Tool in Molecular Construction. *Angew. Chem. Int. Ed.* **39,** 2632–2657 (2000).
7. Liu, Q. & Burton, D. J. A facile synthesis of diynes. *Tetrahedron Lett.* **38,** 4371–4374 (1997).
8. Hattori, T., Kijima, M. & Shirakawa, H. Oxidative polycondensation of acetylene by iodine in the presence of a palladium-copper catalyst. *Synth. Met.* **84,** 357–358 (1997).
9. Han, S. *et al.* A single-crystalline microporous coordination polymer with mixed parallel and diagonal interpenetrating α-Po networks. *CrystEngComm* **13,** 4838–4840 (2011).
10. Bischoff, A., Subramanya, H., Sundaresan, K., Sammeta, S. & Vaka, A. Novel Piperazine Derivatives as Inhibitors of Stearoyl-Coa Desaturase. (2008). at <WO2008157844 (A1)>
11. Jones, L. F. *et al.* Tuning magnetic properties using targeted structural distortion: New additions to a family of Mn6 single-molecule magnets. *Inorganica Chim. Acta* **361,** 3420–3426 (2008).
12. Meng, J.-P. *et al.* Metal–organic frameworks based on rigid ligands as separator membranes in supercapacitor. *Dalton Trans* **44,** 5407–5416 (2015).
13. Tranchemontagne, D. J. *et al.* Hydrogen Storage in New Metal–Organic Frameworks. *J. Phys. Chem. C* **116,** 13143–13151 (2012).
14. Britt, D., Tranchemontagne, D. & Yaghi, O. M. Metal-organic frameworks with high capacity and selectivity for harmful gases. *Proc. Natl. Acad. Sci.* **105,** 11623–11627 (2008).
15. Zheng, M.-X., Gao, X.-J., Zhang, C.-L., Qin, L. & Zheng, H.-G. Assembly of various degrees of interpenetration of Co-MOFs based on mononuclear or dinuclear cluster units: magnetic properties and gas adsorption. *Dalton Trans* **44,** 4751–4758 (2015).
16. Prock, A., Shand, M. L. & Chance, R. R. Solid-state photopolymerization of diacetylenes. *Macromolecules* **15,** 238–241 (1982).
17. Vinod, T. P., Chang, J. H., Kim, J. & Rhee, S. W. Self-Assembly and Photopolymerization of Diacetylene Molecules on Surface of Magnetite Nanoparticles. *Bull. Korean Chem. Soc.* **29,** 799 – 804 (2008).

18. Okawa, Y., Akai-Kasaya, M., Kuwahara, Y., Mandal, S. K. & Aono, M. Controlled chain polymerisation and chemical soldering for single-molecule electronics. *Nanoscale* **4,** 3013–3028 (2012).
19. Bässler, H. in *Polydiacetylenes* (ed. Cantow, H.-J.) **63,** 1–48 (Springer-Verlag, 1984).
20. Offermann, D. A. *et al.* Synthesis and Incorporation into Cyclic Peptides of Tolan Amino Acids and Their Hydrogenated Congeners: Construction of an Array of A–B-loop Mimetics of the Cε3 Domain of Human IgE. *J. Org. Chem.* **77,** 3197–3214 (2012).
21. Austin, W. B., Bilow, N., Kelleghan, W. J. & Lau, K. S. Y. Facile synthesis of ethynylated benzoic acid derivatives and aromatic compounds via ethynyltrimethylsilane. *J. Org. Chem.* **46,** 2280–2286 (1981).
22. Merkul, E., Urselmann, D. & Müller, T. J. J. Consecutive One-Pot Sonogashira–Glaser Coupling Sequence – Direct Preparation of Symmetrical Diynes by Sequential Pd/Cu Catalysis. *Eur. J. Org. Chem.* **2011,** 238–242 (2011).
23. Vilhelmsen, M. H., Jensen, J., Tortzen, C. G. & Nielsen, M. B. The Glaser–Hay Reaction: Optimization and Scope Based on 13C NMR Kinetics Experiments. *Eur. J. Org. Chem.* **2013,** 701–711 (2013).
24. Matsubara, H. *et al.* Syntheses of Novel Fullerene Tweezers and Their Supramolecular Inclusion Complex of C₆₀. *Chem. Lett.* **27,** 1099–1100 (1998).
25. Bleisch, T. J., Doti, R. A., Pfeifer, L. A. & Norman, B. H. Dihydropyrido Pyrimidine Compounds as Autotaxin Inhibitors. (2014). at <WO2014168824 (A1)*>
26. Lever, A. B. P. *et al.* Recent studies in phthalocyanine chemistry. *Pure Appl. Chem.* **58,** (1986).
27. McKeown, N. B. Phthalocyanine-containing polymers. *J. Mater. Chem.* **10,** 1979–1995 (2000).
28. Wöhrle, D. Phthalocyanines in Macromolecular Phases - Methods of Synthesis and Properties of the Materials. *Macromol. Rapid Commun.* **22,** 68–97 (2001).
29. Abel, M., Clair, S., Ourdjini, O., Mossoyan, M. & Porte, L. Single Layer of Polymeric Fe-Phthalocyanine: An Organometallic Sheet on Metal and Thin Insulating Film. *J. Am. Chem. Soc.* **133,** 1203–1205 (2011).
30. Dini, D. *et al.* Nonlinear Transmission of a Tetrabrominated Naphthalocyaninato Indium Chloride. *J. Phys. Chem. B* **110,** 12230–12239 (2006).
31. Dubinina, T. V. *et al.* Synthesis and investigation of spectral and electrochemical properties of alkyl-substituted planar binuclear phthalocyanine complexes sharing a common naphthalene ring. *Inorganica Chim. Acta* **363,** 1869–1878 (2010).
32. Koelsch, C. F. & Whitney, A. G. THE ROSENMUND-von BRAUN NITRILE SYNTHESIS [1]. *J. Org. Chem.* **06,** 795–803 (1941).
33. Xu, W., Xu, Q. & Li, J. Sandmeyer cyanation of arenediazonium tetrafluoroborate using acetonitrile as a cyanide source. *Org Chem Front* **2,** 231–235 (2015).
34. Zanon, J., Klapars, A. & Buchwald, S. L. Copper-Catalyzed Domino Halide Exchange-Cyanation of Aryl Bromides. *J. Am. Chem. Soc.* **125,** 2890–2891 (2003).
35. Cristau, H.-J., Cellier, P. P., Spindler, J.-F. & Taillefer, M. Highly Efficient and Mild Copper-Catalyzed N- and C-Arylations with Aryl Bromides and Iodides. *Chem. - Eur. J.* **10,** 5607–5622 (2004).
36. Cristau, H.-J., Ouali, A., Spindler, J.-F. & Taillefer, M. Mild and Efficient Copper-Catalyzed Cyanation of Aryl Iodides and Bromides. *Chem. - Eur. J.* **11,** 2483–2492 (2005).
37. Cai, J. *et al.* Atomically precise bottom-up fabrication of graphene nanoribbons. *Nature* **466,** 470–473 (2010).
38. Shimotahira, H., Fusazaki, S., Ikeda, I. & Ozoe, Y. A photoreactive probe that differentiates the binding sites of noncompetitive GABA receptor antagonists. *Bioorg. Med. Chem. Lett.* **21,** 1598–1600 (2011).

39. Quesada, E. *et al.* Synthesis and Fluorescence Properties of Novel Transmembrane Probes and Determination of Their Orientation within Vesicles. *Helv. Chim. Acta* **83,** 2464–2476 (2000).
40. Saito, M., Nakano, Y. & Nakamura, H. Compound for organic thin-film transistor and organic thin-film transistor using the compound. (2013). at <http://www.google.com.ar/patents/US8513654>
41. Khanna, B., Parkin, S. R. & Revell, K. D. 2,6-Diarylethynylanthracenes: synthesis, morphology, and electro-optical properties. *Tetrahedron Lett.* **53,** 6383–6387 (2012).
42. Kim, S.-O. *et al.* Organic semiconductor based on phenylethynyl end-capped anthracene. *Thin Solid Films* **519,** 7998–8002 (2011).
43. Espacenet - Bibliographic data. at <http://worldwide.espacenet.com/publicationDetails/biblio?CC=WO&NR=2010096462A1&KC=A1&FT=D>
44. Mandal, P. K. & McMurray, J. S. Pd−C-Induced Catalytic Transfer Hydrogenation with Triethylsilane. *J. Org. Chem.* **72,** 6599–6601 (2007).
45. Shen, R. *et al.* Facile Regio- and Stereoselective Hydrometalation of Alkynes with a Combination of Carboxylic Acids and Group 10 Transition Metal Complexes: Selective Hydrogenation of Alkynes with Formic Acid. *J. Am. Chem. Soc.* **133,** 17037–17044 (2011).
46. Seki, M. & Matsumoto, K. A novel approach to homochiral β-amino acids. *Tetrahedron Lett.* **37,** 3165–3168 (1996).
47. Handa, N. V., Mendoza, K. D. & Shirtcliff, L. D. Syntheses and Properties of 1,6 and 1,7 Perylene Diimides and Tetracarboxylic Dianhydrides. *Org. Lett.* **13,** 4724–4727 (2011).
48. Cakmak, O., Erenler, R., Tutar, A. & Celik, N. Synthesis of New Anthracene Derivatives. *J. Org. Chem.* **71,** 1795–1801 (2006).
49. Wang, J. *et al.* C-9 Fluorenyl Substituted Anthracenes: A Promising New Family of Blue Luminescent Materials. *Org. Lett.* **12,** 3874–3877 (2010).
50. Lee, A. E., Grace, M. R., Meyer, A. G. & Tuck, K. L. Fluorescent Zn2+ chemosensors, functional in aqueous solution under environmentally relevant conditions. *Tetrahedron Lett.* **51,** 1161–1165 (2010).
51. Athans, A. J., Briggs, J. B., Jia, W. & Miller, G. P. Hydrogen-protected acenes. *J. Mater. Chem.* **17,** 2636 (2007).

3. Preparation of $CaCO_3$ particles for solid state reaction

3.1 Calcium carbonate 78
3.1.1 Calcium carbonate characteristics and properties 78
3.1.2 Calcium carbonate formation 80
3.1.3 Historical background 80
3.1.3.1 Calcium carbonate as construction material 81
3.1.4 Modern uses and production 82
3.2 Preparation methods of $CaCO_3$ particles 83
3.3 Preparation of calcium carbonate microparticles 85
3.3.1 Specific surface for coupling reaction on $CaCO_3$ particles 86
3.3.1.1 Results and discussion 86
3.3.2 $CaCO_3$ particles by grinding 87
3.3.2.1 Results and discussion 87
3.3.2.2 Conclusion on $CaCO_3$ by grinding 89
3.3.3 $CaCO_3$ particles *via* spray pyrolysis technique 89
3.3.3.1 Results and discussion 90
3.3.3.2 Conclusion on $CaCO_3$ particles *via* spray pyrolysis technique 110
3.3.4 General conclusion on preparation of $CaCO_3$ particles for solid state reaction 110
3.4 References 110

In the second part of this work, we decided to extend the results obtained in UHV conditions on macroscopic scale. Reactions directly on $CaCO_3$ microparticles were investigated in order to easily recover the final molecule by simply dissolution of the substrate. This approach is technically impossible under UHV conditions. Once the target

molecules are recovered, they are easily analyzed with standard methods (NMR and mass spectroscopy), while under UHV conditions this investigation is more restricted (Figure 3.1).

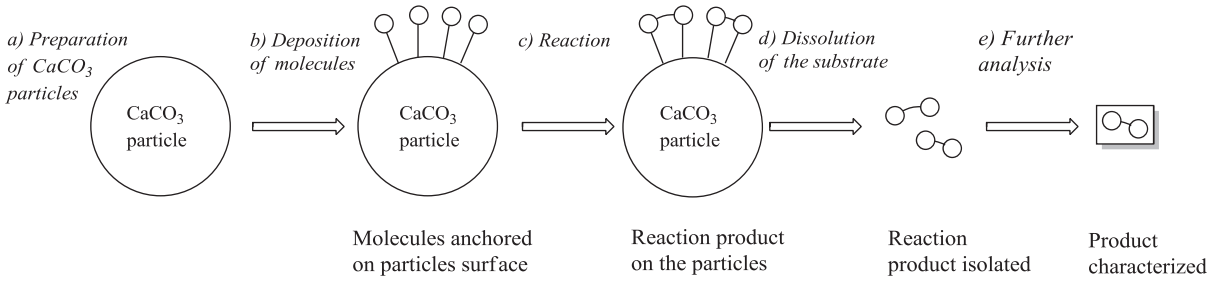

Figure 3.1 Coupling reactions on $CaCO_3$ particles.

In this work we decided to prepare calcium carbonate particles with control of characteristics including size, morphology, and composition. Once the particles are prepared, they will be used for solid state coupling reactions (chapter 4).

3.1 Calcium carbonate

3.1.1 Calcium carbonate characteristics and properties

Calcium carbonate is one of the most abundant mineral of the earth surface (more than 4%) and found in rocks, stalactites, stalagmites biological seashells, shells and bird eggs[1] and is the principal cause of water hardness.

In nature calcium carbonate is found as different polymorphs: calcite, vaterite, aragonite and amorphous calcium carbonate (ACC); however the latter is the most unstable form with short-life time that mainly acts as seed for the others forms crystal growth[2]. The polymorphs have different morphology and crystallographic structure: calcite has a rhombohedral morphology, vaterite spherical and aragonite rod-like (Figure 3.3); the crystallographic structures are reported in Table 3.1.

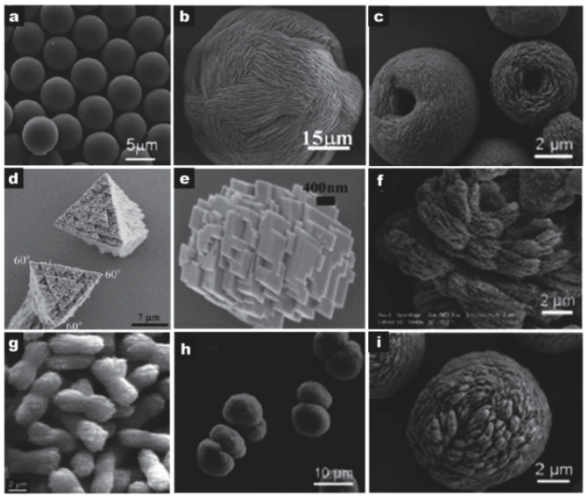

Figure 3.2 a-i) Different type of $CaCO_3$ particles. From ref.[2].

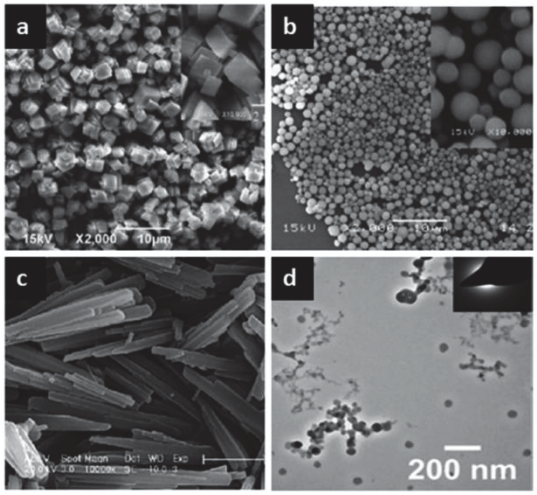

Figure 3.3 Different $CaCO_3$ polymorphs: a) calcite, rhombohedral; b) vaterite, spherical; c) aragonite, rod-like and d) ACC, seed. From ref.[2].

Calcite is the most stable and common polymorph of calcium carbonate[3]. Aragonite, that takes its name from the Spanish village Molina de Aragón, is less stable and it transforms to the calcite in geological times. For this reason it is less common than calcite and is usually found in shells[4]. Aragonite transforms to calcite by heating at 280-350 °C (partial) up to 400 °C (complete) for biogenic aragonite and 380-400 °C (partial) up to 450-470 °C (complete) for inorganic ones[5].

Additionally mechanical grinding causes the two phase transformation of $CaCO_3$ calcite to aragonite and then aragonite to calcite[6].

Vaterite (it takes the name from the German mineralogist Heinrich Vater) is the less stable polymorph and transforms to either calcite (at low temperature) or aragonite

(temperature below 400 °C)[7]. The characteristics of the three polymorphs are summarized in the following table.

	Calcite	**Aragonite**	**Vaterite**
Crystal system	Trigonal	Orthorhombic	Hexagonal
Stability	Stable	Unstable (→ calcite)	Less stable polymorph (→ calcite / aragonite)
Lattice parameter*	a = 4.983 c = 17.019	a = 4.94 b = 7.94 c = 5.72	a = 4.128 c = 8.573
Space group*	$R\bar{3}c$	Pmcn	P 6_3/mmc

Table 3.1 Polymorph of $CaCO_3$. The lattice parameter and space group (marked with *) are reported from PDF database 2004.

3.1.2 Calcium carbonate formation

Calcium carbonate is found mostly in calcite form: chalks, limestone (rock composed mainly by calcite and aragonite) and marbles[8]. The sedimentation is the most common process for those rocks. In a first stage eroded sediments fall down in water and with the time pressure or cementation consolidates these layers. Limestone derives mostly from organic marine organism sedimentation.

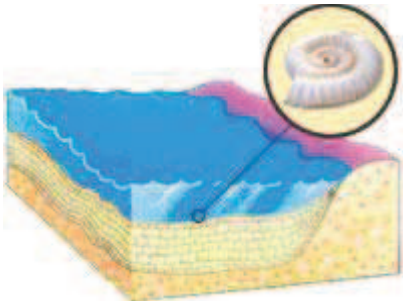

Figure 3.4 Figure representing the sedimentation process: calcium carbonate, present in skeletons of marine organisms, is consolidated with the time by pressure and cementation. From ref.[8].

3.1.3 Historical background

The first examples of human uses of calcium carbonate dates back to the prehistorically time (40,000 BC); in this epoch chalks and limestone powder were used in paintings.

In ancient time chalk was used for different fields such as in road construction or in cosmetics but, the most important development of this material came from the industrial revolution. The growing demand of house construction of this period increased the production of calcium carbonate (mainly as limewash or in paints).

In 1841 precipitated calcium carbonate (PCC) was produced and commercialized for the first time. Calcium carbonate started to be part of daily products such as toothpastes, detergents, paints and in the early 20th century as filler in plastic and rubbers.

In 1960's and 1970's was introduced in paper industry as filler paving the way for ground calcium carbonate (GCC) or precipitated calcium carbonate (PCC) large production[8].

3.1.3.1 Calcium carbonate as construction material

Since ancient time calcium carbonate was used as construction material. In fact one of the oldest description of production and use of lime is Vitruvius' "de Architectura" (13B.C.).

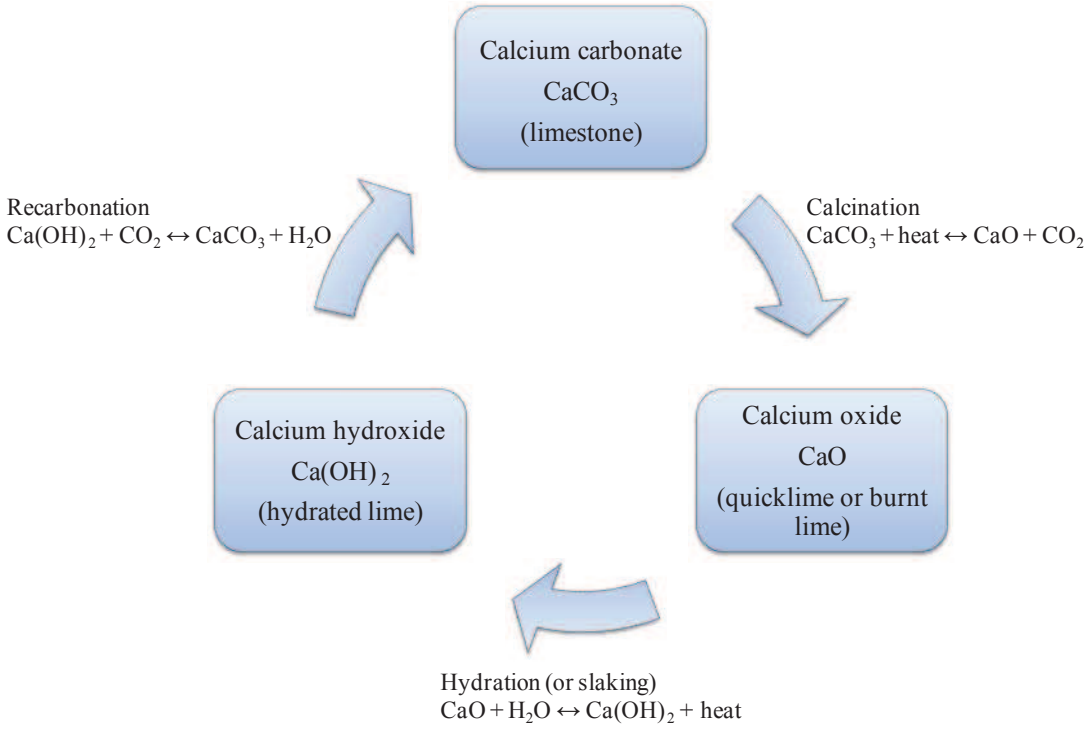

Figure 3.5 $CaCO_3$ life cycle.

The main steps of the cycle (Figure 3.5) are explained here below:

- Calcination: limestone is heated at high temperature in lime kiln (often heated up to 1200 °C) and it is decomposed into quicklime (CaO) and carbon dioxide (CO_2).
- Hydration: exothermic reaction that can occur in two different ways
  - Stoichiometric amount of water is added to obtain hydrated lime (fine powder).

- Excess of water (slaking process) to obtain hydroxide lime in slurry.

- Recarbonation: the last step of $CaCO_3$ life cycle, hydrated lime adsorbs CO_2 and reverts into $CaCO_3$.

The last step is particularly important when lime mortar (constituted of hydrated lime, sand and water) is used to paint the walls. Atmospheric CO_2 converts calcium hydroxide into calcium carbonate, hardening the building wall[9].

3.1.4 Modern uses and production

Today calcium carbonate has a key role in industry and everyday life. Indeed, it is used as filler in paints, coating and plastics[2]; in paper industry it is used for its brightness and light scattering properties. Finally calcium carbonate can be used in health and personal care or in the building field as itself (marble) as a constituent for cement.

Ground calcium carbonate (GCC) and precipitated calcium carbonate (PCC) are the most common industrial methods. In the first one, calcium carbonate is extracted from natural quarry, while in the other it is chemically synthesized from calcium oxide (obtained by calcination process). CaO is then slaked with water to obtain calcium hydroxide; finally $CaCO_3$ precipitates by recarbonation with CO_2. The uses of the two different methods are summarized in the table below.

	GCC	**PCC**
Production	Extraction	Chemical Precipitation
Uses	Filler: - Paper (mainly) - Plastic - Paint - Adhesives	Filler: - Cosmetic - Food/pharmaceuticals - Plastic - Paint/inks - Paper - Adhesives

Table 3.2 GCC in comparison to PCC methods: production and main uses.

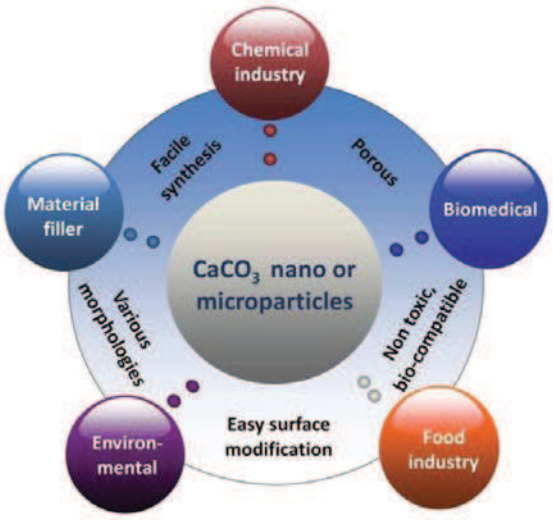

Figure 3.6 Schematic representation of different uses of $CaCO_3$ micro and nanoparticles, from ref.[2].

For its several uses, various studies have been conducted on calcium carbonate synthesis in different morphologies and sizes, as shown in picture above.

Calcite, in particularly, has caught the interest of some research for its possible implication in the origin of life[10–12]. Indeed, in a remarkable paper, Olme and coworkers showed that the modified macroscopic surface aspect of calcite reflects the chirality of the deposited molecules (L or D aspartic acid in their case). Additionally, when calcite is dissolved in aspartic acid solution, the crystals formed in this solution show adsorption and chiral selectivity of two different enantiomers on crystal surfaces[11,12]. These results show the necessity of deeper studies in order to investigate and try to answer to the fundamental questions of homochirality of life.

Recently more and more attention has been devoted to the synthesis of hollow $CaCO_3$ particles for application as drug carrier[13–16]. Several groups proposed different synthesis of $CaCO_3$ particles or assemblies, followed by loading with the anticancer drug doxorubicin (DOX). The *p*H difference between the normal tissue and the tumor tissue (more acidic) let the drug to be locally released[14,16].

3.2 Preparation methods of $CaCO_3$ particles

As calcium carbonate is a very common material, many techniques are known in order to produce it on laboratory scale[2,17].

The two most common methods of calcium carbonate synthesis are the biomimetic and the bubbling method[2]. The first involves the use of organic additives (surfactants for

instance) acting as template or growth modifier (without changing $CaCO_3$ properties) in order to obtain different size or morphology particles. The second, the bubbling method, is the most widespread industrial method[2].

The biomimetic method can be carried out in different ways: the precipitation method (spontaneous precipitation or slow carbonation) and the reverse emulsion method, as shown in Figure 3.7 (a-c). The spontaneous precipitation is obtained by mixing together solutions of additives and CO_3^{2-} and Ca^{2+} ions, while the slow carbonation involves the dissolution of gaseous CO_2 in order to obtain CO_3^{2-} ions (Figure 3.7 a and b respectively). The reverse (W/O) emulsion method consists in mixing together micelles containing the reagents and additives (Figure 3.7c)[2].

The bubbling method, the most common on large scale, uses as well some additives to prevent the common problem of particles aggregation. In this case limestone is used to produce aqueous solution of $Ca(OH)_2$. Then, CO_2 is bubbled into the latter in order to obtain $CaCO_3$ particles (Figure 3.7d)[2].

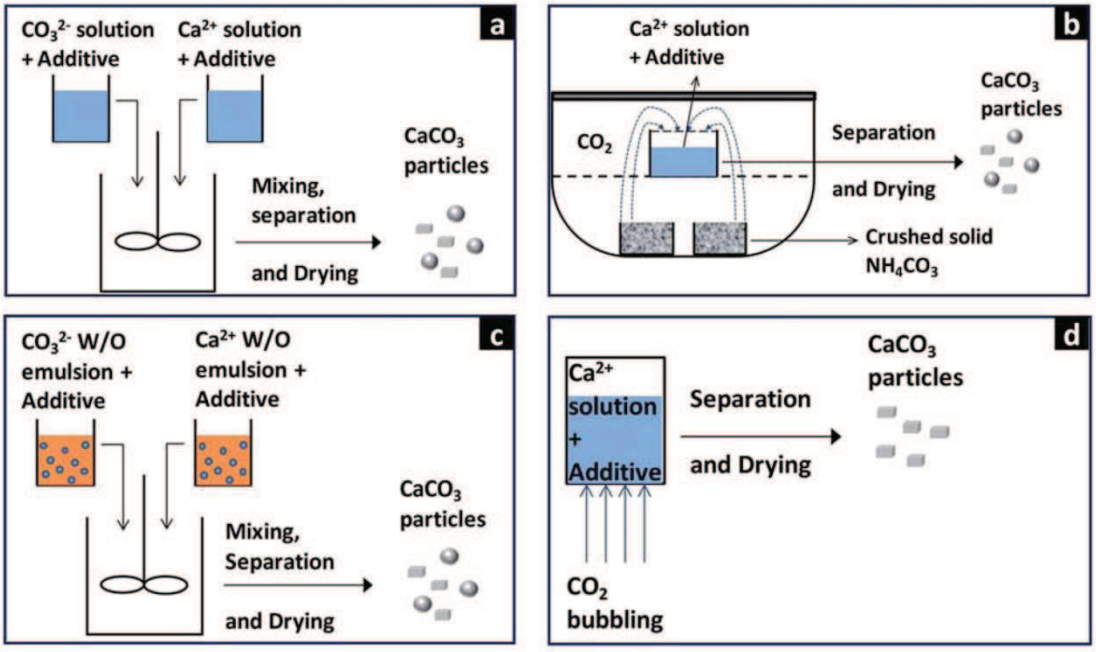

Figure 3.7 Synthesis methods for $CaCO_3$ particles, from ref.[2]. Biomimetic methods: a) spontaneous precipitation; b) slow carbonation and c) reverse emulsion method. Figure d) represents the second method: CO_2 bubbling.

Here we reported a summary table of the two most common methods.

	Biomimetic method	**CO_2 method**
$CaCO_3$ polymorph	Polymorphs ACC, calcite, vaterite and aragonite or mixture	Mainly calcite
Particle size	Both nano and micron size particles Monodispersed particles	Mainly nano size particles Additives necessary to avoid particles aggregation
Type of procedure	One-pot; Different parameters adjustables in order to obtain the desired particles; Reverse emulsion method allow higher reactant concentration inside the micelles	Industrial common method; Synthesis at high *p*H (due to the basic $Ca(OH)_2$); Low temperature synthesis (due to CO_2 solubility)
Uses	Different applications	Mainly industrial applications (filler for papers or paints and so on)

Table 3.3 Summary of main characteristics of the biomimetic and bubbling method for $CaCO_3$ production, readapted from ref.[2].

These methods involve the use of additives (to avoid aggregation) that might leave undesirable traces on particles surface.

Finally, we can just recall some alternatives method for the preparation of calcium carbonate particles: microwave or ultrasound assisted methods, alternating current methods, atomized microemulsion and spray drying methods[2].

In this thesis we developed a new way of preparation of calcite particles by spray pyrolysis technique from calcium acetate aqueous solution; we will detail this method in the next paragraph.

3.3 Preparation of calcium carbonate microparticles

This paragraph is devoted to the two approaches used in this work in order to prepare microparticles of calcium carbonate for solid state reactions.

In order to obtain milligram scale of final material, large specific surface is needed in order to increase the amount of molecules anchored to $CaCO_3$ surface. For this reason the first section described the problem of the specific surface in details (paragraph 3.3.1).

Then, the second section illustrates the first approach investigated in this work in order to obtain calcium carbonate microparticles: by grinding commercial calcium carbonate (paragraph 3.3.2).

The third section deals with the synthesis and complete characterization of calcium carbonate particles by spray pyrolysis technique (paragraph 3.3.3). The general conclusion (paragraph 3.3.4) closes this part.

3.3.1 Specific surface for coupling reaction on $CaCO_3$ particles

In this paragraph we present the estimation of the specific surface. First we evaluate the specific surface area from scanning electron microscopy (SEM) photos of commercial calcium carbonate, and then we estimate the specific surface area an ideal spherical or cubical particle of $CaCO_3$.

3.3.1.1 Results and discussion

3.3.1.1.1 Estimation of specific surface

Commercial $CaCO_3$ (grade of purity 99.99%, Sigma-Aldrich) was analyzed by SEM microscopy in order to evaluate the particles size (Figure 3.8). The product is formed by aggregates of small cubes of 20 μm of side. Having this result in mind, we estimate the specific surface area (SSA) by simply considering a sphere of 10 μm of radius or a cube of 20 μm of side.

$V_{sphere} = 4/3\ \pi r^3 = 4.188\ 10^{-9}\ cm^3$ $\qquad$ $V_{cube} = a^3 = 8\ 10^{-9}\ cm^3$

Volumetric mass density = 2.71 g/cm^3

$Weight_{sphere} = 1.13\ 10^{-8}\ g$ $\qquad$ $Weight_{cube} = 2.168\ 10^{-8}\ g$

$SSA_{sph.} = 1.1\ 10^3\ cm^2/g = 0.1\ m^2/g$ $\qquad$ $SSA_{cube} = 1.1\ 10^3\ cm^2/g = 0.1\ m^2/g$

To sum up, the specific surface of considered $CaCO_3$ leads to 0.1 m^2/g.

By knowing the area occupied from one molecule (for instance 4-iodobenzoic acid dimer) from the nc-AFM results (0.32 nm^2), we can deduce from the SSA previously calculated the quantity of final product (considering 100% yield): ~$1.5\ 10^{-4}$ g.

As we will show later with the BET measurement, this is a very rough approximation to a perfect spherical object with 100% of yield of the reaction.

From this result we conclude that the first step necessary for the coupling reaction is to increase the specific surface. The following parts will introduce the two different approaches used in this work to reach this objective.

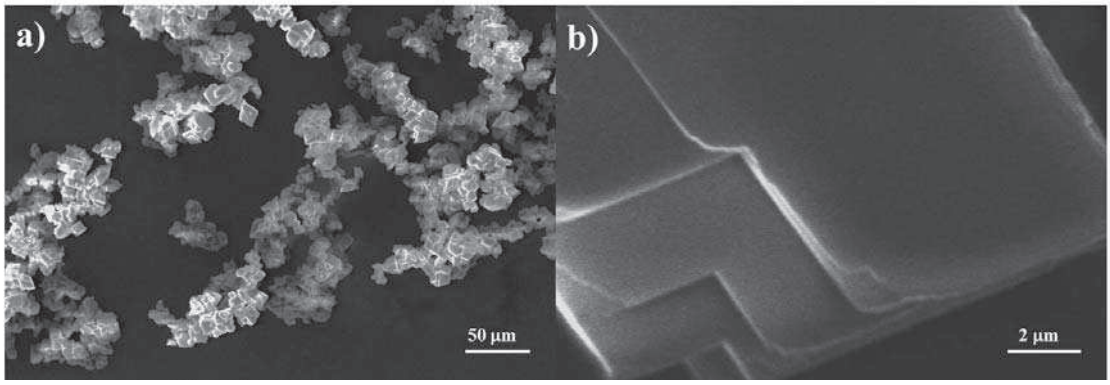

Figure 3.8 SEM images of commercial $CaCO_3$.

3.3.2 $CaCO_3$ particles by grinding

The first approach envisaged in this work, consisted into the preparation of calcium carbonate particles by grinding commercial product in a ball milling machine. Then we characterized these particles by SEM microscopy and BET analysis. This work was done in collaboration with D. Neumeyer (adsorption and BET measurements) from the CEMES laboratory, Toulouse.

3.3.2.1 Results and discussion

3.3.2.1.1 Grinding process

Commercial calcium carbonate was ground into a ball milling machine. The samples were placed in Al_2O_3 jars (45 mL) with 18 balls (10 mm Ø). The jars were filled up to 2/3 of the height with calcium carbonate. The number, the ball diameter and the speed (700 rpm) were maintained fixed, while the time was changed. After 15 minutes of milling (one cycle), the jars warmed up, and a pause was necessary to cool down the system. One to three cycles of 15 min were tested but it turns that there is no difference on the particles dimensions.

In a recent paper, Y. Chen and others analyzed the different effect of rotation speed, media density on particle size distribution and structure of ground calcium carbonate[18].

The authors showed that increasing the rotation speed (from 600 rpm to 1200 rpm) does not decrease the size of the particles, probably due to agglomeration process.

Additionally long grinding time of calcite could favor the two successive phase transitions to aragonite first and to calcite (as previously discussed) visible by XRD; in our case, in principle, it should not change the coupling reaction. Nevertheless, the XRD of

commercial calcium carbonate used in this work, shows the only presence of calcite polymorph even after 60 minutes of grinding treatment.

In the paper previously mentioned, the authors showed also the influence of the media in the grinding process. Passing from glass grinding media to zirconia (higher density media) afforded smaller particles (6.17 μm and 1.76 μm respectively). Finally the SEM images in this paper showed the formation of agglomerations during the grinding process.

Other experiments are in process during the redaction of this manuscript in order to analyze deeper the influence of the time of grinding.

3.3.2.1.2 Characterization

Ground calcium carbonate was analyzed by SEM microscopy. Here below are reported some images of the samples.

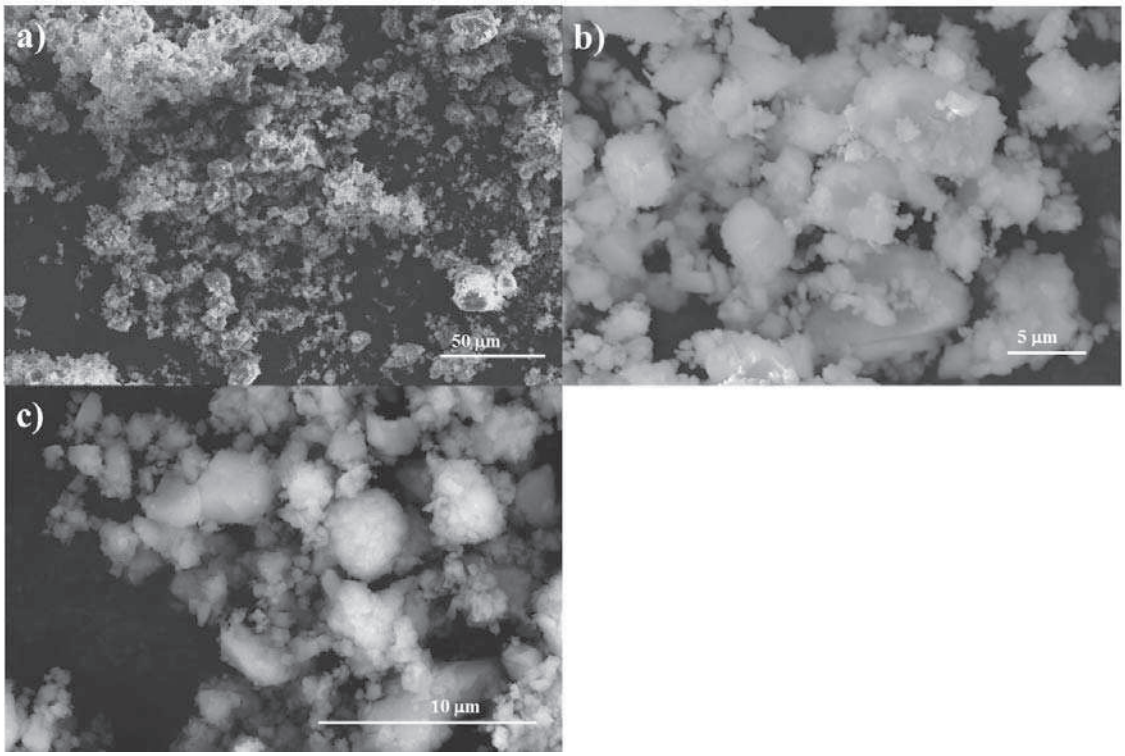

Figure 3.9 SEM images of commercial $CaCO_3$ after grinding.

The sample, as expected, is not completely homogenous, and it is formed by particles of 1-5 μm radius (values estimated from the images).

Ground commercial calcium carbonate was also analyzed by adsorption and BET experiments (the techniques are detailed in Annex). The adsorption isotherms describe the quantity of adsorbed gas on a surface at constant temperature. From the isotherms, the BET equation determines the surface area of the sample.

The measurements were recorded in order to identify the specific surface of calcium carbonate particles. The specific surface of calculated from the BET plot is $a_{S,BET} = 1.3$ (m^2/g).

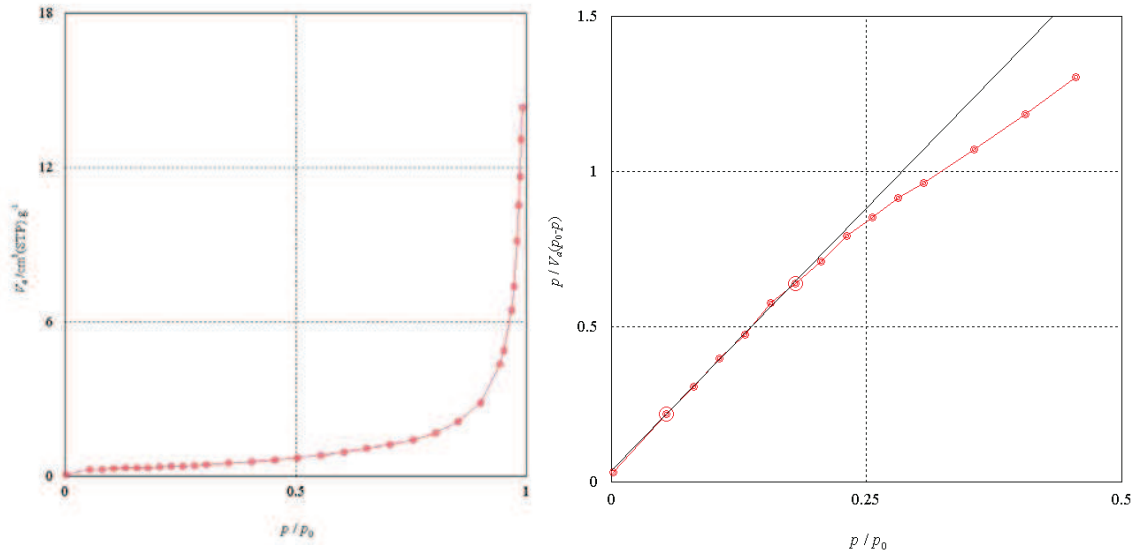

Figure 3.10 Adsorption and BET plot of ground commercial $CaCO_3$. Axes: x = relative pressure p/p_0; y = Va (Standard Temperature and Pressure conditions) for adsorption graph and $y = p/V_a(p_0-p)$ for BET plot.

3.3.2.2 Conclusion on $CaCO_3$ by grinding

The first approach studied in this work in order to improve the specific surface is to grind commercial calcium carbonate. This approach provides calcium carbonate particles with a radius (estimated from the SEM images) between 1-5 μm, specific surface of 1.27 (m^2/g). The grinding destroyed the aggregates, giving more surface accessibility. The ground samples are compatible with our purpose and can be used for the coupling reaction.

3.3.3 $CaCO_3$ particles *via* spray pyrolysis technique

The second approach envisages the synthesis of the calcium carbonate particles *via* spray pyrolysis technique.

The following section presents the synthesis *via* spray pyrolysis, followed by a first characterization (3.3.3.1.2) with IR, TG/DTA, XRD and SEM analysis. Then the purification of selected particles and the second characterization IR, TG/DTA, XRD and SEM conclude the section (3.3.3.1.3 and 3.3.3.1.4).

The work was done in collaboration with D. Neumeyer and Dr. N. Ratel-Ramond, both from CEMES laboratory, Toulouse.

3.3.3.1 Results and discussion

3.3.3.1.1 Synthesis of $CaCO_3$ particles

In this work we decided to use for the first time spray pyrolysis techniques for several reasons: low-cost process[17], simplicity[19], absence of additives in this technique and its availability in our laboratory.

The spray pyrolysis method has been widely studied and used to prepare numerous types of dense or hollow particles, nanoparticles (for instance below 100 nm)[20], multicomponent materials[17,19,21,22], thin films or fibers[20,22].

Spray pyrolysis has been developed at industrial scale by a spin-off from our laboratory named PYLOTE[23].

Spray pyrolysis technique presents several advantages such as the high purity of the final product, low-cost of the process and the possibility to obtain spherical micro and submicron particles with different morphology[24].

The principle of spray pyrolysis can be recalled here. A solution of an appropriate starting material is atomized into small droplets; then, those are transported into a drying zone by a carrier gas. Here the solvent is evaporated and the precursor precipitates. Finally the dry precipitated particles are decomposed in a furnace at appropriate temperature and recovered on a filter.

Many parameters can affect this process, leading to particles with different morphology. The precursor solution (and the stoichiometry of the dissolved salts) determines the composition of the final particles. The size of the atomized droplets and the starting solution concentration can affect the average size and distribution of the final product. In addition to the properties of the starting solution, the morphology of the final product is also influenced by the carrier gas flow rate and the temperature[17]. The residence time of the particle inside of the furnace is affected by the length of the furnace itself.

A variety of different particles can be obtained by modifying some parameters: for instance if the evaporation rate of the solvent is low and the solubility of the product is high, the particles obtained are dense (precipitation into the entire volume) and porous (due to the evaporation of the gas). However, if the evaporation rate is high and the solubility low, the precipitation occurs on the surface and the particles are hollow[25].

A typical spray pyrolysis apparatus consists of (Figure 3.11):

- The atomizer (or nebulizer) to convert the starting solution (for instance metal acetates or nitrates) into droplets.
- The carrier gas (or mixture of gases such as N_2 and H_2, for instance, to prevent oxidation of the materials) that transports the droplets.
- The tubular furnace or reactor (with a specific length) that might have different temperature levels.
- The sampler or precipitator (filter, electrostatic precipitator and so on).

Finally the particles are analyzed with different techniques[17].

As already mentioned the synthesis of inorganic particles *via* spray pyrolysis is often carried out by a starting solution of salt. In this work we focused on the thermal decomposition of calcium acetate:

$$Ca(CH_3CO_2)_2 \rightarrow CaCO_3 + C_3H_6O \quad \text{at 380-400 °C}$$

The decomposition of calcium acetate has been widely investigated in the past years[26–28]. The acetate decomposes at 380-400 °C giving $CaCO_3$ and acetone. The latter is then decomposed into allene or into hydrocarbon radicals[28]. In the past, the decomposition of acetone has been widely investigated in order to understand the mechanism and the possible products[29–34]. A free radical chain mechanism, proposed by Rice and others[30] is commonly accepted. Finally $CaCO_3$ starts to decompose into calcium oxide and carbon dioxide at ~650 °C[28]:

$$CaCO_3 \rightarrow CaO + CO_2 \quad \text{at } T > 650 \text{ °C}$$

The experimental set-up of the spray pyrolysis apparatus used in this work is showed in Figure 3.11. The solid piezoelectric pellet vibrates at 1.65 MHz and generates a spray of droplets transported into a column by a gas stream (air). In the drying zone those droplets are heated (at around 100 °C) and progressively dried in order to obtain spherical particles of the precursor salt by precipitation. Then those particles are transported in a furnace at appropriate temperature (in this work from 250 °C to 750 °C, as reported in Table 3.5) in order to decompose calcium acetate particles into calcium carbonate. Finally, the desired product is collected on an electrostatic filter constituted by two plates inside a quartz tube with a strong potential difference at around 20kV (DDp).

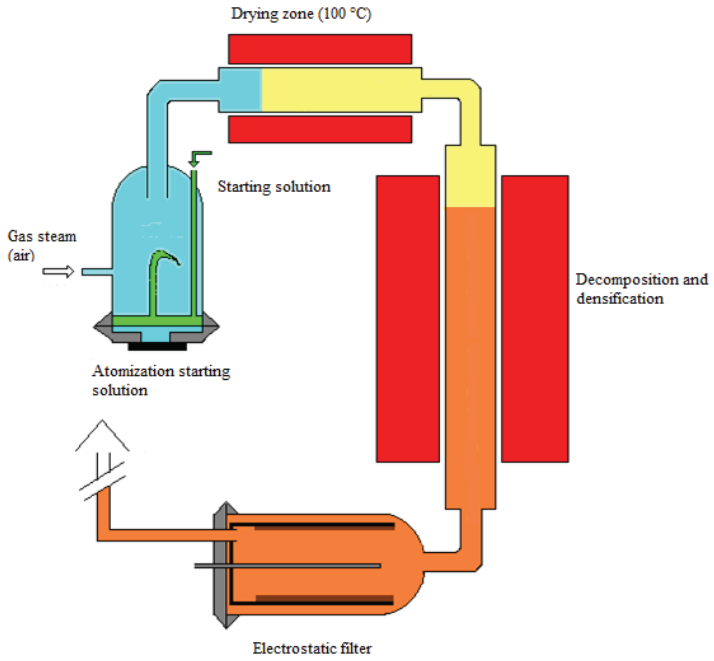

Figure 3.11 Spray pyrolysis system used in this work.

In this work we investigated a set of samples at different decomposition temperatures in order to find the best range for our study.

The table below shows the experimental parameters of the spray pyrolysis set-up. In this work they are constant for all samples.

Parameters	**Drying Z (°C)**	**Filter (°C)**	**Air Flow rate (l/h)**	**Fr (MHz)**	**Filtre (kV)**	**Calcium acetate content (% by weight)**
All samples	100	105	300	1.6	10	15%

Table 3.4 Experimental parameters of spray pyrolysis set-up in this work.

A new set of experiment with different parameters (such as air flow) are in progress at the moment of the redaction of this manuscript.

For clarity reason, in this manuscript the sample X obtained by spray pyrolysis at Y °C will be indicated as: sample X (SP at Y °C).

Sample	**1**	**2**	**3**	**4**	**5**	**6**	**7**	**8**
T (°C)	250	350	400	450	500	550	650	750

Table 3.5 Set of temperature investigated in this work.

On the other hand, the process has some inconvenients such as the high variation in size due to the coalescence of the particles, or the presence of calcium acetate residues in the final product (depending of the decomposition temperature of some samples).

To avoid coalescence, three main options have been proposed[35] in order to decrease particles collisions:

- Decrease the droplet concentration.
- Use parallel (to the drying column walls) gas flow.
- Use laminar regime flow.

The second inconvenient that we encountered in this work is the presence of starting material residues in some samples. In this case, we elaborated an additional purifying treatment (we will detail this point later, in paragraph 3.3.3.1.3).

Finally the system scale-up for industrial purposes requires several modifications[17]; we will not get into details for this point because is not the purpose of this thesis.

3.3.3.1.2 First characterization

This set of samples was characterized in order to investigate the purity and morphology of the particles (FTIR, TG/DTA, XDR and SEM).

3.3.3.1.2.1 Fourier transform infrared spectroscopy (FTIR)

In this paragraph we present the FTIR spectra of starting material (calcium acetate), the reference (commercial $CaCO_3$), the possible side products (CaO and $Ca(OH)_2$) and we compare with our results.

Calcium acetate

The infrared spectrum of calcium acetate hydrate (red in Figure 3.12) is reported in literature; the main band signals obtained in our sample are in agreement with the reference[36]. In the regions between 1600 and 1200 cm^{-1} the spectrum is characterized by the CH_3 bending and C-O stretching vibrations. In the literature the signals at 1350 cm^{-1} and 1413 cm^{-1} are assigned to the symmetric and antisymmetric methyl bending of acetate. In our sample those signals are at 1348 and 1412 cm^{-1}. The symmetric stretching of C-O bond corresponds to a signal at 1446 cm^{-1}, while the antisymmetric is represented by several peaks around 1550 cm^{-1}, both in agreement with the reference. The peaks at 1061 and 1032 cm^{-1} correspond to the vibration of the methyl group (both in agreement with the literature). The peak at 946 cm^{-1} is attributed to the C-C stretching vibration of acetate anion. Below 700 cm^{-1} the spectrum is

characterized by a group of intense sharp peaks corresponding to the vibrations of O-C-O fragment[36]. Between 3600-3000 cm^{-1} the spectrum shows a broad signal assigned to the O-H stretching vibrations.

Calcium carbonate

The absorption bands of calcium carbonate (black in Figure 3.12) can be identified in three main regions: 2646-2423 cm^{-1}, 1833-782 cm^{-1} (CO_3^{2-} out-of-plane bending mode) and 930-730 (CO_3^{2-} out-of-plane bending mode)[37]. The three polymorphs of calcium carbonate, vaterite, aragonite and calcite present different FTIR spectra. Here below we reported a summary table (readapted from the literature[38]) with the vibration frequency (cm^{-1}) of the three polymorphs and our sample of commercial $CaCO_3$.

	ν_1	ν_2	ν_3 *	ν_4 *
Vaterite[a]	1089	877 and 873	1487 and 1445	746 and 738
Aragonite[a]	1083	854	1488 and 1440	713 and 700
Calcite[a]	-	877	1420	713
Calcite[b]	-	876	1422	712

Table 3.6 FTIR of $CaCO_3$ polymorphs. Vaterite[a], aragonite[a] and calcite[a] are from literature[38], while commercial $CaCO_3$[b] is from this work. Vaterite and aragonite present a splitting in the vibrational mode ν_3 * and ν_4 *.

According to the literature, calcite has some characteristic bands that can be easily found in our sample: a broad band at ~1430 cm^{-1} corresponding to asymmetric stretching (ν_3) CO_3^{2-} band, smaller bands at 875 and 712-725 cm^{-1} due to the out-of-plane (ν_2) and in-plane (ν_4) bending respectively[37,38]. A reference in literature shows also a very small band at 1090 cm^{-1} (symmetric stretching ν_1) not visible in our spectra[39]. Finally, additional bands at ~1805 and 2514 cm^{-1} corresponds to $\nu_1 + \nu_4$ and $2\nu_2 + \nu_4$ mode[39,40], are both visible in our spectra. The sample has strong bands due to the presence of bound water (around 3400 cm^{-1}), as reported in literature[37,39,40]. Therefore, the sample analyzed of commercial calcium carbonate corresponds, as expected, to the calcite (results confirmed also by XRD). Table 3.7 summarizes the vibrational frequency assignments of the sample and the literature.

	ν_1	ν_2 (°)	ν_3 (§)	ν_4 (*)	$\nu_1 + \nu_4$	$2\nu_2 + \nu_4$
Ref [38]	-	877	1420	713	-	-
Ref [37]	-	876	1430	712	-	-
Ref [40]	-	874	1425	712	1798	2514
Ref [39]	1090	874	1409	725	1805	-
This work	-	876	1422	712	1804	2512

Table 3.7 FTIR of calcite from the literature and commercial calcium carbonate sample in this work.

Here below we report the FTIR spectra of calcium acetate and commercial $CaCO_3$ (calcite) analyzed in this work. The main characteristic peaks of calcite (877, 1420 and 713cm^{-1}) are assigned on the spectra with symbols reported in the previous table.

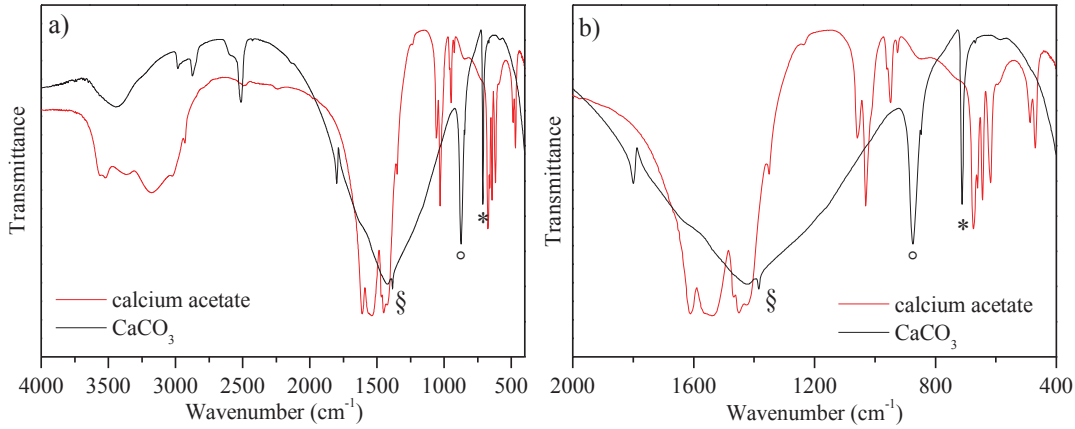

Figure 3.12 a) FTIR of commercial calcium acetate and calcium carbonate between 4000 and 400 cm^{-1}. b) FTIR of commercial calcium acetate and calcium carbonate between 2000 and 400 cm^{-1}. The peaks corresponding to calcite are marked with symbols (§, ° and *), as reported in Table 3.7.

Calcium oxide and calcium hydroxide

Finally CaO and $Ca(OH)_2$ present a different FTIR spectrum. We obtained these compounds as side product after the decomposition of $CaCO_3$ at high temperature. The spectra are known in the literature (reference[41] and SDBA database) and presented the same profile. There are characterized by a sharp peak at 3642 cm^{-1} (O-H bond of hydroxide), a broad peak ~1402-1546 cm^{-1} (C-O bonds from carbonate), 870 cm^{-1} and a wide strong band around 500 cm^{-1} (both corresponding to Ca-O bond).

Experimental samples

Some of the representative spectra obtained for the spray pyrolysis samples are reported in Figure 3.13 and Figure 3.14.

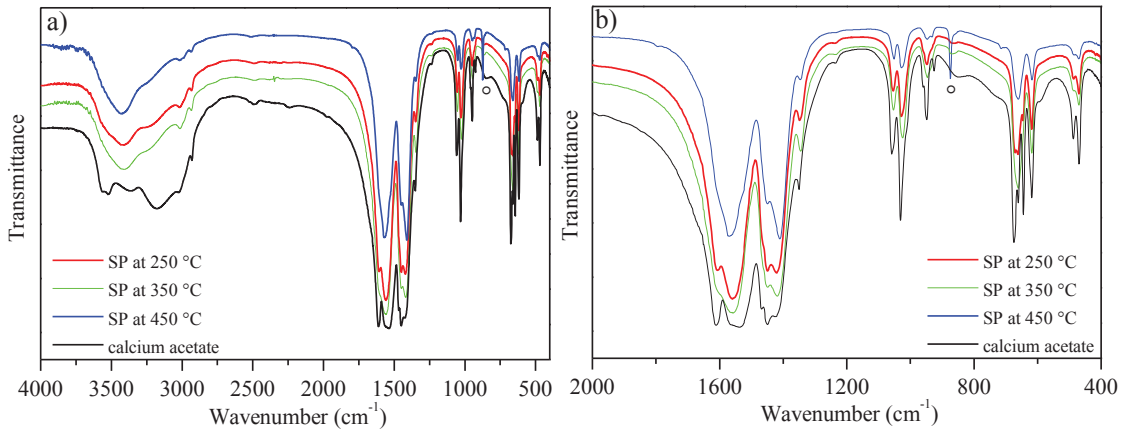

Figure 3.13 a) FTIR of samples 1-2-4 (SP at 250-350-450 °C) and calcium acetate, between 4000 and 400 cm^{-1}. b) FTIR of samples 1-2-4 (SP at 250-350-450 °C) and calcium acetate, between 2000 and 400 cm^{-1}. Only sample 4 (SP at 450 °C) shows a peak corresponding to calcite, marked with a symbol (°), as reported in Table 3.7.

The spectra of samples 1-2-4 (SP at 250-350-450 °C) clearly show an important presence of calcium acetate. Their profile is similar to the calcium acetate spectra: a double band around 1500 cm^{-1}, a peak at 1032 and 950 cm^{-1} and some smaller peaks below 700 cm^{-1}. As we can see from Figure 3.13 sample 4 (SP at 450 °C) shows a peak at 874 cm^{-1} that may be attributed to the calcium carbonate (marked with a symbol in Figure 3.13). Sample 5 (SP at 500 °C) shows the same profile as for the previous samples (the graph is not reported in this manuscript).

Samples 6-7-8, obtained at higher temperature (SP at 550-650-750 °C), show the peaks characteristics of calcite at 1423, 875 and 713 cm^{-1} (marked with symbols in Figure 3.14). Smaller peaks are visible too (1797 and 2512 cm^{-1}). The characteristic peaks of acetate (around 1550; 1032; 950 and below 700 cm^{-1}), on the other hand, are gradually lost.

As expected, when the temperature of the spray pyrolysis experiments increases, the samples present a higher content of calcium carbonate.

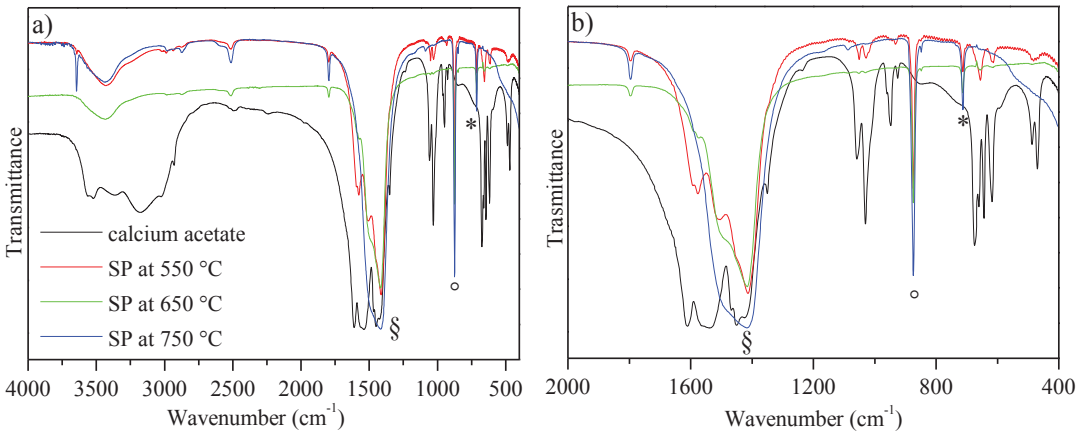

Figure 3.14 a) FTIR of samples 6-7-8 (SP at 550-650-750 °C) and calcium acetate, between 4000 and 400 cm^{-1}. b) FTIR of samples 6-7-8 (SP at 550-650-750 °C) and calcium acetate, between 2000 and 400 cm^{-1}. The peaks corresponding to calcite are marked with symbols (§, ° and *), as reported in Table 3.7. The legend is the same, for clarity reason is not reported in the second graph.

3.3.3.1.2.2 Thermogravimetry/Differential thermal analysis (TG/DTA)

The decomposition of calcium acetate hydrate, calcium carbonate and of all the samples 1-8, was monitored using thermogravimetry (TG) and differential thermal analysis (DTA). The samples were heated up to 1000 °C with a rate of 10 °C/min under oxygen atmosphere in order to be coherent with the spray pyrolysis conditions.

In this paragraph we present the TG/DTA plot of starting material (calcium acetate), the reference (commercial $CaCO_3$) and we compare with our results.

Calcium acetate

The calcium acetate thermal profile is in agreement with the literature data[42,43]. This is characterized by a first step of water molecules loss (between 150-200 °C and 200-240 °C), corresponding to 5% of weight mass loss. Then, between 400 and 520 °C, the calcium acetate decomposes into $CaCO_3$ and acetone, with 37.2% of mass loss[42]. Finally the calcium carbonate decomposes to form calcium oxide between 650 and 765 °C[36,42,43]. Figure 3.15 shows the thermal profile of calcium acetate analyzed in this work. The TG curve shows a first peak, around 400 °C, due to CO_2 generated by the decomposition of calcium acetate into calcium carbonate; the second peak, at 800 °C, can be attributed to decomposition of calcium carbonate.

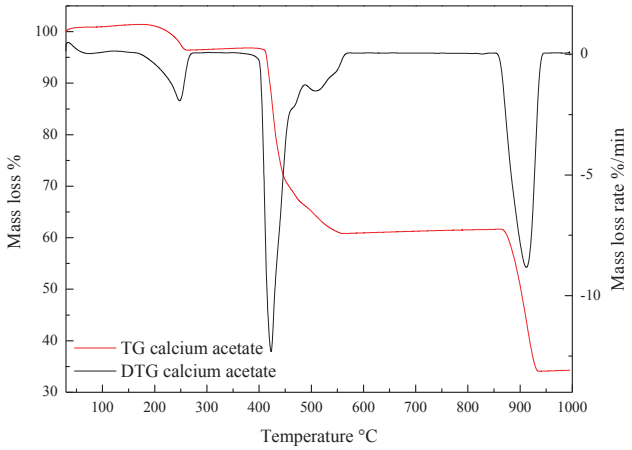

Temp (°C)	Mass Loss (%) Ref [42]	Mass Loss (%) sample
~150-240	5	5
~400-520	37	36
~650-765	27	27

Figure 3.15 TG and DTA plot of calcium acetate analyzed in this work.

Calcium carbonate

The decomposition process of $CaCO_3$ is well known and documented in the literature (see above). In a first step at ~110 °C the carbonate loses the water molecules (2% of mass loss weight), and then it starts to decompose around 650 °C into CaO and CO_2. The sample analyzed in this work is coherent with the literature data[44], as shown in Figure 3.16.

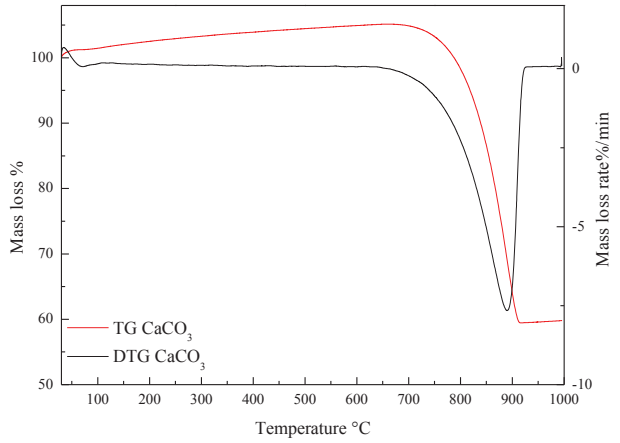

Temp (°C)	Mass Loss (%) Ref[44]	Mass Loss (%) sample
~110	2	-
~650-900	46-48	47

Figure 3.16 TG and DTA plot of commercial calcium carbonate analyzed in this work.

Experimental samples

The thermogravimetric curves of samples 1 and 2 (SP at 250 and 350 °C) at lower temperature display the same profile as calcium acetate (TG curve of sample 1 is reported in Figure 3.17a).

Sample 3 (SP at 400 °C) shows a similar profile with a slight decrement of the first peak due to the decomposition of calcium acetate (29% of weight loss instead of 37%) and consequent increment of second peak due to the decomposition of calcium carbonate (36% of weight loss instead of 26%).

Samples 4-5-6-7-8 (SP at 450-500-550-650-750 °C, respectively) exhibit a gradual reduction of the first peak of decomposition of calcium acetate (from 18% to 1.6% of weight loss) and the increase of the second peak of decomposition of calcium carbonate until 43% of weight loss. TG curves of samples 6 and 8 (SP at 550 and 750 °C) are reported in Figure 3.17 b and c, respectively.

Therefore the thermogravimetric results are coherent with the IR ones: as the temperature of synthesis increases, the content of calcium carbonate increases (as we can see from the second peak that becomes more important). Consequently the calcium acetate content decreases (first peak is lower). The curves of significant samples 1-6-8 (SP at 250-550-750 °C) are reported here below Figure 3.17 a-b-c respectively.

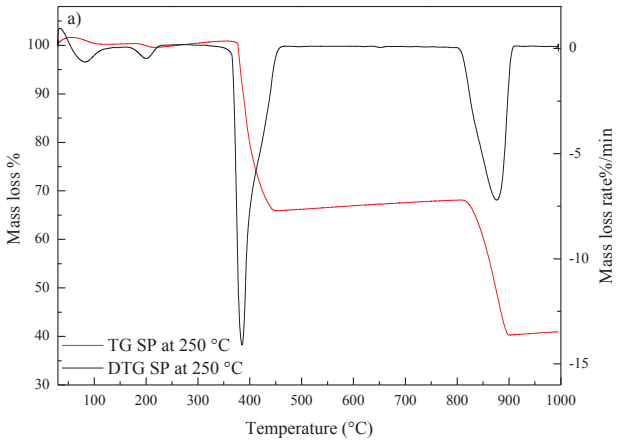

Temp (°C)	Mass Loss (%) sample	
~150-240	2	water
~380-480	36	
~780-930	28	CO_2

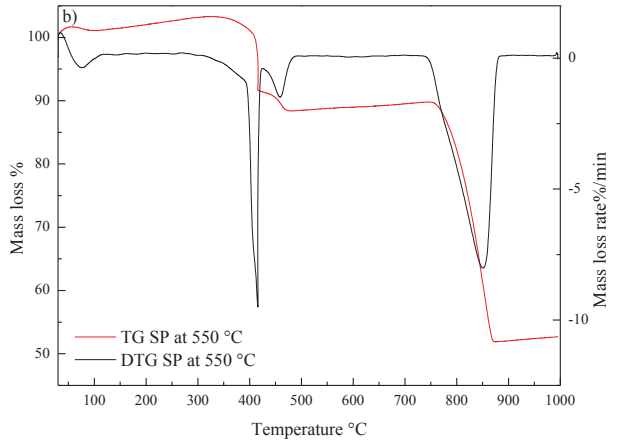

Temp (°C)	Mass Loss (%) sample	
~150-240	1	water
~350-500	16	
~580-930	39	CO_2

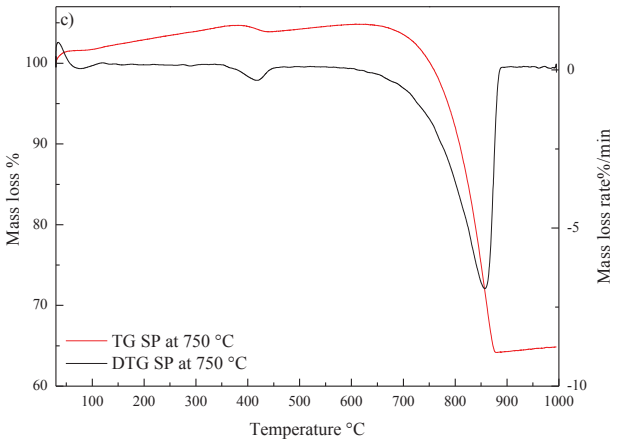

Temp (°C)	Mass Loss (%) sample	
~150-240	<1	water
~350-500	1	
~580-930	43	CO_2

Figure 3.17 a-c) TG and DTA plots of samples 1-6-8 (SP at 250-550-750 °C respectively).

3.3.3.1.2.3 X-ray powder diffraction (XRD)

Samples 1-8 (SP from 250 to 750 °C) were analyzed by XRD analysis in order to identify the calcium acetate or calcite crystalline phases.

In this paragraph we present the XRD patterns of samples compared with starting material (calcium acetate), the reference (commercial $CaCO_3$) and the possible side product (CaO) from the PDF 2004 database.

The XRD patterns of samples 1-2-3-4 (SP at 250-350-400-450 °C) show mainly the presence of calcium acetate hydrate and amorphous phase, while sample 5 (SP at 500 °C) exhibits a pattern of mainly calcite but still amorphous phase. Finally, the patterns of sample 6-7-8 (SP at 550-650-750 °C) show mainly calcite and amorphous phase (broad peak below 20 degree).

The pattern of sample 8 (SP at 750 °C) shows also the presence of small amount of calcium oxide at 37.23 and 53.90 degree (marked with a symbol * in Figure 3.18).

Some significant XRD spectra are reported here below (Figure 3.18). The first pattern shows mainly calcium acetate and amorphous phase (sample 1, SP at 250 °C), while the second pattern (sample 6, SP at 550 °C) calcite and a broad peak at 10-20 degree (amorphous phase). The latter could be attributed to a solid phase not well or not at all crystallized. Finally the third pattern (sample 8, SP at 750 °C) shows two additional small peaks at 37.6 and 54.1 2θ (attributed to CaO). When the spray pyrolysis is performed at high temperature (T >650 °C), CaO is formed as side product. However, when the sample is left to air conditions, CaO converts rapidly into $Ca(OH)_2$,very hygroscopic and not visible with XRD. For this reason, we believe that only traces of CaO are visible with XRD.

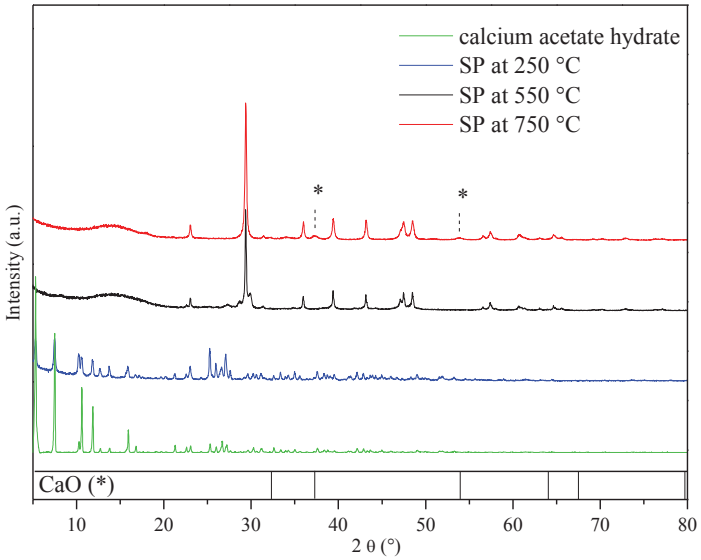

Figure 3.18 XRD patterns of samples 1-6-8 (SP at 250-550-750 °C), calcium acetate hydrate analyzed in this work and CaO reference on the bottom (PDF 2004 database). The peaks in sample 8 (SP at 750 °C) marked with * correspond to CaO.

3.3.3.1.2.4 Scanning Electron Microscopy (SEM)

For better investigating the structure and the dimension of the synthesized particles, SEM analysis was carried out on some relevant samples. The commercial product was also submitted to this analysis as already presented in the previous paragraph. It forms mainly aggregates of small particles of ~1-5 μm radius.

The spray pyrolysis particles analyzed by SEM are shown in the picture below. They have spherical structure, with diameter between 1-5 μm (deduced from the picture).

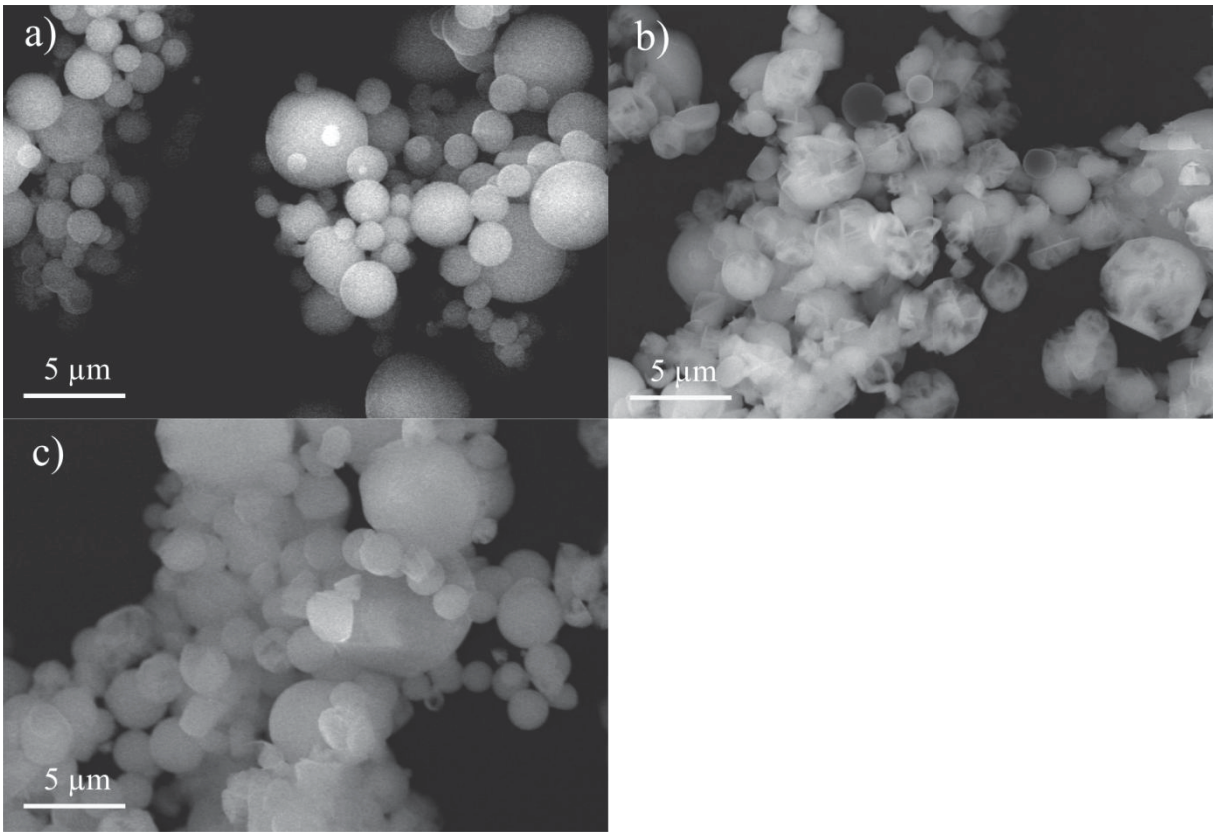

Figure 3.19 SEM images of samples a) sample 1 (SP at 250 °C); b) sample 3 (SP at 400 °C); c) sample 5 (SP at 500 °C).

3.3.3.1.2.5 Summary of first characterization

The first characterization carried out on the particles revealed important differences between the samples synthesized at lower or at higher temperature.

When the synthesis is performed at low temperature (T = 250 °C), the content of calcium acetate is dominant. Increasing the temperature augments the calcium carbonate content, due to the decomposition of calcium acetate (see equations).

Finally, at higher temperature (T> 650 °C) calcium carbonate decomposes into CaO and CO_2.

$$Ca(CH_3CO_2)_2 \rightarrow CaCO_3 + C_3H_6O$$

$$CaCO_3 \rightarrow CaO + CO_2$$

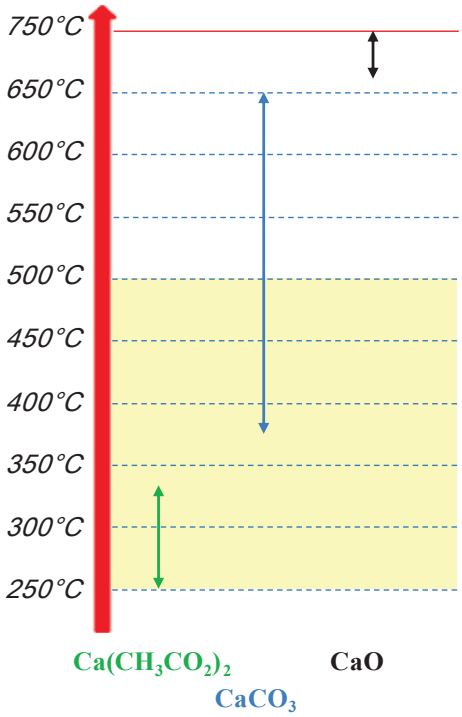

Figure 3.20 Temperature scheme.

In summary, we synthesized microparticles of $CaCO_3$ with different degree of purity (due to the decomposition temperature in the furnace). We discarded samples at temperature T> 500 °C in order to avoid undesirable CaO and we selected samples between 250 and 500 °C for further treatment.

3.3.3.1.3 Heating treatment of selected samples

The most promising samples selected for our purpose are the particles synthesized between 250 and 500 °C. Samples 1-3-5 (SP 250- 400- 500 °C) were selected and submitted to additional treatment. This consisted in heating the samples in a furnace for 5h at 500 °C (gradient 10 °C/min) in order to convert all the acetate residues into $CaCO_3$. A second characterization followed this process.

3.3.3.1.4 Second characterization

After heating treatment, the samples were submitted to a second characterization with the same techniques (FTIR, TG/DTA, XRD and SEM) and additionally BET.

3.3.3.1.4.1 Fourier transform infrared spectroscopy (FTIR)

The samples selected 1-3-5 (SP 250-400-500 °C), reported here in the first graph, exhibit all the same IR profile (Figure 3.21) after heating treatment.

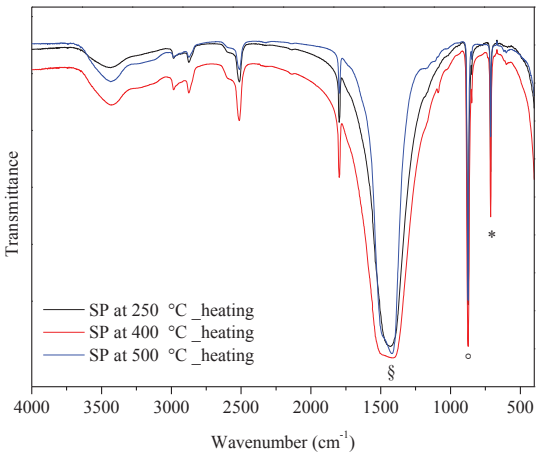

Figure 3.21 FTIR of samples 1-3-5 (SP at 250, 400 and 500 °C respectively) after the heating treatment. The main peaks corresponding to calcite (discussed in Table 3.7) are marked with symbols (§, ° and *).

In order to compare their profiles with the references, sample 3 (SP at 400 °C) is reported in a plot with calcium acetate and carbonate (Figure 3.22). Its profile is very similar to the latter. Moreover, the characteristics peaks of calcite are recognizable in the graph: the broad band at 1427 cm^{-1}, smaller bands at 874 and 717 cm^{-1} are easily identified (marked in the figure with the symbols). Additionally, peaks at 1802 and 2510 cm^{-1} of calcite also visible (all the peaks are reported in Table 3.7).

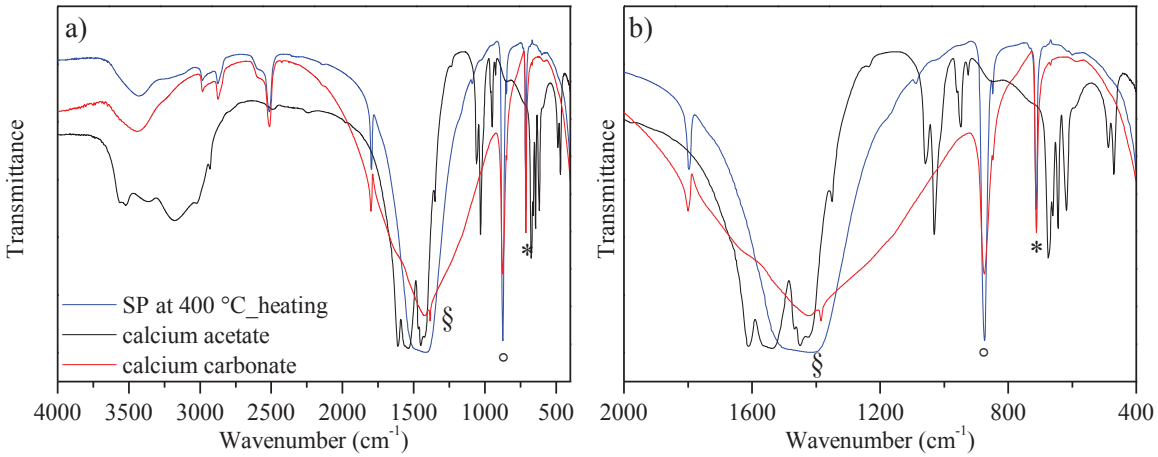

Figure 3.22 a) FTIR of sample 3 (SP at 400 °C) after heating treatment, calcium acetate and calcium carbonate between 4000 and 400 cm^{-1}. b) FTIR of sample 3 (SP at 400 °C) after heating treatment, calcium acetate and calcium carbonate between 2000 and 400 cm^{-1}. The main peaks corresponding to calcite are marked with symbols (§, ° and *), as reported in Table 3.7. The legend is the same, for clarity reason is not reported in the second graph.

3.3.3.1.4.2 Thermogravimetry/Differential thermal analysis (TG/DTA)

Purified samples 1-3-5 (SP at 250-400-500 °C) were also analyzed by thermogravimetric analysis. All the samples display the same profile: the differential thermogravimetric curve shows one mass loss peak between 550 and 800 °C, corresponding to the conversion of $CaCO_3$ into CaO and CO_2. The mass loss peak at ~400 °C, attributed to the decomposition of calcium acetate, completely disappears. All the samples present the same curve, as reported in Figure 3.23. The results are in agreement with the IR data.

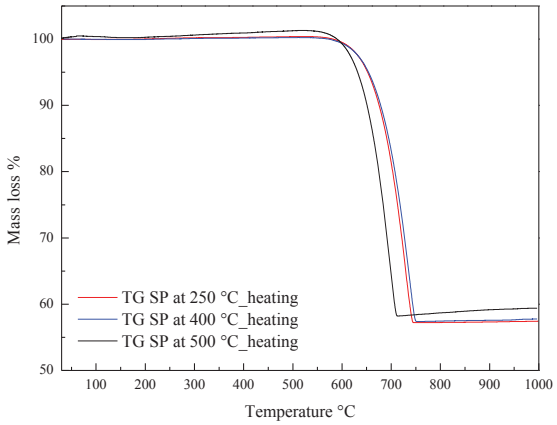

Temp (°C)	**Mass Loss (%) Ref[44]**	**Mass Loss (%) sample**	
~550-800	46-48	43	CO_2

Figure 3.23 TG plots of samples 1-3-5 (SP at 250, 400 and 500 °C) after the heating treatment.

3.3.3.1.4.3 X-ray powder diffraction (XRD)

The purified samples 1-3-5 (SP at 250, 400, 500 °C) were analyzed by XRD. The three patterns show only the presence of calcite. The amorphous broad peak (below than 20 degree) presented in the sample before the treatment, has now disappeared. The heating treatment purified the samples from the amorphous phase.

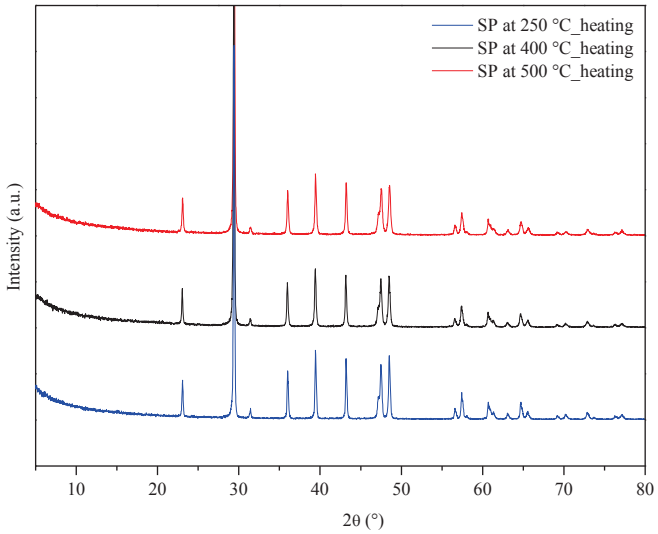

Figure 3.24 XRD patterns of samples 1-3-5 (SP at 250, 400 and 500 °C) after heating treatment.

3.3.3.1.4.4 Scanning Electron Microscopy (SEM) and Transmission Electron Microscopy (TEM)

The purified samples 1-3-5 were also investigated by SEM.

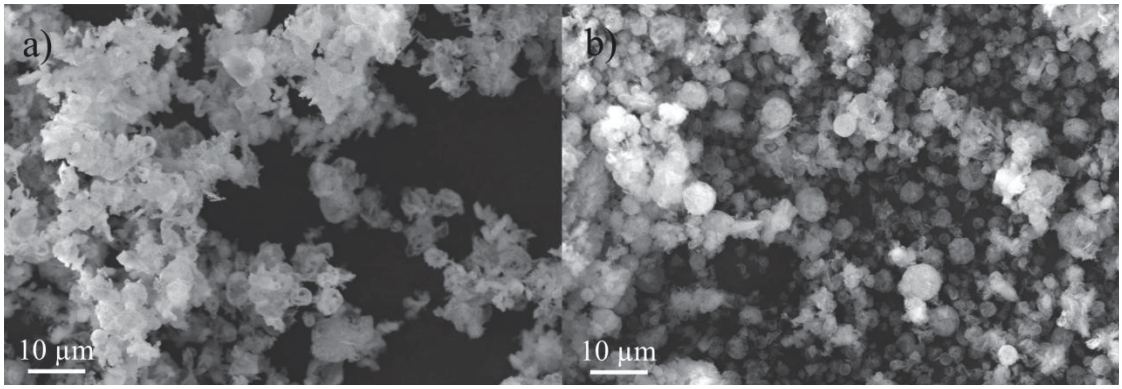

Figure 3.25 SEM images of a) sample 1 (SP at 250 °C) after heating treatment; b) sample 3 (SP at 400 °C) after heating treatment.

Samples 3 and 5 (SP at 400 and 500 °C) show a quite spherical form, after the heating treatment, while sample 1 (SP at 250 °C) lost its spherical form. Indeed sample 1 was mainly constituted by calcium acetate, therefore the heating treatment destroyed the spherical form.

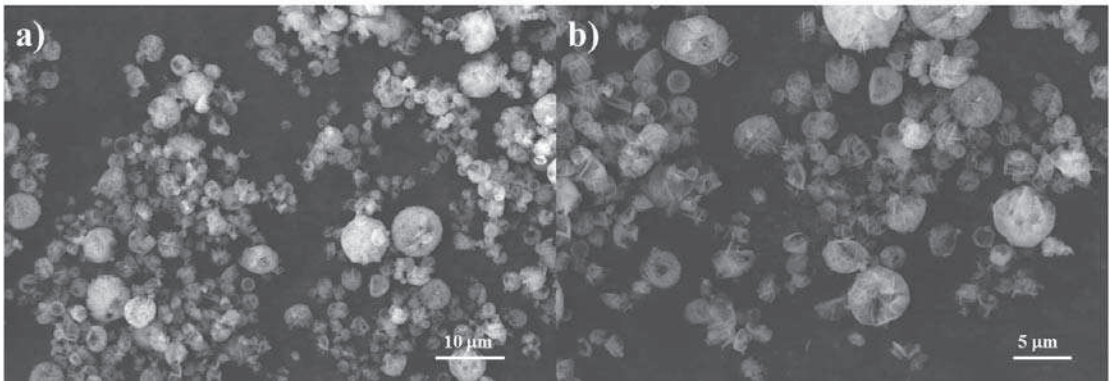

Figure 3.26 SEM images of a-b) sample 5 (SP at 500 °C) after heating treatment.

Sample 5 (SP at 500 °C) was analyzed by TEM. The sample was dispersed in ethanol solution under ultrasounds and then placed on the support. The TEM images are in agreement with the structure identified in SEM images.

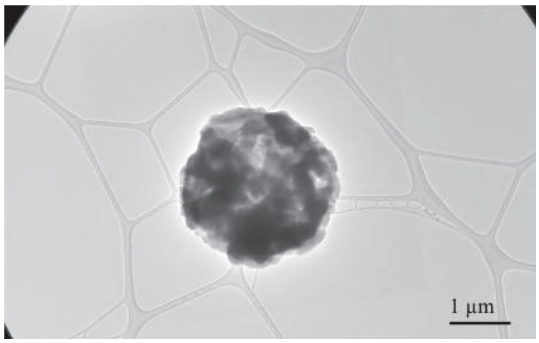

Figure 3.27 TEM image of sample 5 (SP at 500 °C) after heating treatment.

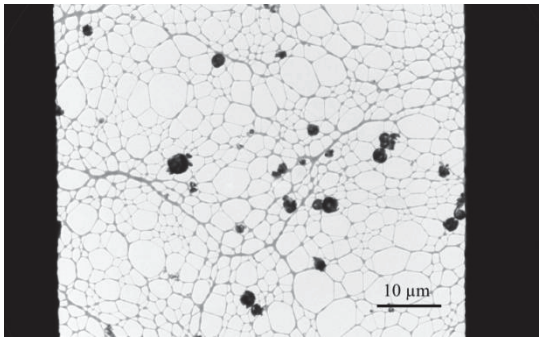

Figure 3.28 TEM image of sample 5 (SP at 500 °C) after heating treatment.

Diffraction of the particles afforded a polycrystalline pattern that corresponds to calcite (reference with PDF database).

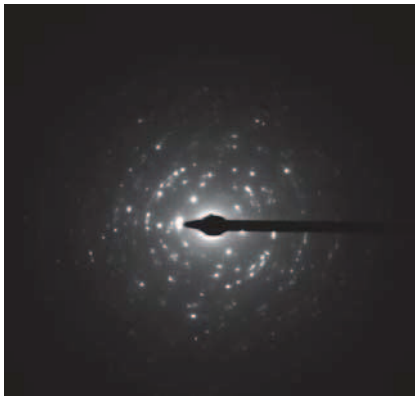

Figure 3.29 Diffraction of sample 5 (SP at 500 °C) after heating treatment.

3.3.3.1.4.5 Adsorption, BET and granulometric analysis (GL)

Finally, the selected samples were analyzed by BET technique in order to calculate their specific surface by adsorption of nitrogen gas.

Here below we report the adsorption of sample 5 (SP at 500 °C) after heating treatment, as example.

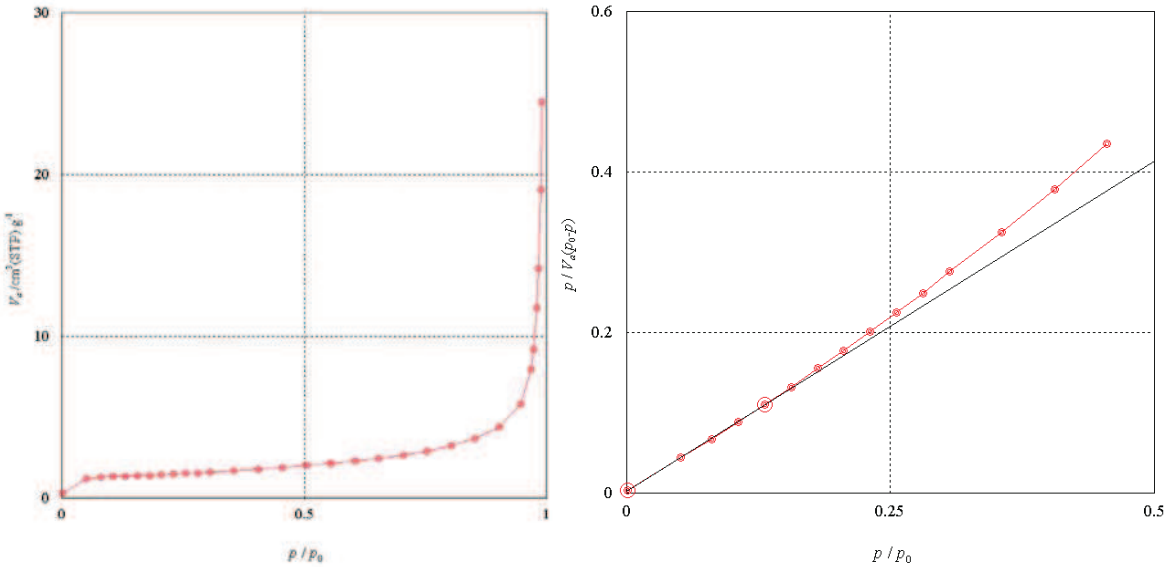

Figure 3.30 Adsorption isotherm and BET plot of sample 5 (SP at 500 °C) after the heating treatment.

The specific surface $a_{S,BET}$ (m^2/g) is calculated from the BET plot. As reported in the summary table, the specific surface value increases from sample 1 to 5.

Sample after the heating treatment	$a_{S,BET}$ (m^2/g)
1 (SP at 250 °C)	2.1
3 (SP at 400 °C)	4.7
5 (SP at 500 °C)	5.0

Table 3.8 Specific surfaces of samples 1-3-5 (SP at 250-400-500 °C) after the heating treatment.

The specific surface of sample 3 and 5 (SP at 400-500 °C) are approximately the same for our purpose. In all three cases, the specific surface is higher than the surface obtained with the grinding method ($a_{S,BET}$ = 1.27m^2/g) and the one of starting commercial material (estimation to $a_{S,EXT}$ = 0.1 m^2/g).

The laser granulometric analysis (LG) experiment on sample 5 (SP at 500 °C) after heating treatment shows the dimension and distribution of the particles. The measurement was carried out in distilled water. Figure 3.31 shows an distribution of the particles of medium radius of d(v,0.5) = 4.3 μm.

The GL analysis on sample 3 (SP at 400 °C) after heating treatment is in progress during the redaction of this manuscript.

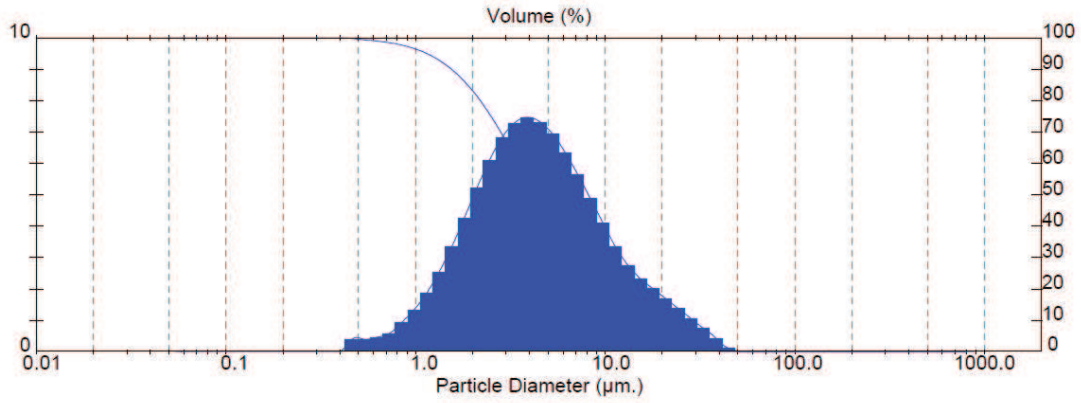

Figure 3.31 LG on sample 5 (SP at 500 °C) after the heating treatment.

3.3.3.1.4.6 Conclusion on second purification

The heating treatment affords the desired product with a good grade of purity, confirmed by FTIR, TG/DTA and XRD analysis. Samples 3 and 5 (SP at 400 and 500 °C) in particularly, even after this treatment maintain their spherical structure, while sample 1 (SP at 250 °C) seems to lose it. Finally, additional BET and laser granulometric analysis gives the specific surface desired.

3.3.3.2 Conclusion on $CaCO_3$ particles *via* spray pyrolysis technique

In this work $CaCO_3$ particles of a few microns size were synthesized by spray pyrolysis technique. A comprehensive spectroscopic and thermal study was carried out on the first set of samples. As the particles obtained were not completely pure, a heating treatment was performed, completed by the same characterization. Finally, the selected samples result in good specimens for coupling reaction.

At the moment of the redaction of this manuscript, the characterization of a new set of samples is still in progress. In this case, some parameters (such as air flow) of the spray pyrolysis technique have been changed in order to deeply investigate the subject.

3.3.4 General conclusion on preparation of $CaCO_3$ particles for solid state reaction

In this chapter we presented the preparation of $CaCO_3$ particles in order to use them for solid state reactions. The two approaches used in this work, the grinding method and the synthesis *via* spray pyrolysis, gives the substrates with a good specific surface (1.3-5 m^2/g) for our work. The grinding method was easily performed by milling the commercial product, while the second approach involves the spray pyrolysis technique. In this case the synthesis was carried out for the first time, so it was completed by a detailed characterization.

3.4 References

1. Faatz, M., Gröhn, F. & Wegner, G. Mineralization of calcium carbonate by controlled release of carbonate in aqueous solution. *Mater. Sci. Eng. C* **25,** 153–159 (2005).
2. Boyjoo, Y., Pareek, V. K. & Liu, J. Synthesis of micro and nano-sized calcium carbonate particles and their applications. *J. Mater. Chem. A* **2,** 14270–14288 (2014).
3. calcite.pdf. at <http://www.handbookofmineralogy.org/pdfs/calcite.pdf>
4. aragonite.pdf. at <http://www.handbookofmineralogy.org/pdfs/aragonite.pdf>
5. Yoshioka, S. & Kitano, Y. Transformation of aragonite to calcite through heating. *Geochem. J.* **19,** 245–249 (1985).
6. Criado, J. M. & Trillo, J. M. Effects of mechanical grinding on the texture and structure of calcium carbonate. *J. Chem. Soc. Faraday Trans. 1 Phys. Chem. Condens. Phases* **71,** 961 (1975).
7. vaterite.pdf. at <http://www.handbookofmineralogy.org/pdfs/vaterite.pdf>
8. The British Calcium Carbonates Federation. at <http://www.calcium-carbonate.org.uk/index.asp>
9. The british lime association. at <http://www.britishlime.org/links.php>
10. Hazen, R. M., Filley, T. R. & Goodfriend, G. A. Selective adsorption of l- and d-amino acids on calcite: Implications for biochemical homochirality. *Proc. Natl. Acad. Sci.* **98,** 5487–5490 (2001).

11. Orme, C. A. *et al.* Formation of chiral morphologies through selective binding of amino acids to calcite surface steps. *Nature* **411,** 775–779 (2001).
12. Addadi, L. & Weiner, S. Biomineralization: Crystals, asymmetry and life. *Nature* **411,** 753–755 (2001).
13. Wei, W. *et al.* Preparation of Hierarchical Hollow CaCO $_3$ Particles and the Application as Anticancer Drug Carrier. *J. Am. Chem. Soc.* **130,** 15808–15810 (2008).
14. Liu, L. *et al.* Biomineralization of Stable and Monodisperse Vaterite Microspheres Using Silk Nanoparticles. *ACS Appl. Mater. Interfaces* **7,** 1735–1745 (2015).
15. Zhang, J. *et al.* Calcium Carbonate Nanoplate Assemblies with Directed High-Energy Facets: Additive-Free Synthesis, High Drug Loading, and Sustainable Releasing. *ACS Appl. Mater. Interfaces* **7,** 15686–15691 (2015).
16. Peng, C., Zhao, Q. & Gao, C. Sustained delivery of doxorubicin by porous CaCO3 and chitosan/alginate multilayers-coated CaCO3 microparticles. *Colloids Surf. Physicochem. Eng. Asp.* **353,** 132–139 (2010).
17. Okuyama, K. & Wuled Lenggoro, I. Preparation of nanoparticles via spray route. *Chem. Eng. Sci.* **58,** 537–547 (2003).
18. Chen, Y., Lian, X., Li, Z., Zheng, S. & Wang, Z. Effects of rotation speed and media density on particle size distribution and structure of ground calcium carbonate in a planetary ball mill. *Adv. Powder Technol.* **26,** 505–510 (2015).
19. Caiut, J. M. A. *et al.* Elaboration of boehmite nano-powders by spray-pyrolysis. *Powder Technol.* **190,** 95–98 (2009).
20. Messing, G. L., Zhang, S.-C. & Jayanthi, G. V. Ceramic Powder Synthesis by Spray Pyrolysis. *J. Am. Ceram. Soc.* **76,** 2707–2726 (1993).
21. Joffin, N. *et al.* Phosphor powders elaborated by spray-pyrolysis: Characterizations and possible applications. *Opt. Mater.* **28,** 597–601 (2006).
22. Patil, P. S. Versatility of chemical spray pyrolysis technique. *Mater. Chem. Phys.* **59,** 185–198 (1999).
23. PYLOTE. at <http://www.pylote.fr/fr>
24. Joffin, N. *Synthèse par pyrolyse d'aérosol et caractérisation de luminophores : Y2O3:Eu3+ et An2SiO4:Mn2+ pour application dans les panneaux à plasma*. (Toulouse, INPT, 2004). at <http://www.theses.fr/2004INPT012G>
25. Che, S., Sakurai, O., Shinozaki, K. & Mizutani, N. Particle structure control through intraparticle reactions by spray pyrolysis. *J. Aerosol Sci.* **29,** 271–278 (1998).
26. Judd, M. D., Plunkett, B. A. & Pope, M. I. The thermal decomposition of calcium, sodium, silver and copper(II) acetates. *J. Therm. Anal.* **6,** 555–563 (1974).
27. Wayne R. Pease, Robert L. Segall, Roger St. C. Smart & Peter S. Turner. Surface Reduction in Low-temperature Formation of Nickel Oxide from Different Nickel Salts. *J. Chem. Soc. Farady Trans.* **1,** 747–758 (1985).
28. Adánez, J., de Diego, L. F. & García-Labiano, F. Calcination of calcium acetate and calcium magnesium acetate: effect of the reacting atmosphere. *Fuel* **78,** 583–592 (1999).
29. Rice, F. O. & Vollrath, R. E. The thermal decomposition of acetone in the gaseous state. *Proc. Natl. Acad. Sci. U. S. A.* **15,** 702–705 (1929).
30. Rice, F. O., Rodowskas, E. L. & Lewis, W. R. The Thermal Decomposition of Acetone. *J. Am. Chem. Soc.* **56,** 2497–2498 (1934).
31. Winkler, C. A. & Hinshelwood, C. N. The Thermal Decomposition of Acetone Vapour. *Proc. R. Soc. Lond. Ser. Math. Phys. Sci.* **149,** 340–354 (1935).
32. Allen, A. O. The Thermal Decomposition of Acetone. *J. Am. Chem. Soc.* **58,** 1052–1053 (1936).
33. Davoud, J. G. & Hinshelwood, C. N. Thermal Decomposition of Acetone. *Nature* **144,** 909–910 (1939).

34. Smith, J. R. E., Phil, D. & Hinshelwood, C. N. The Thermal Decomposition of Acetone. *Proc. R. Soc. Lond. Math. Phys. Eng. Sci.* **183,** 33–37 (1944).
35. Alavi, S. *et al.* Spray Pyrolysis synthesis of submicronic particles. Possibilities and limits. **30A,** 417–424 (2002).
36. Musumeci, A. W., Frost, R. L. & Waclawik, E. R. A spectroscopic study of the mineral paceite (calcium acetate). *Spectrochim. Acta. A. Mol. Biomol. Spectrosc.* **67,** 649–661 (2007).
37. Legodi, M. A., de Waal, D., Potgieter, J. H. & Potgieter, S. S. Rapid determination of CaCO3 in mixtures utilising FT—IR spectroscopy. *Miner. Eng.* **14,** 1107–1111 (2001).
38. Andersen, F. A. *et al.* Infrared Spectra of Amorphous and Crystalline Calcium Carbonate. *Acta Chem. Scand.* **45,** 1018–1024 (1991).
39. Diego Rodriguez-Blanco, J., Shaw, S. & G. Benning, L. The kinetics and mechanisms of amorphous calcium carbonate (ACC) crystallization to calcite , via vaterite. *Nanoscale* **3,** 265–271 (2011).
40. Gunasekaran, S. & Anbalagan, G. Spectroscopic study of phase transitions in natural calcite mineral. *Spectrochim. Acta. A. Mol. Biomol. Spectrosc.* **69,** 1246–1251 (2008).
41. Guan, W. *et al.* A Novel Synthesis Method of Porous Calcium Silicate Hydrate Based on the Calcium Oxide/Polyethylene Glycol Composites. *J. Nanomater.* **2013,** 1–7 (2013).
42. Bilton, M., Brown, A. P. & Milne, S. J. Investigating the optimum conditions for the formation of calcium oxide, used for CO_2 sequestration, by thermal decomposition of calcium acetate. *J. Phys. Conf. Ser.* **371,** 012075 (2012).
43. Niu, S., Han, K., Lu, C. & Sun, R. Thermogravimetric analysis of the relationship among calcium magnesium acetate, calcium acetate and magnesium acetate. *Appl. Energy* **87,** 2237–2242 (2010).
44. Babou-Kammoe, R., Hamoudi, S., Larachi, F. & Belkacemi, K. Synthesis of CaCO3 nanoparticles by controlled precipitation of saturated carbonate and calcium nitrate aqueous solutions. *Can. J. Chem. Eng.* **90,** 26–33 (2012).

4. Coupling reaction on $CaCO_3$ particles

4.1 Reaction on solid surface by mechanochemistry 114
4.1.1 Introduction and objective 114
4.1.2 Experimental 116
4.1.3 Results and discussion 119
4.1.4 Conclusions on reaction by mechanochemistry activation 120
4.2 Coupling reaction on solid surface by thermal activation 121
4.2.1 Introduction and objective 121
4.2.2 Experimental 121
4.2.3 Results and discussion 121
4.2.4 Other reactions studied in this work 125
4.2.5 Conclusions on coupling reaction by thermal activation on $CaCO_3$ microparticles 129
4.3 General conclusion on coupling reactions on solid surface 129
4.4 References 131

In the previous chapter we prepared $CaCO_3$ microparticles with correct specific surface for our purpose (Figure 4.1 a).

In this chapter we will describe the deposition of molecules on those particles (Figure 4.1 b), the reaction activation on the surface (Figure 4.1 c), and the work-up in order to isolate the product (Figure 4.1 d-e).

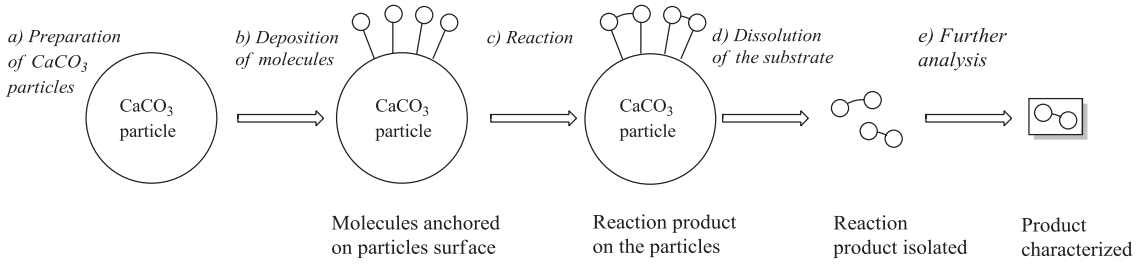

Figure 4.1 Coupling reactions on $CaCO_3$ particles.

We present the two solvent-free activation approaches used in this work: mechanochemistry activation (paragraph 4.1) and thermal conditions (paragraph 4.2). Conclusions and further perspectives on these methods close the chapter.

4.1 Reaction on solid surface by mechanochemistry

4.1.1 Introduction and objective

IUPAC defines mechanochemical reaction as "chemical reaction induced by direct absorption of mechanical energy" (IUPAC *Compendium of Chemical Technology, "the Gold Book"*, ed. Oxford 2nd edition 1997)[1–3]. Even if the first mechanochemical reactions date to the prehistorical times, it is commonly accepted that the first contribution to the modern mechanochemistry are from M. Carey Lea, M. Faraday and F. W. Ostwald in the 19th century[2–4]. During the following century mechanochemistry was widely investigated mostly in eastern-European countries. After the contribution of P. G. Fox's[5] in 1975 the subject became more popular. Today mechanochemistry is recognized as a new green and solvent-free method that interests different fields of science. It ranges from organic to inorganic chemistry, mechanical alloying, catalysis and pharmaceutical field, as summarized in Figure 4.2[2].

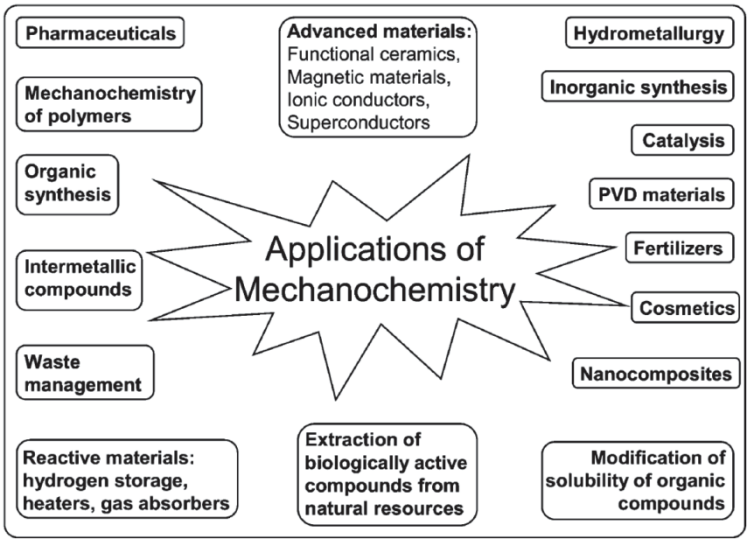

Figure 4.2 Application fields of mechanochemistry, from the ref.[2].

Moreover, the absence of solvent makes mechanochemistry a very interesting method for industrials applications. Figure 4.3 shows the dramatic increase of the number of patents including the terms "mechanochemical" or "mechanochemistry" in the last decades[4].

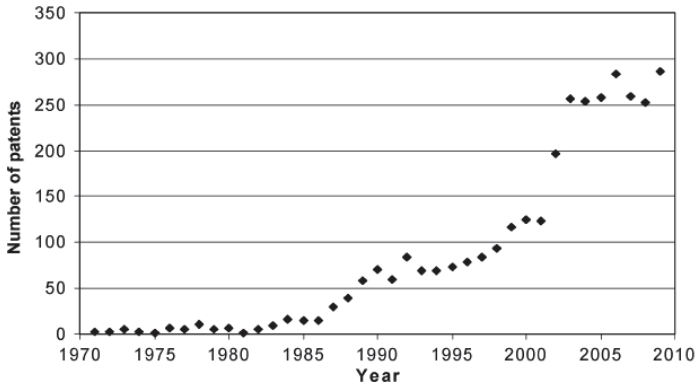

Figure 4.3 Number of patents including the terms "mechanochemical"/ "mechanochemistry" vs. years, from the literature[4].

In this work we decided to use this technique in order to activate the precursor molecule (4-iodobenzoic acid) on $CaCO_3$ (previously milled, as explained in the previous chapter) in order to explore coupling reactions.

The work was done in collaboration with Dr. M. Baltas and Dr. B. Guidetti at the SPCMIB laboratory in Toulouse.

4.1.2 Experimental

Many variables play a crucial role in mechanochemistry reactions (Figure 4.4), often summarized in chemical, technological and process parameters[6]. The first takes into account all the parameters linked to the reaction (such as the type of reaction, the reagents, catalysts or additives). The second considers the type of milling material (the machine, the type and the size of the ball). Finally the last one takes into account all the parameters during the process (speed, time etc.).

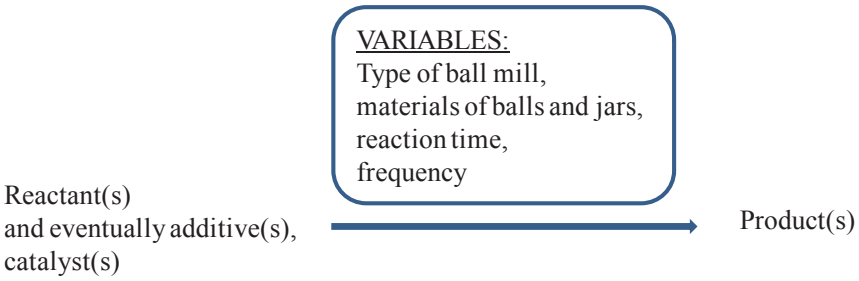

Figure 4.4 Variables in mechanochemistry reaction, readapted from the literature[1].

Different types of milling machines are depicted in Figure 4.5[2]. In this work we used planetary ball mill Pulverisette 7 Premium line, Fritsch (I-d Figure 4.5, Figure 4.6). The principle is explained in Figure 4.6: the planetary turns around a central axis, while the jars rotate around their own axis. The speed of these movements leads to high energy impacts of the balls inside the jars, necessary for grinding.

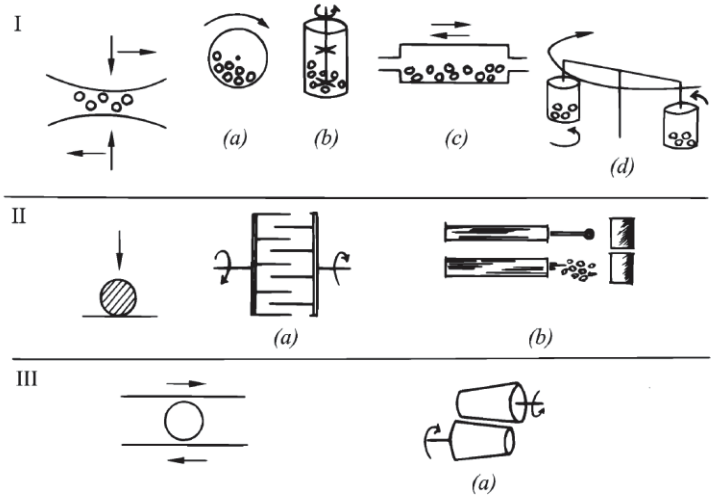

Figure 4.5 Different types of mechanical milling. I-shear + impact: a- ball mill, b-attritor, c- vibration mill, d-planetary mill. II-impact: a-pin mill, b-jet mill. III-shear: a-rollers. Adapted from ref.[2].

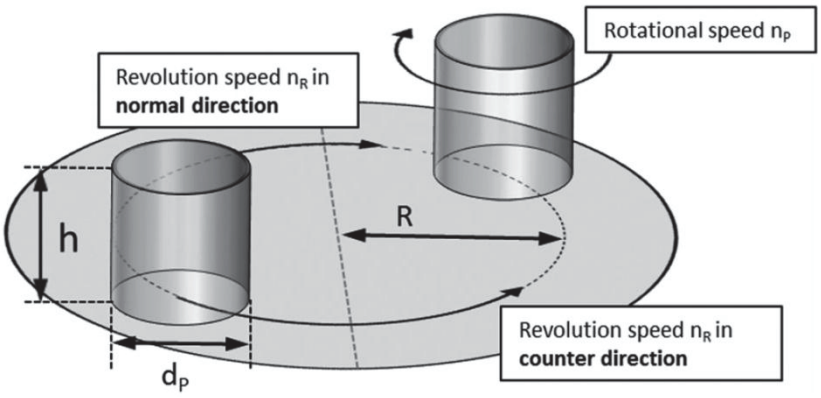

Figure 4.6 Principle of planetary ball mill. From the literature[7].

The kinetic energy is affected different variables, as deduced from:

$$E_{kin}(rot\ or\ osc) = 0.5I\omega^2 = 2\pi^2 I\nu^2$$

where ν_{rot} or ν_{osc} is the rotation or oscillation frequency; and I the moment of inertia (depending from material density). Reaction time *t* and frequency ν affect the reaction. It is well known that increasing *t* leads to higher yields[1]. In most cases a minimum speed is required for an efficient grinding. Increasing the speed often augments the yield. However, in some cases, once arrived to a given value, the reaction efficiency plateaus. Additionally, if the revolution speed is too high, it might yields to undesired side-products. Therefore, the influence of the speed on the yield of reaction depends strictly of the type of reaction studied[1,7].

The type of material of the balls and jars affects the yield, the selectivity and more generally the reaction, as can be deduced from the previous equation. Passing from a light-weight material to a high-weight material, some reactions show an increment in yield, while others not. Therefore, the choice has to be done by taking into account the envisaged reaction and not considering the general rule of higher material density, higher energy transferred[1,7].

Finally also, size and number of balls and other parameters contributed to the success of the reaction in mechanochemistry, as extensively explained in some reviews[1,7]. We will not get into further details.

Although standard mechanochemical reactions use pure products, in this work we mixed the sample with $CaCO_3$ substrate.

In this work all the samples were prepared with the same procedure and with the same amount of calcium carbonate and 4-iodobenzoic acid (0.900g and 0.170g respectively). The reactants were weighted directly in the jars. All the experiments were characterized by a cycle

of mixing followed by a pause in order to cool down the jars. In all the cases the jars were filled up to 2/3 with milling balls and reaction mixture; the other third is necessary for the trajectory of the milling balls.

In a first preliminary experiment (entry 1 and 2 in Table 4.1) reactant (4-iodobenzoic acid) and $CaCO_3$ were ground together in corundum jars (45 ml with 10 mm Ø balls) in a planetary milling machine (Pulverisette). The speed was maintained constant at 700 rpm with 18 balls.

After this preliminary test, all the other experiments (samples 3 to 7 in Table 4.1) were carried out in a more efficient planetary milling machine (Pulverisette 7 Premium line, Fritsch). The new machine allowed testing different number of cycles and different temperatures in order to optimize the reaction. Reactant and $CaCO_3$ (previously milled) were ground together in agate jars (20 ml with 10 mm Ø balls). In this machine it was possible to invert the sense of rotation every cycle; this option was not possible in the preliminary experiment. The speed was maintained constant for all experiments at 750 rpm with 10 balls.

First, we tested different parameters (time and cycles) in order to optimize the reaction conditions (samples 3 to 5). Then, we carried out a second experiment (sample 6) with the optimized parameters and pre-heated $CaCO_3$. Finally, the last experiment (sample 7) was performed in the same conditions as for previous sample, but the jars were filled with argon gas.

Experimental details of all the samples are summarized in Table 4.1.

Sample	**Speed (rpm)**	**Time of mixing**	**Pause (min)**	**Cycle**	**Inversion**	**Comments**
1	700	15 min	/	/	/	
2	700	9 h	15	/	/	
3	750	15 min	5	4	On	
4	750	30 min	5	4	On	
5	750	30 min	5	8	On	
6	750	30 min	5	8	On	$CaCO_3$ pre-heated
7	750	30 min	5	8	On	$CaCO_3$ pre-heated and under Ar atm

Table 4.1 Experimental details of the samples in the coupling reaction activated *via* mechanochemistry.

Once the reaction is finished, the samples were treated with the same procedure. The standard work-up consists in dilution of the reaction mixture in deionized water, then HCl 1M is added slowly in order to dissolve the $CaCO_3$ powder. Then, the aqueous phase is extracted

with dichloromethane; the organic phases were collected together and dried over anh. $MgSO_4$ and the solvent was removed under vacuum.

4.1.3 Results and discussion

As previously mentioned, the first two samples were ground in an old-model planetary ball mill (Table 4.1). In the first case (entry 1) the reaction mixture was ground for 15 minutes and then work-up followed the reaction. In this case only the starting material was found. As reaction time is well known as a key parameter[1,6] of mechanochemistry reactions, in the second case (entry 2) the reaction mixture was ground for 9 hours. Standard work-up followed the reaction and NMR spectrum shows only starting material and traces of 4-iodobenzoic acid.

Sample 3 to 5 (Table 4.1), were carried out in a more recent and efficient model of planetary machine (Pulverisette 7 Premium line, Fritsch). The NMR spectra of these products show the presence of both reactant and benzoic acid. Comparing with sample 2, the peaks of samples 3-5 are finer and the integration is higher. The ratio between the the product and starting material is drastically lower in samples 3-5 than sample 2, showing the more efficient grinding performance of the second mill (Table 4.2).

The product obtained in this reaction was also compared with the reference of commercial benzoic acid and 4-hydroxybenzoic acid (the two products expected from the side reaction with water molecules, Table 4.2).

Entry	δ_1 **(d)**	δ_2 **(t)**	δ_3 **(t)**	**Ratio benzoic acid/starting mat**
Sample 2	7.945	-	7.50	0.02:1
Sample 3	7.945	7.623	7.50	0. 2:1
Sample 4	7.945	7.623	7.50	0.26:1
Sample 5	7.945	7.623	7.50	0.74:1
Ref. benzoic acid	7.95	7.62	7.50	

Table 4.2 NMR ^{1}H chemical shift of samples 2 to 5 and reference of benzoic acid.

As in all the cases we obtained benzoic acid, we speculate on the presence of layers of water molecules on the calcite samples. We suggest a radical mechanism starting with a cleavage of C-halide bond and following reaction with a water molecule (Figure 4.7).

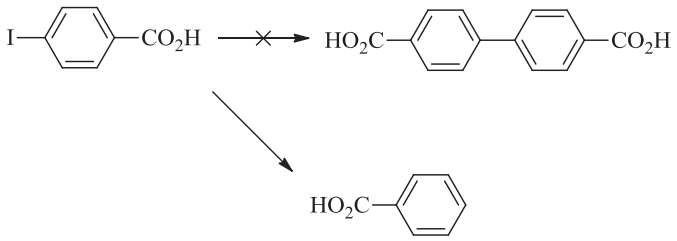

Figure 4.7 Suggested reaction in planetary ball milling machine.

In order to avoid water molecules, a second experiment was carried out (sample 6 in Table 4.1). 4-iodobenzoic acid was mixed with $CaCO_3$ (previously dried for 24 hours in an oven at 200 °C). Then the reaction was conducted with the same conditions (speed, time, pause, cycles and inversion) of sample 5. The spectrum showed that product was again benzoic acid (Table 4.3).

Entry	δ_1 (d)	δ_2 (t)	δ_3 (t)	Ratio benzoic acid/starting mat.
Sample 5	7.945	7.623	7.50	0.74:1
Sample 6	7.945	7.623	7.50	2.63:1
Ref. benzoic acid	7.95	7.62	7.50	

Table 4.3 NMR ^{1}H chemical shift of samples 5 and 6.

Finally the last experiment (sample 7 in Table 4.1) was carried out under argon atmosphere in order to avoid air humidity. $CaCO_3$ was previously dried 24 hours in an oven at 200 °C. All the other parameters were maintained constant (speed, time, pause, cycles and inversion). The NMR spectrum showed the same results and final product (benzoic acid).

4.1.4 Conclusions on reaction by mechanochemistry activation

In this first approach we decided to activate 4-iodobenzoic acid by mechanochemistry. Two preliminary experiments were conducted in a planetary ball mill, but in this case only starting material and traces of benzoic acid were recovered.

The other reactions were conducted in a more efficient planetary ball milling machine (Pulverisette 7 Premium line, Fritsch). In this case different conditions of time and cycles were tested in order to find the ideal parameters. After optimization, we carried out the experiment with pre-heated $CaCO_3$; then with the same conditions and under argon atmosphere. In all the cases we obtained benzoic acid. For this reason, we suggest the presence of layers of water molecules which could explain the preponderance of this side-reaction that affords benzoic acid.

In the case of mechanochemistry reaction, however, the substrate of $CaCO_3$ is not necessary. Therefore the study can be pursued with the same precursor molecule, without the substrate in order to concentrate the reaction mixture.

4.2 Coupling reaction on solid surface by thermal activation

4.2.1 Introduction and objective

The second approach analyzed in this work is thermal activation. The mixture of 4-iodobenzoic acid (precursor) and $CaCO_3$ (previously milled) was heated in a specific furnace under vacuum. Then, once the reaction was finished, the mixture was treated with standard work-up.

4.2.2 Experimental

All the samples were prepared with the same amount of $CaCO_3$ and 4-iodobenzoic acid (0.900 g and 0.170 g respectively). The reactants were weighted directly in the jars.

4-iodobenzoic acid was ground with $CaCO_3$ (previously prepared) in a grinding machine for 15 minutes (Pulverisette). Then the powder was placed in a crucible inside a furnace and preheated for 2 hours at 200 °C under vacuum ($P = 1.8\ 10^{-2}$ mbar) in order to remove all the water molecules and deprotonate the carboxylic acid. Then the temperature was increased to determined values (different temperatures were tested in order to find the best reaction protocol, as will be discussed below).

Once the reaction was stopped, all the samples were treated with the same procedure (standard work-up). Those were diluted in deionized water and $CaCO_3$ was dissolved by adding slowly HCl 1M. The reaction mixtures were then extracted with dichloromethane, dried over anh. $MgSO_4$ and the solvent removed under vacuum.

4.2.3 Results and discussion

Once treated with the standard work-up, all the samples were analyzed by NMR spectroscopy.

In a first experiment we tested this reaction at 400 °C for 1 day (entry 1, Table 4.4). The NMR spectrum shows the complete decomposition of the starting material. For this reason the temperature was decreased at 300 °C (entry 2, Table 4.4). In this case we obtained large amount of starting material, diaryl ether (4,4'-oxydibenzoic acid) (product A) and benzoic acid (product B), Figure 4.8.

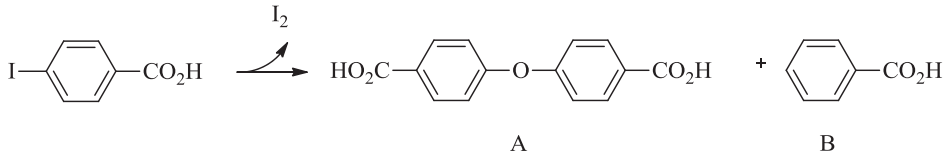

Figure 4.8 Reaction *via* thermal activation.

The reaction conditions were optimized in terms of time and temperature as reported in the summary table below.

Entry	Temp. (°C)	Time	Product A/starting mat.	Product B/ starting mat.
1	400	1 day	Decomposition of all the products	
2	300	1 day	0.06:1	0.06:1
3	300	2 days	0.1:1	0.06:1
4	300	3 days	1:1	2:1
5	300	4 days	Decomposition of all the products	
6	250	3 days	0.15:1	0.08:1
7	260	3 days	0.16:1	0.10:1
8	280	3 days	0.83:1	0.29:1

Table 4.4 Summary of thermal activated experiment parameters and results.

If the reaction is carried out for two days at 300 °C (entry 3), the quantity of starting material is still high. If the time is extended to 3 days (entry 4) the amount of starting material decreases, however the side-product B (benzoic acid) is predominant. If the reaction is too long (entry 5) all the products are decomposed and the NMR spectrum is no more interpretable. For temperature of 250 or 260 °C (entry 6 and 7) the amount of starting material is still high.

Finally, the best condition found is for 3 days at 280 °C (entry 8). In this case, the reaction mixture affords product A, a low amount of starting material and the side-product B is still present.

In all the cases we found I_2 (confirmed by an UV-Vis spectroscopy qualitative test) in a trap at (-20 °C) placed between the pump and the furnace.

Product A was isolated and fully characterized. The reaction mixture obtained at 280 °C was treated with a standard work-up. The separation of starting material and product A was not possible with HPLC system due to the high insolubility of the product mixture; it was then esterificated in standard condition (methanol, conc. sulfuric acid as catalyst)[8]. Flash

chromatography separation (ethyl acetate/pentane 5:95) afforded the esterificated derivative of product A and starting material. Esterificated product A was analyzed by NMR (mono and bidimentional) and mass spectroscopy.

The NMR spectrum of the esterificated product A, shows two doublets and one singlet, and is very similar to the methyl-4-hydroxy benzoate and dimethyl-4,4'-biphenyldicarboxylate ones (Table 4.5). However, the latter could be excluded due to the slightly different chemical shift signals. In order to discriminate between the methyl-4-hydroxy benzoate and the diaryl ether (A), we mixed the two different products (1:1 solution). In this case, the NMR spectrum shows 8 different signals, confirming two different products. The NMR and mass spectroscopy data data are in agreement with the literature[9,10] confirming that the obtained product A is the diaryl ether (4,4'-oxydibenzoic acid).

	δ_1 (d) aromatic	δ_2 (d) aromatic	δ_3 (s) methyl
Product A esterificated	8.055	7.055	3.91
Reference lit.[9,10]	8.06	7.06	3.92
Methyl-4-hydroxy benzoate	7.955	6.885	3.90
Dimethyl-4,4'-biphenyldicarboxylate[10]	8.13	7.69	3.95

Table 4.5 NMR signals of product A esterificated; its reference from the literature; methyl-4-hydroxy benzoate and dimethyl-4,4'-biphenyldicarboxylate.

The yield of this reaction is 16%, represents a "compromise" in terms of time and temperature: in fact too high temperature or over extended time lead to decomposition of the product.

The reaction was also carried out on spray pyrolysis substrate microparticle (SP at 400 °C after heating treatment), and we obtain the same product and benzoic acid as side product.

4.2.3.1 Mechanism discussion

Starting from 4-iodobenzoic acid, thermal activation yielded diaryl ether as main product (Figure 4.8).

Diaryl ethers have been deeply studied due to their interest in industrial and biological field. In fact, these compounds are interesting substructure in the total synthesis of antibiotics (teicoplanin) or anti-HIV agents (chloropeptin)[11–14].

The standard synthesis of diaryl ethers involves the Ullmann coupling of phenol and aryliodide with stoichiometric copper catalyst and drastic conditions[11,12]. D. M. T. Chan and D. A. Evans proposed separately the synthesis of diaryl ether *via* coupling of arylboronic

acids and phenols, in presence of copper(II) catalyst and base. The reaction in this case proceeds at room temperature[15,16]. A. Aranyos and coworkers reported palladium-catalyzed cross-coupling of phenol and aryl halide with very good yield[17]. Metal-free routes were proposed by Z. Liu and coworkers *via O*-arylation of phenol and aromatic carboxylic acid[18] and F. Li and coworkers *via* microwave-assisted coupling reaction of phenols and aryl halide in presence of potassium carbonate[19]. H. J. Cristau and others suggested a milder Ullmann reaction conditions, with low-cost ligands, copper(I) catalyst, base in acetonitrile[11]. Those metal-catalyzed routes are, however, not compatible with the industrial production.

Finally, the most recent studies are focused on diaryliodonium salts. The synthesis from these compounds is actually well known since 1950, but the use of protic solvent, long reaction times, high temperature afforded the target molecules with moderate yield[12,20]. The recent development of new routes for diaryliodonium salts[21], paved the way for their applications[12,20]. In the most recent papers the arylation of phenols is performed in milder conditions in aprotic solvent with diaryliodonium triflates and tetrafluoroborates (soluble in less polar solvent)[12,20]. In Figure 4.9 are summarized the principal synthetic strategies presented in this chapter in order to obtain diaryl ethers. The first strategy includes the metal catalyzed synthesis (such as Ullmann or palladium catalyzed). The second route is metal-free and it involves the diaryliodonium salt. The last route, elaborated in this thesis, is, for the first time, metal and solvent-free.

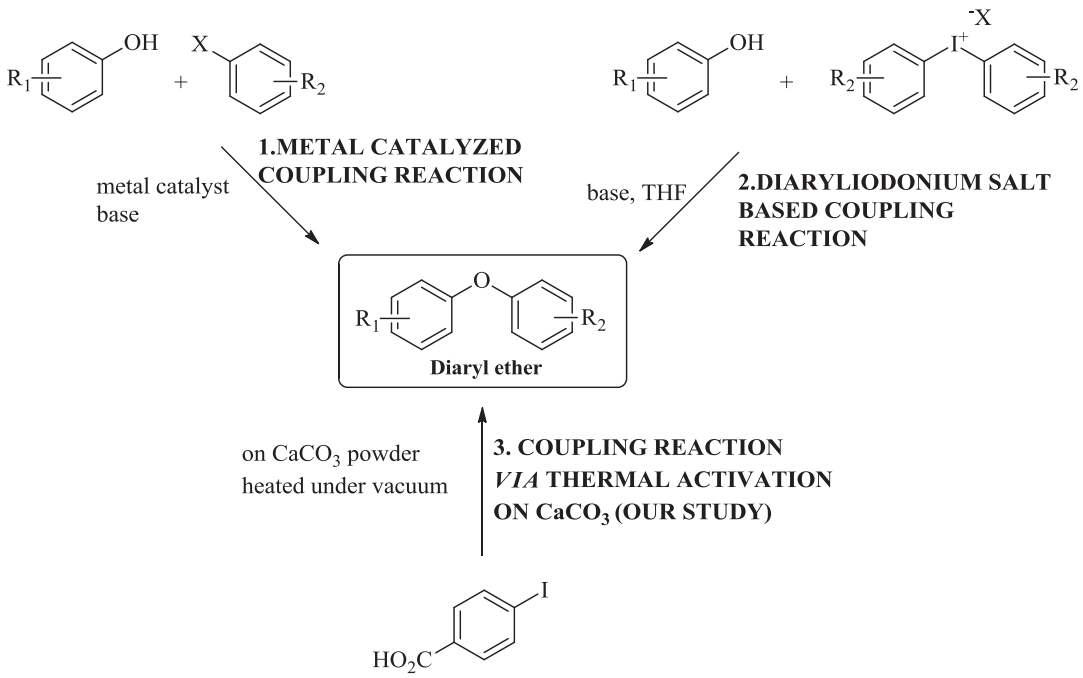

Figure 4.9 Principal synthetic strategies in order to obtain diaryl ethers.

In the third case, for the coupling reaction *via* thermal activation, we suggest a reaction mechanism involving a basic confinement. Even if the sample is dried for 2h at 200 °C, in fact, we suppose the presence of water layers on the particles. $CaCO_3$ is slightly soluble in water but it forms the HCO_3^- and CO_3^{2-} species in equilibrium. The evaporation of water molecules, due to the combined effect of temperature and vacuum, forms a basic confinement environment. In this context, a first halide cleavage step could form the radical and then the phenate molecule (after reaction with a water molecule). Alternatively, the latter could also be formed from the attack of OH^- (basic confinement) to the 4-iodobenzoic acid. Once formed, we suppose that the phenate attacks another 4-iodobenzoic acid and form the diaryl ether.

4.2.3.2 3-iodobenzoic acid

Having in mind the result obtained for the 4-iodobenzoic acid, we decided to extend the study on 3-iodobenzoic acid. We used the same experimental conditions of the previous case.

3-iodobenzoic acid was ground with $CaCO_3$ freshly milled for 15 minutes (same amount as for 4-iodobenzoic experiment). Then the mixture was placed in a crucible and heated under vacuum at 200 °C for 2 hours in order to remove all the water molecules. The temperature was then increased to 280 °C for 3 days. Standard work-up afforded the mixture product/starting material with a molecular ration of 0.43:1. At the moment of the redaction of this manuscript, the esterification followed by purification and complete characterization is still in progress in order to identify the molecule.

4.2.4 Other reactions studied in this work

Another interesting reaction studied in this work is the condensation of 2,3-dicyanonaphthalene in order to obtain phthalocyanine. The reaction has already been reported in UHV conditions on a monolayer of NaCl[22] (chapter 1). With this new approach we tried to extend the study from the UHV conditions to the surface of particles.

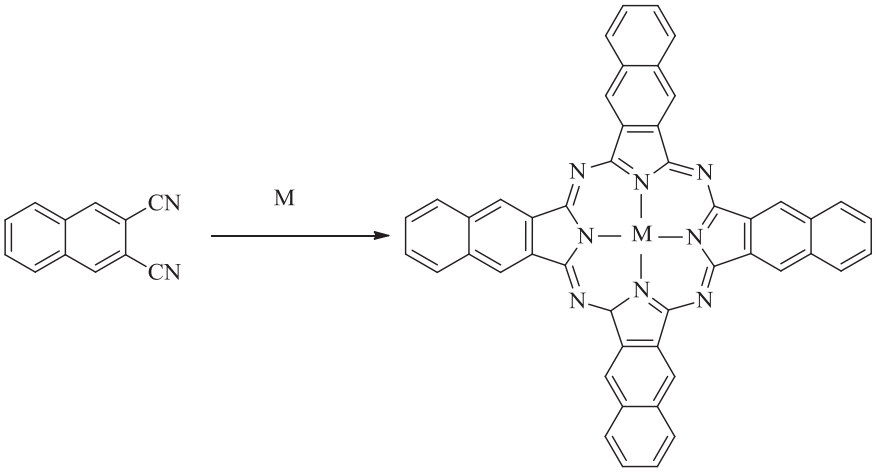

Figure 4.10 Phthalocyanine reaction; M is the metal, for instance Fe.

The reaction was carried out in conditions similar to the previous experiments on benzoic acid derivatives. In all cases 2,3-dicyanonaphthalene was ground with $CaCO_3$ (previously prepared) in a grinding machine for 15 minutes in presence of Fe powder (0.160 g, 7.174 g and 0.040 g respectively) under argon atmosphere. Then, we tested three different conditions, as summarized in Table 4.6.

Entry	Temp. (°C)	Time
1	RT	1 day
2	200	1 day
3	200	4 days

Table 4.6 Summary table of temperature and time parameters in phthalocyanine reaction.

In a first preliminary experiment (entry 1), we analyzed the milling product in order to see if the reaction was already started with milling. However after the work-up, the NMR spectrum shows only the starting material.

In the other two cases (entry 2 and 3) the reaction mixture was placed in a crucible inside the furnace and preheated for 1h30 at 100 °C under vacuum in order to remove all the water molecules. Then the temperature was increased to 200 °C. Standard work-up followed the reaction.

If the reaction is carried out one day (entry 2) the NMR spectrum of the reaction mixture shows one molecule with similar pattern but different chemical shift as main product and traces of starting material. However if the reaction is carried out in the same experimental conditions but for 4 days (entry 3), the NMR spectrum becomes more complicated. It shows several peaks that might be assigned to different products of many reactions occurring at the same time.

The reaction at 200 °C for 1 day (entry 2) is a particularly attractive candidate for our preliminary work because it forms mainly one product. Therefore, the reaction mixture was purified by column chromatography on silica gel (ethyl acetate/dichloromethane/cyclohexane 1:6:3) and the product analyzed by mono and bidimentional NMR spectroscopy. In this case, the compound shows the same pattern of the 2,3-dicyanonaphthalene but different chemical shift.

We suggested two possible products as reported in the picture below (Figure 4.11): naphthalene dicarboxylic anhydride (naphtho[2,3-*c*]furan-1,3-dione, product **1**) or dicarboxylic acid (naphthalene-2,3-dicarboxylic acid, product **2**). In both cases phthalocyanine was not obtained, probably due to the water molecules present $CaCO_3$; additionally metallic Fe did not take part to the reaction.

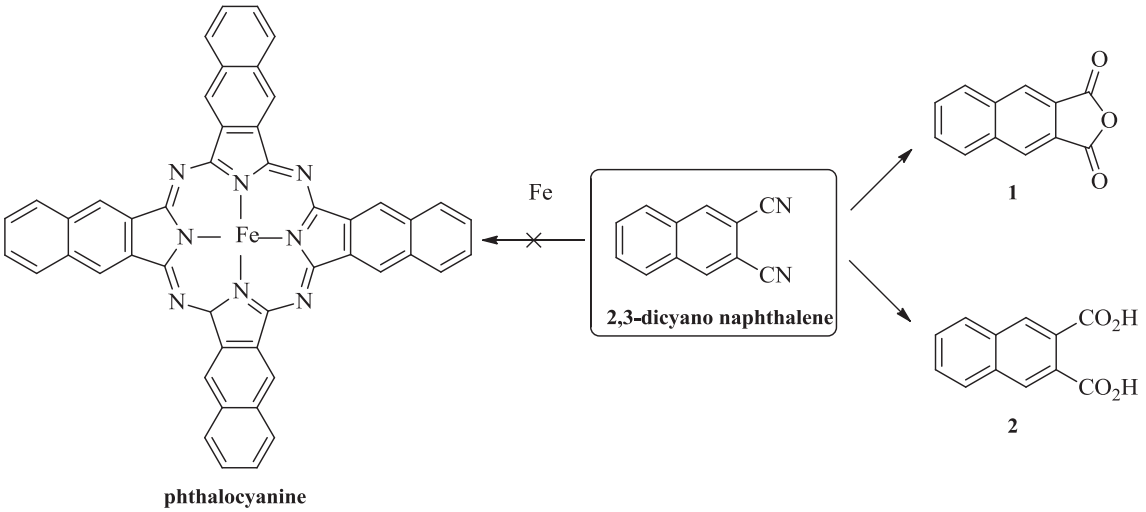

Figure 4.11 Different reaction products from 2,3-dicyanonaphthalene starting material.

The NMR spectrum of anhydride derivative (molecule **1** in Figure 4.11) is already known in literature[23], while the dicarboxylic derivative only in SDBS database. Therefore alone NMR spectroscopy cannot discriminate between the two forms. For this reason we completed the study with also mass spectroscopy and infrared spectroscopy. High resolution mass spectroscopy by chemical ionization (DCI/CH_4) suggests the anhydride form (m/z 198). However, this technique is not enough to discriminate between the two possible products because the carboxylic form could also dehydrate at the moment of the analysis. The infrared spectrum here is reported in the significant range of 4000-1400 cm^{-1}. The starting material 2,3-dicyanonaphthalene is compared to the product of the reaction after work-up and purification (Figure 4.12). The first shows the characteristic peak corresponding to the -CN

group (marked with the symbol * in the graph) at 2224 cm^{-1} in agreement with the literature[24,25]. This peak disappears in the reaction product. Additionally the latter shows a characteristic double peak around 1770-1710 cm^{-1} (marked with the symbol § in the graph). This pattern is typical of anhydride compounds (two double peaks separated by about 60 cm^{-1}). Usually it appears at around 1850-1800 cm^{-1} and 1790-1740 cm^{-1} but it may be shifted due to the conjugation (as in this case). The typical IR spectrum of carboxylic acid (reported in literature[26]) does not present these double bands.

We can conclude that the product obtained from this reaction is the anhydride (product **1** in Figure 4.11).

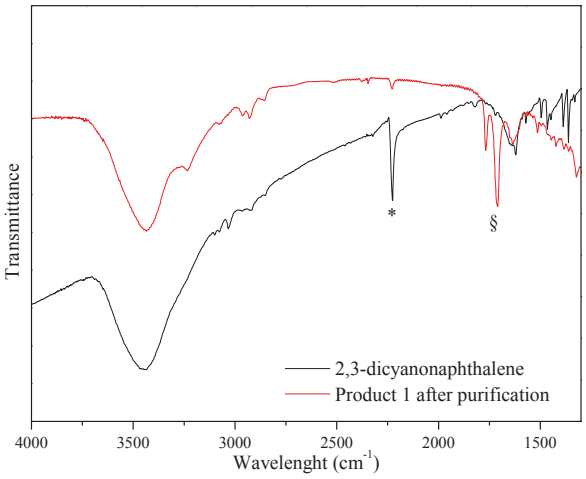

Figure 4.12 FTIR of product **1** after purification and 2,3-dicyanonaphthalene between 4000 and 1400 cm^{-1}.

4.2.4.1 Mechanism discussion

Here we report the two different mechanisms for product **1** and **2**:

- Nitrile hydrolysis in basic conditions:

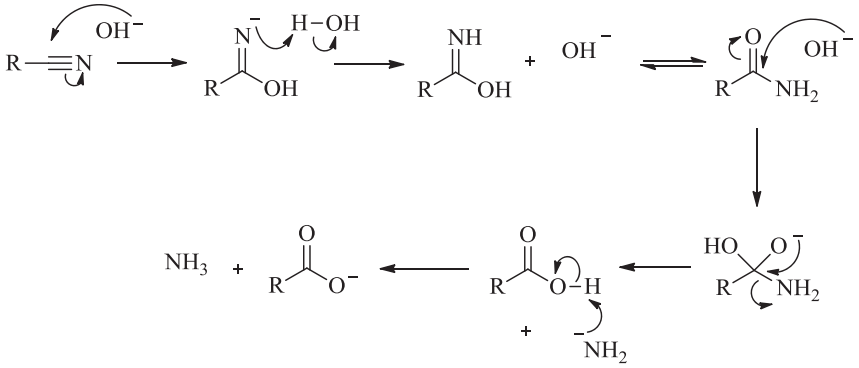

Figure 4.13 Nitrile hydrolysis in basic conditions.

- By heating the carboxylic acid, the corresponding cyclic naphthalene dicarboxylic anhydride (naphtho[2,3-*c*]furan-1,3-dione) can be obtained:

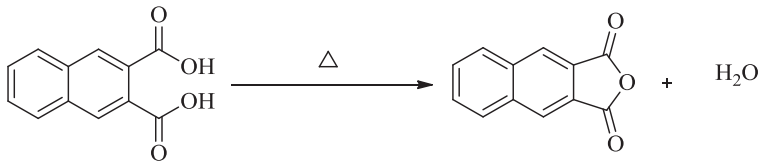

Figure 4.14 Dehydration of carboxylic acid.

In our case, probably, a first step of nitrile hydrolysis occurs in basic conditions followed by dehydration of the carboxylic derivative.

We can conclude for this reaction that the temperature was not high enough to give the phthalocyanine. Moreover, the cyano groups reacted immediately with the water molecules.

In UHV the reaction was more efficient for several reasons: not only the environment is water-free (side reactions are limited), but also the metal atoms sublimated directly on the surface are more reactive than Fe powder used in our experiment.

4.2.5 Conclusions on coupling reaction by thermal activation on $CaCO_3$ microparticles

The second approach studied in this work consists in coupling reaction *via* thermal activation. We optimized the reaction parameters (substrate milling grade, temperature and time) in order to obtain, for the first time, diaryl ether derivative (4,4'-oxydibenzoic acid) with a metal-free and solvent-free method.

In this work we also investigate the condensation of 2,3-dicyanonaphthalene: we obtained and completed characterized the naphthalene dicarboxylic anhydride (naphtho[2,3-*c*]furan-1,3-dione).

Finally we also started the study of the coupling reaction on 3-iodobenzoic acid; at moment of the redaction of the manuscript the complete characterization is in progress.

Further studies should be done to improve the yield and better understand the reaction mechanism.

4.3 General conclusion on coupling reactions on solid surface

In this chapter we presented the reactivity of 4-iodobenzoic acid on $CaCO_3$ *via* two different solvent-free methods.

Once the precursor molecules are grafted to the $CaCO_3$ surfaces, the reaction is activated with two different solvent-free approaches: mechanochemistry and thermal activation.

In the first case, the mixture is milled in a planetary ball mill (Pulverisette 7 Premium line, Fritsch). We investigated different conditions of time and cycles to optimize the reaction. We also carried out the reaction with pre-heated $CaCO_3$ and under argon atmosphere. The product obtained in all the cases (with different molecular ratio) is benzoic acid. We hypothesize the presence of layers of water molecules that could explain this product. In this case, we suggest as future experiment, the synthesis without the substrate of $CaCO_3$ in ultra-dry conditions.

In the second approach we carried out the reaction *via* thermal activation. In this case the molecule obtained is diaryl ether derivative (4,4'-oxydibenzoic acid). With this strategy we also synthesized and completely characterized the naphthalene dicarboxylic anhydride (naphtho[2,3-*c*]furan-1,3-dione).

We can conclude that the main factor affecting this coupling reaction on $CaCO_3$ is the surface chemistry. In fact when the reaction is performed in UHV, the surface of the calcite crystal is cleaved *in situ* and no water molecules are present. The pressure in this case is very low (10^{-9} mbar) and the surface is perfectly clean.

When the precursor molecules are activated by mechanochemistry, we suppose that the presence of water molecules layers leads the competitive reaction to become predominant.

Finally, when the reaction is carried out inside the furnace, the pressure is 10^{-2} mbar, and the presence of water layers favors a basic confinement. In this medium, two mechanisms seem possible: nucleophilic attack on the precursor molecule and the consequent formation of phenate. The latter attacks 4-iodobenzoic acid to afford diaryl ether (4,4'-oxydibenzoic acid).

Technique	**Grade of purity of the surface**	**Pressure**	**Product**
UHV	Very clean: the crystals are cleaved under vacuum	10^{-9} mbar	4,4'-Biphenyldicarboxylic acid
Mechanochemistry activation	Layers of water molecules	Ambient	Benzoic acid
Thermal activation	Basic confinement environment	1.8 10^{-2} mbar	Diaryl ether or naphthalene dicarboxylic anhydride

Table 4.7 Summary of the differences between the three techniques.

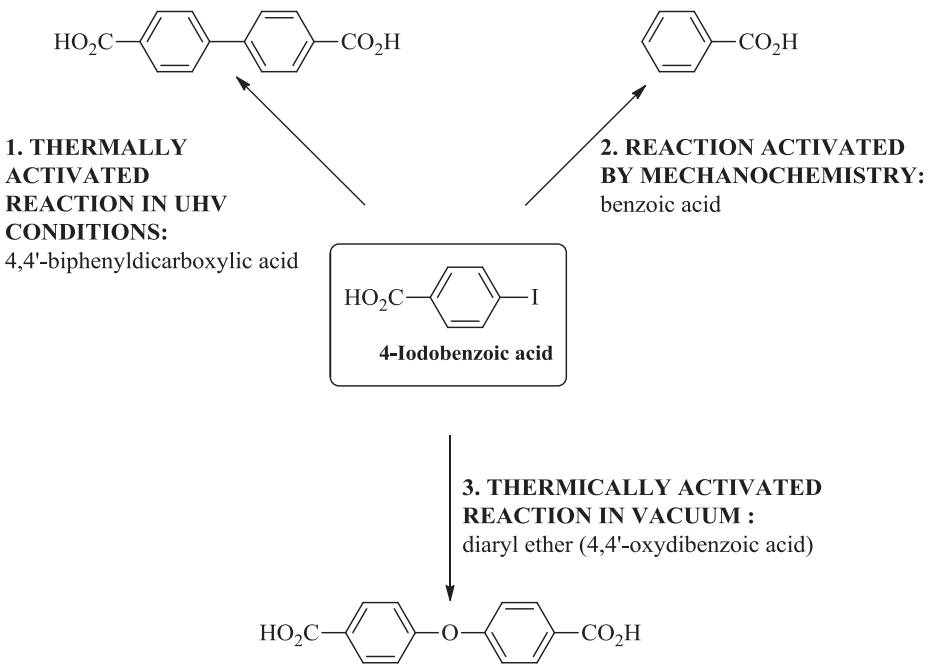

Figure 4.15 Summary of possible reactions from 4-iodobenzoic acid precursor molecule.

4.4 References

1. Stolle, A., Szuppa, T., Leonhardt, S. E. S. & Ondruschka, B. Ball milling in organic synthesis: solutions and challenges. *Chem. Soc. Rev.* **40,** 2317–2329 (2011).
2. Boldyreva, E. Mechanochemistry of inorganic and organic systems: what is similar, what is different? *Chem. Soc. Rev.* **42,** 7719 (2013).
3. Jones, W. & Eddleston, M. D. Introductory Lecture: Mechanochemistry, a versatile synthesis strategy for new materials. *Faraday Discuss.* **170,** 9–34 (2014).
4. James, S. L. *et al.* Mechanochemistry: opportunities for new and cleaner synthesis. *Chem. Soc. Rev.* **41,** 413–447 (2011).
5. Fox, P. G. Mechanically initiated chemical reactions in solids. *J. Mater. Sci.* **10,** 340–360 (1975).
6. Stolle, A., Schmidt, R. & Jacob, K. Scale-up of organic reactions in ball mills: process intensification with regard to energy efficiency and economy of scale. *Faraday Discuss.* **170,** 267–286 (2014).
7. Burmeister, C. F. & Kwade, A. Process engineering with planetary ball mills. *Chem. Soc. Rev.* **42,** 7660–7667 (2013).
8. Ronde, N. J. *et al.* Molecular-Weight-Enlarged Multiple-Pincer Ligands: Synthesis and Application in Palladium-Catalyzed Allylic Substitution Reactions. *ChemSusChem* **2,** 558–574 (2009).
9. Sengupta, S., Sadhukhan, S. K., Bhattacharyya, S. & Guha, J. Palladium-catalyzed reactions of bisarenediazonium salts: two-fold Heck reaction, carbonylation and cross-coupling regimen. *J. Chem. Soc. [Perkin 1]* 407–410 (1998). doi:10.1039/a707378j
10. Hirashima, S., Nobuta, T., Tada, N., Miura, T. & Itoh, A. Direct Aerobic Photo-Oxidative Synthesis of Aromatic Methyl Esters from Methyl Aromatics via Dimethyl Acetals. *Org. Lett.* **12,** 3645–3647 (2010).
11. Cristau, H.-J., Cellier, P. P., Hamada, S., Spindler, J.-F. & Taillefer, M. A General and Mild Ullmann-Type Synthesis of Diaryl Ethers. *Org. Lett.* **6,** 913–916 (2004).

12. Jalalian, N., Ishikawa, E. E., Silva, L. F. & Olofsson, B. Room Temperature, Metal-Free Synthesis of Diaryl Ethers with Use of Diaryliodonium Salts. *Org. Lett.* **13,** 1552–1555 (2011).
13. Deng, H. *et al.* Total Synthesis of Anti-HIV Agent Chloropeptin I. *J. Am. Chem. Soc.* **125,** 9032–9034 (2003).
14. Evans, D. A., Katz, J. L., Peterson, G. S. & Hintermann, T. Total Synthesis of Teicoplanin Aglycon. *J. Am. Chem. Soc.* **123,** 12411–12413 (2001).
15. Chan, D. M. ., Monaco, K. L., Wang, R.-P. & Winters, M. P. New N- and O-arylations with phenylboronic acids and cupric acetate. *Tetrahedron Lett.* **39,** 2933–2936 (1998).
16. Evans, D. A., Katz, J. L. & West, T. R. Synthesis of diaryl ethers through the copper-promoted arylation of phenols with arylboronic acids. An expedient synthesis of thyroxine. *Tetrahedron Lett.* **39,** 2937–2940 (1998).
17. Aranyos, A. *et al.* Novel Electron-Rich Bulky Phosphine Ligands Facilitate the Palladium-Catalyzed Preparation of Diaryl Ethers. *J. Am. Chem. Soc.* **121,** 4369–4378 (1999).
18. Liu, Z. & Larock, R. C. Facile *O* -Arylation of Phenols and Carboxylic Acids. *Org. Lett.* **6,** 99–102 (2004).
19. Li, F., Wang, Q., Ding, Z. & Tao, F. Microwave-Assisted Synthesis of Diaryl Ethers without Catalyst. *Org. Lett.* **5,** 2169–2171 (2003).
20. Jalalian, N., Petersen, T. B. & Olofsson, B. Metal-Free Arylation of Oxygen Nucleophiles with Diaryliodonium Salts. *Chem. - Eur. J.* **18,** 14140–14149 (2012).
21. Merritt, E. & Olofsson, B. Diaryliodonium Salts: A Journey from Obscurity to Fame. *Angew. Chem. Int. Ed.* **48,** 9052–9070 (2009).
22. Abel, M., Clair, S., Ourdjini, O., Mossoyan, M. & Porte, L. Single Layer of Polymeric Fe-Phthalocyanine: An Organometallic Sheet on Metal and Thin Insulating Film. *J. Am. Chem. Soc.* **133,** 1203–1205 (2011).
23. Nishina, Y., Kida, T. & Ureshino, T. Facile Sc(OTf) 3-Catalyzed Generation and Successive Aromatization of Isobenzofuran from o -Dicarbonylbenzenes. *Org. Lett.* **13,** 3960–3963 (2011).
24. Lin, C.-H., Lin, K.-H., Pal, B. & Tsou, L.-D. Iterative synthesis of acenesvia homo-elongation. *Chem Commun* 803–805 (2009). doi:10.1039/B814840F
25. Akai, N., Kudoh, S. & Nakata, M. Matrix-isolation infrared spectrum and optimized structure of 2,3-dicyanonaphthalene in the T1 state. *Chem. Phys. Lett.* **392,** 480–485 (2004).
26. Rzączyńska, Z., Kula, A., Sienkiewicz-Gromiuk, J. & Szybiak, A. Synthesis, spectroscopic and thermal studies of 2,3-naphthalenedicarboxylates of rare earth elements. *J. Therm. Anal. Calorim.* **103,** 275–281 (2011).

General conclusion

The objective of this thesis was to explore covalent coupling on insulating surface of calcium carbonate. For this reason, we first synthesized a series of molecules to be deposited on calcium carbonate in Ultra High Vacuum (UHV) conditions, in order to study various types of reactions: homocoupling of ethynes, photopolymerization, polycondensation and Ullmann reaction.

The molecules comprised a carboxylic acid anchoring group (in order to prevent the formation of clusters or desorption from the surface) and a reactive groups.

Then we also synthesized 2,3-dicyanonaphthalene and naphthalene-2,3,6,7-tetracarbonitrile compounds in order to investigate the polycondensation on calcite in UHV in presence of metal atoms (Fe or Au) to yield the phthalocyanines or polyphthalocyanines.

Those molecules are currently been studied on calcite surface in UHV conditions in Prof. A. Kühnle's group, University of Mainz, Germany.

In the second part of this work we extended for the first time this investigation from the surface in UHV to microparticles surfaces. First, we prepared calcium carbonate microparticles by grinding or by spray pyrolysis (a new method of preparation of these particles) that were fully characterized with different techniques: FTIR, TG/DTG, XRD, SEM and BET. Then, the precursor molecules were deposited on the surface of those particles and the reactions were activated with two different solvent-free methods:

- By grinding in a planetary milling machine (mechanochemical activation).
- By heating the samples in a furnace under vacuum (thermal activation).

Then, the microparticles of $CaCO_3$ were dissolved in weak acids allowing the extraction of the reaction products and their characterization by NMR and mass spectroscopy.

As a prototype reaction, we studied the coupling of 4-iodobenzoic acid which has been shown to give 4,4'-biphenyldicarboxylic acid in UHV.

In the first case (mechanochemical activation) we obtained benzoic acid as the main product, while in the second case (thermal activation) diaryl ether derivative. In both cases the formation of reaction products was interpreted as the presence of water layers.

Perspective works

The short term work envisages completing the deposition and the study of the synthesized molecules on calcite in UHV (ethynes, dimers and naphthalene derivatives).

In particularly the naphthalene-2,3,6,7-tetracarbonitrile compound will be deposited in presence of different metals (such as Mn instead of Fe, that in a previous case on metal surface allows a diminution of activation temperature[1]).

For the reactions on calcium carbonate microparticles, it will be possible to synthesize similar molecules such as polyether derivatives.

For long term work, we envisage to heat the calcium carbonate at high temperature under vacuum (for instance at 10^{-6} mbar) for several hours in order to remove water molecules, then the substrate could be transferred in a glove box to perform the reactions in a water-free environment. The work should be completed with a specific study on water layers on calcium carbonate.

Additionally, we propose to investigate different types of reactions under vacuum. The precursor molecules should have an anchoring group to fix the insulating surface and reactive groups to perform the reaction, possibly without catalyst.

Possible candidates for this objective are the diboronic acids. With these molecules two reactions could be studied: dehydration in order to obtain polymeric structures or esterification.

The reaction envisaged on calcium carbonate microparticles should take into account two main problems that could prevent the result:

- The presence of a layer of water molecules.
- The polymeric structures might be sensible to the water acid work-up used in the previous cases.

To conclude, calcium carbonate represents an appealing material for future applications in UHV conditions, due to its properties and high surface energy (compared to NaCl or other insulating systems). The explorative work conducted in this thesis paved the way for future studies.

On the other hand, as demonstrated in this work, microparticles of this material can be easily prepared and used as substrate for on-surface reactions. The easy work-up allows

recovering different products. In this context, calcium carbonate offers new possibility as substrate for solvent-free reactions.

References

1. Koudia, M. & Abel, M. Step-by-step on-surface synthesis: from manganese phthalocyanines to their polymeric form. *Chem. Commun.* **50,** 8565 (2014).

EXPERIMENTAL PART

Experimental part of Chapter 2

Generalities

Solvents and Reagents

All the solvents were purchased from Sigma Aldrich and Acros Organics. They were dried over molecular sieves 3Å, unless specified differently. NEt_3 was dried over KOH then distilled under reduced pressure. Anhydrous DMF and 1,4-dioxane were bought from Acros Organics and Sigma Aldrich.

All the reagents were purchased from Sigma Aldrich, Acros Organics or TCI. They were employed without additional purification, unless specified.

Chromatographic supports

Chromatographic purifications were carried out on silica gel (Fluka, pore size 6Å, 230-400Å mesh) or with Flash Chromatography SPOT II Armen Instrument (cartridge of silica Agela 60 Å; 20 g; 40 g). TLC preparatives were carried out on silica gel (silica gel 60 F_{254}, Merck). All the reactions were followed by thin layer chromatography (TLC) on silica gel (silica gel 60 F_{254}, Merck or Fluka) and the revelation was carried out with UV lamp (254 or 365 nm) and by indicators (potassium permanganate, cerium ammonoium molybdate or iodine vapors).

Analytical tools and devices

Nuclear magnetic resonance (NMR) spectroscopy

The NMR spectra were recorded on Bruker Advance 300 or 500 MHz spectrometers (Common service of University Paul Sabatier, Toulouse). As internal reference, the solvent residual signals are reported in table below[1]:

Solvent	**$CDCl_3$**	**CD_2Cl_2**	**DMSO**	**CD_3CN**
Ref.^{1}H (ppm)	7.26	5.32	2.50	1.94
Ref.^{13}C (ppm)	77.16	53.84	39.52	1.32 118.26

Table 1 Solvent residual signal, from ref.[1].

All the chemical shift (δ) reported in this manuscript are in ppm. The following abbreviations were employed: s = singlet, d = doublet, dd = doublet of doublets, t = triplet and m = multiplet.

Mass spectroscopy

The mass spectra and high resolution mass (HRMS) spectra were recorded at the common service of University Paul Sabatier (Toulouse), on different instrument in ESI, DCI (CH_4 or NH_3) and APCI modes.

Crystallographic structures

Single crystal structure was recorded by Dr. Nicolas Ratel-Ramond of X-ray service from CEMES/CNRS laboratory (Toulouse) on a Bruker Kappa APEXII CCD diffractomer.

Synthesis

Methyl 4-iodobenzoate (1) [2]

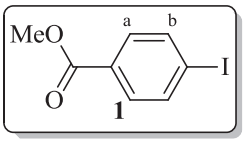

4-Iodobenzoic acid (1 g, 4.03 mmol) was placed in a 250 mL round-bottomed flask and dissolved in MeOH (68 mL). A few drops of conc. H_2SO_4 were added and the solution was refluxed overnight. NEt_3 (0.5 mL) was then added to *p*H 7 and the solvent was removed in vacuum. The residue was dissolved in CH_2Cl_2 and H_2O and the water phase was extracted with CH_2Cl_2 (3 x 30 mL). The combined organic layers were then washed with brine, dried over anhydrous $MgSO_4$ and concentrated under reduced pressure. Final solvent traces were removed under high vacuum to afford the product **1** (0.858 g, 81 %) as a white solid. The compound was used with no further purification.

^{1}H-NMR (300 MHz, $CDCl_3$) δ_H 7.80 (2H, d, J = 8.7 Hz, 2 x Ar-H_b), 7.74 (2H, d, J = 8.7 Hz, 2 x Ar-H_a), 3.91(3H, s, -OCH_3).

Synthesis of methyl 4-((trimethylsilyl)ethynyl)benzoate (2) [3,4]

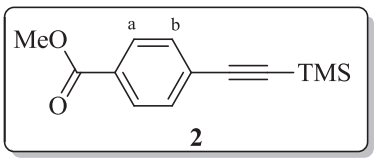

2

A solution of methyl 4-iodobenzoate **1** (2 g, 7.6 mmol, 1 eq) in freshly distilled Et_3N (30 mL) was degassed, under stirring and argon atmosphere for 30 minutes. To this solution, trimethylsilylacetylene (1.2 mL, 8.4 mmol, 1.1 eq) was added and the solution degassed for another 10 minutes. CuI (72.0 mg, 0.38 mmol, 0.05 eq) and $Pd(PPh_3)_2Cl_2$ (160.0 mg, 0.23 mmol, 0.03 eq) were then added and the reaction mixture was stirred at room temperature for 2 hours. The solvent was then removed and the residue was dissolved in EtOAc/hexane (2 : 8), and passed through a silica pad. The combined organic washes were then concentrated to afford the product **2** as an off-white solid (1.66 g, 94 % yield) which was used without further purification.

^{1}H-NMR (300 MHz, $CDCl_3$) δ_H 7.97 (2H, d, J = 8.7 Hz, 2 x Ar-H_a), 7.52 (2H, d, J = 8.7 Hz, 2 x Ar-H_b), 3.91(3H, s, -OCH_3), 0.26 (9H, s, -Si(CH_3)$_3$).

Synthesis of methyl 4-ethynylbenzoate (3) [3,5]

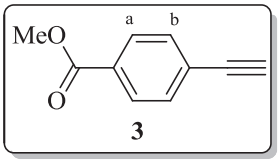

3

4-((Trimethylsilyl)ethynyl)benzoate **2** (1.603 g, 6.89 mmol, 1 eq) was dissolved in a mixture of MeOH:CH_2Cl_2 (1:1, 96 mL) under argon atmosphere. Anhydrous K_2CO_3 was then added (4.69 g, 33.9 mmol, 4.92 eq) and the mixture was stirred at room temperature for 3 hours. CH_2Cl_2 and H_2O were then added and the water layer was extracted with CH_2Cl_2 (3 x 20 mL). The combined organic phases were washed with brine and dried over anhydrous Na_2SO_4, filtered and the solvent was removed in vacuum to afford the product **3** (0.962 g, 87 %) as a solid, which was used with no further purification.

^{1}H-NMR (300 MHz, $CDCl_3$) δ_H 7.99 (2H, d, J = 8.4 Hz, 2 x Ar-H_a), 7.55 (2H, d, J = 8.4 Hz, 2 x Ar-H_b), 3.92 (3H, s, -OCH_3), 3.23 (1H, s, -CH).

Synthesis of dimethyl 4, 4'–(buta-1,3-diyne-1,4-diyl)dibenzoate (4) [6]

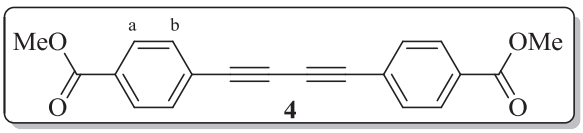

Methyl 4-ethynylbenzoate **3** (0.100 g, 0.624 mmol, 1 eq) was dissolved in dried $^{i}Pr_2NH$ (6.32 mL) and the solvent mixture was degassed under Ar atm. CuI (7.47 mg, 39.2 µmol, 0.063 eq), $Pd(PPh_3)_2Cl_2$ (10.9 mg, 15.5 µmol, 0.025 eq) and iodine (0.120 g, 0.473 mmol, 0.76 eq) were then added while stirring. The reaction mixture was left to react for 6h at room temperature. The solvent was then removed in vacuum; the residue was dissolved in CH_2Cl_2 and washed with a saturated solution of $Na_2S_2O_3$, dried over $MgSO_4$ and evaporated. The compound was dissolved in CH_2Cl_2, passed through a silica pad that was washed with CH_2Cl_2. The combined organic washes were then concentrated to afford the product **4** as a solid (0.080 g, 81 % yield) which was used with no further purification.

^{1}H-NMR (300 MHz, $CDCl_3$) δ_H 8.02 (4H, d, J = 8.4 Hz, 4 x Ar-H_a), 7.59 (4H, d, J = 8.4, 4 x Ar-H_b), 3.93 (6H, s, 2 x -OCH_3).

Synthesis of 4,4'-(buta-1,3-diyne-1,4-diyl)dibenzoic acid (5) [7]

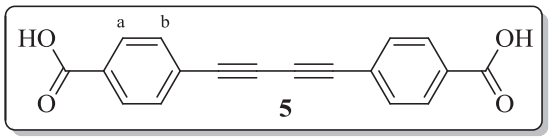

4,4'-(buta-1,3-diyne-1,4-diyl)dibenzoate **4** (0.246 g, 0.772 mmol, 1 eq) was dissolved in THF (18 mL) under stirring. Then a solution of LiOH (0.187 g, 7.81 mmol, 10.12 eq) in H_2O (5.5 mL) was added to the mixture. The reaction was stirred for 5 days, HCl 3M was then added drop by drop until precipitation at pH 2~3. The precipitate was filtrated on funnel and washed with cold H_2O and Et_2O. The product was recovered, dried at the vacuum line (0.137 g, 61 %).

^{1}H-NMR (300 MHz, DMSO) δ_H 7.99 (4H, d, J = 8.4 Hz, 4 x Ar-H_a), 7.75 (4H, d, J = 8.4, 4 x Ar-H_b).

Synthesis of 4-ethynylbenzoic acid (6) [8,9]

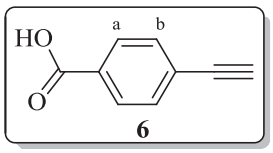

6

Methyl 4-ethynylbenzoate **3** (60 mg, 0.375 mmol, 1 eq) was dissolved in MeOH (0.7 mL) under stirring. Then a solution of LiOH (11 mg, 0.459 mmol, 1.2 eq) in H_2O (0.6 mL) was added to the mixture. The reaction was stirred for 5h. The solvent was then removed in vacuum; HCl 3M was added drop by drop until precipitation at *p*H 2~3 and the solution was extracted with EtOAc. The organic phase was washed with brine, dried over anhydrous Na_2SO_4 and evaporated. Final solvent traces were removed under high vacuum to afford the product **6** (0.023 g, 42 %) as a solid. The compound was used with no further purification.

^{1}H-NMR (300 MHz, $CDCl_3$) δ_H 8.05 (2H, d, J = 8.4 Hz, 2 x Ar-H_a), 7.58 (2H, d, J = 8.5 Hz, 2 x Ar-H_b), 3.25(1H, s, -CH).

Synthesis of methyl 3-iodobenzoate (7) [10]

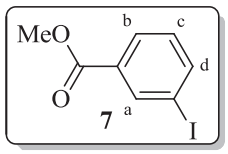

7

To a round-bottomed flask were added 3-iodobenzoic acid (2 g, 8.06 mmol), some drops of conc. H_2SO_4 and MeOH (50 mL). The solution was heated under reflux overnight. The mixture was then cooled at room temperature and diluted with Et_2O (50 mL) and H_2O (50 mL). The water phase was washed with Et_2O (2 x 50 mL). All the organic phases were collected together and washed with a saturated solution of $NaHCO_3$ and brine. The organic phase was then dried over anhydrous $MgSO_4$ and evaporated under vacuum. The product **7** (1.879 g) is a white solid and was obtained with a yield of 89 %.

^{1}H-NMR (300 MHz, $CDCl_3$) δ_H 8.38 (1H, s, Ar-H_a), 8.02-7.99 (1H, m, Ar-H_b), 7.90-7.87 (1H, m, Ar-H_d), 7.19 (1H, t, J = 7.8 Hz, Ar-H_c), 3.92 (3H, s, -OCH_3).

Synthesis of methyl 3-ethynylbenzoate (8) [3,11,12]

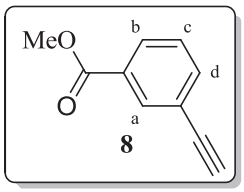

8

Methyl 3-iodobenzoate **7** (1 g, 3.8 mmol, 1 eq), CuI (29 mg, 0.152 mmol, 0.04 eq), $Pd(PPh_3)_2Cl_2$ (53 mg, 75.5 µmol, 0.02 eq) were dissolved in degassed THF (10 mL) in a Schlenk flask. Then trimethylsilylacetylene (0.81 mL, 5.73 mmol, 1.5 eq), NEt_3 (1.06 mL) were added and degassed again for some minutes. The solution was stirred at room temperature under argon atmosphere. After 3h (when all the compound **6** had reacted) was added TBAF [1 M, Sigma Aldrich] in THF solution (7.65 mL) and some molecular sieves (3Å). The reaction was stirred under air atmosphere and at room temperature overnight. The mixture was then filtered on Celite®, washing with Et_2O. The residue was then purified by column chromatography (SiO_2, EtOAc/ hex. 0.5:9.5) to afford the product **8** (0.392 g, 64 %).

^{1}H NMR (300 MHz, $CDCl_3$) δ_H 8.16 (1H, s, Ar-H_a), 8.03-8.00 (1H, m, Ar-H_b), 7.68-7.64 (1H, m, Ar-H_d) , 7.41 (1H, t, J = 7.8 Hz, Ar-H_c), 3.92 (3H, s, -OCH_3), 3.12 (1H, s, -C*H*).

Synthesis of dimethyl 3,3'-(buta-1,3-diyine-1,4-diyl)dibenzoate (9) [11,13]

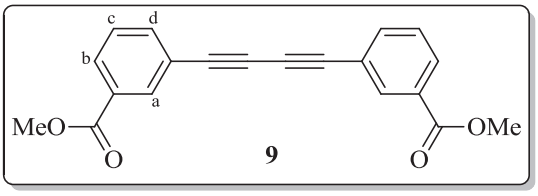

9

In a flask equipped with magnetic stirrer were added CuCl (7 mg, 68.7 µmol, 0.10 eq), TMEDA (0.031mL, 0.207 mmol, 0.30 eq) and CH_2Cl_2 (6 mL). Then molecular sieves (3Å, 1 g) were added and after few minutes methyl 3-ethynylbenzoate **8** (0.111 g, 0.693 mmol, 1 eq). After 2 h (monitored *via* TLC) the reaction was stopped by addition of H_2O (7 mL). The aqueous phase was extracted with CH_2Cl_2 (2 x 10 mL). All the organic phases were collected together and filtered on a short SiO_2 plug with CH_2Cl_2. The organic phases containing the product (monitored *via* TLC) were regrouped and evaporated in order to afford the product **9** (0.100 g, 91 %).

^{1}H NMR (300 MHz, $CDCl_3$) δ_H 8.20-8.22 (2H, m, 2 x Ar-H_a), 8.06-8.03 (2H, m, 2 x Ar-H_b), 7.72-7.69 (2H, m, 2 x Ar-H_d), 7.46-7.41 (2H, m, 2 x Ar-H_c), 3.94 (6H, s, 2 x -OCH_3).

Synthesis of 3,3'-(buta-1,3-diyne-1,4-diyl)dibenzoic acid (10) [7,14]

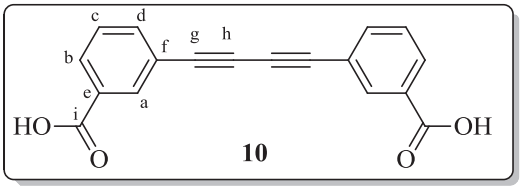

In a small flask dimethyl 3,3'-(buta-1,3-diyine-1,4-diyl)dibenzoate **9** (60 mg, 0.188 mmol, 1 eq) was dissolved in THF (7.2 mL). Then a solution of LiOH (0.092 g, 3.84 mmol, 20.38 eq) in H_2O (4 mL) was added and the mixture stirred at room temperature overnight. HCl 3M (1.2 mL) was then added drop by drop under stirring and ice bath until precipitation at *p*H 2~3. The precipitate was then filtered on funnel and washed with Et_2O and cold H_2O. The product was then recovered from the funnel and dried at the vacuum line (20 mg, yield 37 %).

^{1}H NMR (500 MHz, DMSO) δ_H 8.09 (2H, s, 2 x Ar-H_a), 8.04-8.01 (2H, m, 2 x Ar-H_b), 7.88-7.86 (2H, m, 2 x Ar-H_d), 7.62-7.56 (2H, m, 2 x Ar-H_c).
^{13}C NMR (125 MHz, DMSO) δ_C 166.3 (C_i), 136.5 (C_d), 132.9 (C_a), *131.9* (C_e), 130.7 (C_b), 129.5 (C_c), *120.7* (C_f), 81.2 (C_g), 73.9 (C_h). The chemical shifts in italic were attributed by analogy to molecule **11**.
HRMS (ES-) calculated for [$C_{18}H_9O_4$] 289.0501, found 289.0498.

Synthesis of 3-ethynylbenzoic acid (11) [7,8,15]

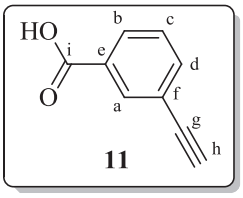

Methyl 3-ethynylbenzoate **8** (91 mg, 0.568 mmol, 1 eq) was dissolved in MeOH (1.5 mL) under stirring and then a solution of LiOH (16 mg, 0.668 mmol, 1.2 eq) in H_2O (1.5 mL) was added to the mixture. The reaction was stirred overnight. Then the solvent was removed in vacuum, then HCl 3M was added drop by drop until precipitation at *p*H 2~3. Then the solution was extracted with EtOAc. The organic phase was washed with brine, dried over

anhydrous $MgSO_4$ and evaporated. Final solvent traces were removed under high vacuum to afford the product **11** (0.045 g, 54 %).

^{1}H NMR (300 MHz, DMSO) δ_H 13.22 (1H, s, -O*H*), *7.97-7.94* (2H, m, Ar-H_{a-b}), *7.73-7.71* (1H, m, Ar-H_d), 7.53 (1H, t, J = 7.8 Hz, Ar-H_c), 4.30 (1H, s, -C*H*). The chemical shifts in italic were attributed by analogy to molecule **10**.

^{13}C NMR (75 MHz, DMSO) δ_H 166.4 (C_i), *135.8* (C_d), *132.2* (C_a), 131.4 (C_e), *129.7* (C_b), 129.2 (C_c), 122.1 (C_f), 82.5 (C_g), 81.7 (C_h). The chemical shifts in italic were attributed by analogy to molecule **10**.

HRMS (DCI-CH_4) calculated for [$C_9H_6O_2$] 147.0446, found 147.0457 (corresponding to the protonated form $[M+H]^+$).

Crystallographic structure of molecule **11** is reported in Annex.

Synthesis of 6,7-dibromonaphthalene-2,3-dicarbonitrile (12) [16,17]

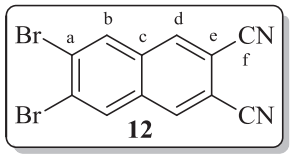

12

1,2-Dibromo-4,5-bis(dibromomethyl)benzene (0.701 g, 1.2 mmol, 1 eq), fumaronitrile (0.150 g, 1.92 mmol, 1.6 eq) and NaI (0.600 g, 4.00 mmol, 3.3 eq) were stirred in DMF (7 mL) at 80 °C, under argon atmosphere for 5h (TLC-control: SiO_2, toluene/acetone 15:0.75). The reaction mixture was cooled to room temperature. The mixture was poured into a 100 mL round-bottomed flask and 20 mL of H_2O were added in order to precipitate a solid; then 10 mL of saturated solution of $Na_2S_2O_3$ was added. The compound was filtered on fritted funnel and washed with saturated solution of $Na_2S_2O_3$, H_2O and Et_2O. The precipitate was finally dried to give the final product **12** (0.293 g, 72 %).

^{1}H NMR (500 MHz, $CDCl_3$) δ_H 8.26 (Ar-H_d), 8.30 (Ar-H_b).

^{13}C NMR (125 MHz, $CDCl_3$) δ_C 134.8 (C_dH), 132.9 (C_bH), 132.5 (C_c), 128.7 (C_a), *115.4 (*Ar-*CN), 111.7 (*C_e-CN*)*. The chemical shifts in italic cannot be assigned with certitude.

HRMS is already reported in literature (reference above).

Synthesis of naphthalene-2,3,6,7-tetracarbonitrile(13) [17]

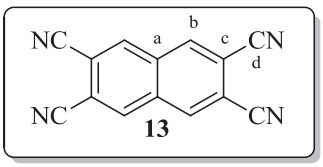

6,7-Dibromonaphthalene-2,3-dicarbonitrile **13** (1.288 g, 3.8 mmol, 1 eq) was stirred with CuCN (1.716 g, 19.1 mmol, 5 eq) in DMF (27 mL) under reflux and argon atmosphere for 5h (TLC-control: SiO_2, toluene/acetone 15:0.75). Then, once the reaction mixture was cooled, a saturated solution of $FeCl_3 \cdot 6H_2O$ was added until precipitation of a solid; the dark precipitate was filtered and washed with NH_4OH (28-30% NH_3 basis). The precipitate was redissolved in 100 mL CH_3CN and heated under reflux. Then the insoluble admixtures were filtered off and the filtrate was evaporated affording the final product **13** (0.700 g, 80 %).

^{1}H NMR (300 MHz, CD_3CN) δ_H 8.69 (4H, s, Ar-*H*).
^{13}C NMR (125 MHz, DMSO) δ_C 136.8 (*C_b*), *133.1 (C_a), 115.6 (C_d), 113.4 (C_c)*. The chemical shifts in italic were assigned by analogy to molecule **12**.
HRMS (DCI-CH_4) calculated for [$C_{14}H_4N_4$] 229.0514, found 229.0504 (corresponding to the protonated form $[M+H]^+$).

Methyl pent-4-ynoate (14) [18]

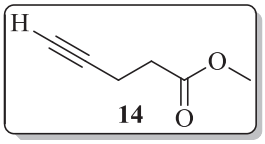

4-pentynoic acid (1 g, 10.19 mmol) dissolved in dry MeOH (20 mL) with few drops of conc. H_2SO_4, was heated at reflux for 24h under argon atmosphere. The product was then extracted with CH_2Cl_2, and the organic phase was washed with saturated solution of $NaHCO_3$, dried over anhydrous $NaSO_4$ and evaporated. The final product is a colourless liquid (0.780 g, 68%).

^{1}H NMR (300 MHz, $CDCl_3$) δ_H 3.70 (3H, s, -OC*H$_3$*), 2.59-2.56 (2H, m, -C*H$_2$*), 2.54-2.50 (2H, m, -C*H$_2$*).

Dimethyl 5,5'-(anthracene-2,6-diyl)bis(pent-4-ynoate) (15) [19]

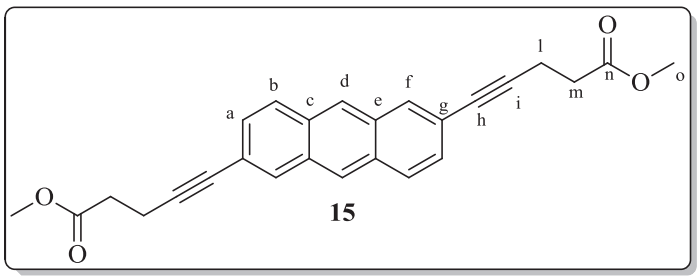

A mixture of 2,6-dibromoanthracene (1 g, 2.97 mmol, 1 eq), methyl pent-4-ynoate **14** (0.82 mL, 7.14 mmol, 2.4 eq), $[Pd(PPh_3)_2Cl_2]$ (41.78 mg, 0.059 mmol, 0.02 eq), CuI (34.01 mg, 0.178 mmol, 0.06 eq), and degassed NEt_3 (30 ml) was heated under reflux and under argon atmosphere for 2 days. After 2 days the catalysts were added again in the same ratio $[Pd(PPh_3)_2Cl_2]$ / CuI (0.02 eq:0.06 eq) and methyl pent-4-ynoate (0.5 mL, 1.5 eq) was added too. The reaction continued for other 3 days in the same conditions (under reflux and argon atmosphere) and the catalysts and the alkyne were added again in the same quantites described above. Once the reaction was finished (monitored *via* TLC), the crude mixture was cooled at room temperature, diluted with CH_2Cl_2 and passed through a short Celite® pad. The solution was evaporated, the crude residual solid was purified by flash chromatography (SiO_2, cyclohex./CH_2Cl_2 70:30→ CH_2Cl_2 pure, with a gradual increment of polarity 20% every time) to afford the product **15** as yellow bright solid (0.787 g, 66%).

^{1}H NMR (300 MHz, $CDCl_3$) δ_H 8.28 (2H, s, Ar-H_d), 8.04 (2H, s, Ar-H_f), *7.90* (2H, d, J = 9 Hz, Ar-H_b), *7.40* (2H, dd, ^3J = 9 Hz, ^4J = 3 Hz, Ar-H_a), 3.75 (6H, s, -OCH_3), 2.84-2.79 (4H, m, -C$_l$$H_2$), 2.72-2.67 (4H, m, -C$_m$$H_2$). The chemical shifts in italic cannot be assigned with certitude.

^{13}C NMR (75 MHz, $CDCl_3$) δ_C 172.7(-*C*O), 131.8 (C_f), *131.7* (C_c or C_e), *131.2* (C_c or C_e), *128.6* (C_a or C_b), *128.5* (C_a or C_b), 126.3 (C_d), 120.9 (C_g), 89.5 (Ar-CC_i), 82.1 (Ar-C_hC), 52.2 (-O*C*H$_3$), 33.8 (-C_mH$_2$), 15.9 (-C_lH$_2$). The chemical shifts in italic cannot be assigned with certitude.

HRMS (DCI/CH_4) m/z 398.1534 $[M-H]^+$ (calculated 398.1518).

Dimethyl 5,5'-(anthracene-2,6-diyl)dipentanoate (16) [20]

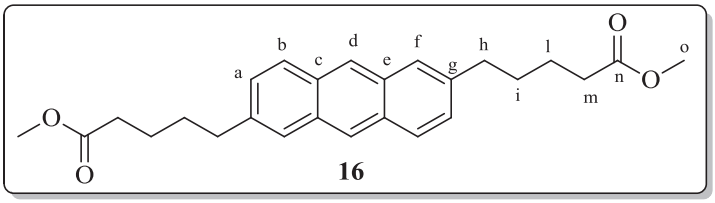

Dimethyl 5,5'-(anthracene-2,6-diyl)bis(pent-4-ynoate) **(15)** (26 mg, 6.53 10^{-2} mmol, 1eq), 10% Pd/C (12 mg, 1.13 10^{-2} mmol of palladium, 0.17 eq of palladium) were stirred in dry MeOH (2.5 mL) under argon atmosphere. Then TES (0.10 mL, 6.49 10^{-1} mmol, 10 eq) was added drop by drop with a microL syringe. The reaction was left run for 4h. The product filtered with CH_2Cl_2 on Celite® pad. Preparative TLC (EtOAc/CH_2Cl_2/cyclohex. 1:3:6) on the crude product afforded the final molecule **16** with a yield of 27% (0.007 g).

^{1}H NMR (300 MHz, CD_2Cl_2) δ_H 8.30 (2H, s, Ar-*H_d*), *7.92* (2H, d, *J* = 9 Hz, Ar-*H_b*), 7.74 (2H, s, Ar-*H_f*), *7.32* (2H, dd, ^3J = 9 Hz, ^4J = 3 Hz, Ar-*H_a*), 3.63 (6H, s, -OC*H_3*), 2.84-2.79 (4H, m, -C_hH_2), 2.36 (4H, m, -C_mH_2), 1.69-1.79 (4H, m, -$C_{i\text{-}l}H_2$). The chemical shifts in italic cannot be assigned with certitude.

^{13}C NMR (125 MHz, CD_2Cl_2) δ_C 174.2 (-*C*O), 139.6 (*C_g*), *131.9* (*C_c* or *C_e*), *131.2* (*C_c* or *C_e*), *128.3* (*C_a* or *C_b*), *127.7* (*C_a* or *C_b*), 126.2 (*C_d*), 125.4 (*C_f*), 51.7 (-O*C*H$_3$), 36.2 (Ar-*C_h*H$_2$), 34.2 (-*C_m*H$_2$), 30.8 (*C_i*H$_2$), 25.0 (*C_l*H$_2$). The chemical shifts in italic cannot be assigned with certitude.

HRMS (DCI/CH_4) m/z 407.2226 $[M\text{-}H]^+$ (calculated 407.2222)

Dimethyl 5,5'-(9,10-dihydroanthracene-2,6-diyl)bis(pent-4-ynoate) (19) [18]

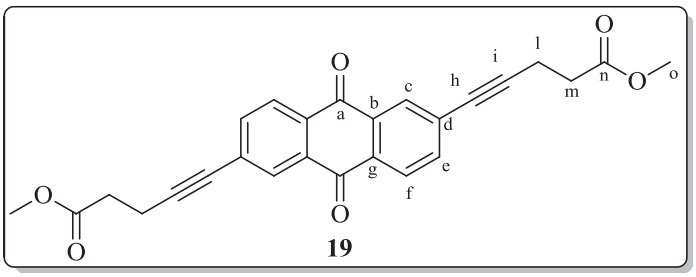

2,6-dibromoanthraquinone (0.105 g, 2.87 10^{-1} mmol, 1 eq) was dissolved in $NHEt_2$ (8 mL) and degassed; then methyl pent-4-ynoate **14** (0.094 mL, 8.18 10^{-1} mmol, 3 eq) was added and degased again. Finally [Pd(PPh$_3$)$_2$Cl$_2$] (19 mg, 2.71 10^{-2} mmol, 0.1 eq) and CuI (5.20 10^{-3} g,

2.73 10^{-1} mmol, 0.1 eq) were added and the reaction was let run under argon atmosphere for 24h at reflux. The crude mixture was cooled at RT and the solvent was removed in vacuum. The crude product was dissolved in CH_2Cl_2, the solution was filtered on Celite® pad and then evaporated. The residue was then purified by column chromatography (SiO_2, EtOAc/cyclohex. 3:7) to afford the product **19** (0.105 g, 85%).

^{1}H NMR (500 MHz, $CDCl_3$) δ_H 8.21 (2H, s, Ar-H_c), 8.17 (2H, d, J = 6 Hz, Ar-H_f), 7.71 (2H, dd, ^3J = 10 Hz, ^4J = 5 Hz, Ar-H_e), 3.73 (6H, s, -OCH_3), 2.78 (4H, m, -C_lH_2), 2.66 (4H, m, -C_mH_2).
^{13}C NMR (125 MHz, $CDCl_3$) δ_C 182.0 (-C_aO), 172.2 (-C_nO), 136.8 (C_e), 133.4 (C_b), 132.1 (C_d), 130.3 (C_c), 130.1 (C_g), 127.4 (C_f), 93.8 (C_i), 80.2 (C_h), 52.1 (-OCH$_3$), 33.2 (C_m), 15.6 (C_l).
HRMS (DCI/CH_4) m/z 429.1349 of the protonated form $[M+H]^+$ (calculated mass 429.1338).

Experimental techniques

The experimental technique used to investigate molecules on calcite surface in UHV conditions is the atomic force microscopy in non-contact operating mode (nc-AFM). The atomic force microscopy was developed by G. Binning, C. F. Quate and C. Gerber in 1986[21] as an extension of scanning probe microscopy (STM). Binning and coworkers substituted the STM tip with a cantilever in order to extend the investigation field from metallic to insulating surfaces. In this work the nc-AFM was used in collaboration with A. Kühnle's group, University of Mainz, Germany.

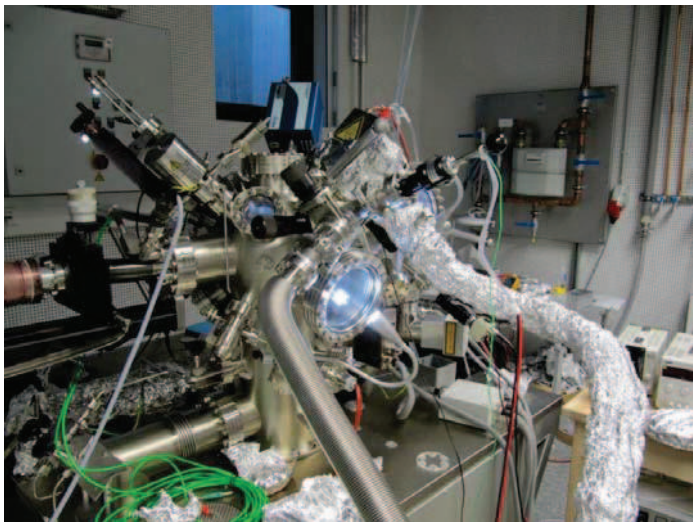

Figure 1 nc-AFM system in Mainz, Germany.

Before starting the scanning sequence with the nc-AFM the calcite crystals are cleaved in the central chamber of the machine. Then those crystals are heated at around 480 K for about one hour to remove surface charges.

Once the substrate is ready, it is transferred inside the nc-AFM chamber (separated to avoid contamination of the microscope) in order to collect images of the surface. Then, the sample is placed again in the central chamber for the sublimation. The molecules inside the crucible are sublimated at given temperature. Once the sublimation is finished, the sample is moved again in the nc-AFM chamber to collect new images. The central chamber is also connected to a UV-lamp and a mass spectrometer for further experiments.

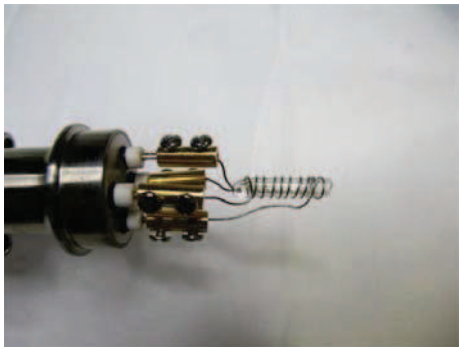

Figure 2 Crucible with sample.

Experimental part of Chapter 3

Grinding of commercial calcium carbonate

Commercial calcium carbonate (Sigma Aldrich) was ground for 15 minutes at 700 rpm in a Pulverizette 7, Fritsch.

Synthesis of particles *via* spray pyrolysis

For the synthesis of calcium carbonate particle, the starting material (calcium acetate hydrate) was purchased from Sigma-Aldrich. All the samples were synthesized from a water solution of calcium acetate (aqueous solution 15% by weight). Then the solution was put in the spray pyrolysis systems. The details are given in chapter 3.

Characterization of calcium carbonate particles

All particles were characterized by Fourier-transform infrared spectroscopy (FT-IR), thermogravimetry and differential thermal analysis (TG/DTA), X-ray powder diffraction

(XRD) and scanning electron microscopy (SEM). Some samples were submitted to an additional treatment and then characterized with the same techniques and additionally adsorption, BET and laser granulometric analysis (LG).

Fourier-transform infrared spectroscopy (FTIR)

The IR spectroscopy is useful in order to identify the different polymorphs (calcite, vaterite and aragonite) of calcium carbonate particles. Additionally, this technique was also used in order to identify the different constituent of the synthesized particles (calcium carbonate, calcium acetate or calcium oxide).

The spectra were recorded between 4000-400 cm^{-1}, using a Perkin Elmer Spectrum 100 FT-IR spectrometer with a resolution of 0.5 cm^{-1}. The samples were prepared as pellets with KBr (Acros Organics) 100 mg for 1 mg of product.

Thermogravimetry and differential thermal analysis (TG/DTA)

The thermal analysis is useful in order to detect the composition of the samples (calcium acetate or calcium carbonate). The experiments were performed in a Setaram Labsys instrument. The samples were heated up to 1000 °C with a rate of 10 °C/min under oxygen atmosphere in order to be coherent with the spray pyrolysis conditions. The crucibles used were in alumina.

The samples 1-3-5 (SP at 250-400-500 °C) after heating treatment were heated up to 1000 °C with a rate of 10 °C/min under air in a thermobalance DIAMOND TG/TDA.

X-ray powder diffraction (XRD)

The powder X-ray measurements were used to identify the different components of our samples (calcium acetate, calcium carbonate and calcium oxide). There were performed with on X-ray Bruker powder diffractometer with Bragg-Brentano set-up, θ-θ geometry. The source is Cu anticathode ($\lambda K_{\alpha 1}$= 1.5405 Å, $\lambda K_{\alpha 2}$= 1.5443 Å). The acquisition conditions were: 2θ = 5 ° - 80 ° and counting time 14 sec by step (step size 0.02 °).

Scanning electron microscopy (SEM)

The SEM images afford important information about the morphology and the structure of the calcium carbonate particles. There were recorded in a Jeol JSM-6490. The images were recorded with a tension of 20 kV and the samples were not metalized before the measurement.

Adsorption and BET

Adsorption experiments and BET treatments were carried out by D. Neumeyer from CEMES Laboratory (Toulouse). The measurements were recorded in order to identify the specific surface of calcium carbonate particles. There were performed in a Belsorp mini instrument. The gas used was nitrogen and the samples were previously degased for 16h under vacuum at 150 °C.

The BET method is one of the most common methods to measure the surface of powders and porous material[22]. The theory, elaborated by Brunauer, Emmett and Teller is based on the adsorption of gas on a porous material. Adsorption isotherms are calculated by the quantity of gas adsorbed at constant temperature (typically 77 K, liquid nitrogen); desorption isotherms are measured by the gas desorption[23,24]. The BET equation is usually applied in the linear form:

$$\frac{1}{X[(P_0/P)-1]} = \frac{1}{X_m C} + \frac{C-1}{X_m C} \cdot \left(\frac{P}{P_0}\right)$$

where X is the amount of the gas adsorbed at relative pressure (P/P_0), X_m is the monolayer capacity (amount of adsorbate as monolayer) and C is constant.

When the BET equation is plotted, the graph should be linear with a positive slope.

- The slope (s) and intercept (i) can be obtained using least squares regression.

$$s = \frac{C-1}{X_m C} \qquad i = \frac{1}{X_m C}$$

- The monolayer capacity (X_m) can be calculated: $X_m = \frac{1}{s+i}$
- Once X_m is determined, the total surface area (S_t) can be calculated with the following equation: $S_t = \frac{X_m N_{av} A_m}{M_v}$

  where N_{av} is Avogadro's number, A_m is the cross sectional area of the adsorbate (16.24 $Å^2$ for nitrogen) and M_v is the molar volume (or molecular weight) of adsorbate.
- Specific Surface Area (S_A) is then determinate by total Surface area (St) divided by sample weight (w): $S_A = \frac{S_t}{w}$

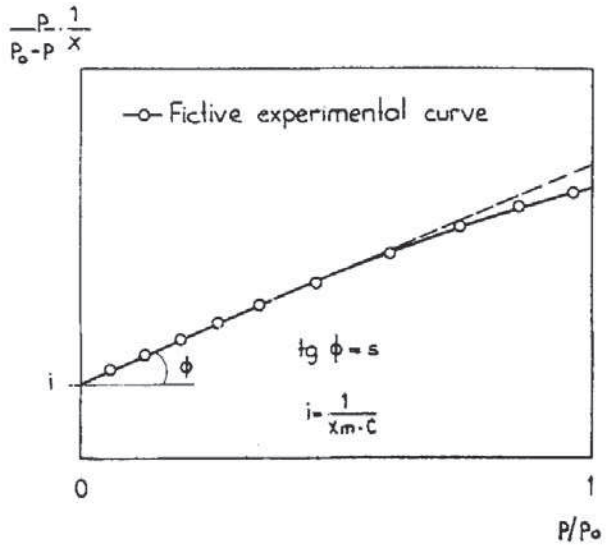

Figure 3 Graph of BET equation, obtained by plotting $\frac{p}{(p_0-p)} \cdot \frac{1}{x}$ as function of the relative pressure p/p_0 from ref.[24].

If such a graph is not obtained, then the BET method is insufficient in obtaining the surface area and other methods are used.

Laser granulometry (LG)

The laser granulometric analysis (LG) experiment was performed on a Malvern Mastersizer S instrument only for one selected sample in order to identify the dimensions of the particles. The measurement was carried out on a sample suspension in distilled water, under ultrasounds with a power probe (750W). The experiment was carried out by D. Neumeyer from CEMES Laboratory (Toulouse).

Transmission electron microscopy (TEM)

Conventional TEM images of the microparticles and the relative diffraction patterns were acquired using a Philips CM20 FEG TEM, working at 200 kV. The sample for TEM characterization was prepared by placing a drop of its ethanol dispersion on carbon-coated copper grid and dried at room temperature. The experiment was carried out by Dr. C. Marcelot from CEMES laboratory (Toulouse).

Experimental part of Chapter 4

Mechanochemistry experiments

Mechanochemistry reactions were performed on a Pulverisette 7 Premium Line, Fritsch as already introduced in the previous chapter.

Thermal experiments

The thermal experiment were performed in a tubular furnace (Thermolyne Sybron 21100) connected to a vacuum pump (Vacuumbrand® RZ6). The system is composed by a quartz tube inserted in a furnace. The tube is connected to a vacuum pump protected by a trap at -20 °C. The reaction mixture powder is placed in a crucible inside the quartz tube. The temperature of the reaction is measured by a thermocouple (Digitron 2029T) inserted between the furnace and the quartz tube.

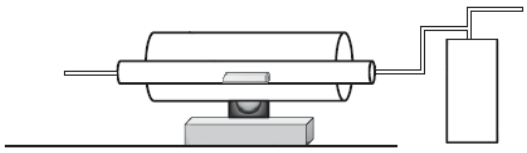

Figure 4 Experimental set-up of the furnace.

References

1. Fulmer, G. R. *et al.* NMR Chemical Shifts of Trace Impurities: Common Laboratory Solvents, Organics, and Gases in Deuterated Solvents Relevant to the Organometallic Chemist. *Organometallics* **29,** 2176–2179 (2010).
2. Shao, M. & Zhao, Y. TTFAQ-cored D/A ensembles: synthesis, electronic properties, and redox responses to transition metal ions. *Tetrahedron Lett.* **51,** 2892–2895 (2010).
3. Feng, Y.-S., Xie, C.-Q., Qiao, W.-L. & Xu, H.-J. Palladium-Catalyzed Trifluoroethylation of Terminal Alkynes with 1,1,1-Trifluoro-2-iodoethane. *Org. Lett.* **15,** 936–939 (2013).
4. Niamnont, N., Siripornnoppakhun, W., Rashatasakhon, P. & Sukwattanasinitt, M. A Polyanionic Dendritic Fluorophore for Selective Detection of Hg2+ in Triton X-100 Aqueous Media. *Org. Lett.* **11,** 2768–2771 (2009).
5. Zanotti, G. *et al.* Synthesis of a novel unsymmetrical Zn(II) phthalocyanine bearing a phenyl ethynyl moiety as sensitizer for dye-sensitized solar cells. *Dalton Trans.* **40,** 38–40 (2010).
6. Fasina, T. M. *et al.* Synthesis, optical properties, crystal structures and phase behaviour of symmetric, conjugated ethynylarene-based rigid rods with terminal carboxylate groups. *J. Mater. Chem.* **15,** 690–697 (2005).

7. Han, S. *et al.* A single-crystalline microporous coordination polymer with mixed parallel and diagonal interpenetrating α-Po networks. *CrystEngComm* **13,** 4838–4840 (2011).
8. Bischoff, A., Subramanya, H., Sundaresan, K., Sammeta, S. & Vaka, A. Novel Piperazine Derivatives as Inhibitors of Stearoyl-Coa Desaturase. (2008). at <WO2008157844 (A1)>
9. Jones, L. F. *et al.* Tuning magnetic properties using targeted structural distortion: New additions to a family of Mn6 single-molecule magnets. *Inorganica Chim. Acta* **361,** 3420–3426 (2008).
10. Offermann, D. A. *et al.* Synthesis and Incorporation into Cyclic Peptides of Tolan Amino Acids and Their Hydrogenated Congeners: Construction of an Array of A–B-loop Mimetics of the Cε3 Domain of Human IgE. *J. Org. Chem.* **77,** 3197–3214 (2012).
11. Merkul, E., Urselmann, D. & Müller, T. J. J. Consecutive One-Pot Sonogashira–Glaser Coupling Sequence – Direct Preparation of Symmetrical Diynes by Sequential Pd/Cu Catalysis. *Eur. J. Org. Chem.* **2011,** 238–242 (2011).
12. Austin, W. B., Bilow, N., Kelleghan, W. J. & Lau, K. S. Y. Facile synthesis of ethynylated benzoic acid derivatives and aromatic compounds via ethynyltrimethylsilane. *J. Org. Chem.* **46,** 2280–2286 (1981).
13. Vilhelmsen, M. H., Jensen, J., Tortzen, C. G. & Nielsen, M. B. The Glaser-Hay Reaction: Optimization and Scope Based on 13C NMR Kinetics Experiments: The Glaser-Hay Reaction. *Eur. J. Org. Chem.* **2013,** 701–711 (2013).
14. Matsubara, H. *et al.* Syntheses of Novel Fullerene Tweezers and Their Supramolecular Inclusion Complex of C60. *Chem. Lett.* 1099–1100 (1998).
15. Bleisch, T. J., Doti, R. A., Pfeifer, L. A. & Norman, B. H. Dihydropyrido Pyrimidine Compounds as Autotaxin Inhibitors. (2014). at <WO2014168824 (A1)*>
16. Dini, D. *et al.* Nonlinear Transmission of a Tetrabrominated Naphthalocyaninato Indium Chloride. *J. Phys. Chem. B* **110,** 12230–12239 (2006).
17. Dubinina, T. V. *et al.* Synthesis and investigation of spectral and electrochemical properties of alkyl-substituted planar binuclear phthalocyanine complexes sharing a common naphthalene ring. *Inorganica Chim. Acta* **363,** 1869–1878 (2010).
18. Shimotahira, H., Fusazaki, S., Ikeda, I. & Ozoe, Y. A photoreactive probe that differentiates the binding sites of noncompetitive GABA receptor antagonists. *Bioorg. Med. Chem. Lett.* **21,** 1598–1600 (2011).
19. Khanna, B., Parkin, S. R. & Revell, K. D. 2,6-Diarylethynylanthracenes: synthesis, morphology, and electro-optical properties. *Tetrahedron Lett.* **53,** 6383–6387 (2012).
20. Mandal, P. K. & McMurray, J. S. Pd−C-Induced Catalytic Transfer Hydrogenation with Triethylsilane. *J. Org. Chem.* **72,** 6599–6601 (2007).
21. Binnig, G. & Quate, C. F. Atomic Force Microscope. *Phys. Rev. Lett.* **56,** 930–933 (1986).
22. International Union of Pure and Applied Chemistry. Reporting physisorption data for gas/solid systems with Special Reference to the Determination of Surface Area and Porosity. *Pure Appl Chem* **57,** pp. 603—619, 1985. (1985).
23. Brunauer, S., Deming, L. S., Deming, W. E. & Teller, E. On a Theory of the van der Waals Adsorption of Gases. *J. Am. Chem. Soc.* **62,** 1723–1732 (1940).
24. Fagerlund, G. Determination of specific surface by the BET method. *Matér. Constr.* **6,** 239–245 (1973).

ANNEX

Annex

X-Ray structure of 3-ethynylbenzoic acid (11)

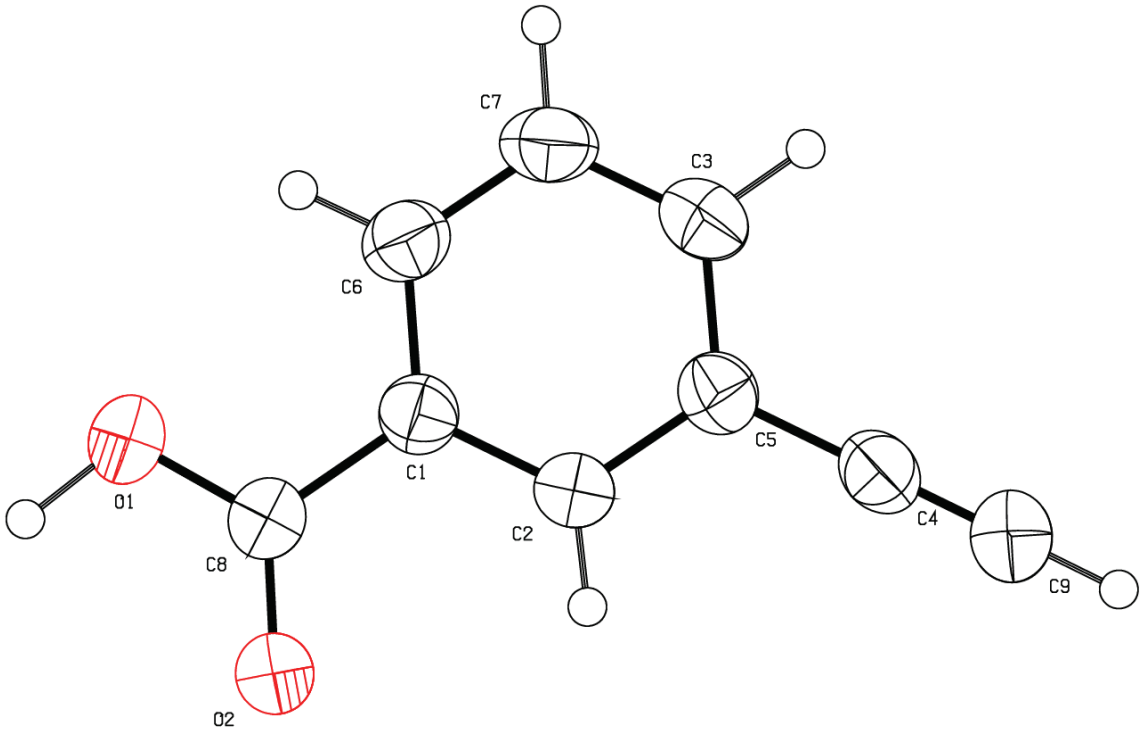

Figure 1 X-Ray structure of 3-ethynylbenzoic acid.

Molecular Formula	**$C_9 H_6 O_2$**
Molecular weight (g/mol)	146.14
Space group	P -1
a (Å)	3.8630 (7)
b (Å)	8.3000 (9)
c (Å)	11.7490 (1)
α (°)	101.4400
β (°)	93.8000
γ (°)	99.8300
Volume ($Å^3$)	361.84 (8)

R factor	R=0.0367 (1086) wR2 = 0.1165 (1317)

Table 1 Selection of crystallographic information of 3-ethynylbenzoic acid structure; all the data are available at the reference online[1].

Crystals were obtained by vapor diffusion of hexane in a solution of 3-ethynylbenzoic acid in CH_2Cl_2.

In 3-ethynylbenzoic acid structure, the carboxylic group forms a dihedral angle of 2.49 (18°) with the plane of benzene ring. Hydrogen bonds link the molecules by pairs *via* O–H···O bonds; in this way they form the acid-acid inversion dimers. The latter are linked by pairs *via* C–H···O bonds forming chains.

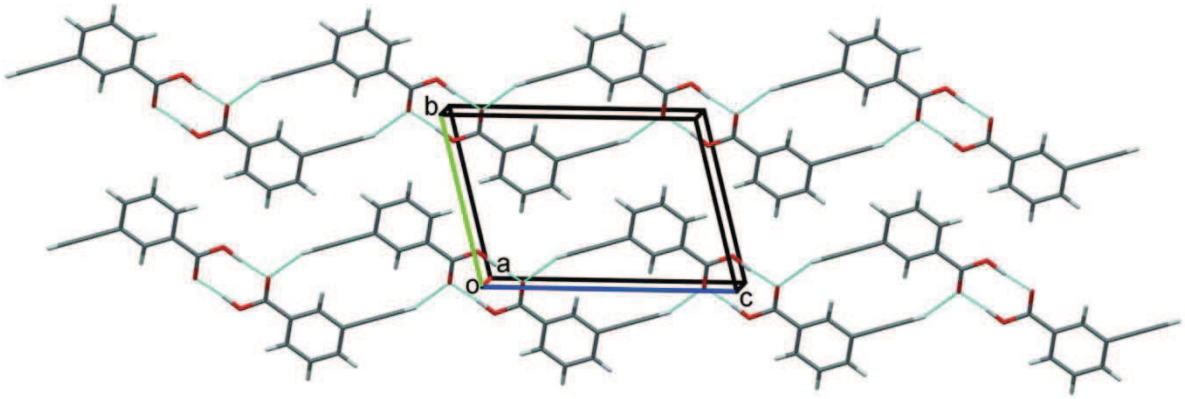

Figure 2 Crystal packing of the 3-ethynylbenzoic acid along *a* axis. From ref.[1].

Reference

1. Venturini, C., Ratel-Ramond, N. & Gourdon, A. Crystal structure of 3-ethynylbenzoic acid. *Acta Crystallogr. Sect. E Crystallogr. Commun.* **71,** o750–o751 (2015).

Résumé en français
Réactions de couplage sur carbonate de calcium

Introduction

Dans les dernières années, la miniaturisation a permis de fabriquer des dispositifs toujours plus petits jusqu'à l'échelle nanométrique. La taille des transistors, par exemple, a été fortement réduite et la densité a augmentée, comme montré à la figure suivante[1].

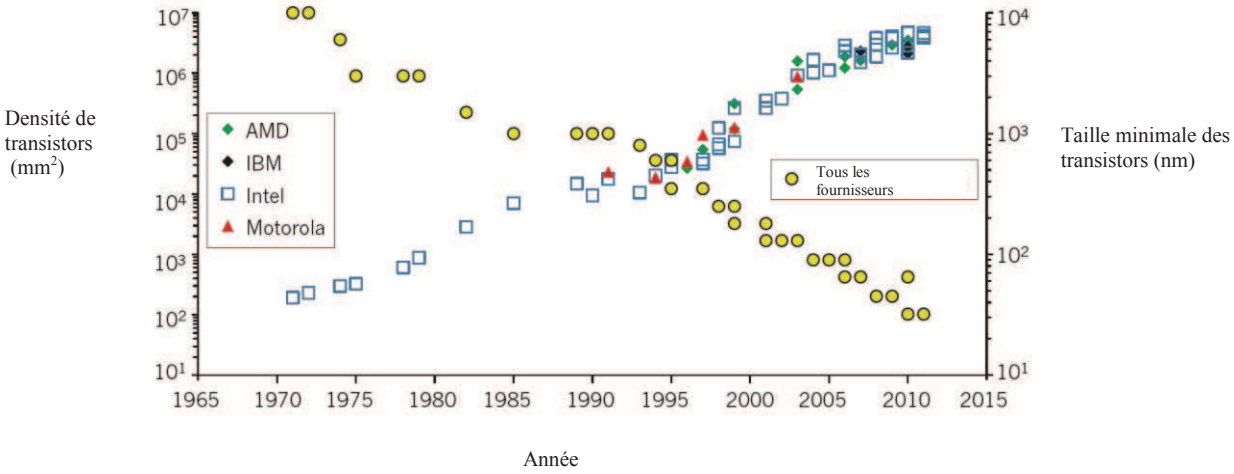

Figure 1 Evolution de la taille et la densité de transistors depuis 1970. Les cercles jaunes montrent la réduction en taille de la longueur du canal du MOSFETs (axe *y* à droite) ; les autres symboles représentent l'augmentation du nombre de transistors par millimètre carré (axe *y* à gauche)[1].

Ce développement a été possible par l'approche « top-down », comme dans le cas de la lithographie (la surface est modifiée pour créer un motif). Cependant cette méthode est proche de sa limite pour des raisons techniques et physiques. Ces limitations ont mené au développement du concept d' « électronique moléculaire ». A. Aviram et M. A. Ratner, dans les années '70, ont proposé l'utilisation de molécule seule comme dispositif électronique « molecular rectifier » ainsi que de circuits électroniques constitués de molécules[2,3].

Ce concept est longtemps resté théorique car le développement technologique n'était pas à la hauteur. Cependant, les futurs progrès scientifiques permettront probablement d'obtenir des dispositifs complexes par synthèse sur surface *via* l'approche « bottom-up ».

Des molécules précurseurs sont assemblées par des liaisons covalentes sur une surface (très propre) afin d'obtenir des structures plus complexes.

Ce couplage covalent a été principalement étudié sur surface métallique pour plusieurs raisons que nous détaillerons plus loin.

Dans ce travail de thèse nous nous sommes proposés d'étudier ces réactions de couplage sur surface isolante de carbonate de calcium.

Ce travail est présenté en deux parties. Dans un premier temps, la synthèse de molécules pour des réactions de couplage en conditions UHV (ultra high vacuum) sur calcite a été abordée.

Dans un second temps, cette étude a été étendue à l'échelle macroscopique (semi-préparative). Dans ce cas, des microparticules de carbonate de calcium ont été préparées par broyage d'un produit commercial ou par synthèse par spray pyrolyse. Ces particules ont été utilisées comme substrat pour des réactions de couplage.

Réactions de couplage sur surface en conditions UHV

Les réactions de couplage sur surface en conditions UHV sont réalisées par sublimation de molécules précurseur directement sur la surface. Ensuite, ces molécules sont activées pour réagir entre-elles afin d'obtenir des structures plus complexes, par formation de liaison covalente, ayant une fonction spécifique (mécanique ou électrique par exemple).

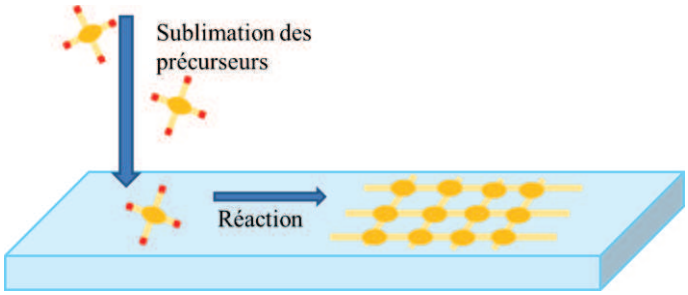

Figure 2 Approche « bottom-up » en UHV.

Cette technique permet d'obtenir des structures 0D, 1D ou 2D directement sur la surface, sans problème de solubilisation (en effet les produits sont sublimés directement sur la surface). Ainsi, il est possible de synthétiser des produits impossibles à obtenir en solution. La surface, en particulier la surface métallique, joue un rôle fondamental. L'interaction très forte entre le substrat métallique et les molécules présente l'avantage de limiter les phénomènes de désorption même à haute température. De plus, la surface agit comme un catalyseur. Pour ces raisons, jusqu'à aujourd'hui, cette approche a été développée sur surface métallique.

Le plus grand défi reste le développement de ces réactions sur des surfaces isolantes, indispensables pour des applications comme l'électronique moléculaire.

Les premières études de réactions de couplage en conditions UHV ont été réalisées sur surface métallique en 2007[4]. Depuis la publication de cet article, plusieurs réactions ont été proposées par cette technique, principalement sur surface métalliques.

Dans un papier remarquable, J. Cai et autres ont obtenu par cette approche, par exemple, des nanorubans de graphène, comme montré à la Figure 3. Dans ce cas, dans une première étape (step 1), un polymère à motif anthracène est obtenu ; puis une réaction de cyclodéhydrogénation conduit au nanoruban de graphène (step 2)[5].

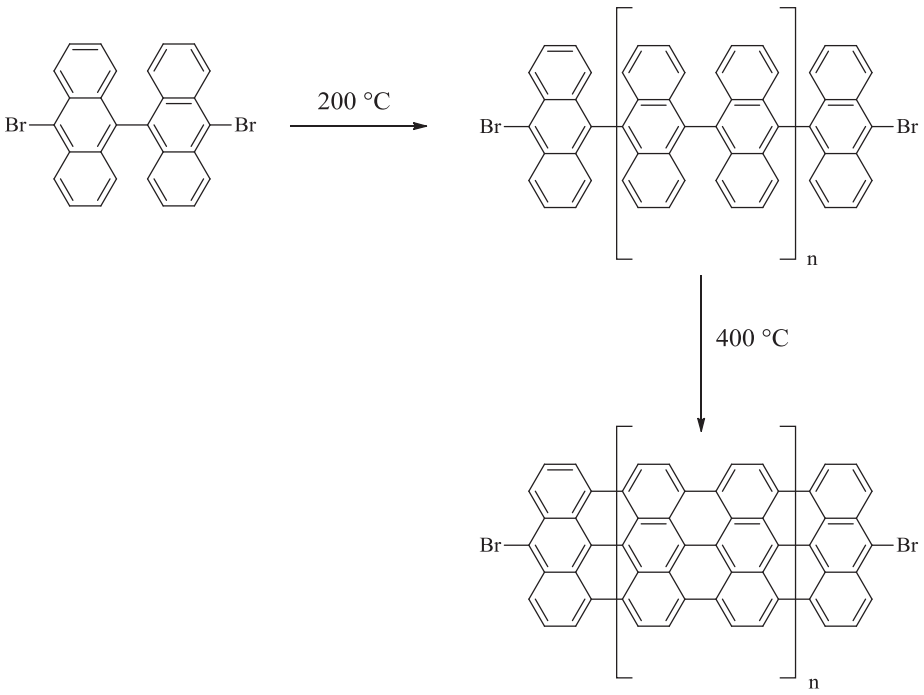

Figure 3 Synthèse d'un nanoruban de graphène : étape 1 formation du polymère linéaire (par réaction d'Ullmann à 200 °C); étape 2 formation d'un nanoruban de graphène (par réaction de cyclodehydrogénation à 400 °C). Réadapté depuis la ref.[5].

Aujourd'hui, les principales études de couplage covalent sur surfaces isolantes ont été menées par les équipes du Prof. A. Künhle (Université de Mayence, Allemagne) et Dr. Gourdon (CEMES-CNRS Toulouse) sur la surface de carbonate de calcium. Ce matériau, a une énergie de surface de 600 mJ/m^2, inférieure à celle d'une surface métallique comme l'or (1000 mJ/m^2) mais supérieure à celle du NaCl (140 mJ/m^2), (Springer book, sous presse).

Sur ce substrat, ils ont récemment démontré le couplage de molécules dérivées de l'acides benzoïque[6–9].

Le mécanisme proposé par ces équipes est présenté à la Figure 4. Le dérivé de l'acide benzoïque est sublimé (étape a), puis déprotoné (étape fondamentale pour le greffage sur la surface de carbonate) spontanément ou par recuit selon le pK_a de la molécule (étape b). Selon

ces chercheurs, la présence du groupe carboxylate affaiblit la liaison phényl-halogène et favorise ainsi le clivage homolytique, lors d'un deuxième recuit (étape c). Le radical obtenu réagit pour donner l'acide biphényldicarboxylique (étape d).

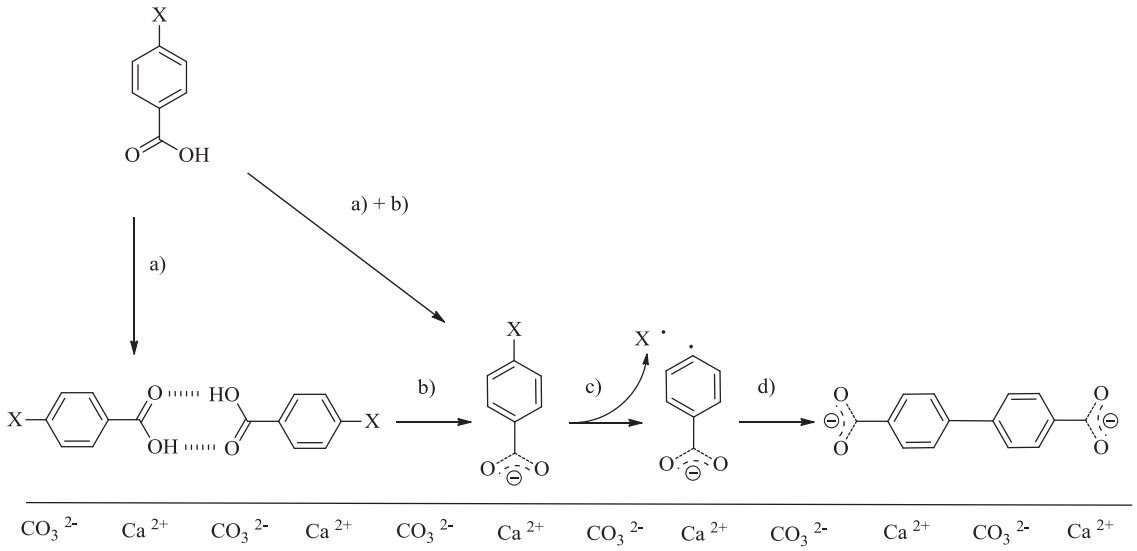

Figure 4 Mécanisme proposé pour la réaction de couplage sur calcite en UHV.

Parmi les exemples les plus intéressants, nous pouvons citer l'acide 3,5-diiodosalicylique[7]. Dans ce cas, le *p*Ka est de 2,07 et la molécule se déprotone spontanément dès sublimation et se fixe sur la surface. Après recuit à 580 K, les molécules obtenues présentent une structure zigzag, comme montré à la Figure 5. Le mécanisme de réaction est présenté à la Figure 6.

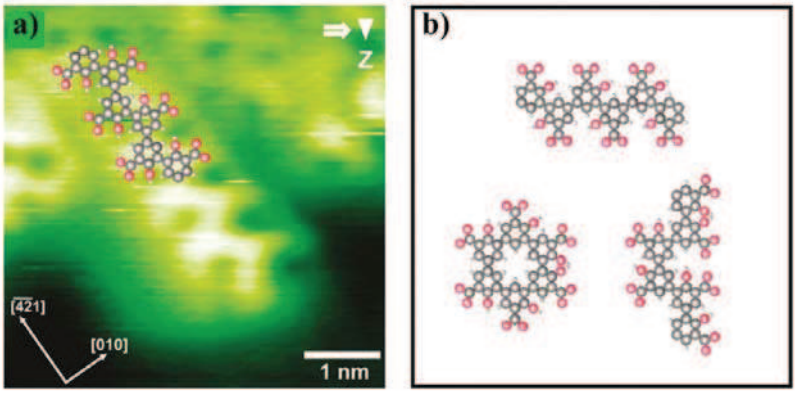

Figure 5 a) Image par nc-AFM du produit du couplage de l'acide 3,5-diiodosalicylique ; b) Représentation de différentes structures possibles pour cette molécule. Réadapté depuis la ref.[7].

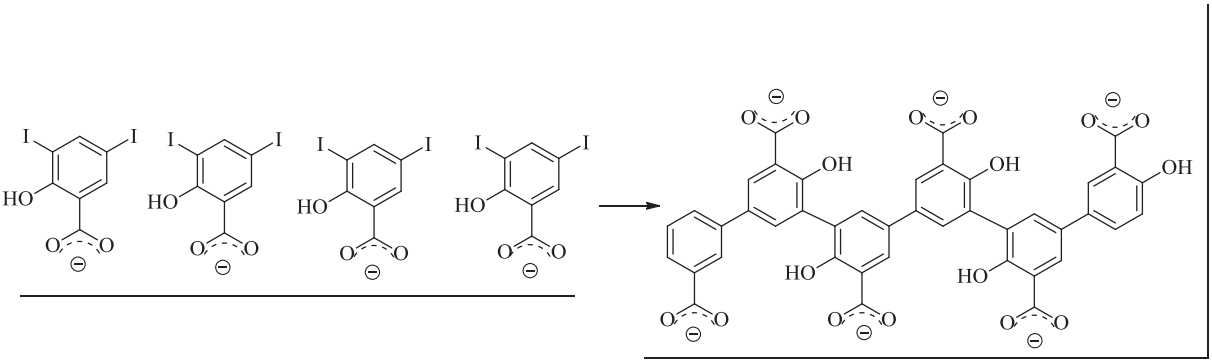

Figure 6 Mécanisme proposé pour la réaction de couplage de l'acide 3,5-diiodosalicylique (gauche vue de côté, droite vue de dessus).

Molécules pour le couplage covalent sur calcite en conditions UHV

Les molécules que nous avons conçues puis synthétisées pour les réactions de couplage sur calcite en UHV, sont caractérisées par un cœur central (idéalement facilement observable par nc-AFM), connecté par des bras à des groupes de greffage (acides carboxyliques) et des groupes réactifs.

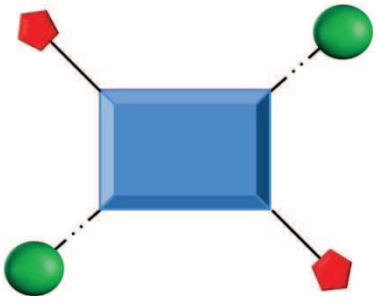

Figure 7 Schéma des molécules cibles pour des réactions de couplage sur calcite en conditions UHV. Le carré bleu représente le cœur central ; le rond vert le groupe de greffage au bout des «bras » et le pentagone rouge le groupe réactif.

Dans un premier temps, nous avons synthétisé deux dérivés de l'acide benzoïque avec la triple liaison en position *para* ou *meta* (molécule **6** et **11** respectivement), pour des réactions d'homocouplage, comme présenté à la Figure 8.

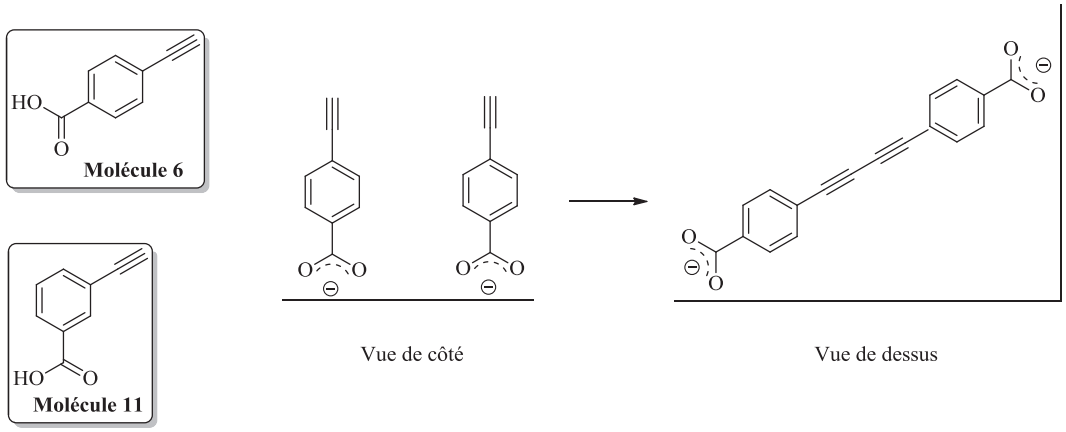

Figure 8 Molécules **6** et **11** pour des réactions d'homocouplage sur calcite en UHV.

La molécule **6**, une fois sublimée, se greffe sur la surface de $CaCO_3$ grâce au groupe carboxylique. Un premier essai de recuit n'a pas permis d'obtenir la réaction de couplage. L'irradiation à 254 nm durant 1h (pour tester une réaction de photopolymérisation) a aussi échoué. La molécule **11** semble réagir directement dans le creuset rendant le dépôt par sublimation impossible.

Des études plus approfondes sont nécessaires afin de mieux comprendre la réaction de couplage.

Puis, nous avons synthétisé les dimères correspondants pour des réactions de photopolymérisation (Figure 9). Les molécules ont été ensuite déposées sur la surface de $CaCO_3$: elles se greffent grâce aux groupes carboxyliques.

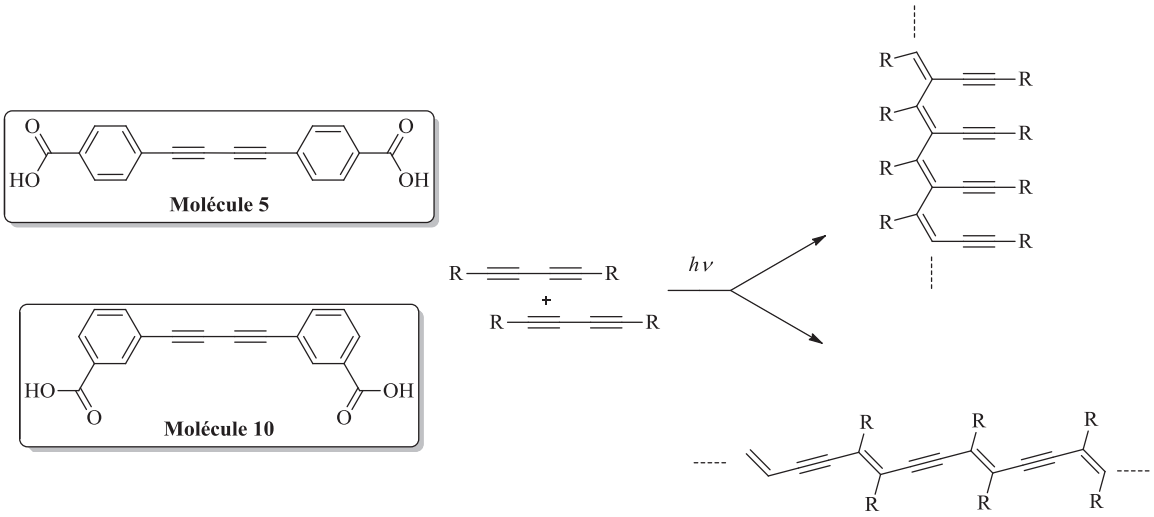

Figure 9 Molécules **5** et **10** pour des réactions de photopolymérisation (deux dérivées possibles).

Un premier test d'irradiation à 254 nm n'a pas donné les résultats attendus. Des études supplémentaires seront menées par l'équipe du Prof. A. Kühnle en Allemagne prochainement.

Nous avons poursuivi ce travail avec la synthèse du naphtalène-2,3,6,7-tetracarbonitrile afin d'obtenir une réaction de polycondensation en présence d'atomes de Fe (Figure 10).

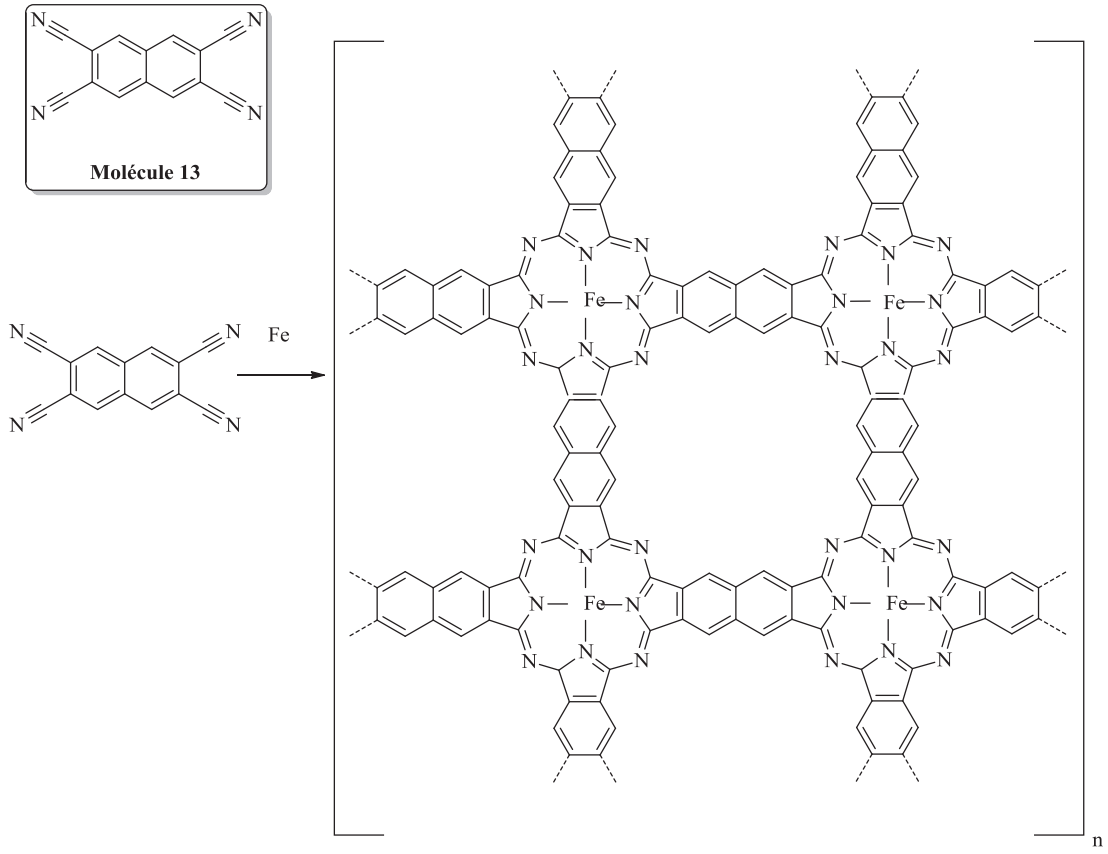

Figure 10 Molécule **13** et réaction de polycondensation en présence de Fe.

La molécule **13** ainsi que le 2,3-dicyanonaphtalène sont actuellement en phase d'étude dans l'équipe du Prof. A. Kühnle en Allemagne.

Enfin, nous avons étudié la synthèse d'un dérivé de l'anthracène. La molécule cible (**18**) est constituée de deux groupes réactifs en positions 9 et 10 (pour obtenir dans une première étape un polymère par réaction d'Ullmann). Deux chaines alkyles en position 2 et 6 sont terminées par des groupes carboxyliques, éléments essentiels pour le greffage sur la surface de calcite.

Pour la synthèse de ce produit, nous avons réussi à synthétiser et caractériser un intermédiaire clé du produit final.

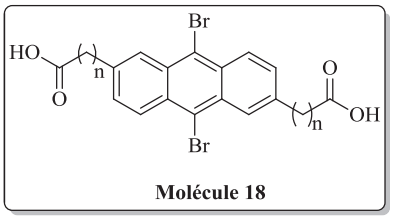

Molécule 18

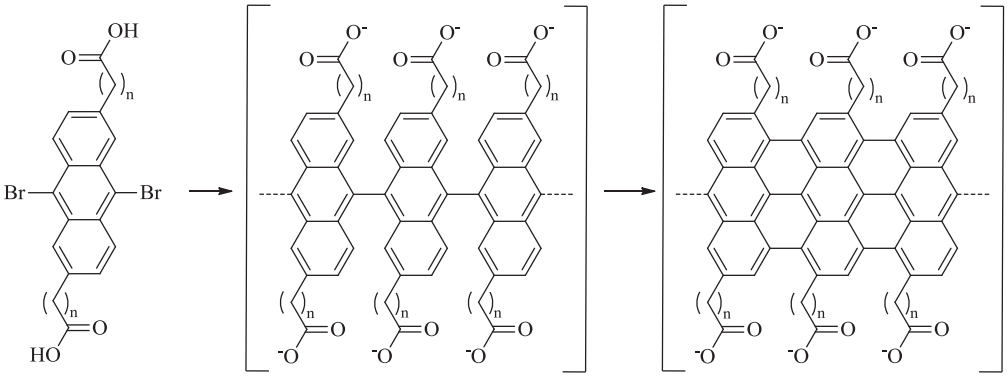

Figure 11 Molécule **18** et synthèse d'un nanoruban de graphène par réaction d'Ullmann suivi par réaction de cyclodéhydrogénation.

Une fois déprotonées et greffées sur la surface, les molécules cibles (**18**) devraient réagir afin d'obtenir dans un premier temps un polymère linéaire (par réaction d'Ullmann). Une réaction de cyclodéhydrogénation (jamais étudié sur cette surface en UHV), devrait mener au nanoruban de graphène.

Les études en UHV présentent plusieurs limitations, par exemple les structures synthétisées ne peuvent pas être exportées de l'environnent UHV pour analyses supplémentaires. De plus, sur isolant le manque de techniques de spectroscopies de surface limite les possibilités de caractérisation.

Pour ces raisons, nous avons étendu le travail effectué en conditions UHV à l'échelle macroscopique, comme représenté sur le schéma suivante (Figure 12).

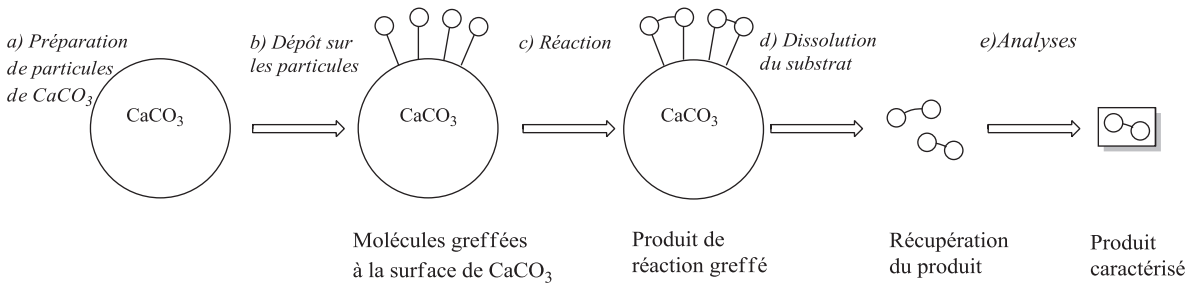

Figure 12 Réaction de couplage sur particules de $CaCO_3$.

Dans un premier temps, nous avons préparé des microparticules afin d'étudier des réactions en phase solide (étape a). Pour la suite nous avons déposé ces molécules cibles sur les microparticules (étape b) puis activé la réaction par différentes méthodes (étape c). Enfin par dissolution du substrat (étape d), nous avons récupéré et caractérisé le produit final (étape e).

Préparation de particules de $CaCO_3$ pour des réactions de couplage en phase solide (étape a)

Afin d'obtenir des particules de carbonate de calcium nous avons choisi deux méthodes différentes.

Par broyage de carbonate de calcium commercial

Dans un premier temps, nous avons broyé du carbonate de calcium commercial (Figure 13) afin d'obtenir des particules présentant une surface spécifique suffisante pour des réactions de couplage (Figure 14).

Le produit commercial a été broyé pour 15 minutes dans une broyeuse planétaire.

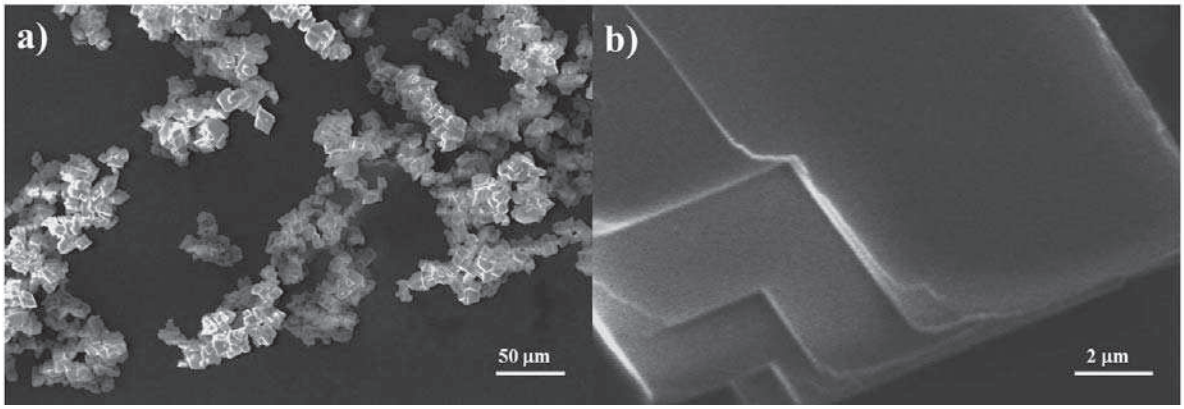

Figure 13 a-b) Images MEB du carbonate de calcium commercial.

Avant broyage, le produit commercial est formé d'agglomérats de formes cubiques. La surface spécifique estimée est de 0.1 m^2/g (chapitre 3).

Après broyage, les agglomérats ne sont plus observables. La surface spécifique déterminée par BET est de $a_{S,BET}$ = 1,3 m^2/g.

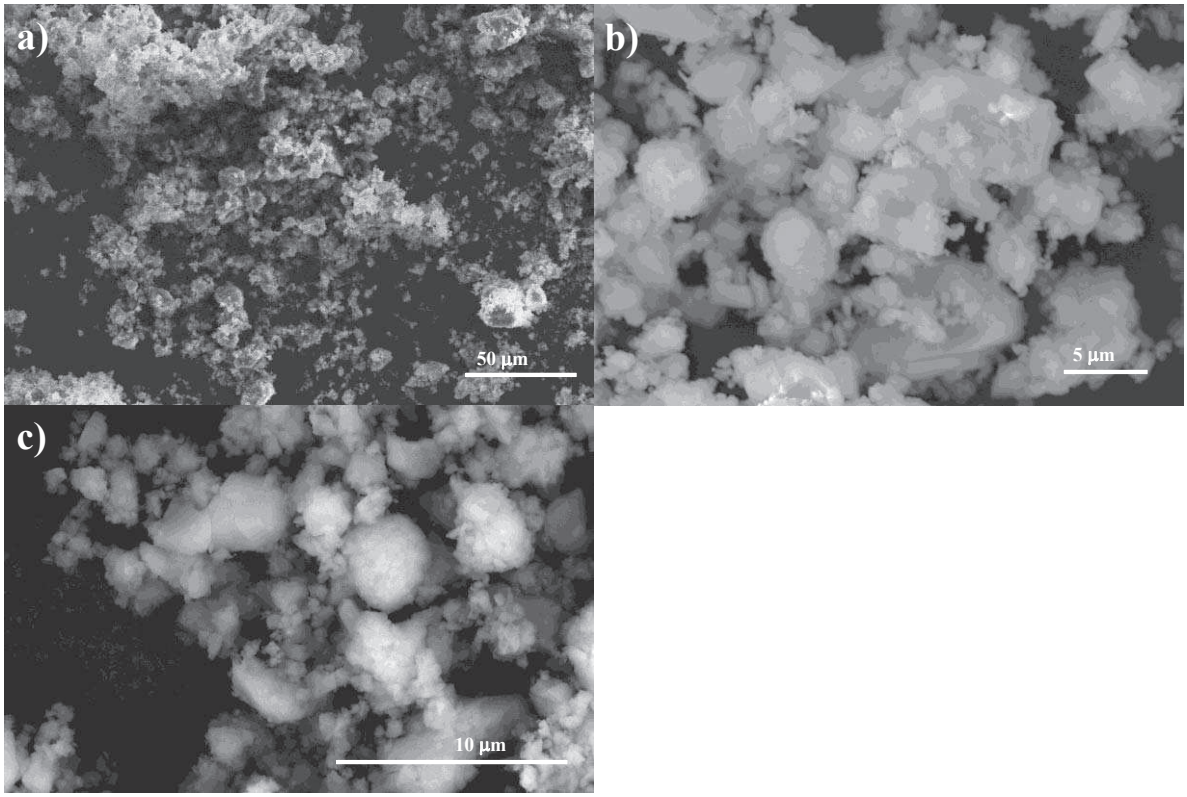

Figure 14 a-c) Images MEB du carbonate de calcium commercial après broyage.

Synthèse par spray pyrolyse

Les microparticules de carbonate de calcium peuvent être préparées par nombreuses méthodes mais nous avons mis au point la préparation par spray pyrolyse (pour la première fois) à partir d'une solution aqueuse d'acétate de calcium.

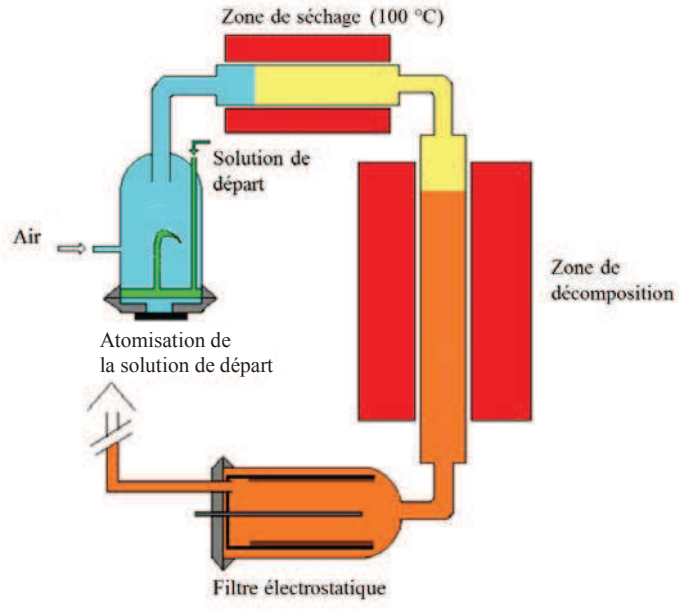

Figure 15 Schéma du dispositif de spray pyrolyse utilisé.

Tout d'abord, des particules d'acétate de calcium sont formées et séchées (à environ 100 °C). Puis elles se décomposent pendant le processus de spray pyrolyse (dans la zone de décomposition présentée à la Figure 15) en carbonate de calcium et acétone (Eq. 1). A plus haute température, le carbonate se décompose en oxyde de calcium (Eq. 2) :

$$Ca(CH_3CO_2)_2 \rightarrow CaCO_3 + C_3H_6O \quad T \sim 380\text{-}400\ °C \qquad \text{Eq.1}$$

$$CaCO_3 \rightarrow CaO + CO_2 \quad T > 650\ °C \qquad \text{Eq.2}$$

Plusieurs températures de pyrolyse ont été étudiées.

Echantillon	**1**	**2**	**3**	**4**	**5**	**6**	**7**	**8**
T (°C)	250	350	400	450	500	550	650	750

Tableau 1 Températures de décomposition des échantillons pendant le spray pyrolyse.

Les échantillons ont été caractérisés par différentes techniques expérimentales : FTIR, ATG/DTG, DRX et MEB.

Les spectres IR des échantillons obtenus à différentes températures de spray pyrolyse (250, 350, 450, 550, 650, 750 °C) sont présentés à la Figure 16 et à la Figure 17. Les spectres du carbonate de calcium et acétate de calcium ont été ajoutés comme références.

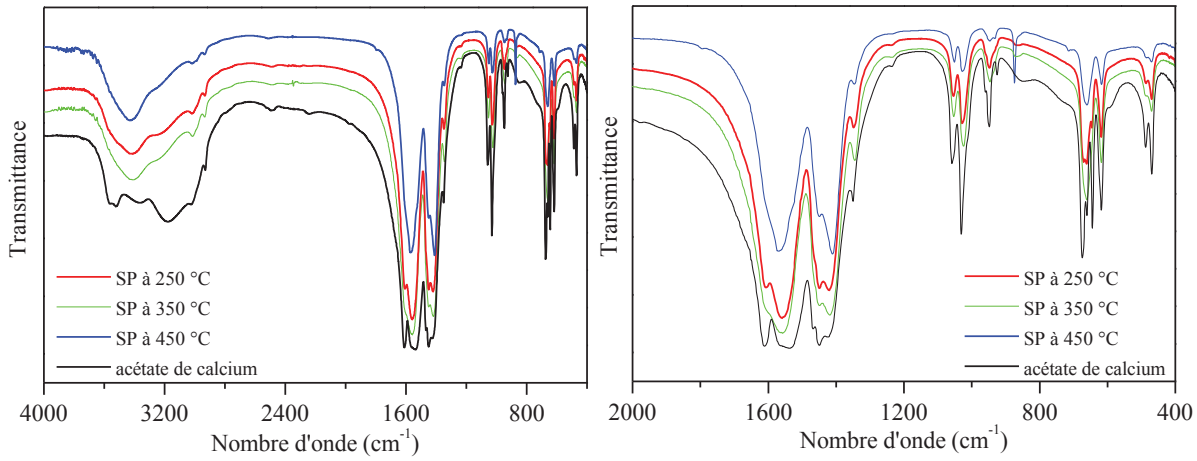

Figure 16) Spectres infrarouge des échantillons 1-2-4 obtenus par spray pyrolyse à différentes températures 250-350-450 °C et de l'acétate de calcium entre 4000 et 400 cm^{-1}. b) Spectres infrarouge des échantillons 1-2-4 obtenus par spray pyrolyse à différentes températures 250-350-450 °C et de l'acétate de calcium entre 2000 et 400 cm^{-1}. Seul l'échantillon 4 (température de spray pyrolyse à 450 °C) présente le pic caractéristique de la calcite (marqué avec le symbole °).

Les spectres IR des échantillons obtenus pas spray pyrolyse à 250-350-450 °C, présentent un profil similaire à celui de l'acétate de calcium (comme présenté sur la Figure 16). Les échantillons élaborés à plus hautes températures (550-650-750 °C) présentent un profil proche de celui du carbonate de calcium (Figure 17).

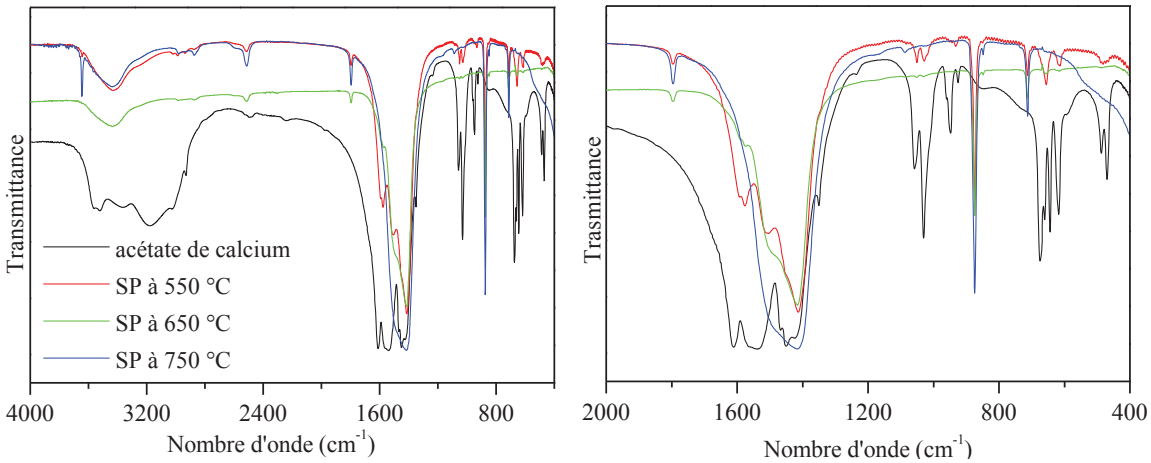

Figure 17 a) Spectres infrarouge des échantillons 6-7-8 obtenus par spray pyrolyse à différentes températures 550-650-750 °C et de l'acétate de calcium entre 4000 et 400 cm^{-1}. b) Spectres infrarouge des échantillons 6-7-8 obtenues par spray pyrolyse à différentes températures 550-650-750 °C et de l'acétate de calcium entre 2000 et 400 cm^{-1}. Les pics correspondants à la calcite son marqués avec les symboles §, ° et *.

L'analyse thermogravimétrique des différents échantillons montre une perte de masse entre 380 et 480 °C caractéristique de la décomposition de l'acétate de calcium en carbonate. Une deuxième perte de masse est observée entre 780-930 °C, caractéristique de la décomposition du carbonate en oxyde de calcium avec formation de CO_2. La comparaison des courbes ATG des différents échantillons (détaillée dans le chapitre 4) montre une perte de masse entre 380 et 480 °C de plus en plus faible pour les échantillons synthétisés à plus hautes températures (par exemple dans l'échantillon 8 - SP à 750 °C in Figure 18). Ainsi, comme l'indiquait la spectroscopie IR, l'augmentation de la température de spray pyrolyse permet l'obtention d'une phase de carbonate de calcium plus pure (Figure 18).

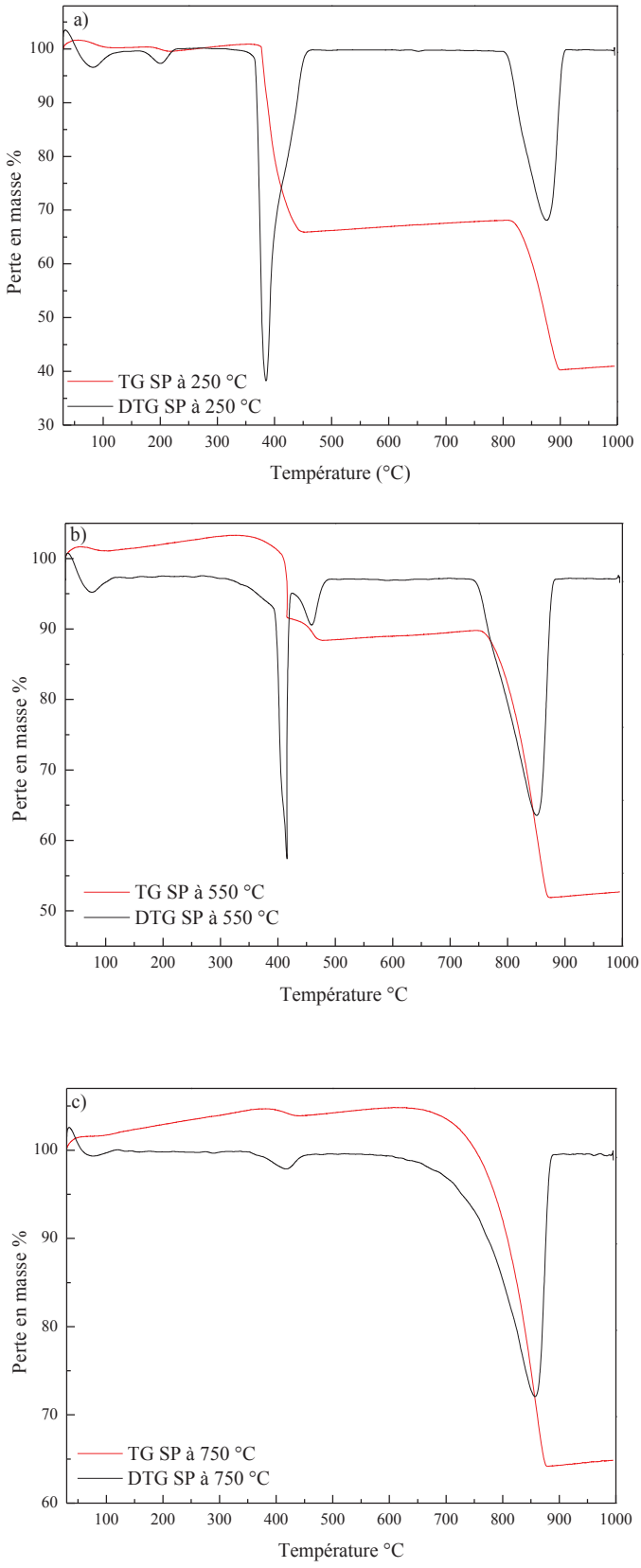

Figure 18 a-c) TG et DTG des échantillons 1-6-8 (obtenus par spray pyrolyse à 250-550-750 °C).

Les spectres de diffraction X de particules obtenues par synthèse à 250-550-750 °C sont présentés à la Figure 19.

Le spectre de diffraction X de l'échantillon à 250 °C présente des pics caractéristiques d'un produit principalement constitué d'acétate de calcium. Au contraire, les spectres des échantillons élaborés à 550 et 750 °C montrent l'obtention de calcaire. Remarquons sur le spectre de l'échantillon élaboré à 750 °C, l'apparition de 2 pics à 2 théta = 37,6° et 54,1° caractéristiques de l'oxyde de calcium.

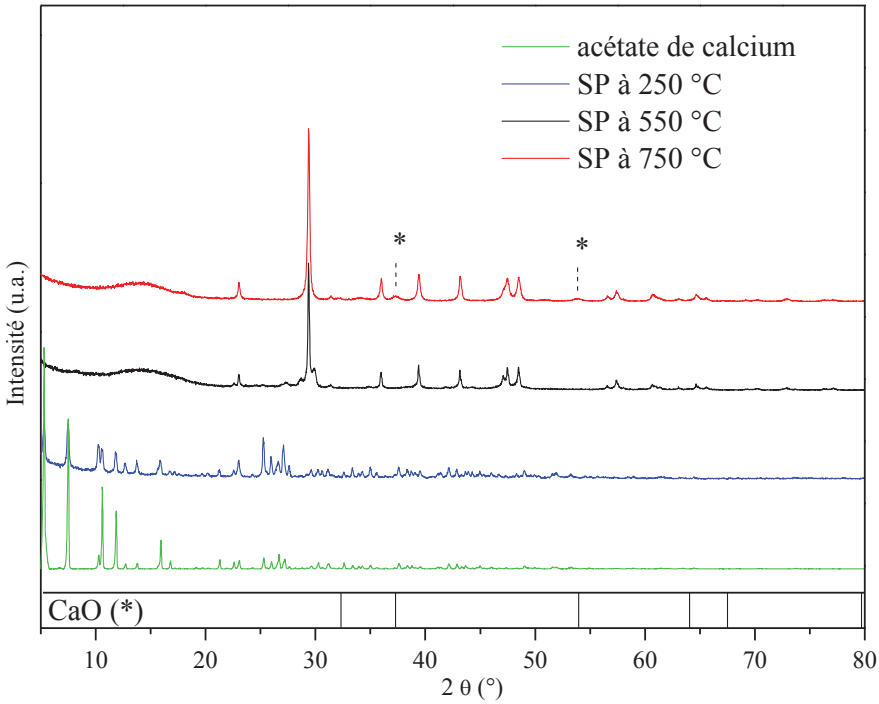

Figure 19 Diffractogrammes de rayons X des échantillons 1-6-8 (obtenus par spray pyrolyse à 250-550-750 °C) et de l'acétate de calcium hydrate (PDF Base des donnés). L'échantillon à 750 °C (en rouge) présente 2 pics caractéristiques de l'oxyde de calcium (CaO) marqués avec le symbole *.

Les images MEB des échantillons sont présentées à la Figure 20. Les particules sont quasi sphériques avec un diamètre compris entre 1 et 5 µm, quel que soit la température de synthèse.

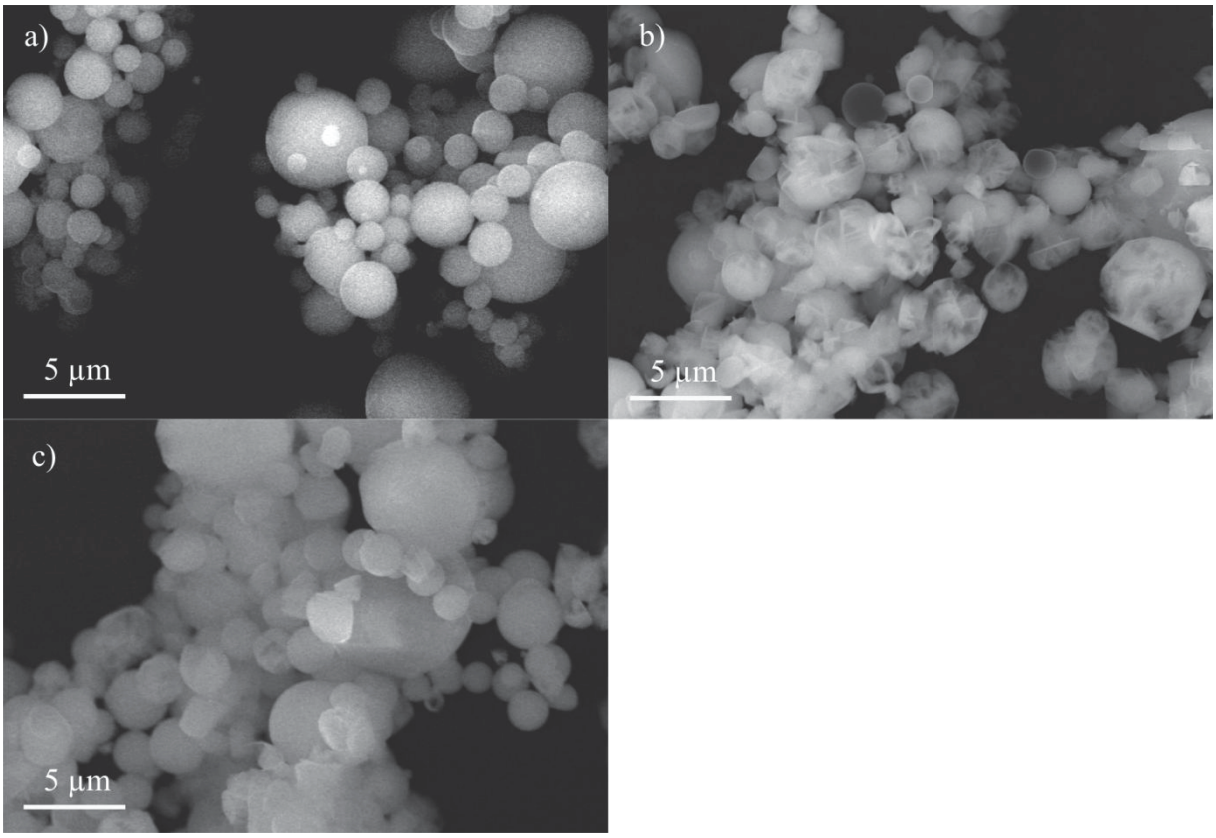

Figure 20 Images MEB a) échantillon 1, température de spray pyrolyse 250 °C ; b) échantillon 3, température de spray pyrolyse 400 °C et c) échantillon 5, température de spray pyrolyse 500 °C.

En conclusion, suivant la température de pyrolyse, les échantillons présentent des compositions en acétate de calcium et carbonate de calcium différentes. A basse température (T = 250 °C) les échantillons sont principalement constitués d'acétate de calcium, alors qu'à température plus haute (T> 500 °C) les échantillons sont principalement composés de carbonate de calcium. A température supérieure (T<650 °C), le carbonate de calcium se décompose en oxyde de calcium.

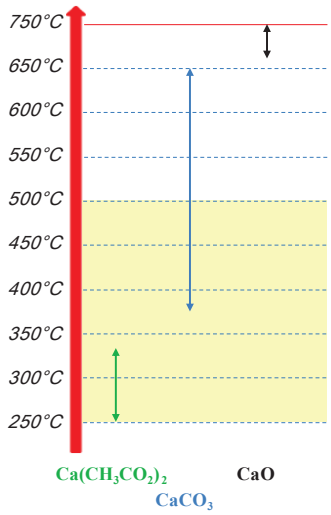

Figure 21 Schéma de températures de spray pyrolyse.

Les échantillons élaborés à température inférieure à 500 °C (zone jaune dans la figure) ont été sélectionnés et soumis à un recuit à 500 °C pendant 5h. Ce traitement thermique permet de purifier les échantillons (FTIR, ATG/DTG, DRX).

Les spectres IR des échantillons après recuit (à la Figure 22 l'échantillon obtenu à 400 °C), présentent une phase unique correspondant à la calcite.

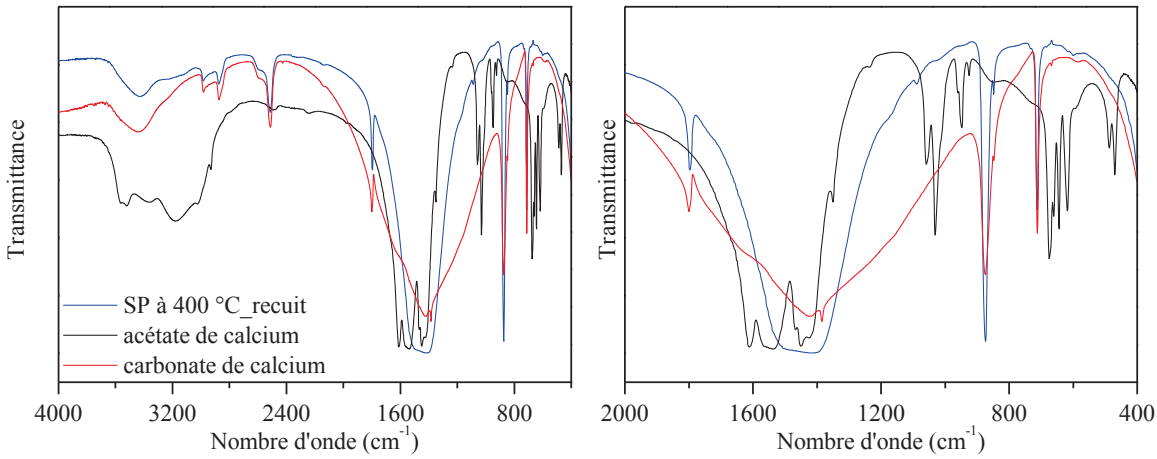

Figure 22 a) Spectres infrarouge de l'échantillon 3 obtenu par spray pyrolyse à 400 °C après le traitement thermique, de l'acétate de calcium et du carbonate de calcium entre 4000 et 400 cm^{-1}. b) Spectres infrarouge de l'échantillon 3 obtenu par spray pyrolyse à 400 °C, de l'acétate de calcium et du carbonate de calcium entre 2000 et 400 cm^{-1}. Les pics correspondants à la calcite son marqués avec les symboles §, ° et *.

L'analyse thermogravimétrique des échantillons après recuit ne montrent plus qu'une seule perte de masse caractéristique de la décomposition du carbonate de calcium en oxyde de calcium (Figure 23).

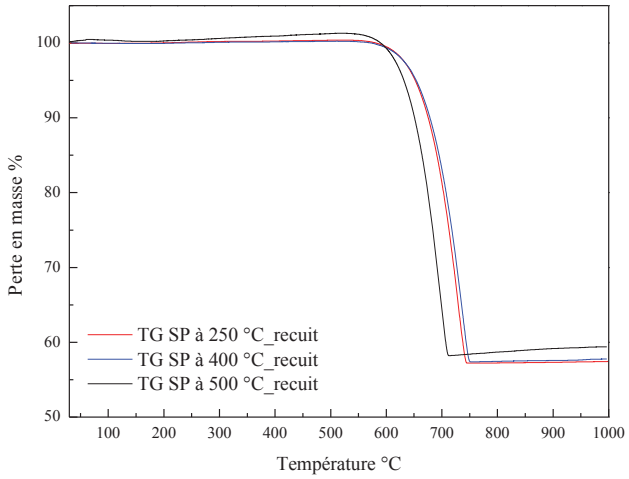

Figure 23 TG et DTG des échantillons 1-3-5 (obtenus par spray pyrolyse à 250-400-500 °C) après le traitement thermique.

Les spectres de diffraction X (Figure 24) des échantillons après recuit confirment la présence d'une phase unique correspondant à la calcite.

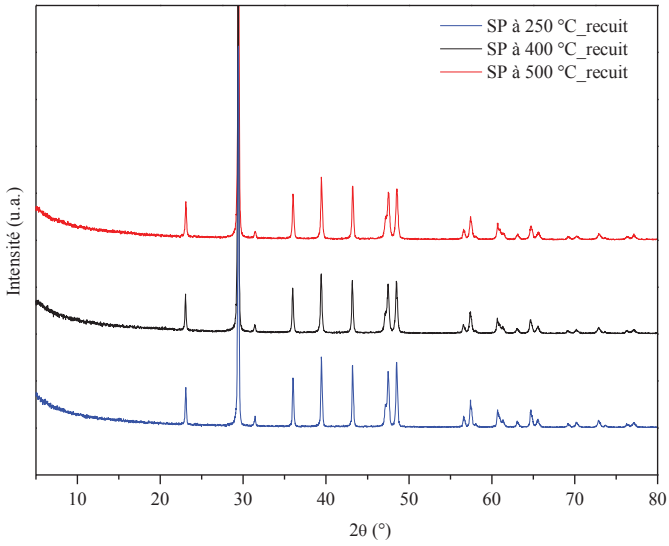

Figure 24 Diffractogrammes de rayons X des échantillons 1-3-5 (obtenus par spray pyrolyse à 250-400-500 °C) après le traitement thermique.

Les images MEB de l'échantillon 5 (obtenu à 500 °C) sont présentées à la Figure 25. Les particules ont presque conservés leur structure sphérique après le traitement thermique.

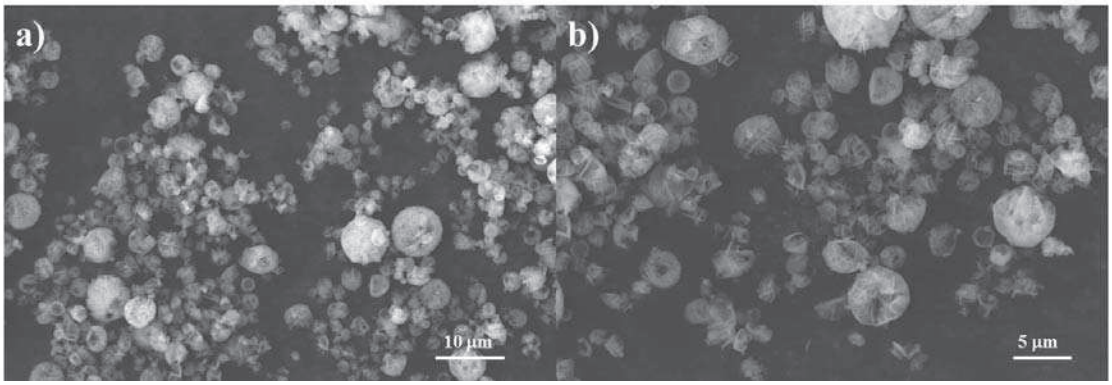

Figure 25 Images MEB de l'échantillon 5 (température de spray pyrolyse 500 °C) après traitement thermique.

Les surfaces spécifiques des échantillons après traitement thermique sont présentées dans le Tableau 2.

Sample	$a_{S,BET}$ (m^2/g)
SP 1 (250 °C)	2,1
SP 3 (400 °C)	4,7
SP 5 (500 °C)	5,0

Tableau 2 Surfaces spécifiques calculée par BET.

Les surfaces spécifiques des échantillons obtenus à 400 et 500 °C sont quasi équivalentes pour l'objectif de réactions de couplage sur ces surfaces. Ces échantillons ont ainsi été sélectionnés comme substrat pour les réactions de couplage. En conclusion pour cette partie, nous avons pu obtenir des microparticules de $CaCO_3$ par spray pyrolyse en deux étapes.

Réactions de couplage sur $CaCO_3$ à l'échelle macroscopique (étapes b-e)

Nous avons étudié des réactions activées par deux méthodes sans solvant :

- Par mécanochimie ;
- Par réaction dans un four sous vide.

Dans un premier temps, nous avons concentré notre étude sur la mécanochimie. Cette technique représente une alternative intéressante à la chimie en solution. Il s'agit d'un broyage avec des billes à haute vitesse des réactifs de départ dans une broyeuse planétaire. Plusieurs réactions ont été reproduites par cette méthode avec de très bons rendements et une bonne sélectivité. La facilité d'usage et les résultats obtenus poussent les chercheurs à étudier de plus en plus cette technique.

La réaction, que nous avons étudiée, a déjà été présentée dans la littérature en conditions UHV. Il s'agit de la réaction de couplage de l'acide 4-iodobenzoïque pour obtenir le biphenyl dicarboxylyque dérivé.

Figure 26 Réaction de couplage de l'acide 4-iodobenzoïque sur calcite en UHV.

Nous avons broyé du carbonate de calcium (avec une surface spécifique correcte), le réactif du départ (acide 4-iodobenzoïque) dans une broyeuse planétaire avec des billes en alumine. Nous avons étudié différentes conditions : vitesse de rotation (700 → 750 rpm), temps de broyage (15 → 30 min), prétraitement du substrat de carbonate de calcium, atmosphère neutre (argon).

Dans tous les cas, nous avons obtenu l'acide benzoïque comme produit final.

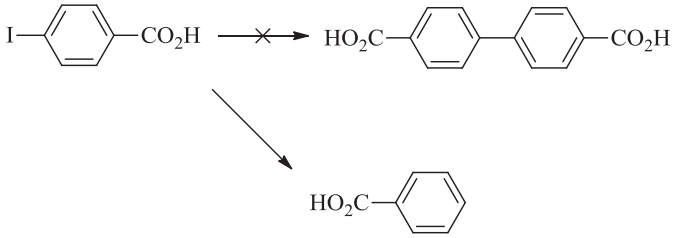

Figure 27 Réaction de couplage de l'acide 4-iodobenzoïque par mécanochimie.

Pour expliquer ce résultat, nous suggérons la présence de plusieurs couches d'eau qui interdit la réaction de couplage entre deux molécules d'acide 4-iodobenzoïque. La réaction parasite avec les molécules d'eau mène à la formation d'acide benzoïque comme produit final.

Dans un deuxième temps, nous avons étudié les conditions d'activation par voie thermique. Le substrat de carbonate de calcium a été broyé avec le produit de départ dans une broyeuse planétaire puis placé dans une nacelle et chauffé dans un four sous vide. Les échantillons ont été chauffés sous vide à 200 °C dans un premier temps pour éliminer l'eau. Ensuite, la température a été maintenue à 280 °C pendant trois jours. Dans ce cas, nous avons obtenu le dérivé éther (produit A à la Figure 28) et l'acide benzoïque comme sous-produit (produit B à la Figure 28).

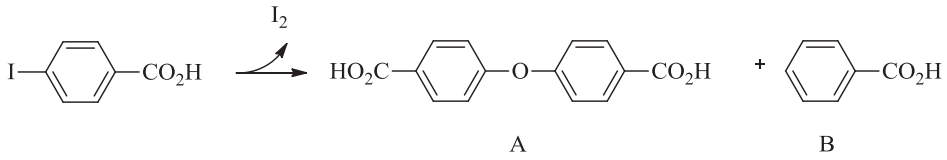

Figure 28 Réaction de couplage de l'acide 4-iodobenzoïque par voie thermique.

Différents paramètres ont été étudiés, présentés dans le Tableau 3. Néanmoins, dans tous les cas, le produit obtenu est le dérivé éther (produit A) et comme sous produit l'acide benzoïque (produit B).

	Temp. (°C)	**Jours**	**Produit A/ Prod. Départ**	**Produit B/ Prod. Départ**
1	400	1 jour	Décomposition des produits	
2	300	1 jour	0.01:1	0.06:1
3	300	2 jours	0.1:1	0.06:1
4	300	3 jours	1 :1	2:1
5	300	4 jours	Décomposition des produits	
6	250	3 jours	0.15:1	0.08 :1
7	260	3 jours	0.16:1	0.10:1
8	280	3 jours	0.83:1	0.29:1

Tableau 3 Résumé des paramètres expérimental et des résultants obtenus par réaction activé thermiquement.

Dans ce cas, nous suggérons la présence d'un milieu basique. En effet, l'action simultanée de l'évaporation d'eau (due à la pompe) et de la solubilisation partielle du carbonate en présence de l'eau restante, forme un milieu basique. Un mécanisme radicalaire ou la formation du phénate mènent probablement à la formation de l'éther (produit A) et de l'acide benzoïque (produit B).

Les différentes techniques expérimentales et leur résultats sont résumés dans le tableau ci-dessous et à la Figure 29.

Technique	**Surface**	**Pression**
UHV	Très propre : les cristaux sont clivés sous vide	10^{-9} mbar
Activation par mécanochimie	Couches des molécules d'eau	Ambiante
Activation thermique	Milieu basique	$1.8 \cdot 10^{-2}$ mbar

Tableau 4 Résumé des différentes techniques.

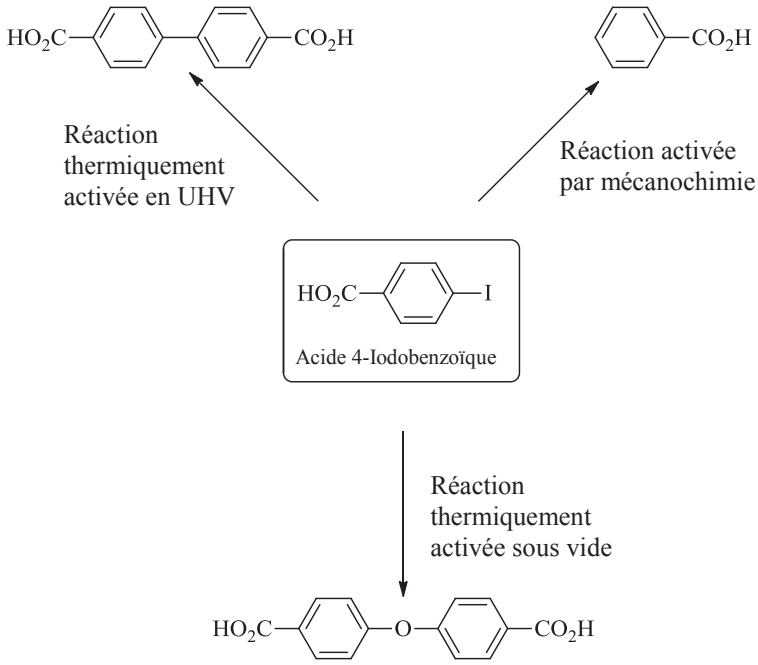

Figure 29 Schéma résumant les résultats suivant les différentes conditionnent de réaction.

Nous avons aussi étudié avec la même technique la réaction de polycondensation du 2,3-dicyanonaphtalène en présence d'atomes du fer.

Dans ce cas, nous avons obtenu l'anhydride correspondant comme montré à la Figure 30 (produit **1**).

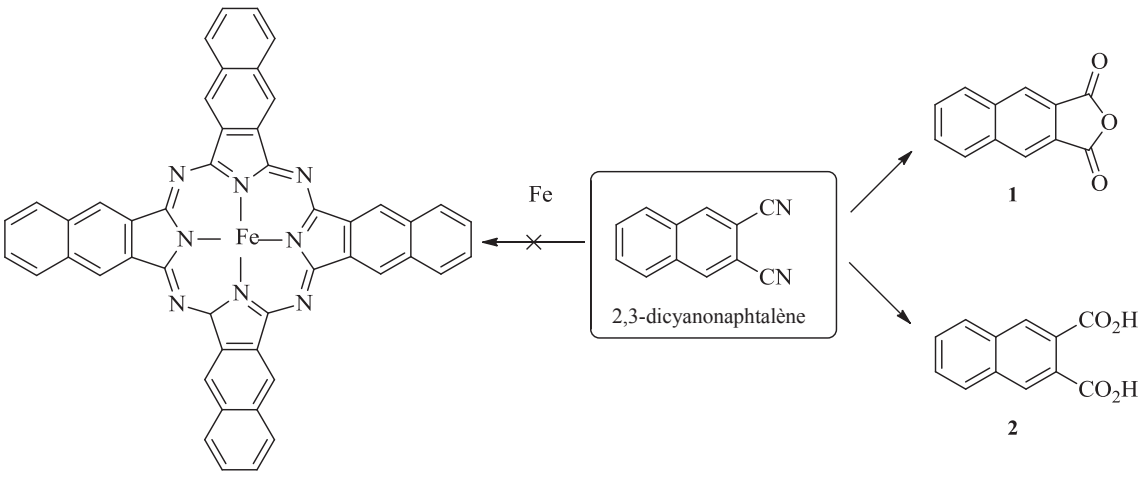

Figure 30 Schéma résumant les réactions à partir du 2,3-dicyanonaphtalène pour voie thermique. Le produit obtenu est le **1**.

La formation de l'anhydride peut également s'expliquer par la présence d'eau basique en surface des microparticules.

Conclusion générale et perspectives

Dans ce travail de thèse, nous avons synthétisé des molécules pour des réactions de couplage innovantes sur la calcite en UHV. Nous avons ensuite étudié ces réactions de couplage en phase solide sur des microparticules de carbonate de calcium obtenues par broyage et spray pyrolyse.

Le dépôt des molécules synthétisées dans ce travail sur calcite en conditions UHV est en cours, en collaboration avec l'équipe d'A. Kühnle.

Pour les études sur les microparticules de carbonate de calcium, nous envisageons la synthèse, par la même technique, de polyéthers. Pour une étude à longue terme, nous envisageons de précuire le carbonate sous vide (à 10^{-6} mbar) pendant plusieurs heures afin d'éliminer les molécules d'eau. La réaction peut être mise en œuvre par la suite dans une boite à gant afin de limiter les interactions avec les molécules d'eau.

Par la suite, nous envisageons l'étude de réaction des acides diboroniques pour étudier les réactions de déshydratation ou d'estérifications sous ultravide.

La même réaction d'estérification peut être envisagée sur les microparticules de carbonate de calcium, néanmoins la présence de couches d'eau ainsi que le work-up acide peuvent empêcher la réaction.

Pour conclure, le carbonate de calcium représente un matériau intéressant pour de futures applications en UHV. De plus, l'élaboration relativement facile de particules permet l'extrapolation des réactions de couplages à l'échelle macroscopique.

Références

1. Ferain, I., Colinge, C. A. & Colinge, J.-P. Multigate transistors as the future of classical metal–oxide–semiconductor field-effect transistors. *Nature* **479,** 310–316 (2011).
2. Does molecular electronics compute? *Nat. Nanotechnol.* **8,** 377–377 (2013).
3. Aviram, A. & Ratner, M. A. Molecular rectifiers. *Chem. Phys. Lett.* **29,** 277–283 (1974).
4. Grill, L. *et al.* Nano-architectures by covalent assembly of molecular building blocks. *Nat. Nanotechnol.* **2,** 687–691 (2007).
5. Cai, J. *et al.* Atomically precise bottom-up fabrication of graphene nanoribbons. *Nature* **466,** 470–473 (2010).
6. Lindner, R. & Kühnle, A. On-Surface Reactions. *ChemPhysChem* **16,** 1582–1592 (2015).

7. Kittelmann, M. *et al.* On-Surface Covalent Linking of Organic Building Blocks on a Bulk Insulator. *ACS Nano* **5,** 8420–8425 (2011).
8. Kittelmann, M., Rahe, P., Gourdon, A. & Kühnle, A. Direct Visualization of Molecule Deprotonation on an Insulating Surface. *ACS Nano* **6,** 7406–7411 (2012).
9. Kittelmann, M., Nimmrich, M., Lindner, R., Gourdon, A. & Kühnle, A. Sequential and Site-Specific On-Surface Synthesis on a Bulk Insulator. *ACS Nano* **7,** 5614–5620 (2013).

Université de Toulouse
Thèse d'Université, spécialité Chimie Moléculaire
Soutenue le 25 novembre 2015
Chiara VENTURINI

On-surface coupling reactions on calcium carbonate

Covalent coupling on metallic surfaces in UHV (Ultra High Vacuum) conditions is a new method for preparing molecular structures otherwise impossible to achieve in solution (graphene nanoribbons, 2D polymers for instance). The major challenge is now to extend these reactions from metallic to insulating surfaces, for future applications as, for instance, in molecular electronics. In particular, the coupling reaction of benzoic acid derivatives, grafted on calcite *via* carboxylic groups, has been demonstrated for the first time in UHV conditions. In the first part of this work, we synthesized precursor molecules for specific reactions (homocoupling of ethynes, photopolymerization, polycondensation and Ullmann reaction) on calcium carbonate in UHV conditions. In the second part of this work we extended this investigation up to the macroscale level (semi-preparative) by grafting molecules on calcium carbonate microparticles, followed by reaction activation and finally by dissolution of the substrate in order to recover the coupling products. The calcium carbonate microparticles were prepared by grinding commercial product or by spray pyrolysis and were fully characterized by FTIR, TG/DTG, XRD, SEM and BET techniques. Then, after grafting of organic reactant, the reactions were activated with two different solvent-free methods: by grinding in a planetary milling machine or by heating the samples in a furnace under vacuum. Whereas in UHV conditions, 4-iodobenzoic acid affords biphenyldicarboxylic acid, mechanochemical condition gives benzoic acid and thermal activation the dibenzoic acid ether.
Keywords: calcium carbonate, coupling reactions, spray pyrolysis, solvent-free reactions, ball milling, surface chemistry

Réactions de couplage sur calcium carbonate

Le couplage covalent sur surface métallique en UHV (Ultra High Vacuum) est une technique émergente permettant de synthétiser des structures moléculaires impossibles à obtenir par la chimie en solution (nanorubans de graphène, polymères 2D par exemple). Aujourd'hui, le plus grand défi reste le développement de ces réactions sur des surfaces isolantes pour différentes applications comme, par exemple, l'électronique moléculaire. En particulier, le couplage de dérivés d'acides benzoïques, greffés sur les surfaces de carbonate de calcium en UHV par des groupes carboxyliques, a été démontré récemment pour la première fois. Lors de ces travaux, nous avons dans un premier temps synthétisé des molécules précurseurs de réactions de couplage (homo-couplage d'éthyne, photopolymérisation, polycondensation et réaction d'Ullmann) sur des surfaces de carbonate de calcium en UHV. Par la suite, nous avons mené cette étude à l'échelle macroscopique (semi-préparatoire), par greffage de molécules sur des microparticules de carbonate de calcium, puis activation de la réaction, et enfin dissolution du substrat afin d'extraire le produit final. Les microparticules ont été obtenues par broyage de produit commercial ainsi que par spray pyrolyse et complètement caractérisées par FTIR, ATG/DTG, DRX, MEB et BET. Les réactions de couplage ont été activées par deux méthodes sans solvant: par broyage dans une broyeuse planétaire ou par traitement thermique sous vide. Alors qu'en UHV le couplage de l'acide 4-iodobenzoïque donne l'acide biphenyldicarboxylique, en mécanochimie nous avons obtenu l'acide benzoïque et par activation thermique l'éther dibenzoïque.
Mots clés: carbonate de calcium, réactions de couplage, spray pyrolyse, réactions sans solvant, mécanochimie, chimie de surface

Centre d'élaboration de matériaux et d'études structurales – CNRS UPS 8011
29 Rue Jeanne Marvig, BP 94347, 31055 Toulouse *Cedex 4*